Imperial College London

Synthesis and Characterisation of Stimuli-responsive Amino Acid-based Polymeric Materials for Drug Delivery

Shiqi Wang

Thesis submitted in accordance with the requirements of Imperial College London for the degree of DOCTOR OF PHILOSOPHY.

Department of Chemical Engineering

Imperial College London

May 2018

Declaration of originality

This thesis is submitted for the degree of Doctor of Philosophy at Imperial College London. I confirm that the research presented in this thesis is my own work. Any results obtained in collaboration have been specifically indicated and acknowledged in the texts.

The research was carried out under the supervision of Dr Rongjun Chen between September 2014 and March 2018. The thesis does not contain any material that has been previously accepted for the award of any qualification at Imperial College London or any other educational institution.

This thesis contains 109 figures, 14 tables and 47452 words excluding the bibliography and the appendix.

Parts of the work have been presented at conferences and workshops, including: the Imperial College PhD Symposium, Department of Chemical Engineering (London, UK, 2015, 2016 & 2017), the 22nd and 23rd CLSS-UK Annual Conference (London, UK, 2016 & 2017), the Materials Research Society Spring Meeting and Exhibit (Phoenix, US, 2017), European Nanomedicine Meeting (London, UK, 2017), BESIG Young Researcher Meeting (Dublin, Ireland, 2016), Warwick Polymer Conference (Coventry, UK, 2016), SNAL Workshop within 3rd World Congress on New Technologies (Rome, Italy, 2017), Workshop on biomaterials and lipid membranes (Salou, Spain, 2015 & 2016), Fundamentals and Applications of Lipid Membrane Biophysics workshop (Horsly Park, UK, 2015), ITN SNAL Summer School on biomaterials, cell membranes and lipid bilayers (Roccalumera, Italy, 2015), 2D Materials and Interfaces workshop (Manchester, 2015).

Parts of the work have been or will be published in the following papers:

Wang, S., Huang, X., Ha, Y., Chin, B., Wen, S., & Chen, R. Cell-penetrating peptide mimicking polymer-based membrane-active nanogels for oral drug delivery. *Manuscript in preparation.*

Wang, S., Attah, R., Li, J., Chen, Y., & Chen, R. (2018). A pH-responsive amphiphilic hydrogel based on pseudopeptides and poly(ethylene glycol) for oral delivery of hydrophobic drugs. *Submitted to ACS Biomaterials Science & Engineering.*

Wang, S.**,** & Chen, R. (2017). pH-Responsive, lysine-based, hyperbranched polymers mimicking endosomolytic cell-penetrating peptides for efficient intracellular delivery. *Chemistry of Materials*, *29*(14), 5806-5815.

Wang, S., Liu, X., Villar-Garcia, I. J., & Chen, R. (2016). Amino acid based hydrogels with dual responsiveness for oral drug delivery. *Macromolecular bioscience*, *16*(9), 1258-1264.

Shiqi Wang

March 2018

Acknowledgements

For the past 3 years during my PhD, I've been thinking so many times about how to write my acknowledgements in my thesis. But when I'm actually writing, I don't know where to start. I would like to thank you all who accompanied me for the good and the bad times in this long journey.

Specifically, my acknowledgement goes to my supervisor, Dr Rongjun Chen, for providing me the opportunity to the project. I have to say the project was beyond my expectation and I really learnt a lot about how to become a professional researcher. I am grateful for all the guidance and suggestions, technically and personally.

Also I would like to acknowledge the support from ITN-SNAL. Thank Prof Nigel Slater, Dr Krishnaa Mahbubani, Prof Carlos Marques, Dr Fabrice Thalmann, Dr Kevin Ward and Dr Ian Tucker for their advice and guidance during my secondments and collaborative work. Thank all SNAL network team members for providing fruitful workshops and online courses.

Many thanks to Prof Paul Luckham for being my academic mentor. I really appreciated his suggestions during ESA and LSR, as well as the discussions at my final stage of PhD. Thank my viva examiners Dr Daryl Williams and Dr Dejian Zhou for their suggestions and comments.

I'm also grateful to all the MSc students and undergraduate students I have been working with: Xiaoxue Liu, Reva Attah, Xiaozhen Huang, Bayan Al-Balushi, Jiali Li, Yitong Chen, Wanyue Ouyang, Youlim Ha, Sim Wen and Benjamin Chin. Their dedicated work made a great contribution towards my PhD.

Thank Mrs Patricia Carry for her patience and support over the three years in department analytical lab. I also thank Dr Mahmoud Ardakani, Dr

Ecaterina Ware, Dr Peter Haycock, Dr Stephen Rothery, Dr Ruth Brooker and Dr Ignacio J. Villar-Garcia for their help in equipment training and sample testing.

Thank Miss Jessica Baldock, Mrs Susi Underwood, Mrs Severine Toson and Mrs Aleksandra Szymanska for their administrative support.

Thank European Union Marie Curie Actions for financially supporting my PhD. Also thank Imperial College Trust and the Old Centralians' Trust for travel funding.

For friends and family, I would first thank mum and dad, for their understanding, encouragement and love forever.

I am grateful to my dear lab buddies, Dr Siyuan Chen, Dr Marie Bachelet and Mr Michal Kopytynski, for their everyday accompany in the daily 'routine'. Thanks for all the sympathy and support when I was feeling low. Also thanks for the helpful discussions about experiments and life. Thank Appaprent Bharma and Gabriella Morrison for proofreading my thesis.

Thank all my friends in SNAL network, especially Anna Sofia Tascini who always cheered me up with her Italian lovely smile. Also thank Mattia Morandi for his great help in imaging during my secondment in Strasbourg.

Special thanks to Dr Chongyu Zhu for his immense technical support in chemical synthesis. Also thank Dr Ruijiao Dong, Mr Yuan Zhao and Dr Yunqing Zhu for their technical consultations.

And finally to my beloved Tianyi, who stands by my side throughout my PhD journey. Without you, I would not have the courage to even start this adventure. Whenever I was depressed, your words and the dishes you cook made me feel life was gonna be better.

To my parents and my husband

When thunders come, raindrops patter;	*打雷要下雨（嘞哦），*
When showers come, find a shelter;	*下雨要打伞（嘞哦），*
When it's cold, wear a warm sweater;	*天冷穿棉袄（嘞哦嘞诶哦），*
When it's hot, get an air cooler;	*天热扇扇子，*
Wisdom is…it's that simple.	*智慧就是——这么简单，*
Why does thunder and rain happen?	*为什么会打雷下雨——为什么，*
Why does winter and summer switch?	*为什么有冬天夏天——是个难题，*
There are so many UNKNOWN MISTERIES OF NATURE,	*不知道的奥秘万万千千，*
*Wisdom is simple? No, it is NOT. Hey!**	*智慧简单——又不简单——嗨！*

------The theme song lyrics of my favourite childhood cartoon *Haier Brothers,* which sparked my interests in science.

*The English version of the lyrics was translated by myself.

Abstract

The delivery of cell-targeted therapeutics, particularly macrodrugs such as proteins and nucleic acids, is of great importance for modern therapy. However, there are many different barriers in the complex bio-environment, which significantly limit the drug availability and efficacy. Herein, this thesis presents the work on development of smart amino acid-based polymeric materials for drug delivery. Specifically, drug delivery vehicles at different length scales with different stimuli-responsive behaviour have been systematically investigated.

A library of anionic, cell penetrating peptide-mimicking, lysine-based hyperbranched polymers have been developed for intracellular drug delivery. Results showed that these polymers destabilised membranes significantly at late endosomal pH, but remained non-lytic at physiological pH. The multivalency effect of the hyperbranched structure further effectively promoted the membrane interactions. Further investigation into endosomal release showed that the hyperbranched polymers could facilitate intracellular payload delivery in Hela cells.

A series of amphiphilic hydrogels have been developed for oral drug delivery. The effects of crosslinking ratio, solid contents and molecular weights of crosslinkers on hydrogels' behaviour were investigated. Also, the *in vitro* model drug loading and release was evaluated. Results suggested that hydrophobic payloads could be successfully incorporated into the hydrogels, and the release in biorelevant buffers was triggered by pH stimulus. Furthermore, by using disulfide-bond containing crosslinkers, the hydrogels responded to the redox trigger in the colon, which led to a faster and more efficient release.

For intracellular drug delivery via an oral route, nanogels were prepared using membrane-active polymers by either physical or chemical crosslinking. The physically crosslinked nanogels were designed to have pH-responsive dissociation. So they could retain model drugs in the acidic gastric fluid, but release them in the neutral intestinal fluid. After dissociation, the polymers were membrane-lytic at slight acidic pH (5.5), which could probably permeabilise cell membranes for intracellular delivery.

Table of Contents

Declaration of originality ..... **i**

Acknowledgements ..... **iii**

Abstract ..... **ix**

List of Figures ..... **xv**

List of Tables ..... **xxvii**

Abbreviations and nomenclature ..... **xxix**

Chapter 1 Introduction **1**

1.1 Drug delivery systems 1

1.1.1 Overview 1

1.1.2 Biological barriers 3

1.1.3 Current challenges and opportunities 6

1.2 Stimuli-responsive systems for overcoming biological barriers 7

1.2.1 pH-Responsive systems 7

1.2.2 Redox-responsive systems 17

1.2.3 pH- and redox-dual responsive systems 21

1.3 Natural/artificial peptides as drug carriers 22

1.3.1 Tumour penetrating peptides 23

1.3.2 Cell penetrating peptides 25

1.4 CPP-mimetic polymers as drug carriers 30

1.4.1 Polycations 30

1.4.2 Zwitterionic polymers and polyanions 33

1.5 PLP and its derivatives 36

1.6 Aims and objectives 39

1.7 Research gaps, novelties and impact 41

1.7.1 Research gaps and novelties 41

1.7.2 Research impact 44

1.8 Thesis outline 45

Chapter 2 Materials and Methods **47**

2.1 Materials 47

2.2 Organic Synthesis 49
2.2.1 Hyperbranched polymer synthesis 49
2.2.2 Hydrogel synthesis 53
2.2.3 Synthesis of physically crosslinked nanogels 55
2.2.4 Synthesis of chemically crosslinked nanogels 56
2.3 Structural and physiochemical properties characterisation 59
2.3.1 Nuclear Magnetic Resonance (NMR) Spectrometry 59
2.3.2 Fourier Transform Infrared (FTIR) Spectroscopy 60
2.3.3 Gel Permeation Chromatography (GPC) 61
2.3.4 X-ray photoelectron spectroscopy (XPS) 61
2.3.5 Differential scanning calorimetry (DSC) 62
2.3.6 Thermo gravimetric analysis (TGA) 64
2.3.7 Dynamic light scattering (DLS) 64
2.3.8 Zeta potential 66
2.3.9 Scanning electron microscopy (SEM) 67
2.3.10 Transmission electron microscopy (TEM) 69
2.3.11 Turbidimetry 69
2.3.12 Fluorescence Spectroscopy 69
2.3.13 Critical aggregation concentration (CAC) determination 71
2.3.14 Rheology analysis 72
2.4 Membrane activity evaluation 73
2.4.1 GUVs formulation 73
2.4.2 GUVs interaction with HPLP5 characterised by confocal microscopy 75
2.4.3 Haemolysis assay 76
2.4.4 Imaging of ghost red blood cells by confocal microscopy. 77
2.5 Mammalian cell based assays 77
2.5.1 Mammalian cell culture 77
2.5.2 Cytotoxicity assay 79
2.5.3 Intracellular delivery of model drugs 80
2.6 Hydrogel swelling studies 80
2.7 Hydrogel loading and release 81

2.7.1 Model drug loading and release 81
2.7.2 Probiotics loading and release 83
2.8 Nanogel loading and release 85
2.8.1 Nile red loading and release in physically crosslinked nanogels 85
2.8.2 Doxorubicin loading and release in chemically crosslinked nanogels 88
Chapter 3 Hyperbranched polymers for intracellular drug delivery 90
3.1 Introduction 90
3.2 Results and discussion 93
3.2.1 Model reactions 93
3.2.2 Polymer synthesis and structural characterisation 99
3.2.3 Physiochemical properties 105
3.2.4 pH-Mediated membrane permeability 111
3.2.5 Cytotoxicity 126
3.2.6 Intracellular delivery of model drugs 127
3.3 Conclusions 130
Chapter 4 Hydrogels for oral delivery 132
4.1 Introduction 132
4.2 pH-Responsive amphiphilic hydrogels 135
4.2.1 Synthesis and structural characterisations 135
4.2.2 Hydrogel morphology by SEM 143
4.2.3 pH-Responsive swelling properties 147
4.2.4 pH-Responsive rheology behaviour 148
4.2.5 Loading and release of model drugs 151
4.3 pH- and Redox-responsive hydrogels 157
4.3.1 Synthesis and structural characterisations 157
4.3.2 Hydrogel morphology by SEM 160
4.3.3 pH-Responsive swelling properties 161
4.3.4 Dual-responsive rheology behaviour 163
4.3.5 Loading and release of model drugs 165
4.3.6 Cytotoxicity 167
4.3.7 Loading and release of probiotics 168

4.4 Conclusions 171
Chapter 5 Nanogels for oral drug delivery 174
5.1 Introduction 174
5.2 Physically crosslinked nanogels 177
5.2.1 Synthesis and morphology 177
5.2.2 pH-Sensitivity and ion tolerance 180
5.2.3 Loading and release of model drugs 183
5.2.4 pH-Mediated membrane activity 189
5.3 Chemically crosslinked nanogels via EDC coupling 191
5.4 Chemically crosslinked nanogels via thiol-exchange 196
5.4.1 Synthesis of polymer precursors (PLP-Py20) 197
5.4.2 Nanogel synthesis and morphology 198
5.4.3 pH-sensitivity, ion tolerance and redox-sensitivity 200
5.4.4 Loading and release of anti-cancer drugs 202
5.5 Conclusions 206
Chapter 6 Conclusions and future perspectives 208
6.1 Conclusions 208
6.1.1 HPLP for intracellular drug delivery 208
6.1.2 PLP-based hydrogels for oral drug delivery 209
6.1.3 PLP-based nanogels as a multi-scale delivery system 210
6.2 Future perspectives 210
6.2.1 Further modification of HPLPs 210
6.2.2 Co-delivery of double payloads and multiple stages of release 211
6.2.3 *Ex vivo and in vivo* performance characterisation 212
Bibliography 214
Appendix A Supplement Figures and Tables 249
Appendix B Permissions summary table for third party copyright works 254
Appendix C Bio1 Form of Haemolysis 263
Appendix D Bio1 Form of Cell Culture 276

List of Figures

Figure 1.1 Multiple biological barriers to intravenous delivery of tumour-targeting drugs. Reprinted from literature (Zhang et al. 2017), copyright 2017, with permission from The Royal Society of Chemistry. 5

Figure 1.2 Biological barriers at different scales in oral drug delivery. Adapted from literature (Wang et al. 2016b), copyright 2016, with permission from Wiley. 6

Figure 1.3 Design of pH-responsive drug delivery systems. Left, gastrointestinal (GI) systems, targeting at biological barriers at macroscopic level; middle, tumour microenvironmental (TME) systems, targeting at barriers at microscopic level; right, intracellular endosomal systems, targeting at barriers at cellular level. Adapted from literature (Gao et al. 2010). 8

Figure 1.4 Common pH-responsive polymers for TME system delivery. (a) polyanions; (b) polycations. 13

Figure 1.5 Common acid-liable bonds used in pH-responsive polymer development. 15

Figure 1.6 Schematic showing of endocytosis and endosomal escape strategies. .. 16

Figure 1.7 Design of redox-responsive drug delivery systems. Left, gastrointestinal (GI) systems, for colon targeting at macroscopic level; middle, tumour microenvironmental (TME) systems, for tumour targeting at microscopic level; right, intracellular delivery systems, for cytoplasmic release at cellular level. 18

Figure 1.8 Schematic showing of the synthetic methods for incorporating the disulfide linkage. 20

Figure 1.9 Dual-responsive carriers for intracellular delivery. 21

Figure 1.10 Schematic representation of the CendR trans-tissue transport pathway. Drugs are depicted as black dots co-administrated with TPPs. The inset shows an electron microscopic image of a CendR endocytic vesicle that is budding from the cell surface into the cytoplasm and contains CendR peptide-coated gold

nanoparticles (dark dots). Reprinted from literature (Ruoslahti 2017), copyright 2017, with permission from Elsevier B.V. 24
Figure 1.11 CPP internalisation pathways. Reprinted from (Koren & Torchilin 2012), copyright 2012, with permission from permission from Elsevier B.V. 26
Figure 1.12 (a) Schematic illustration of a redox-responsive colon targeting system utilizing PEGylated CPP. Reprinted from literature (Lee et al. 2014), copyright 2014, with permission from ACS Publications. (b) TME enzyme-cleavable drug delivery system. Reprinted from literature (D. Zhang et al. 2016), copyright 2016, with permission from Elsevier B.V. 29
Figure 1.13 (a) Guanidine-containing polyacrylates and copolymers synthesised from RAFT polymerisation. Reprinted from literature (Treat et al. 2012), copyright 2012, with permission from ACS Publications. (b) Polyarginine derivatives synthesised by NCA polymerisation. Reprinted from literature (Song et al. 2017), copyright 2017, with permission from The Royal Chemistry Society. 31
Figure 1.14 Schematic illustration of zwitterionic and cationic micelles and their cytotoxicity. Reprinted from literature (Kim et al. 2012), copyright 2012, with permission from ACS Publications 34
Figure 1.15 Chemical structures of anionic amphiphilic membrane-lytic polymers. Adapted from literature (Binder 2008), copyright 2008, with permission from Wiley. 35
Figure 1.16 Structure of PLP and its derivatives. (a) PLP; (b) PLP conjugated with L phenylalanine (PP); (c) PLP conjugated with L-leucine (PL); (d) PLP conjugated with L-valine (PV); (e) PLP conjugated with decylamine (PLP-NDA) 37
Figure 1.17 (a) Concentration-dependent relative haemolysis by PLP (■), PV-75 (●), PL-75 (▲), PP-75 (▼) at pH 6.5. (b) pH-induced haemolysis by PLP (■), PV-75 (●), PL-75 (▲),PP-75 (▼) at 0.025 mg/ml. Reproduced from reference (Chen, Khormaee, et al. 2009b), copyright 2009, with permission from Elsevier B.V. 38
Figure 2.1 HPLP Synthesis Schematic. Reprinted from published paper (Wang & Chen 2017), copyright 2017, with permission from American Chemical Society. .. 52

Figure 2.2 Synthetic scheme of pH-responsive amphiphilic hydrogels..... 54
Figure 2.3 Synthetic scheme of pH- and redox-responsive hydrogels. 55
Figure 2.4 Synthetic scheme of pH-responsive physically crosslinked nanogels 56
Figure 2.5 Scheme of nanogel formation via EDC-coupling..... 57
Figure 2.6 Scheme of nanogel formation via thiol-exchange. 59
Figure 2.7 DLS mechanism. The different scattered light intensity traced in larger and smaller particle dispersions (Jones 2010), copyright 2010, open access under the license of CC BY-SA 3.0. 65
Figure 2.8 (a) Chemical structure of DOPC and DOPS. (b) Scheme of GUV formation. 74
Figure 2.9 Three-way dilution streak plate image 84
Figure 3.1: ^{1}H-NMR spectrum of the product of model reaction1. ^{1}H-NMR (400 MHz, $CDCl_3$): δ (ppm) 0.96 (9H, t, H_f, C*H*$_3$), 1.42 (6H, m, H_e, C*H*$_2$), 1.60 (6H, m, H_d, C*H*$_2$), 3.46 (6H, m, H_c, C*H*$_2$), 6.62 (3H, t, H_b, N*H*), 8.31 (3H, s, H_a, C*H*)..... 94
Figure 3.2: ^{1}H-NMR spectrum of the product of model reaction 2. ^{1}H-NMR (400 MHz, DMSO-d_6): δ (ppm) 3.20 (6H, m, H_f, C*H*$_2$), 3.69 (9H, s, H_e, C*H*$_3$), 4.76 (6H, m, H_d, C*H*), 7.38-7.21 (15H, m, H_c, C*H* on the phenylalanine aromatic ring), 8.43 (3H, s, H_b, C*H*), 9.23 (3H, d, H_a, N*H*). 95
Figure 3.3 Scheme for the model reaction between the monomer analogue, Boc-L-lysine and the crosslinker, 1,3,5-benzenetricarboxylic acid chloride. 96
Figure 3.4 Zoomed-in ^{1}H-NMR spectrum of the product between 8.3 and 9.1 ppm where peaks corresponding to the protons on aromatic rings and amine groups locate. 97
Figure 3.5 The NMR spectra of HPLP3 in different solvents. (a) in DMSO-d_6; (b) in DMSO-d_6 and D_2O (1:2 v/v). The arrow points to the peaks of crosslinkers. 99
Figure 3.6 (a) ^{1}H NMR spectrum of HPLP5 with proton designations. (b) Zoomed-in ^{1}H NMR spectra of HPLP1, HPLP3 and HPLP5 between 6.9 and 9.1 ppm. Reprinted

from (Wang & Chen 2017), copyright 2017, with permission from ACS publications. 100
Figure 3.7 FTIR spectra of HPLPs. Reprinted from (Wang & Chen 2017), copyright 2017, with permission from ACS publications. 103
Figure 3.8 DSC curves of HPLP1, HPLP3 and HPLP5. Reprinted from (Wang & Chen 2017), copyright 2017, with permission from ACS publications. 103
Figure 3.9 TGA curves of HPLP and linear PLP. 104
Figure 3.10 (a) pH-dependent transmittance of different HPLPs at 1.0 mg mL^{-1}; (b) pH-dependent transmittance of HPLP5 at different concentrations. (a) was reprinted from (Wang & Chen 2017), copyright 2017, with permission from ACS publications. 105
Figure 3.11 (a) The excitation spectra of pyrene containing 1.0 mg mL^{-1} PLP solution at pH 3.8 and 5.8. (λ_{em}=390 nm) (b) The intensities in figure (a) were normalised by I_{338}. 106
Figure 3.12 (a) Variations in I_{338}/I_{333} of HPLP1, HPLP3 and HPLP5 at 0.1 mg mL^{-1}. (b) Variations in I_{338}/I_{333} of HPLP1, HPLP3 and HPLP5 at 2 mg mL^{-1}. Reprinted from (Wang & Chen 2017), copyright 2017, with permission from ACS publications..... 107
Figure 3.13 CAC determination for HPLP1 and HPLP5 at pH 7.4. Reprinted from (Wang & Chen 2017), copyright 2017, with permission from ACS publications..... 108
Figure 3.14 Variations in I_{338}/I_{333} of HPLP5 at 0.1, 1 and 2 mg mL^{-1} and the pH-responsive hydrophophobicity variation scheme. 109
Figure 3.15 Hydrodynamic particle size distributions of (a) HPLP1 and (b) HPLP5 at 1 mg mL^{-1} in buffers at pH 4.6 (red) and pH 7.4 (black). Reprinted from (Wang & Chen 2017), copyright 2017, with permission from ACS publications. 110
Figure 3.16 TEM images of HPLP5 at (a) pH 4.6 and (b) pH 7.4 (scale bar 200 nm) with one representative particle shown in their respective insets (scale bar 50 nm). Reprinted from (Wang & Chen 2017), copyright 2017, with permission from ACS publications. 111

Figure 3.17 Phase contrast microscope image of GUVs made of DOPC and DOPS (9:1). 113
Figure 3.18 Selected frames from a time-lapse video of a typical GUV composed of DOPC and Rhodamine-labelled PE treated with HPTS at pH 5.0 in the presence of 1 mg mL^{-1} HPLP5 by confocal microscopy. Scale bar 20 μm. 113
Figure 3.19 Selected frames from a time-lapse video of a typical GUV composed of DOPC, DOPS (9:1) and Rhodamine-labelled PE treated with HPTS at pH 5.0 in the presence of 1 mg mL^{-1} HPLP5 by confocal microscopy. Scale bar 20 μm.....114
Figure 3.20 (a) 3D Confocal image of GUVs composed of DOPC, DOPS (9:1) and Rhodamine-labelled PE treated with HPTS at pH 5.0 in the presence of 1 mg mL^{-1} HPLP5. Red channel slices with the focal plane (b) at the supporting coverslip and (c) at the equator. Scale bar 50 μm. 115
Figure 3.21 UV-vis absorbance spectra of HPLP5 solution (1 mg mL^{-1} in pH 7.4 phosphate buffer), and haemoglobin solution (prepared by lysing red blood cells in deionised water).....117
Figure 3.22 (a) Concentration-dependent relative haemolysis of sheep RBCs in the presence of different HPLPs at pH 5.0. (n=3). (b) pH-dependent relative haemolysis of sheep RBCs in the presence of different HPLPs at 2 mg mL^{-1}. (n=3). Reprinted from (Wang & Chen 2017), copyright 2017, with permission from ACS publications. 118
Figure 3.23 pH-dependent relative haemolysis of sheep RBCs in the presence of 5 μg mL^{-1} melittin in (a) 100 mM phosphate or citrate buffer and (b) in 150 mM NaCl. (n=3). (b) was reprinted from (Wang & Chen 2017), copyright 2017, with permission from ACS publications. 119
Figure 3.24 pH-dependent relative haemolysis of sheep RBCs in the presence of (a) 10 μg mL^{-1} poly(L-lysine) and poly(L-arginine); (b) 2 mg mL^{-1} poly(L-lysine) and poly(L-arginine). (n=3). 121

Figure 3.25 Confocal microscopy images of sheep RBCs treated with different sized FITC-dextran and Texas Red® hydrazide at pH 5.0 in the presence or absence of 1 mg mL^{-1} HPLP5: (a) FITC-dextran 10K and HPLP5; (b) FITC-dextran 70K and HPLP5; (c) FITC-dextran 150K and HPLP5; (d) FITC-dextran 10K in the absence of HPLP5. Scale bar 10 μm. Green channel, FITC-dextran; black and white channel, bright field; red channel Texas Red® hydrazide. Reprinted from (Wang & Chen 2017), copyright 2017, with permission from ACS publications..... 122
Figure 3.26 Confocal microscopy images of sheep RBCs treated with 10 μM FITC-dextran 10K, 1.5 μM Texas Red® hydrazide and 1 mg mL^{-1} HPLP5 at pH 4.5 (top) and pH 7.4 (bottom). Formation of HPLP5 precipitates at pH 4.5 prevented the RBCs being appropriately visualised. Scale bar 10 μm. Reprinted from (Wang & Chen 2017), copyright 2017, with permission from ACS publications..... 124
Figure 3.27 Time-lapse confocal microscopy images of sheep RBCs treated with 10 μM FITC-dextran 10K, 1.5 μM Texas Red® hydrazide and 1 mg mL^{-1} HPLP5 at pH 5.0. From top to bottom: bright field; green channel: FITC-dextran; red channel: Texas Red® hydrazide. From left to right, stomatocytes, spherocytes and ghost cells. Scale bar 5 μm. Reprinted from (Wang & Chen 2017), copyright 2017, with permission from ACS publications. 125
Figure 3.28 Concentration-dependent relative viabilities of HeLa cells treated with different HPLPs for 24 h as determined by alamarBlue® assay. (n=5). Reprinted from (Wang & Chen 2017), copyright 2017, with permission from ACS publications..... 126
Figure 3.29 Concentration-dependent relative viabilities of HeLa cells treated with melittin (a), poly(L-lysine) (b) and poly(L-arginine) (c) for 24 h as determined by alamarBlue® assay. (n=5). (a) was reprinted from (Wang & Chen 2017), copyright 2017, with permission from ACS publications. 127
Figure 3.30 Confocal microscopy images of HeLa cells showing the intracellular distribution of the endocytosed calcein. The cells were treated with (a) 2 mg mL^{-1} calcein only, and (b) both 2 mg mL^{-1} calcein and 1 mg mL^{-1} HPLP5. Images were

collected at 5 hours after 1 hour of uptake. Scale bar 10 μm. Reprinted from (Wang & Chen 2017), copyright 2017, with permission from ACS publications. 128
Figure 3.31 Confocal microscopy images of HeLa cells showing the intracellular distribution of the endocytosed calcein. The cells were treated with 2 mg mL^{-1} calcein and (a) 1 μg mL^{-1} melittin, (b) 10 μg mL^{-1} poly(L-arginine), (c) 10 μg mL^{-1} poly(L-lysine). Scale bar 20 μm. 129
Figure 3.32 Summary scheme of hyperbranched polymers facilitating pH-responsive membrane penetration and endosomal escape. Reprinted from (Wang & Chen 2017), copyright 2017, with permission from ACS publications. 130
Figure 4.1 Schematic showing oral drug delivery hydrogels and their controlled-release behaviour. Adapted from literature (Wang et al. 2016b), copyright 2016, with permission from Wiley. 135
Figure 4.2 FTIR spectra of PLP, PEG and hydrogels of different crosslinkers. 136
Figure 4.3 Zoomed-in FTIR spectra for Gel 1K, Gel 3.4K and PLP from 3000 to 3600 cm^{-1}. 137
Figure 4.4 FTIR spectra of PLP, PEG and hydrogels of different crosslinking ratios. 139
Figure 4.5 FTIR spectra of Gel 3.4K (a) at pH 7.4 and (b) at pH 3.0. 140
Figure 4.6 DSC of lyophilised Gel 1K, Gel 1.5K, Gel 3.4K and PEG. Before lyophilisation, all hydrogel gels were equilibrated in water. 140
Figure 4.7 DSC of lyophilised Gel 0.1, Gel 0.2, Gel 0.5. Before lyophilisation, all hydrogel gels were equilibrated in water. 141
Figure 4.8 SEM images of (a) Gel 1K, (b) Gel 1.5K, (c) Gel 3.4K and (d) PEG only. All the hydrogels were equilibrated in pH 3 buffers before lyophilisation. 143
Figure 4.9 SEM images of Gel 0.1 (left), Gel 0.2 (middle), Gel 0.5 (right). All the hydrogels were equilibrated in pH 3 buffers before lyophilisation. *The images were collected by Reva Attah in Dr. Chen's group. Reproduced from Attah's Master Dissertation (2016).* 144

Figure 4.10 Images of Gel 1.5K equilibrated in different solutions before SEM. Left, at pH 3.0; middle, in water; right, at pH 7.4. *The images were collected by Reva Attah in Dr. Chen's group.* 144
Figure 4.11 DSC curves of Gel 1.5K in pH 3.0 buffer, pH 7.4 buffer and water (second heating cycle). 146
Figure 4.12 The swelling ratios (q) of hydrogels.* p<0.05, **p<0.01. (n=3). *The data were collected by Reva Attah in Dr. Chen's group. Reproduced from Attah's Master Dissertation (2016).* 148
Figure 4.13 The correlation between G', oscillation stress and strain applied in the strain sweep of Gel 0.1. *The data were collected by Reva Attah in Dr. Chen's group.* 149
Figure 4.14 The variations of G' and G'' against angular frequency in the frequency sweep of Gel 0.1 at pH 3.0 and pH 7.4 respectively. *The data were collected by Reva Attah in Dr. Chen's group. Reproduced from Attah's Master Dissertation (2016).* .. 150
Figure 4.15 Confocal images of Nile red loaded hydrogel, fluorescent channel (a,c) and bright fields (b,d). (a), (b) PEG 1K Gel loaded with Nile red in pH 3.0 buffer. (c), (d) Negative control, gel without Nile red. Scale bar, 50 μm. 152
Figure 4.16 3D-Confocal images of Nile red loaded hydrogel in (a) pH 3.0 and (b) pH 7.4. 153
Figure 4.17 24-Hour cumulative release of fluorescein in pH 3.0 and pH 7.4 buffers. (a) Gel 1K and Gel 3.4K; (b) Gel 0.1 and Gel 0.5. ** p<0.01. (n=3). *The data were collected by Reva Attah in Dr. Chen's group.* 154
Figure 4.18 Release kinetics of fluorescein in biorelevent buffers (first 2 hours in SGF and then transferred to SIF for another 24 hours). (n=3). *The data were collected by undergraduate students Jiali Li and Yitong Chen in Dr. Chen's group. Reproduced from their undergraduate research report (2015).* 155
Figure 4.19 Release kinetics of FITC-dextran 10K in biorelevent buffers (first 2 hours in SGF and then transferred to SIF for another 24 hours). (n=3). 156

Figure 4.20 FTIR spectra of different hydrogels and PLP. 158
Figure 4.21 (a) the XPS spectrum of Gel_{CDE} 2; (b) the zoomed-in figure of the sulfur peak. Reprinted from published work (Wang et al. 2016a), copyright 2016, with permission from Wiley. 159
Figure 4.22 SEM images of different hydrogels. (a) Gel_{CDE} 4, (b) Gel_{CDE} 3, (c) Gel_{CDE} 2, (d) Gel_{CDE} 1. Reprinted from published work (Wang et al. 2016a), copyright 2016, with permission from Wiley. 161
Figure 4.23 pH-responsive swelling behaviour of hydrogels. * $p<0.05$. (n=3). Reprinted from published work (Wang et al. 2016a), copyright 2016, with permission from Wiley. *The data were collected by Xiaoxue Liu in Dr. Chen's group.i* 162
Figure 4.24 Schematic showing the differences of polymer network of CDE-crosslinked hydrogels and PEG-crosslinked hydrogels. Red arrows pointed to the intramolecular crosslinking of CDE-crosslinked hydrogels. 163
Figure 4.25 Frequency sweep of Gel_{CDE} 2 at pH 3.0, pH 7.4 and pH 7.4 with the addition of DTT. Reprinted from published work (Wang et al. 2016a), copyright 2016, with permission from Wiley. 164
Figure 4.26 Cumulative release of fluorescein at pH 3.0 and 7.4 after 24 h of incubation. (n=3). Reprinted from published work (Wang et al. 2016a), copyright 2016, with permission from Wiley. *The data were collected by Xiaoxue Liu in Dr. Chen's group.* 165
Figure 4.27 Released kinetics of Gel_{CDE} 2 at pH 3.0, pH 5.0, pH 7.4, and pH 7.4 with 0.1 M DTT. (n=3). Reprinted from published work (Wang et al. 2016a), copyright 2016, with permission from Wiley. 166
Figure 4.28 Images of hydrogels after drug release with 0.1 M DTT for 24h. From left to right: Gel_{CDE} 1, Gel_{CDE} 2 and Gel_{CDE} 3. 167
Figure 4.29 Cytotoxicity of gels evaluated by alamarBlue® assay on HeLa cells. (n=5). Reprinted from published work (Wang et al. 2016a), copyright 2016, with permission from Wiley. 168

Figure 4.30 LGG loading capacity of Gel_{CDE} 1 and Gel_{CDE} 3 in MRS (pH 5.0) and PBS (pH 7.4) respectively. * p<0.05, **p<0.01. (n=3)..... 170
Figure 4.31 (a) LGG amount remained in the hydrogel during release. (b) LGG amount released in the MRS medium. **p<0.01. (n=3)..... 171
Figure 5.1 Schematic showing the responsive behaviour of physically crosslinked (a) and chemically crosslinked (b) nanogels. 176
Figure 5.2 A 2D-map of nanogel hydrodynamic sizes as a function of polymer concentration in DMF and in water. Green numbers represent the Z-average size (nm) of the corresponding formulation measured by DLS; the blue cross means there were not enough particles in the sample for DLS measurement; the red cross means there were large particles in the sample and the data failed to pass the Malvern Zetasizer internal quality test. Each data point was the average of three measurements. 178
Figure 5.3 SEM of nanogels of different formulations. a, b, c and d represent formulations with an average hydrodynamic size of 55.7 ± 0.7 nm, 103.0 ± 2.8 nm, 151.4 ± 3.7 nm and 259.2 ± 3.3 nm respectively (according to DLS measurement). The scale bar represents 1 μm..... 179
Figure 5.4 pH-responsive size and PDI variations of nanogels. (n=3)..... 181
Figure 5.5 The effects of ionic strength on the size and PDI of nanogels. (n=3). ... 181
Figure 5.6 (a) UV absorbance spectra of Nile red loaded nanogels and Nile red in water. Inset figure is the photo of two samples: left, Nile red in water and right, Nile red loaded nanogels. (b) SEM of Nile-red loaded nanogels..... 185
Figure 5.7 The 3D-fluorescence spectra of Nile red in loaded nanogels in (a) water, (b) FaSSIF and (c) FaSSGF. (d) The emission spectra of Nile red loaded nanogels in water, FaSSGF and FaSSIF. 186
Figure 5.8 Nile red release kinetics in bio-relevant buffers, including FaSSIF, FaSSGF and SGF with higher biosurfactant contents. *The data were provided by*

Xiaozhen Huang in Dr Chen's group. Reproduced from Huang's Master Dissertation (2017). 188
Figure 5.9 The membrane-lytic activity of PLP-NDA18 and the physically crosslinked PLP-NDA18 nanogels from pH 4.5 to 7.4. The final concentration of both polymers and nanogels in different buffers is 0.02 mg mL^{-1}. 190
Figure 5.10 (a) Size variations of the chemically crosslinked nanogels during synthesis. (b) SEM of purified EDC-coupling nanogels. 192
Figure 5.11 FTIR spectra of EDC-coupling nanogels crosslinked by PEG 220 diamine (solid red), crosslinker (solid blue) and PLP-NDA18 polymer (black dash). 194
Figure 5.12 Surface EDC-coupling reaction scheme. Intermediates and side products include anhydride (pink), urea (brown) and NHS succinate (green). Reproduced from literature (Sam et al. 2010), copyright 2010, with permission from ACS Publications. 195
Figure 5.13 Synthetic scheme of chemically crosslinked dual-responsive nanogels. 196
Figure 5.14 ^{1}H-NMR spectrum (a) and ^{13}C-NMR spectrum (b) of Py crosslinker. ^{1}H-NMR (400 MHz, DMSO-d_6): δ (ppm) 3.10 (4H, m, H_f, CH_2; H_g, CH_2), 7.31 (1H, m, H_e, CH), 7.77 (1H, m, H_d, CH), 8.18 (3H, s, H_b, NH_3), 8.52 (1H, m, H_a, CH). ^{13}C-NMR (400 MHz, DMSO-d_6): δ (ppm) 34.76 (C_g), 37.67 (C_f), 120.03 (C_e), 121.63 (C_d), 137.93 (C_c), 149.84 (C_b), 158.09 (C_a). 197
Figure 5.15 ^{1}H-NMR spectrum of PLP-Py conjugate, in DMSO-d_6. 198
Figure 5.16 (a) SEM of chemically-crosslinked nanogels. (b) The zoomed-in image showing individual nanogels. 200
Figure 5.17 FTIR spectra of PLP-Py polymer, DOX and DOX-loaded nanogels. Black arrows pointed to typical DOX bands incorporated in nanogels. 203
Figure 5.18 3D-fluorescence spectra of (a) free DOX in water and (b) DOX-loaded nanogels. 204

Figure 5.19 The emission spectra of DOX-loaded nanogels in water, and nanogels in different release media for 2 h. The excitation wavelength was 480 nm. 205
Figure 5.20 (a) Chemical Structure of DOX. (b) A schematic showing of DOX and nanogel in SGF and DIF. 206

List of Tables

Table 1-1 List of common pH-responsive polymers developed for oral drug formulations. Summarised from (Niazi 2009). 10

Table 1-2 pH-responsive Eudragit® polymers and their properties. Summarised from (Thakral et al. 2013). 11

Table 1-3 Summary of research gaps, aims and novelties in the three results chapters. 43

Table 3-1 Details of the peaks in Figure 3.3b. 98

Table 3-2 The amount of crosslinkers in the HPLPs characterised by H-NMR. Original data were presented in (Wang & Chen 2017), copyright 2017, with permission from ACS publications. 101

Table 3-3 The molecular weights and polydispersities of the HPLPs. Original data were presented in (Wang & Chen 2017), copyright 2017, with permission from ACS publications. 102

Table 4-1 PEG-crosslinked hydrogel formulations. *The hydrogel samples were prepared by Reva Attah in Dr. Chen's group.* 136

Table 4-2 CDE-crosslinked hydrogel formulations. Readapted from published work (Wang et al. 2016a), copyright 2016, with permission from Wiley. *The solid content data were collected by Xiaoxue Liu in Dr. Chen's group.* 157

Table 4-3 Atomistic compositions of each hydrogel by XPS and the crosslinking ratio. Readapted from published work (Wang et al. 2016a), copyright 2016, with permission from Wiley. 160

Table 5-1 Nanogel size and distribution in common buffers 182

Table 5-2 pH Responsibility of chemically crosslinked nanogels, which were prepared via EDC-coupling, in 50 mM phosphate buffer at different pHs. 193

Table 5-3 CDE and cystamine crosslinked nanogels before and after treatment of DTT 193

Table 5-4 pH sensitivity and ion tolerance of chemically crosslinked nanogels via thiol-exchange 201
Table 5-5 The size and distribution of nanogels after 50 mM DTT treatment for 24h. 202

Abbreviations and nomenclature

CPP	Cell penetrating peptide
CA	Cystamine
CAC	Critical aggregation concentration
CAP	Cellulose acetate phthalate
CDE	L-Cystine dimethyl ester dihydrochloride
D_2O	Deuterium oxide
DCC	N,N'-Dicyclohexylcarbodiimide
DCM	Dichloromethane
DDS	Drug delivery system
DLS	Dynamic light scattering
DMAP	4-Dimethylaminopyridine
DMEM	Dulbecco's modified Eagle's medium
DMF	N,N-dimethylformamide
DMSO	Dimethyl sulfoxide
DOPC	1,2-Dioleoyl-sn-glycero-3-phosphocholine
DOPS	1,2-Dioleoyl-sn-glycero-3-phospho-L-serine
DOX	Doxorubicin
DSC	Differential scanning calorimetry
DTT	1,4-Dithiothreitol

EDC	N-(3-Dimethylaminopropyl)- N'-ethyl carbodiimide hydrochloride
FaSSGF	Simulated fasted gastric fluid
FaSSIF	Simulated fasted intestinal fluid
FBS	Fetal bovine serum
FITC-dextran	Fluorescein isothiocyanate–dextran
FTIR	Fourier Transform Infrared
G'	Storage modulus
G"	Loss modulus
GI	Gastrointestinal
GPC	Gel permeation chromatography
GSH	Glutathione
GSSG	Glutathione disulfide
GUV	Giant unilamellar vesicles
HA	Haemagglutinin
HER2	Human epidermal growth factor receptor 2
HPLP	Hyperbranched PLP
HPMA	N-(2-hydroxypropyl) methacrylamide
HPMCP	Hydroxypropyl methylcellulose phthalate
HPTS	8-Hydroxypyrene-1,3,6-trisulfonic acid tri-sodium salt
IC_{50}	Half Maximal Inhibitory concentration
LGG	*Lactobacillus rhamnosus GG*

LVR	Linear-viscoelastic regime
MMP	Matrix metalloproteinase
M_n	Number average molar mass
MRS broth	de Man Rogosa and Sharpe broth
M_w	Mass average molar mass
NCA	N-carboxylanhydrides
NDA	Decylamine
NHS	$_N$-Hydroxysuccinimide
NMP	$_N$-Methyl-2-pyrrolidone
NMR	Nuclear magnetic resonance
NRP	Neuropilin
PAMAM	Polyamidoamine
PBAA	Poly(butylacrylic acid)
PbAE	Poly(β-amino ester)
PBS	Dulbecco's phosphate-buffered saline
PDEAEM	Poly(N,N’-dimethylaminoethyl methacrylate)
PDI	Polydispersity index
PEAA	Poly(ethylacrylic acid)
PEG	Polyethylene glycol
PEG 220 diamine	4,7,10-trioxa-1,13-tridecanediamine
PEI	Polyethylenimine

pH_e	Extracellular environment pH
pKa	Logarithmic acid disassociation constant
PLP	Poly (L-lysine isophthalamide)
PLP-NDA18	PLP conjugated with decylamine at a stoichiometric ratio of 18%
PLP-Py20	PLP conjugated with pyridine dithioethylamine at a stoichiometric ratio of 20%
PMAA	Poly(methacrylic acid)
PMLA	Poly(malic acid)
PolyHis	Poly(histidine)
PPAA	Poly(propylacrylic acid)
PVA	Poly(vinyl alchohol)
PVAP	Poly(vinyl acetate phthalate)
Py	Pyridine dithioethylamine
RAFT	Reversible addition fragmentation chain transfer
RBCs	Red blood cells
Rhodamine- PE	Lissamine™ Rhodamine B 1,2-dihexadecanoyl-sn-glycero-3-phosphoethanolamine triethylammonium salt
SD	Standard deviation
SEM	Scanning electron microscopy
SGF	Simulated gastric fluid
SIF	Simulated intestinal fluid

siRNA	Small interfering RNA
SNAL	Smart Nano-objects for Alteration of Lipid bilayers
SPPS	Solid phase peptide synthesis
Tat	Trans-activating transcriptional activator
TEA	Triethylamine
TEM	Transmission electron microscopy
T_g	Glass transition temperature
TGA	Thermo gravimetric analysis
THF	Tetrahydrofuran
T_m	Melting temperaure
TME	Tumour extracellular environment
TPP	Tumour penetrating peptide
XPS	X-ray photoelectron spectroscopy
Z-average	Average particle size measured by DLS

Chapter 1 Introduction

The first Chapter briefly introduces the current status of drug delivery systems (DDSs). Then, the biological barriers to drug delivery at different levels are analysed and discussed. Stimuli-responsive systems have been developed to overcome these barriers, and the recent progress is reviewed with particular focus on pH- and redox-responsive systems, which are most commonly used in drug delivery. After explaining the stimuli, the author introduces different amino acid-based polymeric drug carriers, from both structure and application points of view. Cell penetrating peptide (CPP) and CPP-mimicking polymers are of particular interests due to their great potential for addressing biological barriers. Finally, the project objectives and thesis outline are included, to provide a general idea of the research in this thesis.

1.1 Drug delivery systems

1.1.1 Overview

Drug delivery is an engineered method of administrating pharmaceuticals to achieve therapeutic effects (Tiwari et al. 2012). To maximise the pharmaceutical's efficacy, it is critical to design a DDS with suitable release behaviour. By precisely targeting drugs to the diseased location, the drug dose could be reduced, and toxic side effects minimised. By controlling the release rate, the effective local drug concentration could be maintained, thus leading to a satisfactory therapeutic outcome.

Traditionally, the control over release location and release rate was achieved mainly by delivering drugs via different routes, such as oral, intravenous, subcutaneous, nasal, transdermal and transmucosal (Orive et al. 2003). Different routes have significant differences in release location and

release kinetics. For example, the onset of drug action is much slower in oral administration compared with intravenous injection. Since the swallowed drugs have to be released and absorbed in the gastrointestinal tract, which usually takes up to hours, oral delivery is thus not suitable for emergency situations. In contrast, by intravenous injection, drugs are directly released in veins and distributed to various organs rapidly.

In spite of the significant differences between different delivery routes, it is still impossible to control the release location and rate precisely just by choosing suitable delivery routes. Therefore, more attention has been paid to the development of drug formulations, i.e. by adding excipients and additives to further control the release. These additives are considered as inert components but may improve drug stability in unfavourable conditions. Cyclodextrin, for example, is one of the most widely used additives, which retains hydrophobic drugs in its core and releases them in a sustainable manner (Brewster & Loftsson 2007).

Due to the development of nanotechnology in recent decades, more ‘smart’ drug formations have been proposed for targeted delivery. A well-known example using a passive targeting strategy is Doxil®/Caelyx®, which is a liposomal formulation of an anti-cancer drug doxorubicin. By encapsulation of doxorubicin in PEGylated lipid vesicles, the drugs were better protected from immune clearance (Cagel et al. 2017). As a result, the circulation half-life of doxorubicin increased by 100 times compared with free doxorubicin. An increased amount of drug was thus accumulated at the tumour site, due to the passive-targeting enhanced permeability and retention (EPR) effect (O’Brien et al. 2004).

Further modification of the drug carrier even leads to active targeting effects. Unlike passive targeting formulations, which only rely on the

physiochemical properties (size, shape, charge, rigidity, etc.) of the carriers, active-targeting formulations incorporate affinity ligands which bind specifically to diseased tissues or cells. MM-302, for instance, is a HER2 (Human epidermal growth factor receptor 2)-targeting liposomal doxorubicin, specifically designed for HER2-positive breast cancer patients (Miller et al. 2016). Pre-clinical data suggested that MM-302 had better HER2-overexpressed-cell internalisation profile and significantly lower toxicity towards cardiomyocytes than PEGylated liposomal formulations in animal models (Espelin et al. 2016). Phase I clinical trials further proved that the combination of MM-302 and trastuzumab (Herceptin®, a monoclonal antibody against HER2 receptors) had promising efficacy with less cardiac adverse events (Espelin et al. 2016).

1.1.2 Biological barriers

No matter what DDS is used, drugs have to bypass multiple biological barriers before reaching the final target sites. These biological barriers are natural defensive systems developed during evolution to protect human being from foreign hazardous materials. Due to their protective nature, they also become major obstacles for drug delivery. Especially for those macromolecular drugs such as proteins or DNA, the delivery efficiency is usually insignificant (Mitragotri et al. 2014). On one hand, their relatively large size makes them impermeable to most bio-membranes; on the other hand, their exquisite structure is susceptible to degradation by the biological environment.

According to their scales, biological barriers fall into three categories: macroscopic, microscopic and cellular barriers (Zhang et al. 2017). Macroscopic barriers refer to those organs that have potential degradation or clearance effects towards biomacromolecular drugs. Microscopic barriers mainly refer to the epithelium, which is a specific type of tissue composed of

densely packed cells with specific junctions between each other. Epithelial layers cover the surfaces of blood vessels, cavities and organs, thus protecting the tissues that lie beneath from external hazards. Cellular barriers include the lipid bilayer cell membrane and lysosomal degradation. These final barriers prevent biomacromolecules from reaching their subcellular nanoscopic targets.

Different drug administration routes lead to the exposure to different barriers. For example, the main barrier to transdermal delivery is the 10-20 μm stratum corneum at the microscopic level (Bouwstra et al. 2003). To permeate through, the drug carriers must translocate through the stratum corneum lipids and densely packed stratum matrix cells, before diffusion into the epidermis (Proksch et al. 2008).

For intravenous delivery of tumour-targeting drugs, the barriers are more complicated (Figure 1.1). After administration, the macroscopic barrier, namely the mononuclear phagocyte system, quickly recognises and transports them to liver and spleen for clearance. The microscopic obstacles are related to the specific abnormal tumour extracellular environment (TME). The disorganised vascular structure and high interstitial pressure make it difficult for drugs to penetrate and distribute in the tumour. Cellular barriers pose a final challenge for delivery. Considering the fact that the cell membrane is impermeable to biomacromolecules, most nano-sized materials rely on endocytosis pathways to get internalised (Whitehead et al. 2009). However, the subsequent acidification during endosome maturation and lysosomal degradation is vital to fragile biomacromolecules (Shete et al. 2014). Without endosomal escape, it is almost impossible to have a satisfied potency.

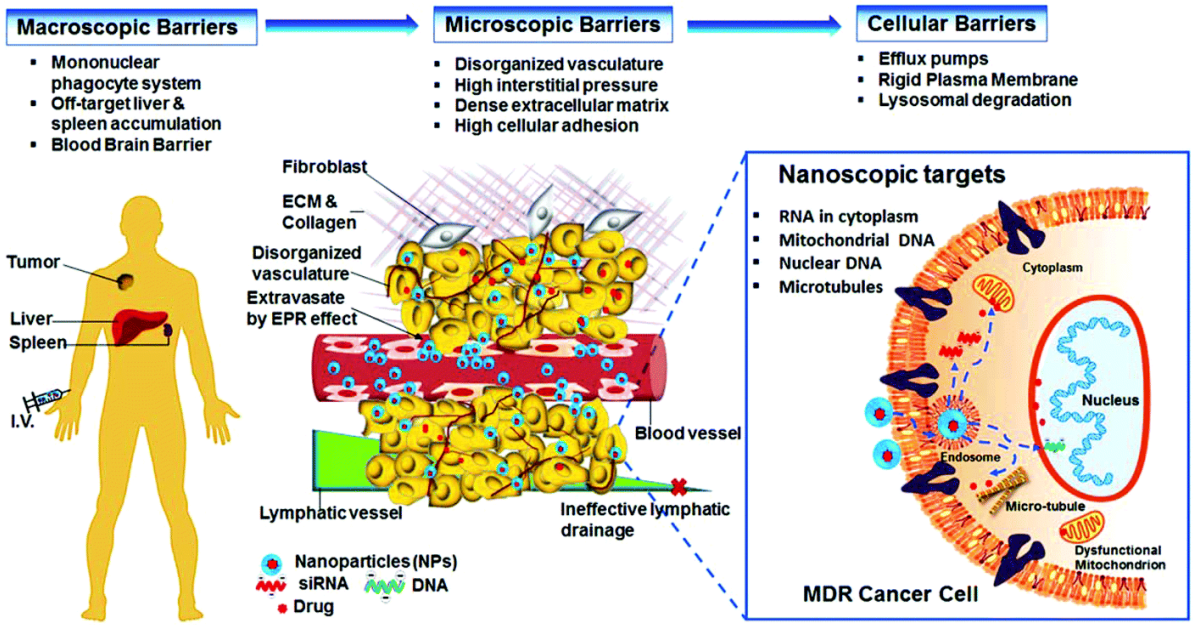

Figure 1.1 Multiple biological barriers to intravenous delivery of tumour-targeting drugs. Reprinted from literature (Zhang et al. 2017)**, copyright 2017, with permission from The Royal Society of Chemistry.**

Another major drug administration route is oral. Unlike intravenous delivery that exposes drugs directly to the macrophages in the blood, oral administration aims to deliver drugs through the digestive system. This poses more obstacles before adsorption (Figure 1.2). Macroscopic barriers in this route include the harsh acidic gastric environment and highly enzymatic intestinal environment which may degrade macromolecular protein-based drugs completely (Choonara et al. 2014). Microscopic barriers refer to the epithelium along gastrointestinal (GI) tract, especially intestinal epithelium which exhibits a large surface area. Despite the high permeability to small molecules and electrolyte, the uptake of biomacromolecules is prohibited due to tight junctions which restrict the transport of payloads larger than 600 Da (Ensign et al. 2012). Finally, the cellular barriers in oral delivery are almost the same as that in other administrative routes. These final barriers also limit the drug efficacy.

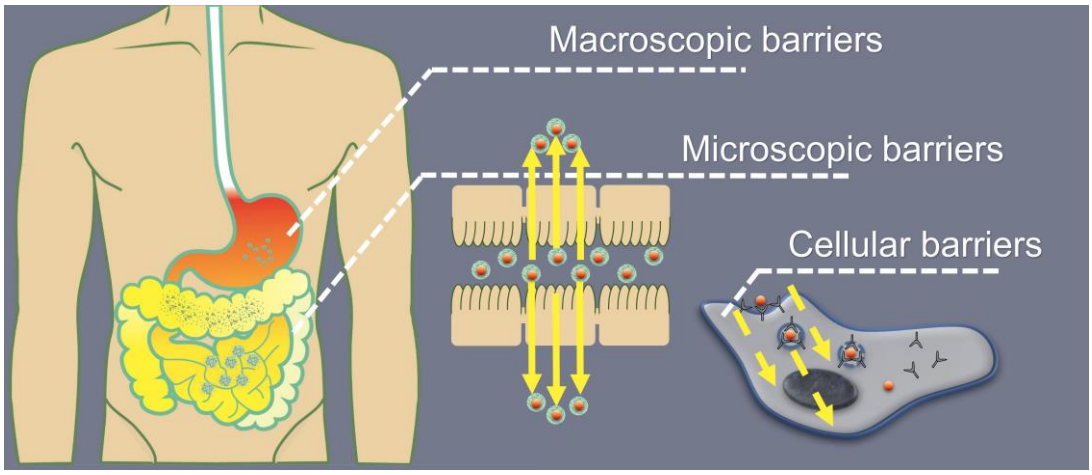

Figure 1.2 Biological barriers at different scales in oral drug delivery. Adapted from literature (Wang et al. 2016b)**, copyright 2016, with permission from Wiley.**

1.1.3 Current challenges and opportunities

Due to the above mentioned biological barriers at multiple levels, the drug delivery efficacy is significantly limited. Especially for those macromolecular drugs such as DNA, RNA and proteins, the *in vivo* obstacles including degradation, quick clearance and the lack of permeability pose great challenges for delivery. Although a large number of papers about innovative design and versatile functionalities of the carriers have been published, not many have discussed the subsequent administration routes and related biological barriers. The ignorance of *in vivo* barriers significantly limits the clinical potential. Therefore, the formidable challenge for drug developers is how to overcome these multiple biological barriers by rational design of the carriers.

To address this challenge, one of the foremost tasks is to better understand how drug carriers interact with biological barriers. Though there has been rapid progress in recent two decades, the current understanding of the interaction between nano-sized materials and biological systems is still in a simplified version compared with what is happening in reality. Due to this

incomplete understanding, sometimes there are contradictory opinions on drug carrier development. For example, multivalency was considered to be a beneficial factor which facilitates the interaction between carriers and cell receptors (Gillies & Fréchet 2005). However, recent evidence suggested that a high density of ligands might lead to adverse effects, such as cytotoxicity and higher haemolytic effects (Jain et al. 2010; Mishra et al. 2010). Furthermore, it was reported that the higher density could even hinder the recognition of receptors due to steric hindrance between densely packed ligands (Kesharwani et al. 2014). Without comprehensive understanding of the interactions between drug carriers and the carriers, it is impossible to design the carriers rationally.

1.2 Stimuli-responsive systems for overcoming biological barriers

Based on the current understanding of biological systems, a variety of stimuli-responsive systems have been proposed to overcome biological barriers. The basic design is to utilise the physiochemical differences naturally existing in biological environment as triggers for controlled release of drugs. Up to date, drug delivery systems in response to numerous stimuli have been reported, among which pH and redox stimuli are extensively investigated. Since pH and redox variations in biological systems have been systematically studied and validated, this section focuses on the recent development of DDSs related to these stimuli.

1.2.1 pH-Responsive systems

pH is one of the most important physiochemical parameters of a biological environment. It varies significantly in different biofluids. For instance, the standard pH of blood is slightly alkaline (between 7.35 to 7.45), while the pH of gastric juice is very acidic (between 1.5 to 3.5 depending on fasted or

fed). The blood pH is buffered by carbonic acid-bicarbonate pairs, while gastric acidic pH is maintained by proton pump H^+/K^+ ATPase on stomach parietal cells (Aburub et al. 2008).

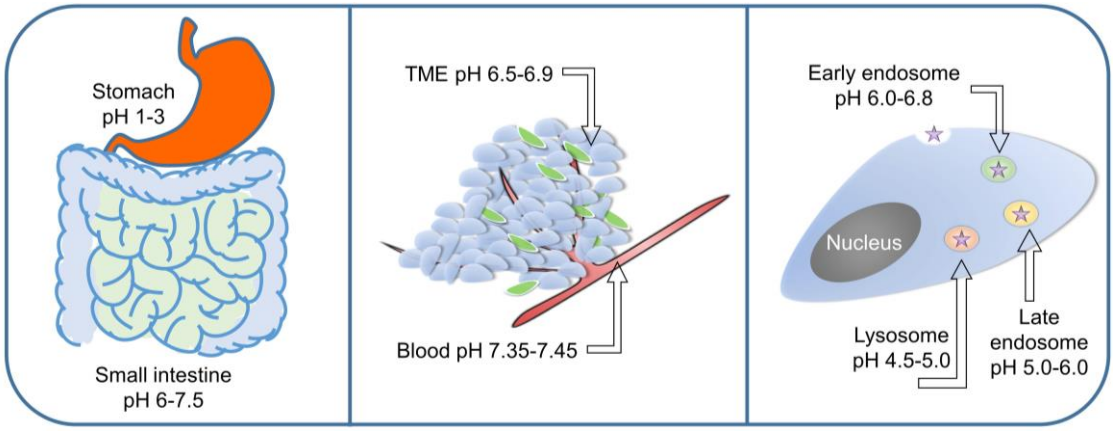

Figure 1.3 Design of pH-responsive drug delivery systems. Left, gastrointestinal (GI) systems, targeting at biological barriers at macroscopic level; middle, tumour microenvironmental (TME) systems, targeting at barriers at microscopic level; right, intracellular endosomal systems, targeting at barriers at cellular level. Adapted from literature (Gao et al. 2010)**.**

Due to physiological pH differences, controlled-release systems that sense and respond to pH triggers are of special interest. According to their designed purposes, these pH-responsive systems could be largely attributed to three categories, namely gastrointestinal (GI) systems, tumour microenvironmental (TME) systems and intracellular endosomal systems (Figure 1.3) (Gao et al. 2010). Carriers in these three systems should respond to their corresponding pH ranges. For GI systems, the pH increases from around 1.5-3.5 in stomach to around 7.5 in intestine. The corresponding drug carriers are designed to resist the strong gastric acid while generally release payloads in neutral environment. The pH of TME, however, is only slightly acidic (pH 6.5-6.9) due to the accumulation of lactic acid under hypoxia. The corresponding pH-triggered vehicles are thus formulated to be sensitive in this pH range but stable at standard blood pH. Similarly, intracellular endosomal

systems work in the slightly acidic pH range between 4.5 and 6.8, which represents the gradual acidification during endosome maturation.

pH-responsive polymers for gastrointestinal (GI) system delivery

The pH-responsive GI system drug carriers are mostly designed for oral delivery, to treat gastrointestinal diseases locally, or systematic diseases remotely. Some examples of pH-responsive polymers used for oral drug formulations are listed in Table 1-1 (Niazi 2009). These polymers have been extensively formulated as enteric coatings for capsules or tablets. On the one hand, the coating polymers protect drug contents from dissolution in the stomach, thus reducing related side effects such as indigestion, heartburn and stomach pain. These side effects were widely reported for non-steroidal anti-inflammatory drugs like ibuprofen. On the other hand, the pH-responsive coating could be used to deliver anti-inflammatory drugs to intestines for the local treatment of inflammatory bowel diseases, constipation and metabolic disorders.

Cellulose derivatives such as cellulose acetate phthalate (CAP) and hydroxypropyl methylcellulose phthalate (HPMCP) have been used as enteric polymers for more than 50 years (Pinto 2010). These polymers could be easily prepared by chemical modification of natural polysaccharides, thus favoured by pharmaceutical scientists. The modified CAP or HPMCP contain pH-sensitive phthalate groups with a pKa around 5.5. The dissolution pH of final polymers could be adjusted by simply varying the modification degrees. Generally, CAP or HPMCP are formulated along with other enteric polymers for sustained intestinal release (Kelley et al. 2012; Niazi 2009).

Table 1-1 List of common pH-responsive polymers developed for oral drug formulations. Summarised from (Niazi 2009)**.**

Chemical /commercial name	Dissolution pH	Representative payloads
Cellulose acetate phthalate (CAP, Aquateric®)	6.2	Diclofenac, Ibuprofen
Hydroxypropyl methylcellulose phthalate (HPMCP)	4.5-5.5	Diltiazem, Rabeprazole, Lovastatin, Mycophenolic acid
Poly(methacrylic acid-co-methyl methacrylate) (Eudragit®)	5.5-7.0	Mesalazine (5-ASA), Sulfasalazine, Budesonide
Poly(vinyl acetate phthalate) (PVAP, Coateric®)	5.0	Aspirin, Erythromycin

Eudragit® and PVAP are polyvinyl enteric polymers synthesised by radical polymerisation of pH-sensitive vinyl polymers. Regarded as inert excipients, these pH-sensitive polyvinyls are soluble in bio-fluids but not degradable. Due to the synthetic nature, the structures and physiochemical behaviours of these polyvinyls are tunable, especially the Eudragit® series (Table 1-2) (Thakral et al. 2013). Eudragit E series are cationic with tertiary amine groups. Accordingly, they are used for drug release in gastric environment due to their higher solubility in acidic environments. On the contrary, Eudragit L and S series are anionic, which means they are solubilised in slightly acidic or neutral fluids. These properties make them more suitable for intestinal release. Currently, there are several Eudragit® coated drugs on the market, namely Asacol, Entocort, Colo-pleon, *etc*. More formulations are in clinical trials. (Patra et al. 2017)

Table 1-2 pH-responsive Eudragit® polymers and their properties. Summarised from (Thakral et al. 2013)**.**

Name	Chemical composition	Solubility	Applications
Eudragit E	Poly(butyl methacrylate, (2-dimethyl aminoethyl) methacrylate, methyl methacrylate) 1:2:1	Soluble in gastric fluid up to pH 5	Film coating
Eudragit L	Poly(methacrylic acid, methyl methacrylate) 1:1	Soluble in intestinal fluid from pH 6	Enteric coating
Eudragit S	Poly(methacrylic acid, methyl methacrylate) 1:2	Soluble in intestinal fluid from pH 7	Enteric coating

Though some pH-responsive polymers have been approved as enteric coatings to control small-molecular drug dissolution, not many succeeded in oral delivery of macromolecular drugs larger than 1000 Da. One reason is the lack of further delivery carriers which transfer macromolecular drugs through the epithelium, as discussed in section 1.1.2. The other reason is the lack of protection against intestinal enzymatic degradation.

pH-responsive polymers for tumour microenvironmental (TME) system delivery

Compared with more than 50 years of practice on pH-responsive polymeric carriers for GI system delivery, the study of pH-responsive carriers for TME system delivery has been thriving in the past 10 years. Currently, chemotherapeutic drugs are predominantly administered systematically via intravenous injection, due to the metastatic nature of the cancer cells. In this case, the pH-responsive drug delivery systems for TME are mostly designed and formulated as nanocarriers.

According to ^{31}P-nuclear magnetic resonance spectroscopy results, the average extracellular environment pH (pH_e) of solid tumours (6.84) is lower than the average pH_e of normal tissues (7.33) (Tian & Bae 2012). This is due to the hypoxia and subsequent accumulation of acidic metabolites (Neri & Supuran 2011). However, tumours are heterogeneous, which means the pH_e slightly varies from 6.5 to 7.2, depending on the tumour types and phases.

Though TME is more acidic than normal physiological environment, the pH difference is not that significant, compared with the pH variation in the GI tract. This requires the pH-responsive polymers for TME system delivery to be able to change their physiochemical properties within this narrow pH range. Currently, there are two main strategies to design these polymers. One is to polymerise monomers with a pKa (logarithmic acid disassociation constant) in a range between 6.5 and 7.2. The pH decrease at TME triggers the protonation/deprotonation of the polymers, leading to swelling/collapse of the nanocarriers and the release of payloads. The other method is to incorporate susceptible chemical bonds which cleave at tumour pH_e. The cleavage could also trigger the collapse of the nanocarriers to release drugs or exposure of some ligands which may further enhance the delivery.

As shown in Figure 1.4, there are mainly two types of the polymers: polyanions and polycations with pKa of approximately 6.8. The polyanions, which bear carboxylic acids groups or sulphonamide groups, are hydrophilic and negatively charged at physiological pH. When the pH drops to tumour pH_e, they become protonated and more hydrophobic. The polycations, however, contain secondary or tertiary amine groups, which are not charged at physiological pH, so become protonated and cationic at tumour pH_e.

Hoffman and Stayton *et al.* studied systematically poly(acrylic acid) and their analogue polyanions (El-Sayed et al. 2005), including poly(methacrylic

acid) (PMAA), poly(ethylacrylic acid) (PEAA), poly(propylacrylic acid) (PPAA), poly(butylacrylic acid) (PBAA) and *etc.* It was found that when increasing the alkyl chain length of the acrylic acid monomer, the pKa of polymer increased as well, from 4.8 for PAA, 5.5 for PMAA, 6.3 for PEAA, 6.7 for PPAA, to 7.4 for PBAA (Pack et al. 2005). Besides the homopolymers listed above, different combinations of these acrylic acid monomers led to copolymers with tunable pKa (Stayton et al. 2010). These polymers were usually formulated along with other materials such as liposomes, inorganic nanoparticles, as the pH-sensitive coatings.

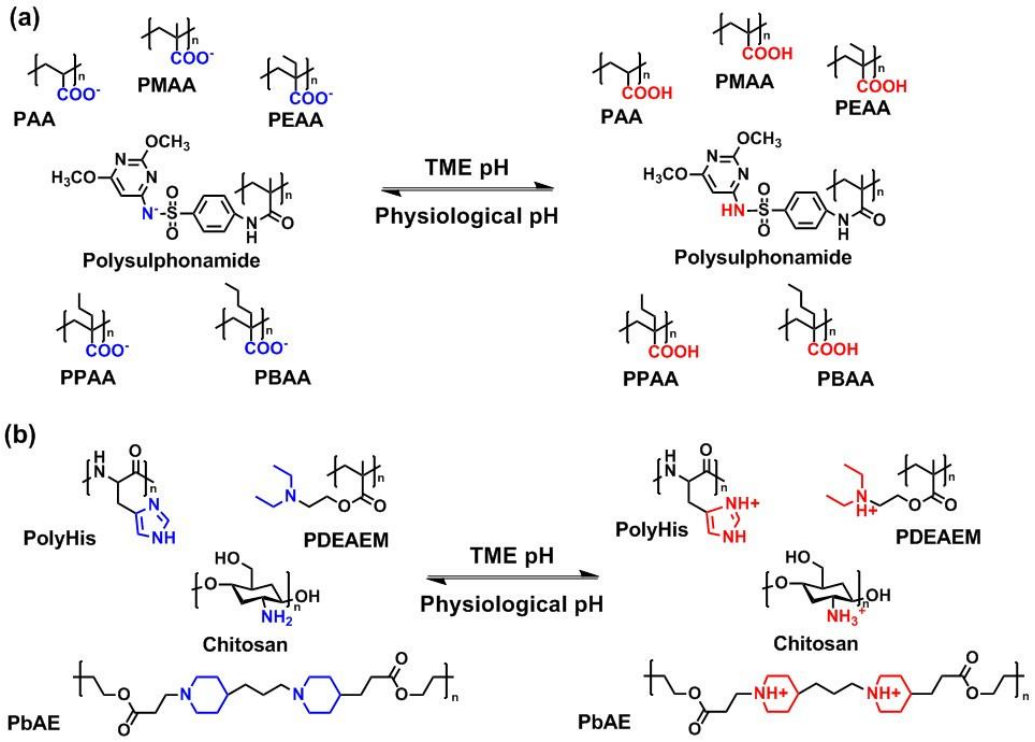

Figure 1.4 Common pH-responsive polymers for TME system delivery. (a) polyanions; (b) polycations.

Besides poly(acrylic acid) and their analogues, polymers with sulphonamide groups are also regarded as promising anionic carriers (Tian & Bae 2012). Compared with carboxylic acid polymers, polysulphonamides are more sensitive to a narrower pH range (Liu et al. 2014). In the previous report,

oligo sulphonamides were conjugated with PEG and shielded cationic ligands (trans-activating transcriptional activator, Tat). Additionally, sulphonamide itself has been used as an antibacterial drug, and more evidence showed that it could inhibit tumour-associated proteins (Monti et al. 2013). Thus, polysulphonamides may enhance the anti-cancer drug efficacy as both carriers and therapeutics.

Polycations, on the other hand, are also widely used. Examples of the cationic polymeric carriers include chitosan (pKa~6.5 (Mi et al. 2008)), poly(histidine) (PolyHis) (pKa~7.0 (Liu et al. 2011)), poly(β-amino ester) (PbAE) (pKa~6.4, (Min et al. 2010)) and poly(N,N'-dimethylaminoethyl methacrylate) (PDEAEM) (pKa~6.6 (Schmalz et al. 2010)). When conjugated with hydrophilic segments (such as PEG), these polymers could form micelles at physiological pH. When the pH decreases at TME, the polymer undergoes a hydrophobic-hydrophilic phase transition. Subsequently, the micelle becomes destabilised and drugs encapsulated could be released.

Another trend in TME targeting delivery is to develop acid-liable polymers (Kanamala et al. 2016). The most common acid-liable chemical bonds are listed in Figure 1.5. These acid-liable bonds are often used to link polymer and drugs, to generate polymer-drug conjugates. In the TME environment, the conjugate can be cleaved and drugs are released. Besides, these bonds are also widely used for PEG conjugation. Well-known for its stealth effects, PEG is considered as an essential for avoiding rapid renal clearance and extending circulation lifetimes. When exposed to the acidic TME environment, PEG conjugated via acid-liable bonds can be cleaved and expose the internal drugs/ligands for better targeting.

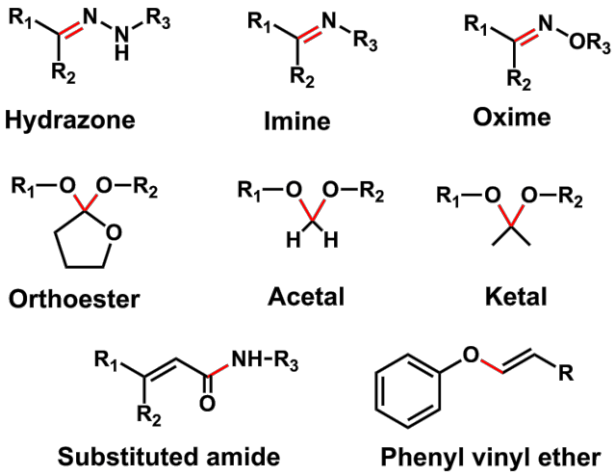

Figure 1.5 Common acid-liable bonds used in pH-responsive polymer development.

pH-responsive polymers for intracellular delivery

Like the TME delivery system, the pH-responsive intracellular delivery system requires polymers to change physiochemical properties within the acidic endosomal/lysosomal pH range (6.0-6.8 in early endosome, 5.0-6.0 in late endosome and 4.5-5.0 in lysosome) (Mukherjee et al. 1997). This range is slightly wider than the TME range. Therefore, in theory, the polymers for TME delivery are also applicable for intracellular delivery.

However, in addition to the pH-responsiveness in acidic endosomal/lysosomal environment, qualified polymers have to be able to facilitate endosomal escape. As shown in Figure 1.6, following uptake by endocytosis, the fate of the nanocarrier and encapsulated payload can differ according to its attempted 'escape strategy'. For example, the nanocarrier can be trapped in the endosome and subsequently degraded in the lysosome or can undergo exocytosis. Common endosomal escape strategies include endosome rupture, membrane fusion and membrane pore formation.

Endosome rupture is caused by a 'proton-sponge' mechanism mostly attributed to cationic carriers such as polyethylenimine (PEI) and polyamidoamine (PAMAM). As shown in Figure 1.6, during the acidification in

endosomes, cationic polymers such as PEI get protonated and absorb a large number of protons pumped into endosomes. As more protons pumped in by V-ATPase on the membrane, more anions such as chloride as well as water also get retained in the endosomes. The endosomes keep swelling and finally burst to release all contents, which may trigger cellular apoptosis (Martens et al. 2014).

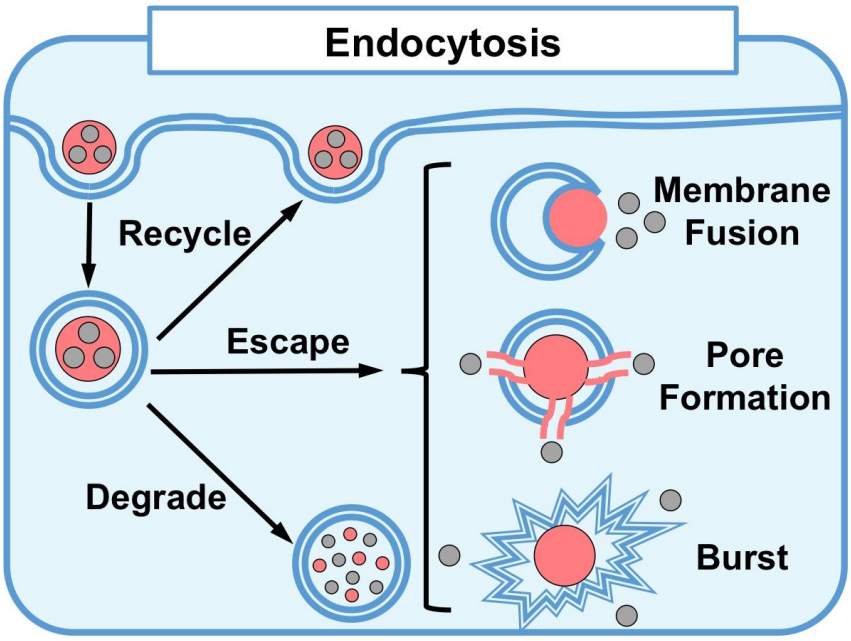

Figure 1.6 Schematic showing of endocytosis and endosomal escape strategies.

Membrane fusion and pore-formation are considered as less cytotoxic compared with endosome rupture (Kauffman et al. 2015). By temporarily or permanently changing the membrane permeability, payloads could be released from endosomes without significant leakage of endosomal contents. Many bacteria and viruses use this strategy to escape from endosomes and deliver their genes into cytoplasm. For example, haemagglutinin (HA) from influenza virus is a pH-responsive fusogenic protein. During acidification in the endosome, HA undergoes conformational changes from random coil to α-helix (Bolhassani 2011). This destabilises the endosomal membrane and releases

viral genes into the cytoplasm. There are some other synthetic peptides and peptide-mimicking polymers (such as GALA, p28, poly (arginine)), which facilitate endosomal escape by membrane fusion or pore-formation (Li et al. 2004; Tan et al. 2017). More details about these peptides and polymers are discussed in section 1.4.

Other pH-responsive DDSs

Besides the three major pH-responsive DDS categories described above, there are some other examples of temporary local pH decrease in diseased tissues. For instance, bacterial infections generally reduce local pH due to anaerobic fermentation and subsequent inflammation (Mura et al. 2013). The acidity could be utilised as a target for antibiotic delivery (Alvarez-Lorenzo et al. 2016). By better manipulating the release of antibiotic via pH-responsive DDSs, the local antibiotic concentration could be boosted, thus achieving better antimicrobial efficacy.

1.2.2 Redox-responsive systems

Redox is another prevalent physiochemical trigger. In a biological environment, there are abundant redox couples such as glutathione (GSH)/ glutathione disulfide (GSSG) and cysteine/cysteine (Banerjee 2012). These thiol/disulfide couples, along with related enzymes, serve as natural ‘buffering’ reagents that regulate the local redox potential. Like the great variation of pH in biofluids, the redox potential differs in different biological environments. For example, the cytoplasm is highly reducing, with GSH/GSSG ratio of around 100 (Saito et al. 2003). However, the lumen of endoplasmic reticulum is oxidising, with approximately 1 to 1 GSH/GSSG ratio (Saito et al. 2003).

A great number of drug delivery systems utilising the redox potential differences in biological environments have been developed (Huo et al. 2014;

Deng et al. 2015). According to their purposes and the biological barriers involved, there are three main categories, as shown in Figure 1.7. Similar to pH-responsive systems, redox-responsive systems also cover several administration routes, and overcome biological barriers at different levels. Carriers in these three systems use different reductive mechanisms for drug release.

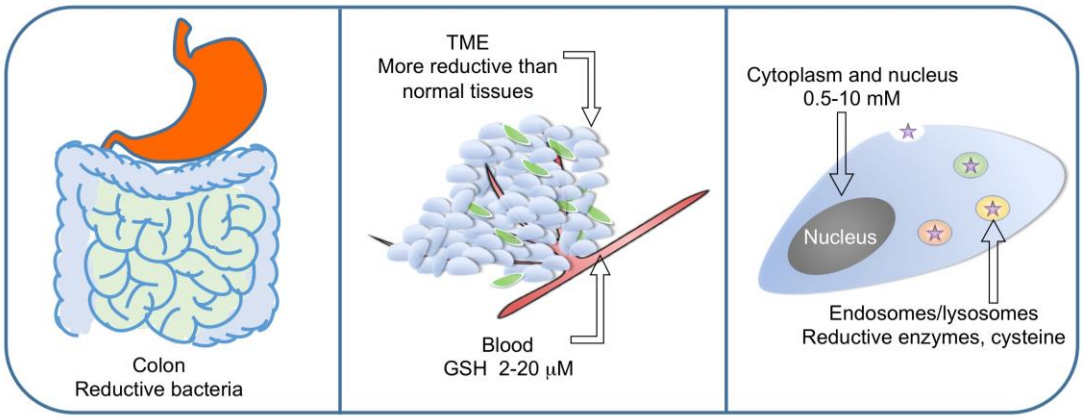

Figure 1.7 Design of redox-responsive drug delivery systems. Left, gastrointestinal (GI) systems, for colon targeting at macroscopic level; middle, tumour microenvironmental (TME) systems, for tumour targeting at microscopic level; right, intracellular delivery systems, for cytoplasmic release at cellular level.

For oral delivery in GI systems, bacteria in the colon are found to have highly reductive proteins which trigger the redox-responsive release. According to the literature, the redox potential in colon is -415 ± 72 mV, which is much lower than the standard reduction potential of disulfide (about -250 mV) (Wilding et al. 1994). Thus, the corresponding disulfide bond-based carriers could be formulated for colon-specific targeting. For instance, Lim *et al.* studied many poly(disulfide)s with linear or branched structures. The results showed that these polymers could be degraded in colon bacteria (*B. fragilis*) containing colonic simulated buffers (Lim et al. 2013; Lau & Lim 2016; Mat Yusuf et al. 2017).

For tumour-related delivery, higher GSH concentration was found in tumour cells (4-7 folds more than normal cells), due to the abnormal metabolism (Opstad et al. 2003; Bobko et al. 2012; Kuppusamy et al. 2002). Also, there are reports about GSH efflux into extracellular matrix, especially after chemotherapy or radiotherapy treatment (Traverso et al. 2013; Khramtsov & Gillies 2014). It could be expected that the tumour related environment is favoured by redox-responsive DDSs (Cho et al. 2012; Deng et al. 2015). However, there is no direct evidence about *in vivo* TME redox potential, possibly due to difficulties in the characterisation. Thus, one should be careful to interpret redox-responsive carriers' potential for tumour-targeting delivery.

At a cellular level, there are some reductive enzymes and cysteine in endosomes/lysosomes which could be used as a redox trigger for endosomal escape. The cytoplasm, however, is more reducing, with a GSH concentration of 0.5-10 mM, more than 100 folds than that in the blood (Cheng et al. 2011). Therefore, disulfide linkage is frequently used for the payloads that require cytoplasmic release. For instance, RNA payloads could be conjugated to endosomal-lytic polymers and released in cytoplasm (Kumar et al. 2012; Dowdy 2017).

Unlike pH-responsive systems which have massive chemical structure varieties, most redox-responsive systems rely on disulfide linkage, derived from natural redox couples. Besides disulfide, diselenide bond, with lower bond energy compared with disulfide, has been recently proposed as another promising redox-responsive linker (Zeng et al. 2013; H. Xu et al. 2013; Ma et al. 2010). The low binding energy of diselenide means more sensitive drug carriers could be formulated with better control over the release profile. Despite this advantage, diselenide-based materials are not widely used, probably due to the difficulty from synthetic perspectives (Huo et al. 2014). Other than

disulfide and diselenide, there are a few reports about other novel linkers such as trimethyl-locked benzoquinone (TMBQ) (Bae et al. 2015; Bae et al. 2014), N-isopropyl, 4-N-amino-2,2,6,6-tetramethylpiperidin-1-oxyl-4-yl (TEMPO) (Bertrand et al. 2016; Fu et al. 2010) and aromatic azo compounds (Roldo et al. 2007; Pinto 2010). These strategies are, however, still in their infancy and need more validation.

Though most redox-responsive polymers just use disulfide bonds as the sensitive linkage, the incorporation of the bonds could be versatile (Huo et al. 2014). As shown in Figure 1.8, polymers could be synthesised as block-copolymers via disulfide linkage. In this case, if the hydrophobicity of block A and B varies, the copolymers self-assembly into micelles in aqueous system (Deng et al. 2015). Once the disulfide bonds in the middle of the blocks are cleaved, the micelles break and the cargos are released. Besides forming linkage for block copolymers, disulfides can be incorporated in the polymer repeating unit, achieved by using disulfide monomers, or polymerising di-thiol monomers. These polymers could be degraded completely by reducing reagents, resulting in fast and thorough release. Disulfide bonds could be conjugated to the polymer pendant groups as well. This strategy is particularly favoured by payload conjugation (Vlieghe et al. 2010). When exposed to redox-triggers, the payloads could be released *in situ*. Finally, disulfide-containing crosslinkers could be used for nanoparticle development. The nanoparticles would become destabilised and disassociated when redox-trigger is presented.

Figure 1.8 Schematic showing of the synthetic methods for incorporating the disulfide linkage.

1.2.3 pH- and redox-dual responsive systems

Due to the coexistence of pH- and redox-triggers in biological environments, as shown in Figure 1.3 and Figure 1.7, the combination of both triggers and the development of dual responsive DDSs have attracted much attention (Cheng et al. 2013). Common approaches include conjugating pH-responsive polymers listed in section 1.2.1 with payloads via disulfide crosslinkers, developing dual-responsive monomers, copolymerisation of pH-responsive monomers with disulfide monomers, and crosslinking pH-responsive micelles with disulfide crosslinkers (Li et al. 2016; McKinlay et al. 2016; Yang et al. 2016; Zhang et al. 2012; Chen et al. 2011; Dai et al. 2011).

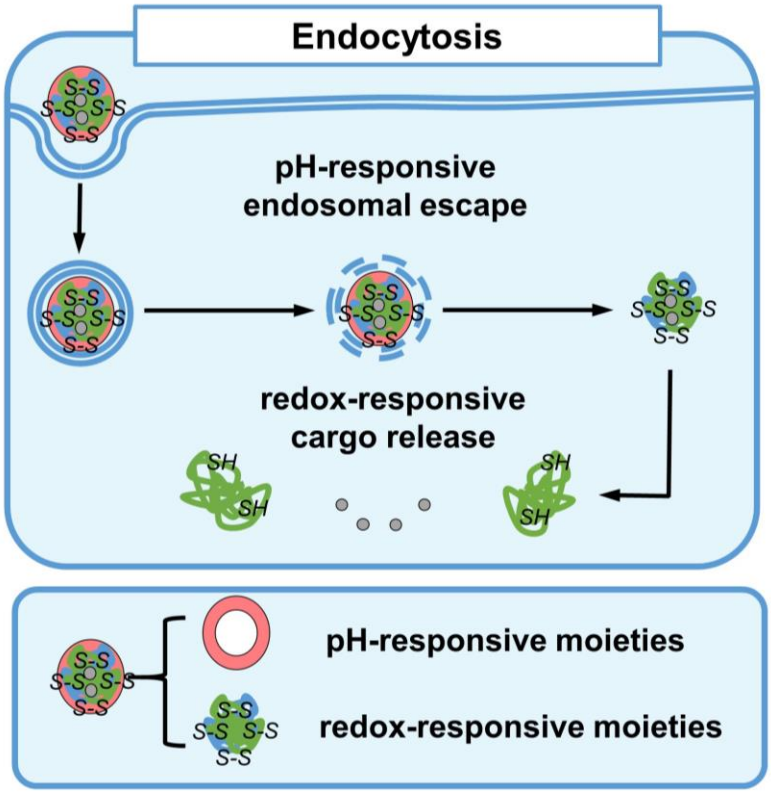

Figure 1.9 Dual-responsive carriers for intracellular delivery.

The majority of current studies particularly focus on the intracellular delivery potential of pH- and redox-responsive DDSs. As shown in Figure 1.9, pH-responsive moieties are used to facilitate the endosomal escape, and the

following redox-responsive moieties are cleaved by GSH in the cytoplasm for the release. Compared with pH-responsive systems, the addition of redox-trigger enables better control over the release, especially in regard to release in the cytosol. Compared with redox-responsive systems, the introduction of pH-responsive endosomal escape polymers improves the availability of macromolecular payloads, and allows intracellular compartment targeting. However, the incorporation of dual-triggers generally increases the complexity of the carriers, which may require more synthetic steps and higher expenses. The possible crosstalk between pH- and redox-responsiveness is another issue that needs more consideration.

1.3 Natural/artificial peptides as drug carriers

Apart from synthetic stimuli-responsive polymers, natural/artificial peptides represent another important class of drug carriers due to their potential for overcoming biological barriers. Defined as shorter amino acid chains (50 or fewer amino acids), peptides are found as either free amino acid segments or fractions of proteins (Daffre et al. 2008). Generally, they are used as bioactive ligands and formulated either as peptide-drug conjugates or as surface ligands along with other materials (e.g. inorganic nanoparticles, liposomes or polymer micelles) (Vlieghe et al. 2010). Most pharmaceutical peptides are naturally existing, such as antimicrobial peptides found in marine fish (Jia et al. 2000). However, with the development of solid phase peptide synthesis (SPPS), more and more artificial peptides have been synthesised (Barany et al. 1987; Merrifield 2006). These synthetic peptides were first used as natural mimics to study the key amino acid residuals in the structure (Schlaad & Antonietti 2003). Later, library synthesis and high-throughput screening made it possible for selecting artificial peptides with better efficacy than their natural counterparts (Mäde et al. 2014).

Commonly used peptides in pharmaceutical context fall into two classes: tumour penetrating peptides (TPPs) and cell penetrating peptides (CPPs). TPPs overcome the microscopic barriers in cancer treatment via tumour-targeting and penetrating capabilities, while CPPs are more suitable for intracellular delivery via their membrane permeability. In this section, the origin, development, mechanism and pharmaceutical applications of TPPs and CPPs are reviewed.

1.3.1 Tumour penetrating peptides

Tumour penetrating peptides (tumour-homing peptides) describe a series of peptides that recognise target receptors in tumours and deliver payloads to these sites (Teesalu et al. 2013). Tumour-specific receptors include integrins, fibrin deposits, overexpressed tumour antigens, epithelium cells, lymphatics and stromal cells within tumours (Feron 2010). The first TPP discovered was LyP-1 (sequence: CGNKRTRGC). LyP-1 was found to accumulate in tumour lymphatics and not in normal lymphatics (Laakkonen et al. 2002). Later, the groundbreaking iRGD (sequence: CRGDKGPDC) was identified, with extensive accumulation in extravascular tumour tissues (Sugahara et al. 2009).

As shown in Figure 1.10, the molecular basis of TPPs' activity was revealed, which is related to the key sequence R/KXXR/K at C-terminal (Teesalu et al. 2009). Instead of direct recognition and binding, these peptides accumulate in tumour via a complex multi-step process. First, they bind to a primary tumour-specific receptor. Then, a protease cleaves the peptide and reveals the C-terminal R/KXXR/K motif, which binds to the second receptor neuropilin-1 (NRP-1) or neuropilin-2 (NRP-2). The binding activates the subsequent endocytotic/exocytotic transport pathway (named CendR pathway). By activating CendR pathway, the anti-cancer drug efficacy was

found to increase significantly. Moreover, the rapid drug distribution throughout the whole tumour could be achieved as well (Ruoslahti 2017).

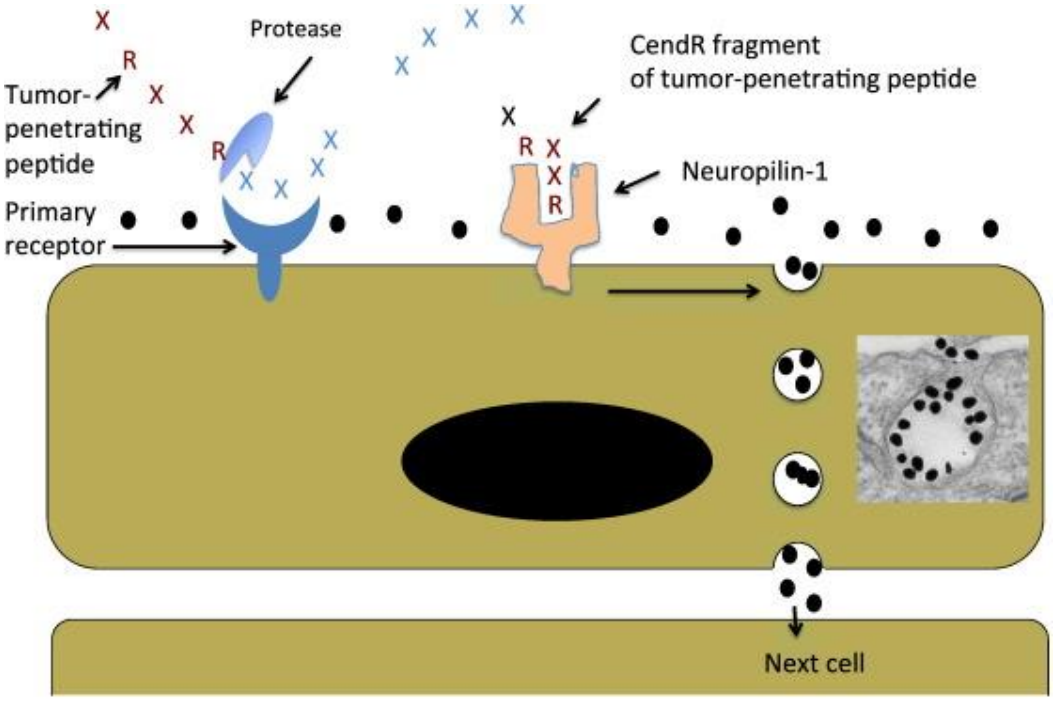

Figure 1.10 Schematic representation of the CendR trans-tissue transport pathway. Drugs are depicted as black dots co-administrated with TPPs. The inset shows an electron microscopic image of a CendR endocytic vesicle that is budding from the cell surface into the cytoplasm and contains CendR peptide-coated gold nanoparticles (dark dots). Reprinted from literature (Ruoslahti 2017)**, copyright 2017, with permission from Elsevier B.V.**

A major advantage of TPP is that it enhances drug delivery not only to covalently conjugated drugs, but also co-administrated drugs that are not attached to the peptide. Due to the relative large size of the endocytic vesicles in the CendR pathway (an average diameter of 200 nm), a large amount of extracellular fluids could be internalised at once (Ruoslahti 2017). Thus, drugs, as well as nanoparticles, could take this opportunity and sneak into cells. Several preclinical studies have shown that the co-administration of iRGD and anti-cancer drugs led to better efficacy (Akashi et al. 2014; Sugahara et al. 2010). The universal enhancement was observed for drugs with various sizes

and formulations, including a small molecular drug doxorubicin, a monoclonal antibody trastuzumab, a liposomal formulated doxorubicin and a nanoparticle formulation nab-paclitaxel (Sugahara et al. 2010). The encouraging results of iRGD made it ready for clinical trials.

1.3.2 Cell penetrating peptides

Cell penetrating peptides describe a series of peptides capable of delivering cargos into the cytoplasm via endocytosis or direct cell membrane penetration. The first CPP reported is Tat from HIV-1 virus (Zorko & Langel 2005). Subsequently, more viral penetrating peptides were revealed, such as PreS2 from Hepatitis-B, HA2 from influenza, VP22 from herpes simplex virus-1, p28 from azurin, etc. Up to date, there are hundreds of CPPs and derivatives reported (Milletti 2012; D. Zhang et al. 2016; Kauffman et al. 2015). A few of these have entered into clinical trials. KAI-9803 is a Tat conjugated protein inhibitor under investigation for the treatment of cardiovascular diseases. PsorBan® is being trialled for its topical delivery of anti- inflammatory drugs.

Though the few first reported CPPs are arginine-rich and cationic, later studies found the sequence of CPPs can be diversified, with positive or negative net charge. Some CPPs are hydrophobic without charge. Cationic CPPs usually have many arginine and lysine residues, while amphiphilic ones bear both hydrophobic and hydrophilic residues. Many amphiphilic CPPs form helical secondary structures, which are believed to play a key role in membrane binding. Hydrophobic CPPs are mostly composed of nonpolar residues. The majority of CPPs are actually amphiphilic, which comprise both cationic and anionic peptides (Milletti 2012).

Due to the great variety in sequence and physiochemical characteristics, the cellular uptake mechanism also varies significantly (Figure 1.11). Some

CPPs penetrate cell membranes in an energy-independent way, causing the accumulation of transient/permanent pores. These pores facilitate the entry of the desired cargo. Others rely on receptor-mediated endocytosis or macropinocytosis, and manage to destabilise endosomal membranes for payload translocation. It is worth noticing that the cytoplasmic internalisation mechanisms are not exclusive to each other. One or multiple strategies could be adopted, depending on the size of the cargo, as well as the local concentration of CPPs. Previous live-cell analysis results showed that Tat-fusion proteins (>50 amino acids) and peptides (<50 amino acids) translocated into cells by distinct modes. Tat-fusion peptides distributed into the cytoplasm directly, whilst most fusion proteins first ended up in cellular vesicles (Tünnemann et al. 2006). Other studies on arginine-rich CPPs suggested that the cellular uptake mechanism varied from endocytosis, to transduction when the concentration increased from 2 μM to 10 μM (Brock 2014).

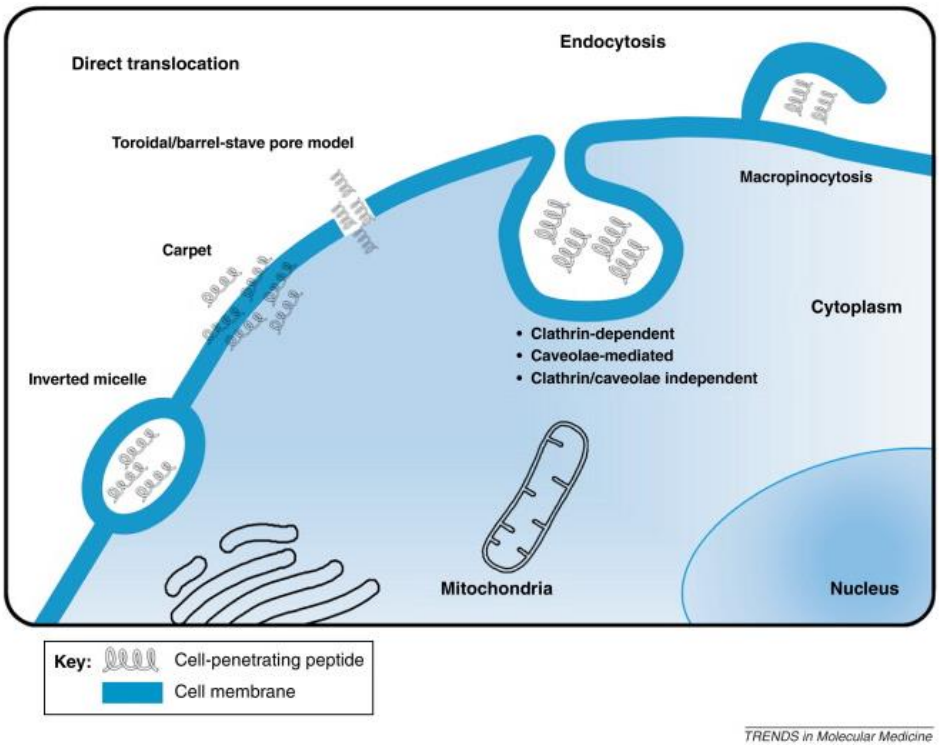

Figure 1.11 CPP internalisation pathways. Reprinted from (Koren & Torchilin 2012)**, copyright 2012, with permission from permission from Elsevier B.V.**

Despite their capability for membrane destabilisation, CPPs are potentially cytotoxic due to non-specific binding to plasma membranes in physiological conditions (Rizzuti et al. 2015). The binding has been reported to result in less organised lipid membranes, and the transient influx of Ca^{2+} into cytoplasm *in vitro* (Melikov et al. 2015; Palm-Apergi et al. 2009). Though there is evidence showing some mammalian cells recovered from the injury and replaced the damaged membrane (Lorents et al. 2012), the potential systematic toxicity *in vivo* remains a big concern for CPP applications. Unfortunately, there is limited *in vivo* safety data available, and controversial opinions existed over this issue. Some claimed that CPPs did not pose systematic damage at the effective dose, even after one-month nasal administration of penetratin-insulin formulation in rats (Feron 2010). Others showed that the arginine-rich CPP conjugated formulation could damage liver and kidney in mice (Deas et al. 2007). Since currently available animal studies use different CPPs, formulations and administration routes, they are not comparable. More systematic studies are needed for the solid understanding of the safety landscape of CPPs.

Because the potential toxicity mainly results from non-specific binding to plasma membranes, it is possible to minimise the binding in physiological conditions by introducing pH-responsive moieties. In a pH-responsive CPP, the membrane-binding affinity is suppressed at physiological pH. However, once acidified in the endosomes, the membrane-lytic potency becomes activated, thus facilitating the cargos to escape from endosomes and enabled the cytoplasmic delivery. Though the endocytic trafficking of CPPs followed by endosomal escape is generally energy-dependent and slower compared with direct membrane translocation, it poses less non-specific cytotoxicity to cells, without sacrifice of CPPs' potency.

As introduced in Section 1.2.1, pH-responsive moieties could be introduced by pH-liable linkages, or pH-responsive segments. Jin *et al*. used the former strategy, by conjugation of succinic acid on Tat lysine residues to shield its positive charge. The pH-sensitive succinyl amides were cleaved at late endosomal pH (5.0) within 2h of incubation, and the released Tat maintained the membrane-lytic activity (Jin et al. 2013). The addition of pH-responsive segments was also achieved by designing chimeric peptides, such as Tat-HA2 (Wadia et al. 2004). HA2 is a pH-responsive CPP derived from influenza, which requires the endosomal acidification for activation. The Tat-HA2 fusion proteins increased the endosomal escape efficiency significantly compared with Tat alone. Moreover, the glutamate residues on HA2 helped to block Tat from binding to negatively charged proteins and membranes (Lee, Erazo-Oliveras, et al. 2010; Lee, Johnson, et al. 2010). Some other papers modified CPPs by introducing pH-responsive histidine residues, by adding them to the N or C terminals or replacing lysine with histidine (Lo & Wang 2008). As mentioned in Section 1.2.1, histidine is well known for its endosomal escaping capacity at acidic pH due to the proton sponge effect. Thus, the membrane-lytic activity histidine-modified CPPs could be adjusted by environmental pH, and the toxicity was significantly lower than original ones under physiological conditions.

Apart from introducing pH-responsive moieties, local administration without systematic exposure is another strategy to maximise the efficacy and avoid side effects. It is indeed the administrative route adopted by the first few CPPs in the clinical trials. However, the results did not seem to be of great significance. KAI-9803, a Tat-conjugated protein kinase C inhibitor, was used for cardiovascular diseases via intracoronary injections. Phase II clinical studies on KAI-9803 was completed in 2011, but the results were not published online. Another formulation was designed for the topical delivery of anti-inflammatory

drug cyclosporine A (commercial name PsorBan®) (Rothbard et al. 2000; Vivès et al. 2008). Unfortunately, the phase IIb clinical study was interrupted due to slow release profile compared with clearance (Guidotti et al. 2017).

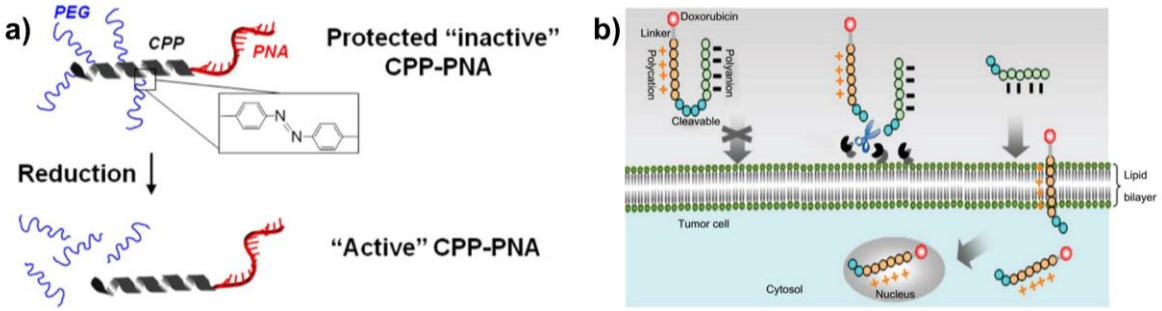

Figure 1.12 (a) Schematic illustration of a redox-responsive colon targeting system utilizing PEGylated CPP. Reprinted from literature (Lee et al. 2014)**, copyright 2014, with permission from ACS Publications. (b) TME enzyme-cleavable drug delivery system. Reprinted from literature** (D. Zhang et al. 2016)**, copyright 2016, with permission from Elsevier B.V.**

Since the local administration results are unfavourable, more attention has been paid to applying CPPs in systematic delivery tailored with targeting groups. Some novel interesting designs utilise specific enzymes in targeting environments to trigger the release. For instance, Lee *et al.* tried to conjugate PEG on a variety of CPPs via azobenzene linkage (Lee et al. 2014) (Figure 1.12a). This system aimed to deliver nucleic acid to colon mucosa using local bacterial azoreductase as a trigger, which could reduce the azobenzene linkage, and the PEG was detached subsequently. This led to the activation of the CPP, which facilitated the subsequent localisation of the PNA in colon mucus cells. Another example was to use the overexpressed enzymes found within the TME, namely matrix metalloproteinase (MMP), to trigger the release. As shown in Figure 1.12b, the positively charged arginine-rich CPP was conjugated with negatively charged oligopeptides via an MMP-substrate domain (PLGLAG). The CPP could be stabilised by polyanions in physiological environment. Thus, non-specific binding could be minimised. When exposed to the TME, the

substrate domain could be cleaved and the CPP released with payloads. The activated CPP then transported payloads into tumour cells (Shi et al. 2012).

1.4 CPP-mimetic polymers as drug carriers

Though CPPs have been proved to be capable of intracellular translocation, the costs of peptide production and purification are generally high (Chen & Harrison 2007; David et al. 2012). Therefore, synthetic polymers which mimic CPP's functions have been developed as cost-effective analogues (Hamid Akash et al. 2015). Most of CPP-mimetic polymers are cationic, like arginine-rich CPPs. A few are anionic, which mimic the glutamate-containing HA2. In this section, the synthesis and applications of CPP-mimetic polymers are reviewed.

1.4.1 Polycations

Inspired by the arginine-rich domain of Tat peptide, most CPP-mimetic polycations incorporate arginine or guanidine groups. A common method is to conjugate guanidine on methacrylate monomers, and copolymerise with other functionalised methacrylate monomers by controlled radical polymerisation (Treat et al. 2012). In this way, block copolymers were generated with micelle-forming potentials. Another popular method is to use ring-opening polymerisation of amino acid N-carboxylanhydrides (NCA) to synthesise polyarginines. Like controlled radical polymerisation, NCA is also a living polymerisation method with controllable molecular weight and narrow polydistribution (Hadjichristidis et al. 2009; Deming 1997; Deming 2000). It was developed specifically for amino acid monomers, which could be degraded *in vivo*. Other guanidine-incorporated polymer backbones include poly(disulfide) (Bang et al. 2013; Gasparini et al. 2014), oligocarbonate (Cooley et al. 2009) or oligophosphoesters (McKinlay et al. 2016). Compared with polyacrylates and

polypeptides, the monomer synthesis is more complicated, which limits their development.

McCormick *et al.* first tried to polymerise a guanidine-containing methacrylate monomer via aqueous reversible addition fragmentation chain transfer (RAFT) polymerisation as shown in Figure 1.13a (Treat et al. 2012). Both homopolymer (M_n=18.1 KDa by GPC) and copolymer with N-(2-hydroxypropyl) methacrylamide (HPMA) (M_n=39.8 KDa by GPC) showed endosomolytic effects. Others have used similar synthetic strategies to load anionic RNA or drugs (Buerkli et al. 2014; Tabujew et al. 2014; Tan et al. 2017; Li et al. 2017).

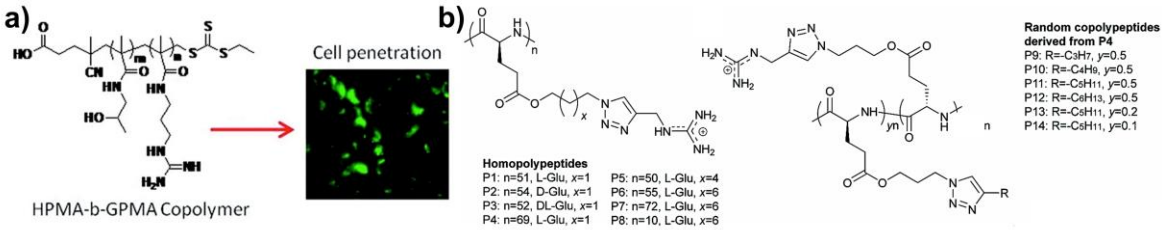

Figure 1.13 (a) Guanidine-containing polyacrylates and copolymers synthesised from RAFT polymerisation. Reprinted from literature (Treat et al. 2012)**, copyright 2012, with permission from ACS Publications. (b) Polyarginine derivatives synthesised by NCA polymerisation. Reprinted from literature** (Song et al. 2017)**, copyright 2017, with permission from The Royal Chemistry Society.**

Though guanidine-containing polyacrylates were prepared readily with controllable molecular weight, the polymers adopted random coil conformation in aqueous environment, thus lacking the functional α-helical structure for membrane permeation (Song et al. 2017). In this case, the membrane translocation resulted from the strong interaction of positively charged guanidine groups with negatively charged lipid membranes (Herce et al. 2014). Therefore, polyarginines with secondary structures were considered to have better membrane permeability.

Cheng *et al.* systematically studied a series of polyarginine derivatives as shown in Figure 1.13b. Their results showed that these helical polyarginine-mimetic polymers had stronger membrane penetration capability than common CPPs such as Tat and Arg9 (Tang et al. 2013). Moreover, introducing 10% hydrophobic alkyl chains led to significant improvement in cell penetration. The best candidate of these series even outperformed the commercially available transfection assay Lipofectamine 2000 in DNA and siRNA (small interfering RNA) delivery (Tang et al. 2013).

Besides linear backbones, dendritic and branched cationic CPP mimics have been developed as well. Though there is no non-linear CPP found in nature, artificially presenting CPPs on dendritic polymers such as poly(amidoamine) was achieved (Kang et al. 2005; Juliano 2006; Carberry et al. 2012; Tarallo et al. 2013). The dendritic structure of non-linear carriers benefits their cargos for longer circulation time due to the decreased elimination by kidneys (Fox et al. 2009). Systemic studies about the generation-dependent cellular uptake suggested that CPP conjugated generation 2 (G2, 18 branches) scaffold was significantly more efficient in cellular delivery than generation1 (G1, 6 branches). Further increases in generation (G3, 54 branches) only led to comparable results, though with more synthetic complexity (Kaufman et al. 2017).

Instead of conjugation CPPs on dendrimers, some reports synthesised branched or dendritic polypeptide CPP mimics via the SPPS method. Geit *et al.* reported a systematic study of 2- and 4-branched polyarginines conjugated with nucleic acids (Saleh et al. 2010). Like their linear counterparts, the total number of arginines was a determinate factor in their cellular delivery efficiency. However, the branched structure only had a slightly positive effect on the cell penetrating capacity. Wender *et al.* studied guanidinium-rich dendritic CPP

mimetics with more branching structures, and found 9- and 12-branched ones exhibited better uptake than 3- and 6-branched ones (Wender et al. 2008). Unfortunately, more branched polymers had higher cytotoxicity compared with their linear counterparts.

1.4.2 Zwitterionic polymers and polyanions

Though CPP-mimetic polycations have been extensively studied, their cytotoxicity remains an unavoidable problem. Like their arginine-rich mimics, the non-specific membrane binding originates from electrostatic interactions. This usually leads to a high cytotoxicity and poor *in vivo* activity (Kauffman et al. 2015). Therefore, zwitterionic and anionic CPP-mimetic polymers have been developed to mimic the amphiphilic CPPs.

A comparative study of cationic and zwitterionic guanidine containing polymers found that the negative counterions reduced the cytotoxicity of carriers, without sacrifice of cellular uptake capacity, shown in Figure 1.14 (Kim et al. 2012). Further studies showed that these zwitterionic polymers conjugated with platinum drugs enhanced the drug delivery efficiency (Abd Karim et al. 2014). A recent paper suggested that instead of using zwitterionic monomer, random distribution of cationic guanidine-monomers and anionic MMA monomers on the polymer chain would lead to similar cellular uptake with negligible cytotoxicity (Khine et al. 2016). However, in the same paper, the authors found that the pure PMMA without guanidine components had very limited cellular uptake.

There are not many anionic amphiphilic CPP mimetics reported up to date. However, some anionic amphiphilic polymers have been reported with pH-responsive membrane permeability (Binder 2008). This characteristic has been observed in amphiphilic CPP HA2 which changes its conformation at

endosomal pH and induces membrane fusion for the release of viral cargos (Lee, Johnson, et al. 2010; Wadia et al. 2004). Therefore, from a functional point of view, these anionic amphiphilic polymers mimic CPPs, though with structural differences.

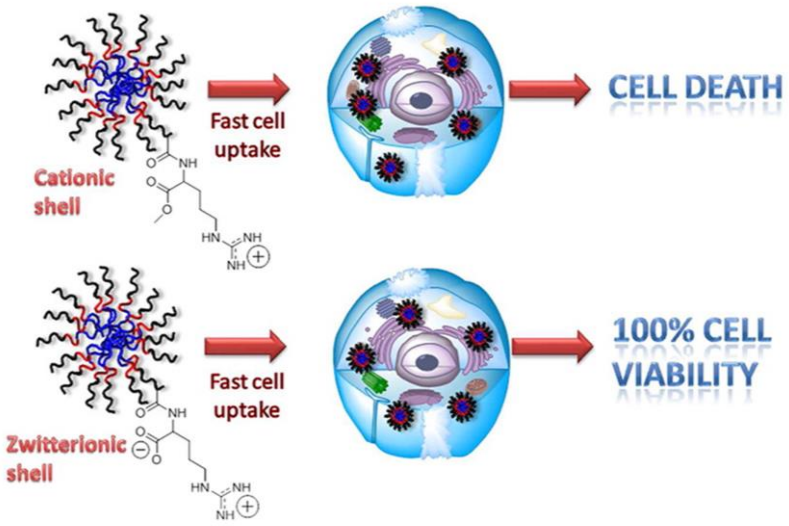

Figure 1.14 Schematic illustration of zwitterionic and cationic micelles and their cytotoxicity. Reprinted from literature (Kim et al. 2012)**, copyright 2012, with permission from ACS Publications.**

Most anionic amphiphilic membrane-lytic polymers developed are shown in Figure 1.15, including PEAA **1** (Lackey et al. 1999), cholesterol-modified poly(acrylic acid) **2** (Lee et al. 2007), poly(styrene-*alt*-methacrylic acid) **3** (Binder 2008), and poly(malic acid) copolymers **4** (Ding et al. 2011). PEAA and derivatives, as discussed in section 1.2.1, represents a series of polymers with acrylic acid monomer-based polymers, which could change their conformation and membrane permeability when pH decreases (El-Sayed et al. 2005). Introducing hydrophobic moieties such as cholesterol (**2**), benzyl rings (**3**), or long alkyl chains (Vial et al. 2007) significantly boosted the membrane binding, due to the increased hydrophobicity (Marie et al. 2014). However, the

enhanced hydrophobicity also increased non-specific binding and irreversible membrane lesion, which lead to higher cytotoxicity (Ding et al. 2011).

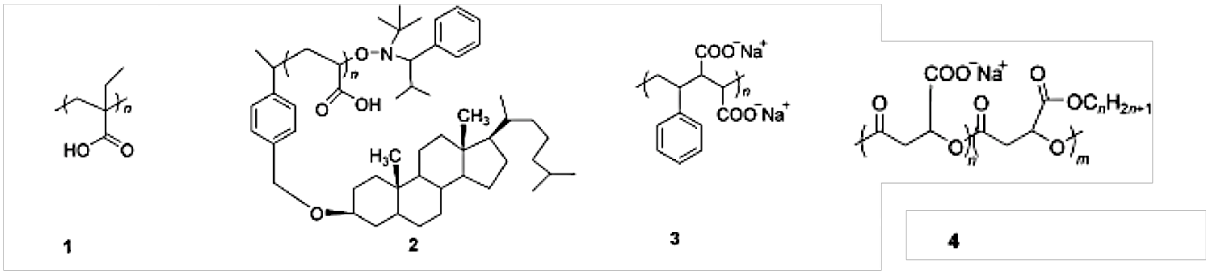

Figure 1.15 Chemical structures of anionic amphiphilic membrane-lytic polymers. Adapted from literature (Binder 2008)**, copyright 2008, with permission from Wiley.**

Though poly(acrylic acid) derivatives have been developed for more than 20 years, the alkyl backbone and non-biodegradability remain an obstacle for their bio-related applications. Poly(malic acid) (PMLA) and its derivatives (**4**), however, are naturally occurring and biodegradable. Recently, there are some reports about the functionalisation and applications for anti-cancer drug delivery (Ding, Helguera, et al. 2013; Ding, Portilla-Arias, et al. 2013; Huang et al. 2012; Ding et al. 2011). Moreover, the polymer-drug conjugate was reported to overcome the blood-brain barrier for brain tumour inhibition (Ding et al. 2010). The conjugation of oligopeptides, such as trileucine, trilysine or tritryptophan, could adjust the membrane-permeation affinity, critical pH for permeation, and even the permeation mechanism (Ding et al. 2017).

PMLA could be obtained from microbial fermentation or chemical synthesis. Natural PMLA was first isolated from the culture broth of *P. polycephalum* (Fischer et al. 1989). Although the subsequent optimisation of the fermentation process made it possible to achieve a sustained production, the crude PMLA synthesised by microbial fermentation needs to be carefully purified and processed. Moreover, it is impossible to control the molecular weight, polydispersity and the chirality of these products. As a result, the

mixture usually contains three isomers (α-type, β-type, and α,β-mixed type) (Lee & Holler 2000). The inhomogeneity and batch-to-batch variation of the mixture are not favourable for pharmaceutical applications. Chemically synthesised PMLA via ring-opening polymerisation or polycondensation, on the other hand, provides more predictable structures. Unfortunately, the reaction conditions of both methods were rather demanding, as they required either vacuum, high temperatures, or metal catalysts (Osanai & Nakamura 2000; He et al. 2006; Wang et al. 2010; J. Wang et al. 2014).

1.5 PLP and its derivatives

Another bio-derived anionic amphiphilic polymer, which is based on L-lysine isophthalamide, has been developed for almost 20 years (Figure 1.16) (Eccleston et al. 1999; Eccleston et al. 2000). The L-lysine derivative polymer, poly (L-lysine isophthalamide) (PLP), has a relatively hydrophobic backbone and hydrophilic carboxyl side groups. The amphiphilicity makes it possible to self-assemble in aqueous systems. Furthermore, it is pH-sensitive due to the presence of a large number of carboxyl pendent groups. When the pH is low, the carboxyl groups are protonated, which leads to agglomeration of PLP. As the pH increases, the deprotonation of carboxyl groups enables PLP to have a large density of negatively charges on polymer chains. The repulsion of negative charged groups enables the polymers to undergo conformational changes from agglomeration to free random coils. As a result, PLP is able to redissolve in the solution.

Compared with other pH-responsive anionic amphiphilic polymers, PLP has several advantages. First, it can be synthesised by a one-pot polycondensation of two commercially available monomers (L-lysine methyl ester, and isophthaloyl chloride) at room temperature without catalysts, which is simple, economical and suitable for large-scale production. Second, the two

monomers were carefully chosen, with considerations in respect of safety and biocompatibility. As an amino acid derivative, L-lysine methyl ester is considered as non-hazardous according to European Regulation (EC) No.1272/2008 (Sigma-Aldrich 2012). Phthalate-based polymers, such as cellulose acetate phthalate, hydroxypropyl methylcellulose phthalate and poly(vinyl acetate phthalate) have been approved by FDA as inactive excipients for decades (FDA/Center for Drug Evaluation and Research 2017). Preliminary *in vitro* cytotoxicity study showed that PLP and its derivative polymers were biocompatible with the IC_{50} (concentrations inhibiting 50% of cell growth relative to non-treated control cells) higher than 2000 μg mL^{-1} (Chen et al. 2005). Moreover, the numerous carboxyl side groups of PLP could be functionalised by coupling with different compounds, such as hydrophobic amino acids to adjust its pH-responsiveness (Khormaee et al. 2010; Chen, Khormaee, et al. 2009b), or protein payloads (Liechty et al. 2009) and siRNA (Khormaee et al. 2013) for intracellular delivery.

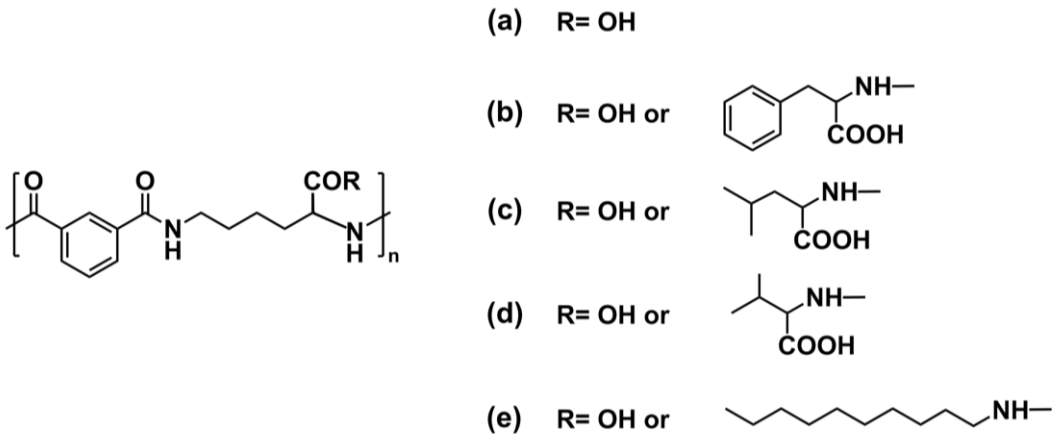

Figure 1.16 Structure of PLP and its derivatives. (a) PLP; (b) PLP conjugated with L phenylalanine (PP); (c) PLP conjugated with L-leucine (PL); (d) PLP conjugated with L-valine (PV); (e) PLP conjugated with decylamine (PLP-NDA).

However, the membrane lytic ability of PLP is also quite low at late endosomal and lysosomal pH (approximately 15% identified by haemolysis

study) (Yue et al. 2005a), thus limiting further application of PLP as drug carriers. As a result, efforts have been made to develop PLP derivatives with tunable pH-responsive ranges and better membrane-lytic activity by coupling different molecules onto PLP side chains (Figure 1.16) (Chen, Khormaee, et al. 2009b; Yue et al. 2005b; Chen et al. 2005; Chen et al. 2008; Khormaee et al. 2010; Chen et al. 2017).

According to a detailed study about different PLP conjugates with valine, leucine, and phenylalanine, the pH-responsive cell membrane-lytic activity has been shown to be dependent on three factors: concentration, grafting degree and hydrophobicity of grafting group (Chen, Khormaee, et al. 2009b). In the haemolysis study, a higher polymer concentration led to a higher activity (Figure 1.17a)(Chen, Khormaee, et al. 2009b). However, at a low concentration (0.025 mg/ml), those polymers grafted with phenylalanine (PP-75) and leucine (PL-75) were able to disrupt lipid membrane with high efficiency at a pH range from 5.0 to 7.0, but showed negligible haemolysis at pH 7.4 (Figure 1.17b). The specific pH-responsive membrane-disruptive activity made these polymers permeable at endosomal pH without disrupting cell membranes at physiological pH, which indicates they could be promising candidates for drug delivery.

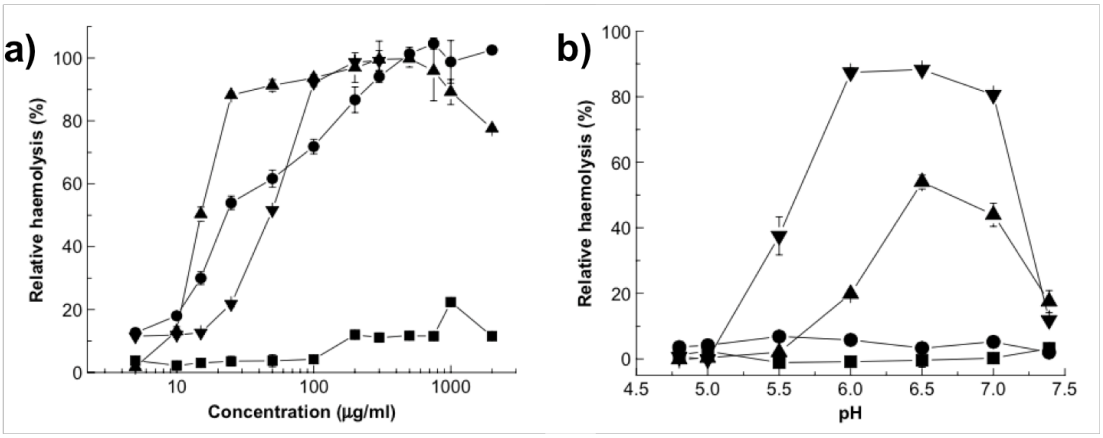

Figure 1.17 (a) Concentration-dependent relative haemolysis by PLP (■), PV-75 (●), PL-75 (▲), PP-75 (▼) at pH 6.5. (b) pH-induced haemolysis by PLP (■), PV-75 (●), PL-75 (▲),PP-75 (▼) at 0.025 mg/ml. Reproduced from reference (Chen, Khormaee, et al. 2009b)**, copyright 2009, with permission from Elsevier B.V.**

Recently published results about PLP conjugated with alkyl side chains also confirmed that grafting hydrophobic moieties on the side chain could boost the membrane-lytic activity at endosomal pH (Chen et al. 2017). Compared with PLP grafted with phenylalanine and leucine, PLP conjugated with decylamine (PLP-NDA) showed similar membrane-lytic activity at a much lower grafting density (18% substitution). Considering the fact that NDA is a long aliphatic chain (10 saturated hydrocarbon units), PLP-NDA has a comb-like structure which may facilitate the membrane interaction. When reducing the alkyl side chain length to 7 saturated hydrocarbons, the maximum haemolysis has been reduced by half at the same pH and polymer concentration (Chen 2017). This suggests that the chain length of pendant alkyl groups and the structure of the comb-like polymers may have an effect on the membrane-lytic activity.

Besides the modifications of PLP to adjust the pH-responsiveness and membrane-lytic activity, another interesting trend is to formulate hydrogels based on PLP (Watkins & Chen 2015). A recently publish paper has reported the hydrogels prepared by crosslinking PLP with an amino acid derivative (L-lysine methyl ester) in an aqueous environment. Resulted hydrogels had pH-dependent swelling behaviour due to the protonation and deprotonation of PLP. Controlled-release studies based on model drugs proved that the hydrogel system was suitable for oral delivery of various payloads including hydrophobic fluorescein and hydrophilic macromolecules such as different sized fluorescein isothiocyanate–dextran. This suggests the great potential of crosslinked PLP materials as oral delivery carriers.

1.6 Aims and objectives

In order to overcome the biological barriers at different scales, this project aims to develop a series of novel stimuli-responsive biomimetic polymer-based materials. Specifically, the author focuses on crosslinked PLP

such as hyperbranched polymers, nanogels and hydrogels. These three polymeric materials bear similar CPP-mimicking pseudopeptidic structure but function in different scales for overcoming different biological barriers.

In the development of each material, there are three major aspects: synthesis, structural effects on physiochemical behaviours, and the evaluation of their capabilities of overcoming biological barriers. Some specific key questions to be addressed in this project are listed below.

Hyperbranched PLP polymers (HPLPs)

- Can HPLPs be synthesised via a simple and robust method?
- Is the hyperbranching degree controllable?
- What are the effects of hyperbranching degrees on the physiochemical properties?
- Do HPLPs have pH-responsive membrane-lytic activity?
- What are the effects of hyperbranching degrees on the membrane-lytic activity?
- What are the possible mechanisms of HPLPs interaction with model lipid membranes?
- Are HPLPs cytotoxic?
- Can HPLPs enhance intracellular delivery?

PLP-based hydrogels

- Can PLP-based hydrogels be synthesised with adjustable crosslinkers?
- Is the pH-responsiveness of the hydrogels adjustable?
- What are the effects of crosslinkers on hydrogel network?
- Can PLP-based hydrogels load different payloads?
- Can PLP-based hydrogels control the release in gastrointestinal fluids?

- How does the incorporation of redox-responsive moieties affect the release?
- Are PLP-based hydrogels cytotoxic?
- Can dual-responsive hydrogels load probiotics for colon-targeted delivery?

PLP-based nanogels

- Can PLP-based nanogels be reproducibly synthesised?
- Are the sizes of the nanogels adjustable?
- Are PLP-based nanogels stable?
- Does in situ loading of hydrophobic payloads affect the properties of nanogels?
- Can nanogels control the release in gastrointestinal fluids?
- What strategies can be used to introduce redox-responsiveness to PLP-based nanogels?
- How does the redox-responsiveness affect the release?

1.7 Research gaps, novelties and impact

1.7.1 Research gaps and novelties

The research presented here looks to develop crosslinked PLP-based materials, not only new polymers with hyperbranched structures, but also highly-crosslinked 3D polymer networks-- nanogels and hydrogels. The series of polymeric materials based on CPP-mimicking polymers are designed to overcome biological barriers at different scales. The research gaps and key novelties of each part are specified below, and also summarised in Table 1-3.

Firstly, previously published work on anionic CPP-mimetic polymers only focused on linear polymers, such as PLP and its derivatives as listed in Section 1.5 However, little attention has been dedicated to branched CPP-mimetic

polymers. The work presented in this thesis first reports a series of anionic, CPP-mimicking, hyperbranched polymers, which caused complete membrane disruption at late endosomal pH while remained non-lytic at physiological pH. The multivalency effect of their hyperbranched structures further enhanced their interaction with cell membranes compared with linear counterparts, thus leading to significantly enhanced membrane-lytic activity. These polymers enhanced the endosomal escape of endocytosed payloads, which proves their capability of overcoming biological barriers at cellular level.

Secondly, previously published preliminary studies on PLP-based hydrogels introduced these hydrogel systems as potential oral drug carriers. However, the effects of crosslinkers' size and structure on crosslinked polymer networks, and the subsequent controlled-release behaviour were not clarified. The work presented in this thesis reports novel PLP-based hydrogels prepared by a range of different crosslinkers, including L-cystine dimethyl ester and PEG diamine with different molecular weights, to study the effects of crosslinkers. The infrared spectra, swelling behaviour, morphology and dynamic rheology of hydrogels were examined to reveal the network details. Further introduction of redox-responsiveness enabled the hydrogel network to disassociate in colonic environment, which could be used for the oral delivery of probiotics.

Thirdly, the work presented in this thesis first reports on the development of CPP-mimetic polymer based nanogels via surfactant-free physically or chemically crosslinking in mild, aqueous solutions. The physically crosslinked nanogels with tunable sizes could accommodate hydrophobic payloads *in situ*, and the release was controlled by pH-dependent disassociation. After disassociation, the polymers were membrane-lytic at slightly acidic pH (5.0-6.0), thus could further facilitate the drug delivery in intestinal cells.

Table 1-3 Summary of research gaps, aims and novelties in the three results chapters.

	Research gaps	Sub-project aims	Novelties
Chapter 3 Hyperbranched polymers for barriers at cellular level	• No anionic non-linear CPP-mimetic polymers developed • Limited understanding about hyperbranching degree on the physiochemical properties and membrane-permeability of CPP-mimetic polymers	• To develop a novel and simple method for hyperbranched anionic polymers preparation • To characterise the structural effects on the polymer properties, investigate the membrane-permeability and explain the mechanism	First report of anionic non-linear CPP-mimetic polymers
Chapter 4 Hydrogels for barriers at macroscopic level	• Limited bioavailability of hydrophobic payloads via oral route • Limited understanding about the effects of crosslinkers on polymer networks, and the subsequent controlled-release behaviour in PLP-based hydrogel systems	• To develop a series of hydrogels, with pH- and redox-responsiveness to overcome the macroscopic barriers for hydrophobic payloads • To characterise the crosslinked polymer networks prepared by different crosslinkers, investigate the controlled release behaviour in simulated GI fluids	Novel PLP-based hydrogels with pH- or dual-responsiveness for hydrophobic payloads delivery
Chapter 5 Nanogels for barriers at macroscopic & cellular level	• Limited drug bioavailability due to low permeation in intestinal cells • No surfactant-free synthesis of CPP-mimetic polymer based nanogel reported	• To develop carriers with permeability to intestinal cell membranes • To develop a simple and robust method for CPP-mimetic polymer based nanogel preparation	First report of CPP-mimetic polymer based membrane-active nanogels

1.7.2 Research impact

The work undertaken in this project lays a solid foundation for similar polymeric materials development. As the preparation of these materials is simple and adaptable, with great tolerance to different starting reagents, more branched or dendritic polymers, nanogels and hydrogels can be developed via the same methodology. For example, the nanogels reported in this thesis were prepared by physically crosslinking PLP-NDA18 using a surfactant-free nanoprecipitation method. The same method could be applied to other polymers such as PLP-NDA10 and even PLP, to prepare similar nanogels with different levels of hydrophobicity and potentially different controlled-release profiles.

The polymeric materials developed in this project are of potential interest to pharmaceutical sectors. These stimuli-responsive drug delivery vehicles can be prepared easily and cost-effectively, and suitable for mass production. Moreover, they are capable of overcoming biological barriers and delivering payloads efficiently to target sites. Specifically, hyperbranched polymers developed are capable of delivering payloads into the cytoplasm. This property could be used for cell engineering *in vitro*. The hydrogels are suitable for oral delivery of small hydrophobic payloads into the intestine and colon. Preliminary studies showed probiotics could be loaded and released as well, which further proves their potential as oral delivery carriers. The nanogels, developed in the last part of this thesis, had pH-responsive membrane-lytic activity, which could be used for oral delivery of payloads into intestinal cells.

This project is also part of the Marie Curie Initial Training Network with a topic of “Smart Nano-objects for Alteration of Lipid bilayers (SNAL)”. My research focuses on the synthetic part, with an experimental polymer chemistry

perspective to understand how to design polymeric drug carriers rationally, especially those CPP-mimicking polymers related carriers. Specifically, the CPP-mimetic hyperbranched polymers revealed the mechanisms enabling these materials to traverse across biological barriers, by using different model lipid membrane systems. Other SNAL partners, from either biophysical or theoretical modeling background, focus on the same topic but use different research tools, such as computational simulation, small-angle X-ray scattering and cryo-transmission electron microscopy, to reveal how the similar PLP-based pseudo-peptides permeablise lipid membranes (Wang & Bresme 2017; Kluzek et al. 2017). The collaborative nature of this project, spanning scientific disciplines, drives a complete understanding of interactions of lipid membranes with nano-objects.

1.8 Thesis outline

This thesis has 6 Chapters, outlined as follows:

Chapter 1 generally introduces the background of drug delivery systems, biological barriers and current challenges in this field. Particularly, stimuli-responsive polymers, cell penetrating peptides and their synthetic mimics are discussed, which provides the focus of the research in this thesis.

Chapter 2 describes the materials and methods used in this work, including synthesis of all the materials, physiochemical properties characterisation, biological models for membrane-activity evaluation, model drug loading and release, and cytotoxicity assays.

Chapter 3 describes a series of lysine-based, CPP-mimicking, hyperbranched polymers for intracellular drug delivery applications. The synthesis was designed and optimised with detailed structural characterisation. The polymers' physiochemical properties were evaluated by several

complementary methods, to demonstrate the polymer behaviour in aqueous solutions. The interactions between these polymers and lipid membranes were tested using model lipid membranes to identify the membrane-lytic ability as well as the mechanism. Finally, the intracellular delivery of a model drug was performed, and the results were compared with a commercially available CPP and other CPP-mimicking polymers.

Chapter 4 describes the design and synthesis of PLP-based hydrogels for oral delivery applications. PLP was crosslinked with different crosslinkers via an EDC-coupling reaction. The swelling behaviour, SEM morphology and dynamic rheology of hydrogels were examined to reveal the network details and to evaluate the responsive properties. The loading and release profiles were investigated on several model drugs, including probiotics.

Chapter 5 describes the design and synthesis of PLP-based nanogels, which combine the advantages of hydrogels and CPP-mimetic polymers. The nano-sized drug carriers were formulated by either physically or chemically crosslinking, with adjustable sizes. Cargos could be loaded in situ during nanogel formation and the release with pH- or redox- triggers was investigated.

Chapter 6 summarises the research in this thesis and presents conclusions. Future perspectives are also discussed based on current achievements.

Chapter 2 Materials and Methods

In this Chapter, all materials and methods used in this thesis are listed and described in detail. Materials including chemicals, solvents, reagents, assays, bacteria strains and mammalian cell lines are sorted based on their suppliers. Methods include the preparation and characterisation of various drug carriers, polymer and lipid membrane interaction evaluations, model drug loading and release *in vitro* and *ex vivo*, and cytotoxicity of these drug carriers.

2.1 Materials

L-Lysine methyl ester dihydrochloride, L-phenylalanine methyl ester dihydrochloride, polyoxyethylene bis(amine) (with various average molecular weights of 1K, 1.5K, 3.4K and 8K Da) and N,N'-dicyclohexylcarbodiimide (DCC) were purchased from Alfa Aesar (Heysham, UK).

Sodium phosphate dibasic, potassium chloride, potassium carbonate, sodium chloride, citric acid, sodium citrate, potassium phosphate monobasic, dimethyl sulfoxide (DMSO), 4-dimethylaminopyridine (DMAP), triethylamine (TEA), sulphuric acid (H_2SO_4), acetic acid, N-methyl-2-pyrrolidone (NMP), HEPES, Texas Red® hydrazide, Hoechst 33342 and LysoTracker® Red DND 99 were purchased from Thermo Fisher Scientific (Leicestershire, UK).

Magnesium sulphate ($MgSO_4$), sodium fluorescein, L-cystine dimethyl ester dihydrochloride (CDE), N-hydroxysuccinimide (NHS), N-(3-dimethylaminopropyl)- N'-ethyl carbodiimide hydrochloride (EDC), 1,4-dithiothreitol (DTT), isophthaloyl chloride, 1,3,5-benzenetricarboxylic acid chloride, 1-butanamine, tetrahydrofuran (THF), pyrene, deuterium oxide (D_2O), DMSO-d_6, chloroform-d, calcein, 4,7,10-trioxa-1,13-tridecanediamine, decylamine (NDA), cysteamine hydrochloride, Aldrithiol™-2, cystamine

dihydrochloride, fluorescein isothiocyanate–dextran (FITC-dextran, with various average molecular weights of 10K, 70K and 150K Da), 8-hydroxypyrene-1,3,6-trisulfonic acid tri-sodium salt (HPTS), poly(vinyl alchohol) (PVA, Mowiol® 28-99, M_w~145 kDa), sucrose, glucose, melittin from honey bee venom, poly(L-lysine) hydrobromide (with average molecular weights of 70-150 kDa), poly(L-arginine) hydrochloride (with average molecular weights larger than 70 kDa), Nile red, Doxorubicin hydrochloride (DOX), de Man Rogosa and Sharpe (MRS) broth powder, de Man Rogosa and Sharpe Agar powder, Dulbecco's modified Eagle's medium (DMEM), Dulbecco's phosphate-buffered saline (PBS), fetal bovine serum (FBS), trypsin-ethylenediaminetetraacetic acid (EDTA) and penicillin-streptomycin were purchased from Sigma-Aldrich (Dorset, UK).

Methanol, ethanol, acetone, N,N-dimethylformamide (DMF), diethyl ether (Et_2O), chloroform, dichloromethane (DCM), triethylamine, sodium hydroxide and hydrochloric acid (HCl) were purchased from VWR International Ltd (Lutterworth, UK).

1,2-Dioleoyl-sn-glycero-3-phosphocholine (DOPC), 1,2-dioleoyl-sn-glycero-3-phospho-L-serine (DOPS) and Lissamine™ Rhodamine B 1,2-dihexadecanoyl-sn-glycero-3-phosphoethanolamine triethylammonium salt (rhodamine PE) were purchased from Avanti (Alabama, US). AlamarBlue® was purchased from AbD serotec (Oxfordshire, UK).

Defibrinated sheep red blood cells (RBCs) were obtained from TCS Biosciences Ltd (Buckingham, UK) and used within 1 week upon delivered. *Lactobacillus rhamnosus GG* (LGG, ATCC 53103) and HeLa cells were kindly provided by Dr Krishnaa Mahbubani from Cambridge University.

MRS broth and MRS agar were made according to instructions with ultrapure water from a Millipore Milli-Q Gradient System. After mixing the powders with water, all broth and agar solutions were autoclaved at 121 °C for 20 min. When the MRS agar cooled down to around 50 °C, it was poured into Petri dishes and allowed to cool down and solidify. All solidified plates were stored upside down in fridge sealed with Parafilm and used within 1 month.

Pyrene was recrystallised in acetone before use. DMSO and DMF were dried by molecular sieves (4 Å) before use. Other chemicals were used as received without further purification.

2.2 Organic Synthesis

2.2.1 Hyperbranched polymer synthesis

2.2.1.1 Model reactions

Model reactions, the use of simplified model molecules to perform similar reactions, are commonly designed for investigation of the possibility of a complicated reaction, optimisation of the reaction condition and identification of the chemical shift of typical molecules in NMR spectra. For hyperbranched polymer synthesis, model reactions between small molecules were needed to acquire a better understanding of the reactivity of crosslinkers and the characteristic peaks in NMR spectra.

Model reaction 1 (1,3,5-benzenetricarboxylic acid chloride and butylamine)

1,3,5-benzenetricarboxylic acid chloride (0.250 g, 0.942 mmol, 1 equiv.) and TEA (0.475 mL, 3.41 mmol) were dissolved in 5 mL precooled THF, while 1-aminobutane (0.279 mL, 2.83 mmol, 3 equiv.) was dissolved in another 10 mL THF separately. Add 1,3,5-benzenetricarboxylic acid chloride solution slowly to aminobutane solution by a dropping funnel. The reaction mixture was

stirred overnight at room temperature after which a white suspension had formed. For purification of the products, the reaction mixture was poured into 30 mL deionised water, which was subsequently extracted with Et_2O (4 × 10 mL, upper layer). The combined Et_2O was dried on $MgSO_4$, filtered and concentrated *in vacuo*. The final products were white powders, which were dissolved in chloroform-d for NMR analysis.

Model reaction 2 (1,3,5-benzenetricarboxylic acid chloride and L-phenylalanine methyl ester hydrochloride)

1,3,5-benzenetricarboxylic acid chloride (0.64 g, 2.4 mmol, 1 equiv.) and TEA (0.73 g, 7.2 mmol, 3 equiv.) were dissolved in 5 mL precooled DCM, while L-phenylalanine methyl ester hydrochloride (1.55 g, 7.2 mmol, 3 equiv.) and TEA (0.73 g, 7.2 mmol, 3 equiv.) were dissolved in another 50 mL DCM separately. Add 1,3,5-benzenetricarboxylic acid chloride solution slowly to L-phenylalanine methyl ester solution by a dropping funnel. The mixed solution was slowly brought to room temperature and stirred overnight. After the reaction, the solution was filtered to remove triethylamine hydrochloride, and the dichloromethane was successively washed with HCl (10 mM) and deionised water twice. After that, the dichloromethane was dried on $MgSO_4$, filtered and concentrated *in vacuo*. The final products were white powders, which were dissolved in chloroform-d for NMR analysis.

Model reaction 3 (1,3,5-benzenetricarboxylic acid chloride and N_α-(tert-Butoxycarbonyl)-L-lysine (Boc-L-lysine))

Boc-L-lysine (0.4 mmol) and potassium carbonate (0.4 mmol) were dissolved in 1 mL pre-cooled deionised water. 1,3,5-benzenetricarboxylic acid chloride (0.1 mmol) were dissolved in 0.5 mL pre-cooled acetone. The acetone solution was dropped into aqueous solution very slowly, and the reaction was

allowed to proceed for 1 h at room temperature. For different products yield calculation, two drops of in situ reaction solution were mixed with DMSO-d_6 for NMR characterisation. For purification, products precipitated out after neutralisation with HCl. The white precipitation was redissolved in NaOH solution. Then HCl was used to precipitate it out again. The precipitation was collected by centrifuge. The purification cycle was repeated three times. The final precipitation was dried in an oven. The dried products were dissolved in DMSO-d_6 or a mixture of D_2O and DMSO-d_6 for NMR characterisation.

Model reaction 4 (1,3,5-benzenetricarboxylic acid chloride and L-lysine methyl ester dihydrochloride)

L-Lysine methyl ester dihydrochloride (0.01 mol) and potassium carbonate (0.04 mol) were dissolved in 50 mL pre-cooled deionised water. 1,3,5-benzenetricarboxylic acid chloride (0.01 mol) was dissolved in 50 mL pre-cooled dry acetone. The acetone solution was dropped into aqueous solution slowly, and white precipitation quickly forms. The precipitation was collected and washed with deionised water. The final precipitation was insoluble in all solvents and thus impossible to get characterised by either NMR or GPC.

2.2.1.2 HPLP synthesis

Hyperbranched poly(L-lysine isophthalamide) (HPLP) with different branching degrees were prepared by a polycondensation reaction followed by ester hydrolysis.

Polycondensation

Typically, 50 mL deionised water was pre-cooled in a fridge (4 °C), and 50 mL acetone was pre-cooled in a freezer (-20 °C) one day before the reaction. Then L-lysine methyl ester dihydrochloride (0.01 mol, 1 equiv.) and potassium

carbonate (0.04 mol, 4 equiv.) were dissolved in the pre-cooled deionised water, while isophthaloyl chloride (0.01 mol, 1 equiv.) and 1,3,5-benzenetricarboxylic acid chloride (0.1 mmol, 0.3 mmol, 0.5 mmol, 0.8 mmol to 1 mmol; 1-10%) were dissolved in the pre-cooled acetone. The acetone solution was slowly dropped into the aqueous solution by a dropping funnel, and an ice bath was used to cool down the reaction. All the reactants were mixed thoroughly by stirring during dropping and the following reaction. After 0.5h, the polymer products precipitated in the solution. The precipitation was washed with deionised water for three times to remove excess solvent and impurities, before drying in an oven at 55 ˚C overnight.

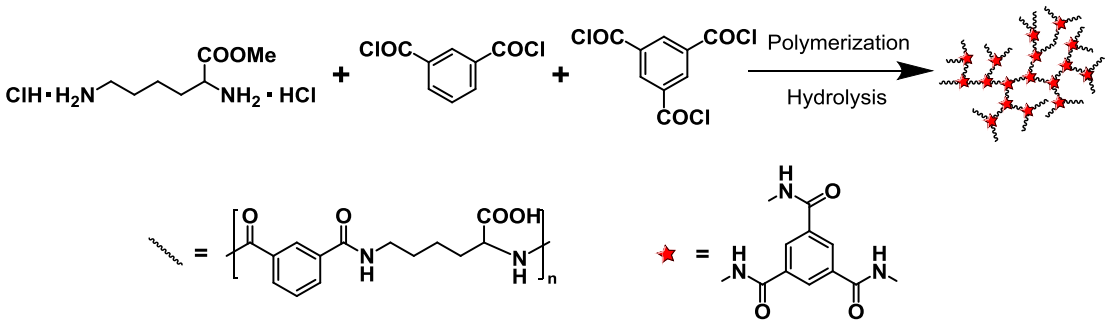

Figure 2.1 HPLP Synthesis Schematic. Reprinted from published paper (Wang & Chen 2017)**, copyright 2017, with permission from American Chemical Society.**

Ester hydrolysis and purification

Dried polymer samples were dissolved in 200-300 mL DMSO. Sodium hydroxide (2.5 equiv per polymer repeat unit) was dissolved in anhydrous ethanol (40 mL). After addition of sodium hydroxide solution to polymer solution, the hydrolysis was allowed to proceed for 0.5h. Hydrolysed hyperbranched polymer precipitation was collected by vacuum filtration. To remove excessive DMSO, polymer precipitation was re-dissolved in a minimum volume of deionised water and precipitated again by adding 1 M HCl. Then the precipitation was collected and dissolved in 1 M NaOH solution. This

precipitation cycle was then repeated three times. Finally, the polymer solution was dialysed against deionised water in a Visking membrane tubing (Medicell, M_w cut-off 12 - 14 kDa) for 3 days. Dialysis water was replaced twice per day.

To acquire polymers in acidic form (in which carboxyl groups were protonated), 1 M HCl was added to the solution, and the precipitation was collected and lyophilised subsequently. To acquire polymers in salt form (in which carboxyl groups were deprotonated), the pH of the dialysed solution was first adjusted by 0.04 M NaOH solution and then lyophilised to yield white fibrous products. The lyophilisation was performed on a VirTris BenchTop Pro freeze dryer. Samples were first frozen in a -20 °C freezer and then placed in the chamber of the freeze dryer. The lyophilisation lasted 3 days until no ice was observed. Dehydrated polymer samples were stored at room temperature before characterisations.

Acidic form polymers were mainly used for structural characterisations including NMR, FTIR, GPC, DSC and TGA. Salt form polymers were used for preparing aqueous solutions and physiochemical behaviour study.

2.2.2 Hydrogel synthesis

2.2.2.1 Synthesis of pH-responsive amphiphilic hydrogels

PLP was first synthesised as previously reported in the literature (Eccleston et al. 1999). Briefly, the polycondensation of L-lysine methyl ester dihydrochloride and isophthaloyl chloride, followed by ester hydrolysis. After preparation, PLP was characterised by ^{1}H-NMR to confirm the structure before use. The salt form PLP was used for hydrogel preparation.

All hydrogels were prepared by an EDC-coupling reaction between PLP and PEG bis(amine) (M_n= 1KDa, 1.5 KDa and 3.4 KDa respectively) in aqueous

solutions as shown in Figure 2.2. In the typical procedure of hydrogel preparation, 100 mg PLP was dissolved in 700 μL of deionised water, and PEG bis(amine) (0.2 molar equivalent of PLP residual) was dissolved in 200μL of deionised water separately. The PEG solution was added to the PLP solution and mixed uniformly by a vortex mixer, after which EDC (2 molar equivalents of PLP residual) and NHS (0.5 molar equivalent of PLP residual) solution was added. The final volume of the mixture was 1.5 mL in a plastic vial with a diameter of 12 mm. The final solution was left overnight at room temperature for gelation. The synthesised hydrogel was then dialysed against deionised water for three days to eliminate impurities and then stored in deionised water before characterisation.

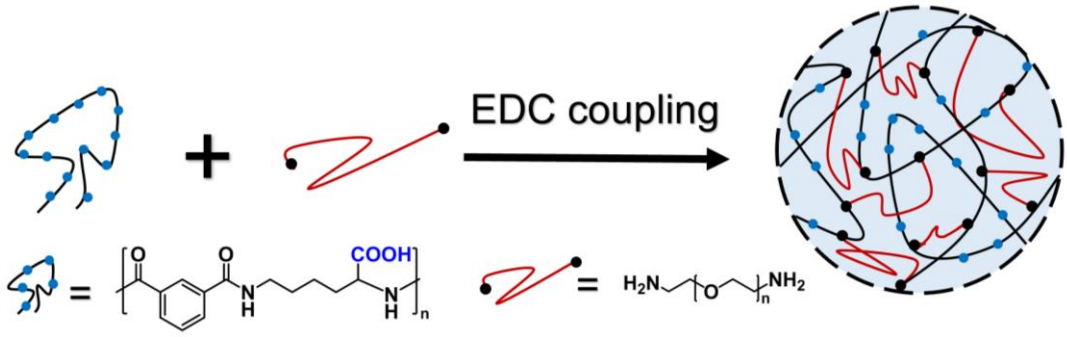

Figure 2.2 Synthetic scheme of pH-responsive amphiphilic hydrogels.

2.2.2.2 Synthesis of pH- and redox-responsive hydrogels

The pH- and redox-responsive hydrogels were prepared via a similar method mentioned in Section 2.2.1.1. Instead of PEG bis(amine), L-cystine dimethyl ester dihydrochloride was used as the crosslinker (Figure 2.3). In this case, 100 mg, 75 mg, 50 mg and 25 mg PLP were dissolved in 1 mL deionised water to yield 10.0%, 7.5%, 5.0% and 2.5% PLP (wt%) aqueous solution. CDE (0.2 molar equivalent of PLP residual) were added and mixed uniformly by a magnetic stirrer. Subsequently, EDC (2 molar equivalents of PLP residual) and NHS (0.5 molar equivalent of PLP residual) were added to the same solution.

The final volume of the mixture was set at 1.5 mL, the same as in Section 2.2.2.1. After the solution became cloudy, the magnetic stirrer was removed, while the cloudy mixture was left at room temperature overnight to form hydrogels. The hydrogels were purified by dialysis against deionised water for a week, and the water was changed once per day. All prepared hydrogels were stored in deionised water at room temperature before use.

Some hydrogel disks were freeze-dried to calculate solid contents, which were defined as below:

$$\%m = \frac{m_d}{m_w} \times 100 \qquad \text{(Equation 2.1)}$$

Where $\%m$ is solid content, m_w and m_d are the weight of hydrogel disk before and after lyophilisation respectively.

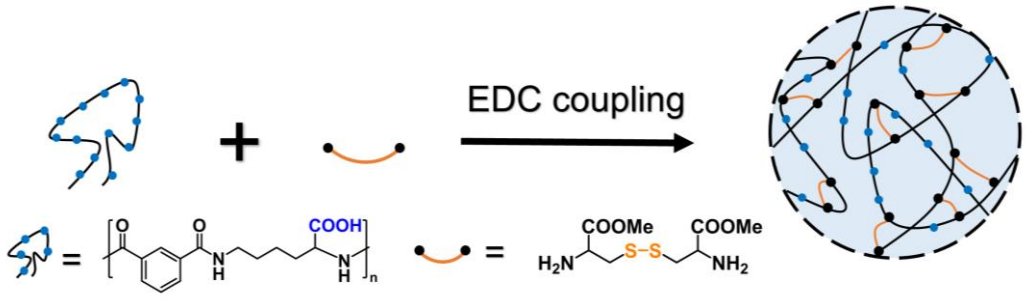

Figure 2.3 Synthetic scheme of pH- and redox-responsive hydrogels.

2.2.3 Synthesis of physically crosslinked nanogels

PLP-NDA polymers were first prepared according to literature (Chen et al. 2017). Briefly, decylamine was conjugated to PLP by a DCC-coupling reaction. PLP-NDA was characterised by ^{1}H-NMR spectra to confirm the structure before use.

The physically crosslinked nanogels were prepared by nano-precipitation of PLP-NDA polymers. Acidic PLP-NDA was dissolved in DMF first

at various concentrations, from 1.25 mg mL^{-1} to 250 mg mL^{-1}. The polymer DMF solution was dropped into deionised water by a pipette with vigorous stirring. Once the dropping finished, the reaction was allowed at room temperature for another 1 h. The particle sizes of polymer self-assemblies were measured by DLS. Then the crude nano-precipitation dispersion was dialysed against deionised water in a Visking membrane tubing (Medicell, M_w cut-off 12 - 14 kDa) for 3 days to remove DMF completely. Water was replaced three times per day. The dialysed nanogels aqueous dispersion was stored in 4 °C fridge before use.

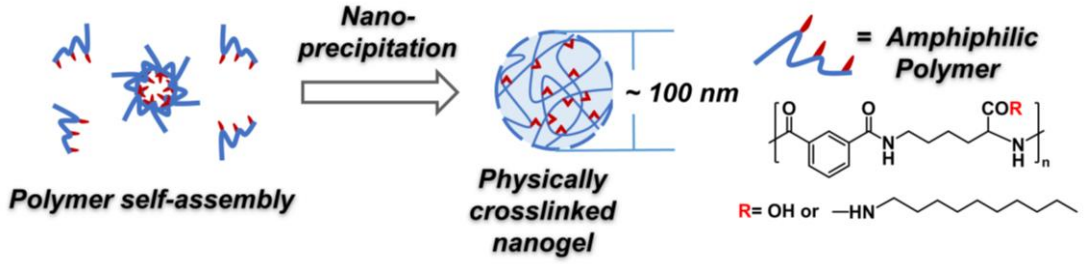

Figure 2.4 Synthetic scheme of pH-responsive physically crosslinked nanogels

2.2.4 Synthesis of chemically crosslinked nanogels

2.2.4.1 Nanogel synthesis via EDC-coupling

EDC-coupling nanogels were prepared based on physically crosslinked nanogels. Instead of nanoprecipitation in deionised water, 40 μL PLP-NDA (25 mg mL^{-1} in DMF, 1 mg in total) was dropped into a solution containing EDC (6.6 mg, 10 molar equivalents of PLP-NDA residual), NHS (4.0 mg, 10 molar equivalents of PLP-NDA residual) and crosslinkers such as L-cystine dimethyl ester dihydrochloride, or cystamine dihydrochloride, or 4,7,10-trioxa-1,13-tridecanediamine (PEG 220 diamine). Two negative controls were also prepared with the same settings. One was physically crosslinked nanogel without EDC, NHS or any crosslinker molecules. The other was with EDC and

NHS but without crosslinkers, to eliminate the effects of these two catalysts on the final products. The reaction mixture was stirred vigorously at room temperature for 1 h. Then it was dialysed against deionised water in a Visking membrane tubing (Medicell, M_w cut-off 12 - 14 kDa) for 3 days to remove DMF, excessive EDC, NHS and other impurities.

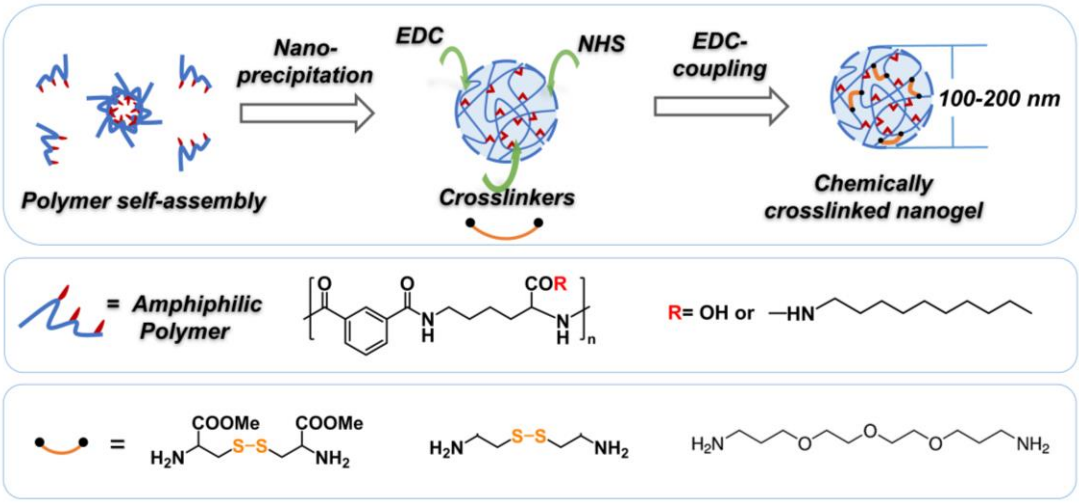

Figure 2.5 Scheme of nanogel formation via EDC-coupling

2.2.4.2 Nanogel synthesis via thiol-exchange

Synthesis of pyridine dithioethylamine hydrochloride crosslinker

Pyridine dithioethylamine hydrochloride was synthesised according to literature (Lelle & Peneva 2014). Briefly, 2,2′-dithiodipyridine (2.2 g, 10 mmol) was dissolved in 5 mL methanol mixed with acetic acid (0.4 mL, 7 mmol). Cysteamine hydrochloride (5.7 g, 5.0 mmol,) dissolved in another 4 mL methanol, was added slowly to 2,2′-dithiodipyridine. The reaction mixture was stirred overnight at room temperature. The product was precipitated out in cold diethyl ether (50 mL) and purified by redissolving in methanol (3 mL) and reprecipitating in cold ether (50 mL) twice. The white powder obtained was dried in air overnight before NMR analysis.

Conjugation of pyridine dithioethylamine hydrochloride on PLP

Pyridine dithioethylamine hydrochloride was conjugated to PLP via an EDC coupling reaction. PLP salt (100 mg) was first dissolved in 2mL 0.1 M phosphate buffer (pH=7.4). EDC (69.5 mg, 0.36 mmol, 1 molar equivalent to PLP repeating units) and NHS (41.7 mg, 0.36 mmol, 1 molar equivalent to PLP repeating units) were added to PLP solution, following by adding pyridine dithioethylamine hydrochloride (16.0 mg, 0.07 mmol, 0.2 molar equivalent to PLP repeating units). The reaction mixture was stirred at room temperature overnight and dialysed against deionised water for 24 h in a Visking membrane tubing (Medicell, M_w cut-off 12 - 14 kDa), during which the deionised water was changed 3 times. After dialysis, the solution was acidified by 1 M HCl and centrifuged at 10000 rpm for 5 mins. The precipitation was collected and lyophilised. The lyophilisation process was the same as specified in Section 2.2.1. The final polymer (PLP conjugated with pyridine dithioethylamine at a stoichiometric ratio of 20%, PLP-Py20) was charachterised by NMR before use.

Nanogel formation via thiol-exchange

One the one hand, pyridine disulfide groups on PLP-Py20, could be cleaved by reducing reagents. On the other hand, the revealed thiol groups after cleavage could attack another pyridine disulfide groups on PLP-Py20, which leads to crosslinking (Figure 2.6). Based on this mechanism, thiol-exchange nanogels were prepared via similar experimental settings as EDC-coupling nanogels. PLP-Py20 was nanoprecipitated in the aqueous environment, which containing DTT as a reducing reagent. Instead of the coupling reaction between carboxylic acids groups on polymers and amine groups on crosslinkers, this time, the polymer self-crosslinked by the thiol-exchange reaction on pyridine disulfide groups.

In a typical experiment, HEPES (10 mM, pH=7) was used as the aqueous buffer, to which DTT (0.25 mg, 1.6 mmol, 0.5 molar equivalent to pyridine dithio groups on PLP-Py20) was added. PLP-Py20 (5 mg) was dissolved in 0.5 mL DMF solution. The HEPES solution was poured into PLP-Py20 DMF solution quickly under vigorous stirring. The mixture turned milky immediately, and it was left stirring for 1 h at room temperature. The nanogel dispersion was dialysed against deionised water in a Visking membrane tubing (Medicell, M_w cut-off 12 - 14 kDa) for 3 days to remove impurities.

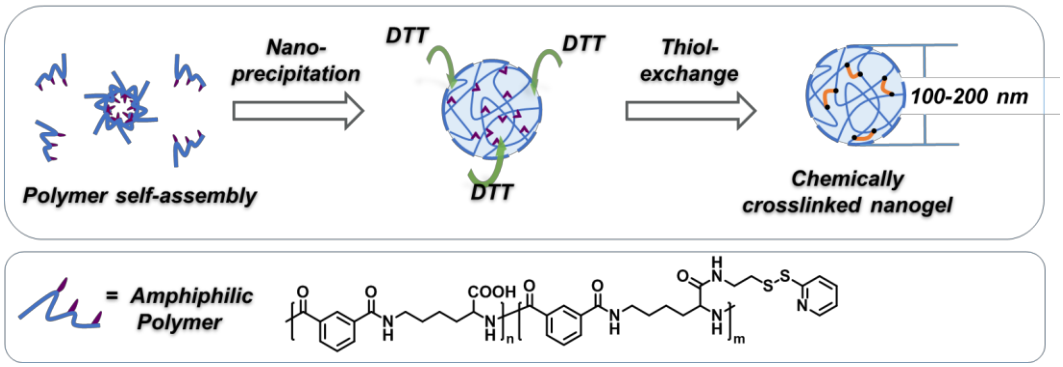

Figure 2.6 Scheme of nanogel formation via thiol-exchange.

2.3 Structural and physiochemical properties characterisation

2.3.1 Nuclear Magnetic Resonance (NMR) Spectrometry

NMR is the most commonly used technique for molecular structure analysis. By measuring the nuclear spin of protons or carbon-13 in a magnetic field, the chemical environment and the relative quantity of protons or carbons will be deduced by chemical shift values and peak integrations.

NMR samples were dissolved in 0.75 mL deuterated solvents, such as DMSO-d_6 or D_2O or a binary solvent containing both DMSO-d_6 and D_2O. All ^{1}H- and ^{13}C-NMR spectra were obtained on an Avance III 400 MHz NMR spectrometer (Bruker, Switzerland) at room temperature. A typical ^{1}H-NMR sample was scanned from -4 ppm to 16 ppm, 16 times. A typical ^{13}C-NMR

sample was scanned from -31 ppm to 251 ppm, 104 times. All samples contained trace tetramethylsilane (TMS) as an internal standard for calibration.

MestReNova (version 8.0) was used for NMR data analysis. For a ^{1}H-NMR spectrum, the chemical shift was first calibrated by TMS's peak at 0 ppm. Then the baseline was corrected by automatic baseline correction in the software. After that, the chemical shifts and peak integrations were acquired, and the peak assignation was performed. For a ^{13}C-NMR spectrum, the chemical shift was also calibrated by TMS. However, only the chemical shifts were acquired but not peak integration due to the decoupling of ^{13}C.

2.3.2 Fourier Transform Infrared (FTIR) Spectroscopy

FTIR spectroscopy is another important technique used for molecular structural analysis. By measuring the absorption of infrared light (500-4000 cm^{-1}), FTIR spectra give information about major functional groups in the sample, such as hydroxyl, carboxyl, amide, *etc*. Unlike NMR designed for solution samples, FTIR is suitable for a wide range of samples, including solids, liquids and even gases. Also, it is widely applied to mixture samples instead of pure chemicals.

Based on these features, in this study, FTIR was used for all samples including polymers, hydrogels and nanogels for different purposes. For HPLPs, it was utilised to verify the structure as a supplement to NMR. For hydrogels, it was used to study the crosslinking and pH-responsive behaviour. For nanogels, it was used to confirm drug loading.

All FTIR data was recorded by a Spectrum 100 Fourier Transform Infrared instrument (PerkinElmer, USA) with a Specac Quest ATR diamond accessory. In a typical measurement, a background scan was first performed, and then the lyophilised polymers, or lyophilised hydrogel or lyophilised

nanogel samples (around 1 mg) were applied on to the plate. The sample scan from 4000 cm^{-1} to 600 cm^{-1} was repeated for 8 times with a resolution of 1 cm^{-1}. The final data presented was an average of 8 scans, exported by PerkinElmer Spectrum software. *Note: chemically crosslinked nanogel samples with or without DOX loading (Section 5.4.4) were provided by undergraduate student Wanyue Ouyang.*

2.3.3 Gel Permeation Chromatography (GPC)

Gel permeation chromatography (GPC)/ Size exclusion chromatography (SEC) is a widely used technique for measuring the molecular weight and molecular weight distribution of natural and synthetic polymers. It is based on liquid chromatographic techniques that separate individual polymer chains by their size in solution instead of their chemical properties.

In this study, HPLPs were fully dissolved in NMP at 1 mg mL^{-1} followed by filtration using 0.45 μm PTFE filters for GPC measurements. The column used was the Mixed D packed column (300-mm long and 7.5-mm wide) with polystyrene/polydivinylbenzene from Polymer Laboratories UK. Detection was made by UV absorbance using a Knauer diode array Smartline 2600 detector at 270, 300, 350, and 370 nm, respectively. The system was operated at 80 °C and a constant flow rate of 0.5 mL min^{-1}. Polystyrene standards (5.8 x 10^2, 9.7 x 10^2, 2.96 x 10^3, 1.988 x 10^4, 1.854 x 10^5, 5.23 x 10^5, and 5.0 x 10^6 Da) were used for calibration.

2.3.4 X-ray photoelectron spectroscopy (XPS)

XPS spectroscopy was used for identification of the elemental composition of materials. When a sample was irradiated by high energy X-rays, the electrons at the surface manage to escape. The number and kinetic energy of escaped electrons were detected and analysed by an energy analyser.

Though XPS was routinely used for inorganic samples, nowadays there are also used for polymeric samples such as hydrogels.

XPS data were acquired with the help of Dr Ignacio J. Villar-Garcia from Department of Materials, Imperial College London.

All XP spectra were recorded using a K-alpha^{+} XPS spectrometer equipped with an MXR3 Al Kα monochromated X-ray source ($h\nu$ = 1486.6 eV). X-ray gun power was set at 72 W (6 mA and 12 kV). With this settings, the intensity of the Ag $3d_{5/2}$ photoemission peak for a standard Ag sample, recorded at 20 eV pass energy, was 5×10^6 counts s^{-1} and the full width at half maximum was 0.58 eV. Binding energy calibration was made by Au $4f_{7/2}$ (84.01 eV), Ag $3d_{5/2}$ (368.20 eV) and Cu $2p_{3/2}$ (932.55 eV). Charge compensation was achieved using the FG03 flood gun using a combination of low energy electrons and the ion flood source. Survey scans were recorded using 200 eV pass energy, 1 eV step size and 100 milliseconds dwell times. All high-resolution spectra were recorded using 20 eV pass energy, 0.1 eV step size and 1 second dwell times. Samples were prepared by pressing the lyophilised hydrogels onto a carbon-based conductive tape and analysed at an electron take-off angle normal to the surface concerning the analyser. The pressure during the measurement of XP spectra was $\leq 1 \times 10^{-8}$ mbar.

Thermo Avantage software was used for data interpretation. Shirley or two-point linear background subtractions were applied, and Thermo scientific sensitivity factors were used for quantification analysis. Peaks were fitted using GL(30), a combination of a Gaussian (70%) and Lorentzian (30%).

2.3.5 Differential scanning calorimetry (DSC)

DSC is a thermoanalytical technique which measures the heat absorbed or released when heating up or cooling down a sample. It is often used to detect

physical transformations such as phase transitions. However, it is sometimes used for chemical reactions such as oxidation.

In this study, DSC was used for polymer samples, lyophilised hydrogels and hydrated hydrogels for different purposes. For HPLPs, it was used to define the glass transition temperature (T_g). For lyophilised hydrogel samples, which were typically dehydrated crosslinked polymer network, DSC measured the crystallisation behaviour of PEG crosslinkers, to identify the homogeneity of the network. For hydrated hydrogels in different solutions, it was interesting to use DSC to measure the melting point of ice within hydrogel networks. The melting points were then correlated with the environment of water in hydrogels.

HPLP samples

Typically, the HPLPs in acidic form were weighed and filled in a Tzero Aluminum Hermetic pan (5-10 mg per sample). The pan was sealed and tested using a TA Q200 differential scanning calorimeter. In one cycle, samples were heated to 200 °C and then cooled to 0 °C. The thermal cycle was repeated twice, and the ramp rate was 10 °C per minute. The data of the second cycle was used, and T_g was analysed by TA DSC software.

Hydrogel samples

Hydrogel samples used in DSC study were provided by MSc student Reva Attah, via the same synthetic method specified in Section 2.2.2.1.

Lyophilised hydrogel samples were cut into small pieces and weighed in a Tzero Aluminum Hermetic pan (5-10 mg per sample). The sealed pan was heated to 80 °C and then cooled to -60 °C in one thermal cycle. The cycle was repeated three times, and the ramp rate was 10 °C per minute. The data of the second cycle was used.

Hydrated hydrogels samples were equilibrated in 0.1 M citrate buffer (pH 3.0) or 0.1 M phosphate buffer (pH 7.4) for 48 h before DSC analyses by a TA Q200 differential scanning calorimeter. Typically, hydrated hydrogel samples were cut into small pieces (0.5-1 mg) and sealed in a Tzero Aluminum Hermetic pan, which was heated to 40 °C and then cooled to -50 °C in one thermal cycle. The thermal cycle was repeated three times, and the ramp rate was 10 °C per minute. Data of the second cycle was used and analysed by TA DSC software.

2.3.6 Thermo gravimetric analysis (TGA)

TGA measures the mass loss of samples with increasing temperature. It reveals details about the decomposition of polymer chains, which is highly dependent on the covalent links in the structure. TGA data of the HPLPs was collected using a TA Q500 thermogravimetric analyser. Typically, samples were placed in a platinum pan and heated in the nitrogen atmosphere from 30 °C to 500 °C. The ramp rate was 10 °C per minute.

2.3.7 Dynamic light scattering (DLS)

DLS is a convenient technique to measure the hydrodynamic size and size distribution of polymers or nanoparticles in solution. When a beam of laser is directed at the sample, it will be scattered by the particles in the sample dispersion. Due to Brownian motion of the small particles, the scattered light intensity constantly fluctuated over time. Because the movement of small particles is faster than large particles in the dispersion, the corresponding scattered intensity trace will be more ‘noisy’ (as shown in Figure 2.7). An autocorrelation function will be generated based on the scattered intensity trace, which reflects the movement of scatters. The average particle size (Z-average), as well as PDI, will be extracted based on the autocorrelation function.

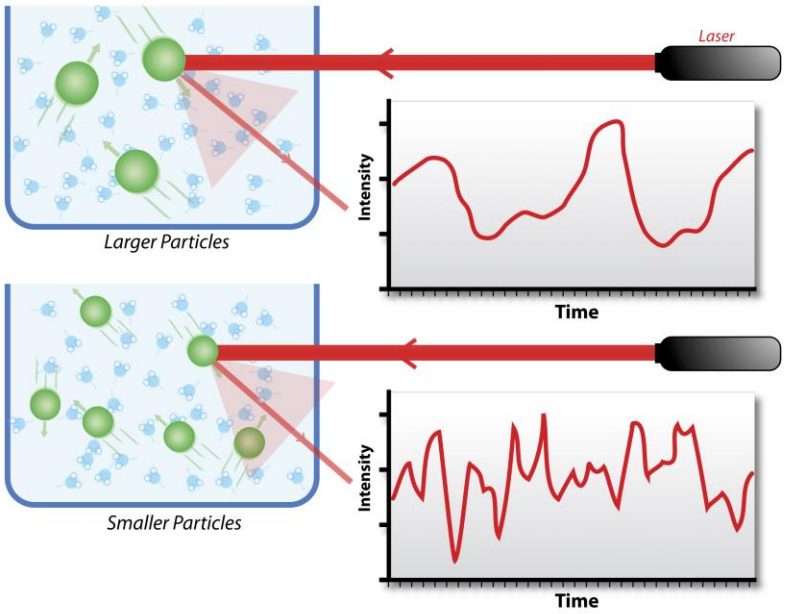

Figure 2.7 DLS mechanism. The different scattered light intensity traced in larger and smaller particle dispersions (Jones 2010)**, copyright 2010, open access under the license of CC BY-SA 3.0.**

In this thesis, DLS was used to study the size and PDI of polymers and nanogels in different environments. Especially for nanogel study, DLS was intensively used for identification of nanogel formation and responsiveness. All the samples in this thesis were measured by a dynamic light scattering platform (Zetasizer Nano S, Malvern, UK).

HPLP samples

Polymer stock solutions (10 mg mL^{-1}) were diluted by 10 times with citric buffer at pH 4.6 or phosphate buffer at pH 7.4. Before DLS measurements, samples were left for equilibration for 48 h and then 0.45 μm cellulose filters were used to filter large particles out of the polymer sample solutions. 0.5 mL solution was added to a polystyrene micro-UV cuvette, and the dynamic light scattering was measured at an angle of 90° in a 10-mm diameter cell at 25 °C. For each sample, the measurement was repeated 3 times, and in each

measurement, the scan was repeated 13 times. The final particle sizes and PDI were calculated by Malvern software.

Nanogel samples

For un-purified nanogels samples, DLS was measured without any filtration. For dialysed nanogels, both filtrated (via a 0.22 μm cellulose filter) and un-filtrated samples were measured. For nanogels in different buffers, dialysed nanogels were 10 times diluted in the specific buffer and DLS was measured after overnight stabilisation. For each measurement, 0.5 mL solution was added to a polystyrene micro-UV cuvette, and the dynamic light scattering was measured at an angle of 90° in a 10-mm diameter cell at 25 °C. The final particle sizes and PDI were calculated by Malvern software. *Note: physically crosslinked nanogel samples for pH and ion tolerance study (Section 5.2.2) were provided by Xiaozhen Huang.*

2.3.8 Zeta potential

Like DLS, Zeta potential is considered as another critical parameter for nanoparticles, because it indicates the particle stability. The dispersions with absolute Zeta potential value above 40 mV are regarded as very stable, while those between 30-40 mV are moderately stable. The dispersions with less than 10 mV Zeta potential are unstable.

Although the Zeta potential cannot be measured directly, it can be calculated based on the electrophoretic mobility of particles in the dispersion. For electrophoretic mobility measurement, an electric field is applied to the particles across the dispersion. Particles with zeta potentials migrate towards the electrode with opposite charge. The velocity can be measured by the laser phase shift caused by particle movement. Multiple theoretical models have been used to fit electrophoretic mobility to determine the Zeta potential. The

most commonly used ones are Smoluchowski's model which fits aqueous solutions, and Huckle’s model which fits organic solutions.

In this thesis, Zeta potential was used to study the stability of nanogels in different environments. All samples were measured by a Brookhaven ZetaPLAS Potential Analyzer (Holtsville, US). The sample preparation was the same as DLS samples. Six measurements were performed for one sample, and each measurement contained 20 scans. The mobility data was fit by Smoluchowski's model by ZetaPLAS software.

2.3.9 Scanning electron microscopy (SEM)

Electron microscopy is a technique to observe fine details of materials in nanometre ranges. The samples can be either nanomaterials such as polymer nanoparticles, or thin-cut pieces of bulky materials such as lyophilised hydrogels. SEM is suitable to observe the surface morphology of materials since the surface is scanned by a focused electron beam and secondary electrons excited by the beam are collected for imaging. TEM, on the other hand, is suitable for internal structure identification since transmitted electrons are collected for imaging.

Sample preparation is a critical step for SEM and TEM imaging. For both techniques, samples have to be imaged in a high vacuum environment, which means only dehydrated samples could be used. During dehydration, the morphology of samples could undergo irreversible changes such as phase separation, which lead to artefacts. These artefacts should be taken into consideration when interpreting data.

Besides artefacts caused by dehydration, another possible artefact comes from sputter-coating. For SEM imaging of non-conductive samples, heavy metals such as gold or platinum have to be used as a coating layer to

increase the secondary electron emission. After coating, the signal/noise ratio will be improved, but the roughness of surface will be sacrificed a bit. For nanomaterials, the diameter may also increased.

Hydrogels samples

Hydrogel samples used form SEM study were provided by MSc students Reva Attah (PEG-crosslinked hydrogels in Section 4.2.2) and Xiaoxue Liu (CDE-crosslinked hydrogels in Section 4.3.2).

Hydrogel samples were equilibrated in different buffers for 48 h before lyophilisation. The lyophilised samples were carefully cut into tiny pieces (less than $1mm^3$) and attached to a conductive tape. Before imaged by SEM, all samples were coated with gold by an EMITECH K550 coater. The current was 20 mA and the coating time was 2 min. The coating led to approximately 12 nm gold layer. All images were acquired by a JEOL JSM-5610LV electron microscope with an accelerating voltage of 20 kV.

Nanogels samples

Nanogels samples were prepared by dropping 5 μl nanogel solution on a silica substrate, which was cleaned with chloroform, ethanol and deionised water separately and dried in an oven before use. The substrate was attached to sample holder via a conductive tape. Tiny droplets (5-10 μl) of nanogels dispersions were then carefully dropping on the substrate, and drying in the air at room temperature overnight. Before imaged by SEM, all samples were coated with platinum by a Q150T Turbo-Pumped Sputter Coater. The current was 120 mA and coating layer was 10 nm. All images were acquired by a LEO Gemini 1525 FEGSEM electron microscope with an accelerating voltage of 5 kV. *Note: chemically crosslinked nanogels used in SEM study were provided by undergraduate student Wanyue Ouyang.*

2.3.10 Transmission electron microscopy (TEM)

TEM was used to visualise hyperbranched polymer aggregations. Samples were prepared by dropping HPLP solution on a 200-mesh copper grid coated with a holey carbon film. The grid was dried in the air overnight before TEM measurement. Images were captured by a JEOL 2000FX TEM (USA) with the help of Dr Mahmoud Ardakani.

2.3.11 Turbidimetry

Turbidimetry was employed to determine the pH- and concentration-dependent phase separation of the polymers in aqueous solution. Citric acid/trisodium citric buffer solutions in a pH range from 3.0 to 6.2 were prepared by mixing 0.1 M citric acid solution and 0.1 M trisodium citric solution in different ratios. Final pH of each buffer was measured by a pH meter. HPLP polymers (salt form) were dissolved in phosphate-buffered saline at pH 7.4 by sonication. The concentrations of polymer stock solutions were 10 mg mL^{-1} and 1 mg mL^{-1} respectively. The stock solutions were diluted by 10 times or 5 times with citric buffer solutions at different pHs and left for 48 h before UV measurement. 0.8 mL solution was added to polystyrene micro-UV cuvette, and the transmittance of the solution was measured at 480 nm using a GENESYS 10S UV/Vis spectrophotometer.

2.3.12 Fluorescence Spectroscopy

Fluorescence spectra of pyrene

Fluorescence spectra of pyrene (a probe molecule) were used to evaluate the hydrophobicity of polymer aggregates. Specifically, significant changes in both emission and excitation spectra of pyrene occur when it migrates from polar to non-polar environments, including a redshift from 333 to

338 nm in the excitation spectrum. Therefore, in this study, the ratio of the intensities at 338 nm to 333 nm (I_{338}/I_{333}) in the excitation spectra was used to indicate the polarity of pyrene environments; the higher the ratio, the more hydrophobic the pyrene environment.

Typically, 1 mmol L^{-1} pyrene stock solution was prepared in methanol and stored in the dark. This pyrene stock solution was diluted with citric buffers at different pHs to make the final concentration of pyrene at 6×10^{-7} M. Polymer stock solutions (10 mg mL^{-1} and 1 mg mL^{-1}) were diluted by 10 times or 5 times with pyrene-containing citric buffer solutions. Each sample was wrapped with foil and left in the dark for 24 h before fluorescence measurement. 0.8 mL solution was added to a poly(methyl methacrylate) micro-UV cuvette and the excitation spectra (λ_{em}=390 nm) were obtained using a Jobin Yvon Horiba Fluoro Max-4 spectrofluorimeter at right-angle geometry. The width of the bandpass filter for emission was 1 nm, and that for excitation was 5 nm.

Fluorescence spectra of Nile red

Similar to pyrene, Nile red is also a hydrophobic molecule which has environment-dependent fluorescence. In the nanogel study, Nile red was used as a hydrophobic model drug for controlled-release investigation. The fluorescence spectra of Nile red were recorded to estimate its surrounding environment.

The nanogel samples used in this experiment were provided by undergraduate students Sim Wen and Benjamin Chin.

The 3D-fluorescence spectra of the Nile red loaded nanogel in different solutions were measured (for water λ_{ex}=550-610 nm, λ_{em}=630-670 nm; for released solutions λ_{ex}=500-560 nm, λ_{em}=590-660 nm). To prepare the samples, 1 mL Nile red loaded nanogels were added to 10 mL deionised water, 10 mL

simulated gastric fluid, or 10 mL simulated intestinal fluid separately. The 3D-fluorescence spectra were recorded by a Jobin Yvon Horiba Fluoro Max-4 spectrofluorimeter at right-angle geometry, with an emission and excitation bandpass filter of 5 nm for water sample, 2 nm for simulated intestinal fluid and simulated gastric fluid samples.

After examining the 3D spectra, emission spectra of the Nile red loaded nanogel in different solutions were measured from 600 to 700 nm. The optimised excitation wavelength for each solution was used (water λ_{ex}=570 nm, simulated gastric fluid λ_{ex}=515 nm, simulated intestinal fluid λ_{ex}=530 nm). The bandpass filter was 2.5 nm for both emission and excitation, via the same Fluoro Max-4 spectrofluorimeter at right-angle geometry.

Fluorescence spectra of DOX

The 3D-fluorescence spectra of the free DOX in water and DOX-loaded nanogels were measured (λ_{ex}=410-510 nm, λ_{em}=530-630 nm) to investigate the DOX environment. Free DOX sample was prepared by 100X diluting 1 mg mL^{-1} DOX stock solution in deionised water. The final DOX concentration was 10 μg mL-1. DOX-loaded nanogels samples were measured directly without dilution. The 3D-fluorescence spectra were recorded with a bandpass filter of 2.5 nm for both emission and excitation, by a Jobin Yvon Horiba Fluoro Max-4 spectrofluorimeter at right-angle geometry.

2.3.13 Critical aggregation concentration (CAC) determination

The CAC of HPLPs was determined via fluorescence spectra of pyrene via the same method mentioned above. For concentrations lower than CAC, the I_{338}/I_{333} of pyrene will stay the same which reflect the nature of polymers. However, after the concentration reaches CAC, the aggregations formed with hydrophobic cores will accommodate pyrene and changed I_{338}/I_{333}. A linear

increment of I_{338}/I_{333} will be observed until the concentration is high enough to accommodate all pyrene molecules in the hydrophobic environment.

For sample preparation, polymer stock solutions were diluted in 0.1 M pH 7.4 phosphate buffer containing 6×10^{-7} M pyrene. The sample was protected from light exposure for 24 h before fluorescence measurement. 0.8 mL solution was added to a poly(methyl methacrylate) micro-UV cuvette and the excitation spectra (λ_{em}=390 nm) were obtained using a Jobin Yvon Horiba Fluoro Max-4 spectrofluorimeter at right-angle geometry. The width of the bandpass filter for emission was 1 nm, and that for excitation was 5 nm. The ratio of intensities at 338 nm to 333 nm (I_{338}/I_{333}) in the excitation spectra was plotted against concentration to identify the CAC.

2.3.14 Rheology analysis

Rheology is a useful analytical method for hydrogel samples, to reveal the mechanical properties and even the details of the gelation process. In this study, rheology analysis was used to study the stimuli-responsiveness of hydrogels, especially the effects of those stimuli on hydrogel networks.

Hydrogel samples used in rheology analysis were provided by MSc students Reva Attah (PEG-crosslinked hydrogels in Section 4.2.4) and Xiaoxue Liu (CDE-crosslinked hydrogels in Section 4.3.4). The data in Section 4.2.4 were collected by Reva Attah under my supervision, while the data in Section 4.3.4 were collected together by Xiaoxue Liu and the author.

Rheological measurements were performed on a TA-AR2000ex Rheometer with parallel plate geometry (8 mm in diameter) at 25 ^{o}C. Hydrogels were cut into disks of 1-2mm thick by a special Hole Puncher (8 mm inner diameter) to make sure the final slice exactly fit the plate. For the pH-responsiveness study, the post-swelling hydrogel disks were soaked in different

pH buffers at room temperature for 48 h before measurement. As for the redox-responsiveness study, the hydrogel disks were immersed in DTT solution (5 molar equivalents to CDE in the hydrogel) for 48 h at room temperature.

For all measurements, oscillation mode was used. First, the linear viscoelastic region (LVR) and critical strain of the hydrogel disks were obtained by carrying out a dynamic strain sweep on the disks at a constant angular frequency of 1 rad s^{-1} while varying strain from 0.1% to 100%. Storage modulus (G') and loss modulus (G'') against strain were tested. Then, for PEG crosslinked gels, frequency sweep featured a constant strain of 0.5% and varying angular frequency from 1 rad s^{-1} to 100 rad s^{-1}. For CED crosslinked gels, the constant strain was set to 1% for frequency sweep, and the range of angular frequency was also from 1 to 100 rad s^{-1}. G' and G'' against angular frequency were recorded.

2.4 Membrane activity evaluation

To study the interaction between HPLPs and lipid membranes, different membrane models with different complexities were employed, including giant unilamellar vesicles (GUV) and sheep red blood cells.

2.4.1 GUVs formulation

In this study, GUVs were formulated with different lipid compoennts, namely DOPC and DOPS (the chemical structures of both lipids are shown in Figure 2.8a). Lipid stock solutions were prepared as follows:

- DOPC (in chloroform, 10 mg mL^{-1})
- Fluorescent DOPC (DOPC 80 μL with 1% PE (lissamine Rhodamine B) 12.8 μL, in chloroform, 10 mg mL^{-1})
- DOPC: DOPS 9:1 (in chloroform, 10 mg mL^{-1}, v/v)

- Fluorescent DOPC: DOPS 9:1 (DOPC and DOPS mixture 80 μL with 1% PE (lissamine Rhodamine B) 12.8 μL, in chloroform, 10 mg mL^{-1})

Buffer solutions were prepared as follows:

- pH 5.0 100 mM PB buffer with 0.1 M sucrose (273 mosm)
- pH 5.0 100 mM PB buffer with 0.1 M glucose (269 mosm)
- pH 7.4 100 mM PB buffer with 0.1 M sucrose (307 mosm)
- pH 7.4 100 mM PB buffer with 0.1 M glucose (304 mosm)

The osmolality of above buffer solutions was measured by a Gonotec Osmometer Gonotec Osmomat 3000 basic (Berlin, Germany). The mechanism is to measure the freezing point of the solution and fit the value with predetermined calibration. Here, the osmolality values are just for reference to make sure that the buffers used inside and outside GUV have roughly the same osmolality. If there's a huge difference on the osmolality, the GUVs will either shrink or swell and become less stable.

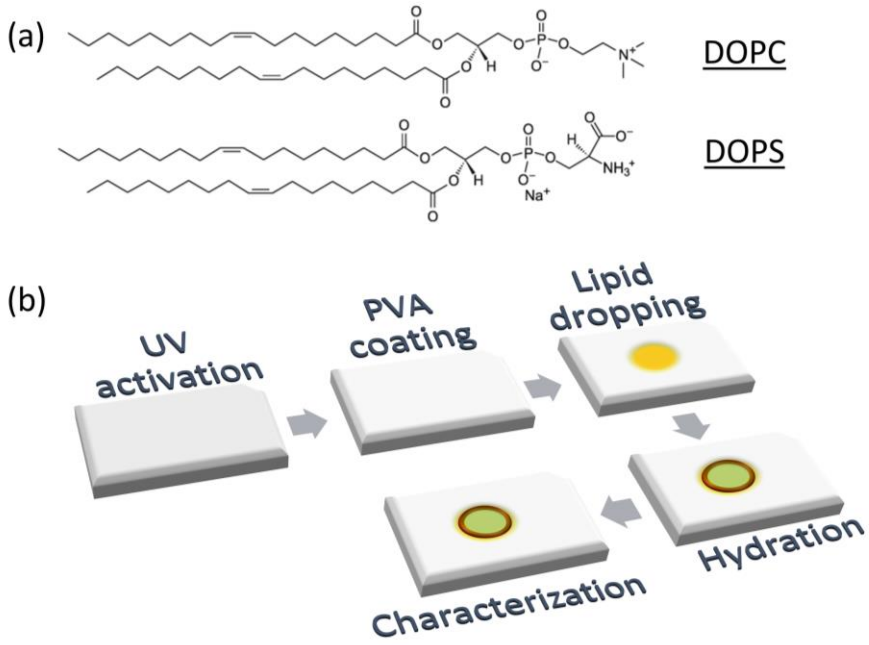

Figure 2.8 (a) The chemical structure of DOPC and DOPS. (b) Scheme of GUV formation.

GUVs used in this studied were all prepared by gel-assisted method (Figure 2.8b). Briefly, a 5% (w/w) solution of PVA was prepared by stirring PVA in water while heating at 90°C. PVA-coated substrates were prepared by following steps. Firstly, microscope glass slides were cleaned with ethanol three times, flowed by drying with compressed air. Then all glass slides were exposed to UV light for 1 h for surface activation. After that, 100 µL PVA was spread evenly on the slides, which were subsequently dried in an oven for 0.5 h at 80°C and cooled down in the fridge overnight. 5 µL lipid stock solution was dropped onto the substrates, followed by drying in the desiccator for 0.5 h. Then rubber spacers were attached to substrates to form chambers filled with sucrose buffer inside. The hydration lasted 5 h before GUVs harvesting. GUVs were stored in the fridge at 4°C and used within 48 h.

2.4.2 GUVs interaction with HPLP5 characterised by confocal microscopy

HPLP5 stock solution was prepared by dissolving salt form polymers in pH 7.4 100 mM PB buffer at 10 mg mL^{-1}. After vortex and overnight stirring, the solution was filtrated by 0.2 µm cellulose filter unit before use. HPLP5 was diluted 10 times by pH 5.0 100 mM PB buffer with 0.1 M glucose and 20 µM HPTS. The pH of the final solution was measured and adjusted to pH 5 or pH 7.4 manually.

For confocal microscopy, an observation chamber was made on a glass slide. The same rubber spacers were used filled with first 50 µL HPLP5 glucose and HPTS containing solution and then 150 µL GUVs hydrated in pH 5.0 100 mM phosphate buffer with 0.1 M sucrose. 1-2 drops of deionised water were added to the chamber to stabilise GUVs during observation. Confocal images were recorded by a Laser Scanning Confocal Microscope Zeiss LSM-510

inverted. The excitation wavelength for HTPS was 488 nm and for Rhodamine B was 543 nm. Images were further processed by Image J and Volocity.

2.4.3 Haemolysis assay

Haemolysis was used to evaluate red blood cell membrane damage quantitatively, by measuring the leakage of haemoglobin by UV absorbance. If polymer, nanogels or other membrane penetrating molecules cause significant defects on RBC membrane, haemoglobin will be released from cells and diffuse into buffers. By comparing the haemoglobin leakage with positive and negative controls, the membrane-lytic activities of these molecules can be deduced.

In this experiment, sheep RBCs were used and the related safety document (Bio1 Form) was enclosed in the Appendix for reference. RBCs were first washed three times with 150 mM NaCl solution before use to remove protective reagents and cell debris. For each wash step, 1 mL RBCs in an Eppendorf tube were centrifuged at 4000 rpm, and the supernatants were removed. 1 mL fresh 150 mM NaCl was added and mixed with RBC pellets by gently shaking the tube upside down a few times. Then RBCs were redispersed in different pH buffers or different pH NaCl solutions at a density of 1-2 x 10^8 cells mL^{-1}. HPLPs, PLP-NDA18, melittin, poly(L-lysine), poly(L-arginine) and PLP-NDA18 based nanogel stock solutions were first prepared and then diluted in RBCs containing buffers. The final volume of each sample was kept at 1 mL. These samples were incubated in a 37 °C water bath for 1 h with linear shaking at 120 rpm. After incubation, the samples were centrifuged at 4000 rpm, and the absorbance of the supernatant was measured at 540 nm by a GENESYS 10S UV/Vis spectrophotometer (Thermo Fisher Scientific, USA). RBCs incubated with buffers only (without any membrane-disruptive molecules) were used as negative controls, while RBCs incubated with deionised water were used as positive controls. Three replicates were used for each sample and

results were presented as mean ± standard deviation (SD). The haemolysis percentage was calculated as below:

$$Haemolysis\ (\%) = \frac{A_{540}(Sample) - A_{540}(Negative\ Control)}{A_{540}(Positive\ Control) - A_{540}(Negative\ Control)} \times 100\%$$

(Equation 2.2)

2.4.4 Imaging of ghost red blood cells by confocal microscopy.

RBCs were first washed three times with 150 mM NaCl solution before use to remove protective reagents and cell debris. After washing, RBCs were resuspended in the pH 5.0 citrate buffer (100 mM) or pH 7.4 phosphate buffer (100 mM) at a density of 1-2 $\times 10^7$ cells mL^{-1}. FITC-dextran with different molecular weights (10K, 70K and 150K Da, with a final concentration at 10 μM) and Texas Red® hydrazide (with a final concentration at 1.5 μM) were added to RBCs suspension, followed by the addition of HPLP5 (final concentration at 1 mg mL^{-1}). RBCs in buffers without HPLP5 were served as negative controls. Confocal images were taken by an LSM-510 inverted laser scanning confocal microscope (Zeiss, Germany) at the excitation wavelengths of 488 nm for FITC-dextran (green channel) and 543 nm for Texas Red® hydrazide (red channel). For videos of haemolysis, images were taken every second for 15 min.. All images were processed with Image J.

2.5 Mammalian cell based assays

2.5.1 Mammalian cell culture

HeLa cell (Biosafety Level 2) was used in this study for cytotoxicity evaluation and intracellular delivery. The risk assessment document (Bio1 Fom) of cell culture was attached in the Appendix for reference. The adherent cells

were cultured in DMEM medium containing 10% (v/v) FBS, 100 units mL^{-1} penicillin and 100 μg mL^{-1} streptomycin unless specified. These cells in cell culture flasks were observed under an optical microscope on a daily basis to check the density and morphology. Every 2-3 days, cells with a confluence of 70-80% were passaged to new flasks to maintain the growth. In a typical cell passaging experiment, cells were trypsinised by trypsin-EDTA in a 37 °C incubation for approximately 3 min until more than 70% of cells became detached. Then an equal amount of cell culture medium was added to deactivate trypsin, and the bottom of cell culture flask was gently washed with cell suspensions. The suspension was centrifuged at 4000 rpm for 5 min to allow cells sedimentation. Then the supernatant was removed, and cell pellets were resuspended in the fresh culture medium by pipetting. The cell suspensions were added to 3 new flasks in a humidified incubator with 5% CO_2 at 37 °C.

For long-term storage, cells were cryopreserved in liquid nitrogen following standard methods. Briefly, cells were harvested, and the density was identified by a haemocytometer. Then, the harvested cells were centrifuged at 4000 rpm for 5 min and resuspended in cryopreservation medium which contained 5% DMSO (v/v), 10% FBS (v/v) and 85% DMEM. The final cell density in the cryopreservation is between 5 x 10^6 to 1 x 10^7 cells mL^{-1}. Cell aliquots were placed into cryogenic storage vials (1mL per vial) and then transferred to a Mr Frosty™ in a -80 °C freezer. After overnight incubation at -80 °C, cryogenic storage vials were transferred to liquid nitrogen.

For thawing frozen cells from liquid nitrogen, a water bath was preheated to 40°C. Then cryogenic storage vials were placed into the water bath with gentle shaking. Once all the ice has melted, the cell suspension was centrifuged at 4000 rpm for 5 mins, and the cryopreservation medium was removed. The

cell pelleted was resuspended in fresh cell culture medium and transferred into culture flasks for incubation.

2.5.2 Cytotoxicity assay

The cytotoxicity of materials was evaluated by the alamarBlue® assay. The mechanism of the alamarBlue® assay was to evaluate the live cell metabolic activity. The active reagent of alamarBlue® is non-fluorescent and able to permeate into cells. In live cells, this reagent could be reduced by intracellular enzymes to generate a highly fluorescent product. By measuring the fluorescence intensity of the cell media, the average metabolic activity could be calculated.

In a typical cytotoxicity experiment, HeLa cells were seeded in 96-well plates at a density of 2-10×10^4 cells mL^{-1} and cultured for 24 h. Then tested materials (e.g. HPLP, hydrogel, melittin, poly(L-lysine) poly(L-arginine)) were prepared in DMEM at different concentrations and filtered with a 0.22 μm filter unit. The cells were treated with these materials for 24 h, while those cells treated with culture medium were used as controls. The material-containing medium was then removed, and cells were washed with PBS, followed by the addition of 10% alamarBlue® (v/v). The plate was further incubated at 37 °C, 5% CO_2 for 4 h before measurement of the fluorescence at 525 nm excitation/ 580-640 nm emission wavelengths by a microplate reader (GloMax®-Multi+ Microplate Multimode Reader, Promega). The wells with alamarBlue® but without cells served as background. Cell viability was calculated from fluorescence readings of the wells. Five replicates were used for each sample and results were presented as mean ± SD.

2.5.3 Intracellular delivery of model drugs

Calcein is a membrane-impermeable fluorescent molecule served as a model drug. HeLa cells were seeded in a MatTek glass-bottom petri dish at a density of 5×10^5 cells mL^{-1}. The cells were incubated for 24 h, before the addition of 2 mL serum-free DMEM containing 2 mg mL^{-1} calcein and 1 mg mL^{-1} HPLP5. Those cells incubated with calcein in the absence of HPLP5 were used as the control. After 1 h incubation, the medium containing calcein was removed, and the cells were washed with PBS for three times. Fresh complete DMEM medium was added for a further incubation of 5 h. Cells were stained with Hoechst 33342 (for nuclei visualisation) and LysoTracker® (for endosome and lysosome visualisation) for 20 min in the incubator just before imaging. A Zeiss LSM-510 inverted laser scanning confocal microscope was used for recording images. The excitation wavelength was 405 nm for Hoechst 33342 (blue channel), 488 nm for calcein (green channel) and 543 nm for LysoTracker® (red channel). All images were processed with Image J.

2.6 Hydrogel swelling studies

Hydrogel samples used in swelling studies were provided by MSc students Reva Attah (PEG-crosslinked hydrogels in Section 4.2.3) and Xiaoxue Liu (CDE-crosslinked hydrogels in Section 4.3.3). The data in Section 4.2.3 were collected by Reva Attah and the data in Section 4.3.3 were collected by Xiaoxue Liu under my supervision.

Before swelling studies, each hydrogel was taken out of the deionised water and cut into disks (with a diameter of 11-12 mm and a thickness of approximately 2 mm). Then the disks were immersed either in 0.1 M citrate buffer at pH 3 or in 0.1 M phosphate buffer at pH 7.4 for 48h at room temperature, after which their wet weight (m_w) were measured. These samples

were soaked in deionised water again for 48 h, followed by lyophilisation (VirTis BenchTop Pro freeze-dryer) to obtain the dry weight (m_d). The swelling ratio *q* was defined as follows:

$$q = \frac{m_w}{m_d} \quad \text{(Equation 2.3)}$$

Three replicates were used for each sample and results were presented as mean ± SD. Student's paired samples *t*-test was performed to show the statistical difference.

2.7 Hydrogel loading and release

2.7.1 Model drug loading and release

Hydrogel samples used in model drug loading and release were provided by MSc students Reva Attah (PEG-crosslinked hydrogels in Section 4.2.5) undergraduate students Jiali Li and Yitong Chen. Reva Attah did the model drug fluorescein loading in PEG-crosslinked hydrogels, and the subsequent release in pH 3.0 and pH 7.4 buffers. Jiali Li and Yitong Chen did the same model drug loading, but release in biorelevent buffers. MSc student Xiaoxue Liu prepared the CDE-crosslinked hydrogel samples used in Section 4.3.5, and did the loading and release in different pH buffers. The author did the release kinetics and release in DTT containing buffers.

Model drug fluorescein loading

Hydrogel disks were first equilibrated in pH 3.0, 100 mM citrate buffer for 48h at room temperature. After 48h, each disk was rinsed with deionised water and then immersed in 2 mL of loading solution, which contained 5 mg mL^{-1} sodium fluorescein dissolved in pH 7.4, 20 mM phosphate buffer. After 48 h, 5.4 µL 14%HCl (v/v) was added to the loading solution to collapse the hydrogels

for another 24h. After loading, the remained fluorescein unloaded was transferred to a 100 mL volumetric cylinder. The cylinder was topped up by pH 7.4, 100 mM phosphate buffer until the total volume reached 100 mL. The absorbance of this solution was quantified by UV absorbance at 488 nm. The fluorescein concentration was calculated based on the calibration curve in pH 7.4, 100 mM phosphate buffer. Then the amount of fluorescein loaded (m_l) was calculated by subtraction of unloaded portions from the total fluorescein added.

Fluorescein release

Biorelevent buffers such as simulated gastric fluid (SGF) and simulated intestinal fluid (SIF) were used for drug release study, to mimic the *in vivo* environments. SGF was prepared by dissolving NaCl (2.0 g) and HCl (7 mL) in deionised water, and more deionised water was added to make the final volume to 1 L. The pH of the final solution was determined by a pH meter (pH~1.2). Simulated intestinal fluid (SIF) was prepared by dissolving KH_2PO4 (6.8 g) in 500 mL deionised water, followed by adding 0.9 g NaOH. The well-mixed solution was then topped up with deionised water to 1 L, and the pH was adjusted to 6.8.

For release study, fluorescein-loaded hydrogel disks were placed in 10 mL different release buffer respectively. For constant release at acidic pH and neutral pH, the release buffers were pH 3.0 20 mM citrate buffer and pH 7.4, 20 mM phosphate buffer. For GI tract mimicking release, the buffers were SIF and SGF. The release samples were placed in a water bath at 37 ºC with gentle agitation. At pre-determined time points, samples of 100 µL were taken out of each tube and replaced with fresh 100 µL of the respective buffer. The samples were diluted in pH 7.4, 100 mM phosphate buffer before their absorbance was read via a UV/Vis spectrophotometer (GENESYS 10S). The percentage of released drugs was calculated as follows:

$$\%\ released = \frac{m_r}{m_l} \times 100 \qquad \text{(Equation 2.4)}$$

Where m_r is the amount of released drug at a specific time point, and m_l is the amount of drug loaded into the hydrogels. Three replicates were used for each sample and results were presented as mean ± SD. Student's paired samples *t*-test was performed to show the statistical difference.

Nile red loading

Nile red stock solution was prepared in acetone at a concentration of 20 mg mL^{-1}. Then 1 µL Nile red stock solution was added to 10 mL pH 3.0 100 mM citrate buffer and pH 7.4 100 mM phosphate buffer respectively. The solutions were bath sonicated for 0.5 h to get Nile red dispersion at a final concentration of 2 µg mL^{-1}. Hydrogel disks were soaked in Nile red dispersion for 24 h at room temperature before imaging by confocal microscopy (Laser Scanning Confocal Microscope Zeiss LSM-510 inverted). The excitation wavelength used was 543 nm. Confocal images were processed by Image J and Volocity.

2.7.2 Probiotics loading and release

Preparation of LGG single colonies

LGG stock strain provided by Dr Krishnaa Mahbubani was defrosted from -80 °C and poured into a 50-mL falcon tube with 30 mL MRS broth. The tube was incubated in a shaking incubator overnight at 37 °C.

A single colony of bacteria was obtained by a streak plate method (Figure 2.9). Briefly, thoroughly mixed bacteria samples were transferred to an agar plate by a sterile inoculation loop. The loop was dragged gently forward and backwards in a zigzag pattern several times to leave streaks on one side of the plate. Then a new sterile loop was used to drag some bacteria from the

first streaks and continued moving in a zigzag pattern. The second streaks were perpendicular to the first ones, with one or two overlapping points. The procedure was repeated once to obtain third streaks.

The agar plate was kept in an incubator at 37 °C for two days. Isolated colonies would be available on second and third streaks (Figure 2.9). Then the plate was stored in fridge as a working stock of the strain.

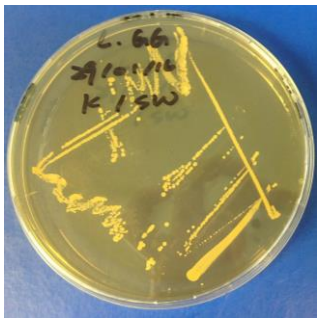

Figure 2.9 Three-way dilution streak plate image.

LGG loading

Hydrogels were prepared as previously described in Section 2.2.2.2. To study the solid contents' effects on loading and release, GEL1 and GEL3 were used to represent high and low solid content hydrogels respectively.

A LGG single colony was seeded in 30 mL MRS broth and incubated at 37 °C in a shaking incubator overnight. The bacteria suspension was diluted, and OD_{600} was measured. The suspension was then centrifuged at 2000 g for 20 min. The supernatant was discarded, and white sticky bacteria pellet was resuspended in 10 mL PBS or fresh MRS broth as loading solutions. Hydrogels were cut into quarters and placed into different loading solutions. These loading solutions were incubated at 37 °C in a shaking incubator for 24 h.

For the extraction of loaded LGG, hydrogels loaded with LGG were crashed onto a 40 μm mesh by a syringe rubber plunger head and ground into

tiny pieces. The pieces were washed by fresh MRS broth to pass through the 40 μm mesh. 4 mL MRS in total was used to wash away all fragments from the mesh, and the suspension was kept for 10 min before bacteria counting, to make recover bacteria from the stressed state.

Then the amount of extracted LGG was quantified by drop-plate technique. In brief, the MRS with loading LGG and hydrogel pieces were diluted by 10^1, 10^2, 10^3, 10^4 and 10^5 times by fresh MRS. Then 5 replicate drops of each dilution (10 μL per drop) were dispensed simultaneously onto an agar plate. Once the dropped MRS dried, the plate was incubated at 37 °C for two days before CFU counting. The results were presented as mean ± SD. Student's paired samples *t*-test was performed to show the statistical difference.

LGG release

Hydrogel quarters loaded with bacteria were placed in 10 mL MRS broth, incubated in a shaking incubator at 37°C. The bacteria released were quantified by the drop plate method at different time points. The bacteria remained in the hydrogels was also quantified by the extrusion method described above. The results were presented as mean ± SD. Student's paired samples *t*-test was performed to show the statistical difference.

2.8 Nanogel loading and release

2.8.1 Nile red loading and release in physically crosslinked nanogels

Nile red loading

Nile red was loaded *in situ* during nanogel synthesis. First, a stock solution was prepared by dissolving Nile red (10 mg) in DMF (1 mL). PLP-

NDA18 (10 mg) was dissolved into another 400 µL DMF, followed by the addition of 100 µL Nile red stock solution. The mixture was then dropped into 50 mL deionised water under vigorous stirring. Once the PLP-NDA18 Nile red solution was added, the deionised water became purple. After addition all PLP-NDA18 and Nile red, the mixture was left stirring another hour, before dialysis against deionised water for three days. The deionised water was replaced twice a day. The dialysed Nile red containing nanogel dispersion was stored in a 4 °C fridge before use. During all this experiment, Nile red containing solutions were protected from light by foil.

The amount of the loaded Nile red was determined by a modified extraction method. Specifically, a 5 mL aliquot of Nile red-loaded nanogel solution was lyophilised, and the powders were re-dissolved in DMSO. The fluorescence of Nile red in DMSO was then measured by a GloMax®-Multi+ Microplate Multimode Reader (Promega, USA) at the excitation wavelength of 570 nm and the emission wavelength of 610-640 nm. Triplicate samples were used for each experiment.

Preparation of biorelevent buffers

SGF and SIF were prepared as described in Section 2.7.1.

Simulated fasted gastric fluid (FaSSGF) was prepared as previously reported in the literature (Aburub et al. 2008). Briefly, sodium taurocholate (41 mg), lecithin (13 mg) and NaCl (2.0 g) were weighed and added to deionised water (500 mL). The mixture was stirred until a clear solution was obtained and topped up with DI water to 1 L, after which 1 M HCl was added to adjust the pH to 1.6.

Simulated fasted intestinal fluid (FaSSIF) was also prepared as previously reported (Söderlind et al. 2010). NaOH (0.34 g), NaH_2PO4

(anhydrate, 3.48 g) and NaCl (6.20 g) were added to 1 L deionised water. Then the solution was adjusted to pH 6.5 with 1 M HCl. Biosurfactant sodium taurocholate (1.65 g) and lecithin (0.152 g) was added. Further sonication for 2 h using a probe tip sonicator (amplitude 100%, pulse 1s on and 1s off) was performed until a clear solution was obtained. The pH of the FaSSIF buffer was determined by a pH meter.

SGF with a high amount of biosurfactant (SGF-biosurfactant) was prepared as a control, by mixing 500 mL SGF buffer with 0.825 g sodium taurocholate and 0.076 g lecithin. The mixture was sonicated for 2 h using a probe tip sonicator (amplitude 100%, pulse 1 s on and 1 s off) to obtain a clear solution.

Nile red release

1 mL Nile red-loaded nanogel dispersion was added to a dialysis bag (M_w 12-14 kDa cut-off) and the bag was placed in 15 mL release solution (FaSSGF, FaSSIF or SGF-biosurfactant). The release was performed in a shaking water bath at 37 °C with gentle agitating. At specific time intervals, the release sample in the dialysis bag was transferred to a new tube with 15 mL fresh release solution. The previous tube with released Nile red was removed from the water bath, lyophilised to eliminate aqueous nanogel medium and re-dissolved in DMSO for fluorescence measurement (excitation: 570 nm, emission: 610-640 nm). Triplicated samples were used for release experiment.

At the same time, a series of time-dependent negative controls were run in parallel to define the release maximum at each time point. 1 mL Nile red-loaded nanogel dispersion was directly added to 15 mL corresponding release solution incubated in the same shaking water bath at 37 °C. Triplicate samples for each time intervals. At specific time point, negative control tubes for that

time point were removed from the water bath for lyophilisation, and the fluorescence was measured via the same method for released samples mentioned above. Cumulative release (%) was calculated based on the normalisation of the negative control:

$$\%\, released = \sum_0^t \frac{F_{released-t}}{F_{control-t}} \times 100 \qquad \text{(Equation 2.5)}$$

Where $F_{released\text{-}t}$ represents the average fluorescence intensity of the released sample at a specific time point and $F_{control\text{-}t}$ represents the average fluorescence intensity of the negative control at that point. The cumulative release was the sum of all the released percentage from the starting point to time t.

2.8.2 Doxorubicin loading and release in chemically crosslinked nanogels

Doxorubicin was loaded *in situ* during nanogels synthesis. First, a stock solution was prepared by dissolving doxorubicin hydrochloride (10 mg) in DMSO (10 mL). Then 5 mg PLP-Py20 was dissolved in 1 mL DOX-DMSO stock solution. Subsequently, 4.5 mL HEPES (10 mM pH=7.0) containing DTT (0.25 mg, 1.6 μmol, 0.5 molar equivalent to pyridine groups on PLP-Py20) was quickly added to DOX-DMSO under vigorous stirring. The mixture was stirred at room temperature for 1 h, before dialysis against deionised water for 3 days. The deionised water was replaced twice a day. The dialysed DOX containing nanogel dispersion was filtered by 0.22 μm filter unit and stored in a 4 °C fridge before use. During all these steps, DOX solutions were protected from light by foil.

DOX release was performed in SGF, and SIF with or without 10 mM DTT. 0.1 mL DOX-loaded nanogel dispersion was added into a 1 mL released buffer,

and the emission fluorescence spectra of the released solution was recorded by a Jobin Yvon Horiba Fluoro Max-4 spectrofluorimeter at right-angle geometry. The excitation wavelength was 480 nm, and the bandpass filter was 2.5 nm for both emission and excitation.

Chapter 3

Hyperbranched polymers for intracellular drug delivery

This Chapter describes a series of lysine-based, CPP-mimicking, hyperbranched polymers for intracellular drug delivery applications. The polymers were synthesised via a polycondensation method. Before setting up the method, several model reactions were used to verify the reactivity of crosslinkers and the reaction conditions. The polymer structures were characterised by NMR, GPC, FTIR, DSC and TGA. Then their physiochemical properties were evaluated by turbidimetry, fluorescence spectroscopy, DLS, and TEM, to demonstrate pH-induced conformational changes in aqueous solutions. The interactions between these polymers and lipid membranes were tested using model lipid membranes to optimise the membrane-lytic ability and elucidate the mechanism. Finally, the intracellular delivery of a model drug was performed.

This Chapter is partially based on the publication (Wang & Chen 2017). Figures, tables and texts were reproduced and reprinted with permission from ACS Publications.

3.1 Introduction

Inefficient intracellular delivery is a critical barrier to the screening and development of biomacromolecular therapeutic agents for medical application (Torchilin 2014; Mitragotri et al. 2014). If biomacromolecules such as oligonucleotides, peptides and proteins are presented to target cells, the following endocytosis causes them to be entrapped in endosomes and eventually degraded in lysosomes by various enzymes (Shete et al. 2014; Leader et al. 2008). Therefore, it is of great importance to design smart carriers

to facilitate the escape of biomacromolecules from endosomes into the cytoplasm.

Cell-penetrating peptides (CPPs) are considered as promising carriers for intracellular delivery (F. Wang et al. 2014). Derived from natural peptides of virus or bacteria, these peptides can interact with lipid membranes and translocate viruses or bacteria into the cytoplasm. Most CPPs are cationic and arginine-rich (Ramsey & Flynn 2015). The positive charge is believed to play an essential role in cell-penetration because of the electrostatic interaction with negatively charged cell membranes (Futaki et al. 2001). However, there are a few anionic CPPs, such as fusogenic peptides derived from the N-terminal sequence of the influenza virus hemagglutinin subunit HA2 and p28 derived from azurin (Milletti 2012). These peptides are amphiphilic, which facilitates their interaction with cell membranes. Compared with most cationic CPPs with a direct membrane penetration ability even at physiological pH, the membrane activity of anionic amphiphilic CPPs is pH-dependent. The membrane-lytic activity of anionic amphiphilic CPPS at physiological pH is negligible, while increases significantly at endosomal pH due to pH-triggered conformational changes (Li et al. 2004; Zorko & Langel 2005). Because of this, anionic CPPs are considered to be more biocompatible than cationic ones, thus demonstrating a promising potential for cytoplasmic drug delivery (Kauffman et al. 2015).

Despite the intensive research on linear CPPs in the past two decades, nowadays increasing interest has been focused on development of branched multivalent CPPs, with higher cell penetration efficiency, higher serum stability, reduced biodegradation and higher loading capacities than linear CPPs (Eggimann et al. 2014). Attention has thus far been mainly paid to cationic branched CPPs based on grafting of natural linear CPPs such as TAT to a

hyperbranched or dendritic polymer backbone (Angeles-Boza et al. 2010), or the synthesis of branched arginine-rich polypeptides as natural mimics (Saleh et al. 2010; Futaki et al. 2002). The results showed that a certain degree of branching could enhance the membrane penetration efficiency, but could also unavoidably lead to an increased cytotoxicity (Saleh et al. 2010).

Although many linear or branched CPPs have been reported for intracellular delivery of macromolecules or even nanoparticles, there are potentially severe side effects including significant non-specific binding to cell membranes (Bolhassani 2011). Also, the prohibitively high costs limit their application in large scales (Chen & Harrison 2007; David et al. 2012). Biomimetic amphiphilic polymers, which have similar membrane-penetrating potentials, are thus considered as more cost-effective and safer alternatives. Previous studies mainly focused on guanidine-containing polymers which mimic arginine-containing CPPs. For instance, there are reports about guanidine-based methacrylamide copolymers (Treat et al. 2012; McKinlay et al. 2016), guanidinium-rich oligocarbonate (Cooley et al. 2009), and poly(disulfide)s (Gasparini et al. 2014; Fu et al. 2015) as effective molecule transporters. Despite the high potency, their strong ionic interaction with negatively charged cell membranes and the subsequent high cytotoxicity of those positively charged polymers remains a big issue. The non-specific membrane bindings may also lead to poor *in vivo* activity and systematic toxicity (Lv et al. 2006). In contrast, little attention has been paid to non-cationic biomimetic membrane-penetrating polymers.

Recently, a series of negatively charged, easy-to-prepare, pH-responsive polyamides has been developed to mimic influenza viral fusogenic CPPs (Eccleston et al. 1999; Chen et al. 2005; Chen, Eccleston, et al. 2009; Chen et al. 2017). The linear, amino acid-based, parent polymer, poly(L-lysine

isophthalamide), only showed limited membrane-lytic capacity at lysosomal pH (Eccleston et al. 2000). By grafting hydrophobic pendant groups, the pH-responsive conformational change and endosomolytic activity could be manipulated (Chen, Khormaee, et al. 2009b; Chen et al. 2005; Chen, Khormaee, et al. 2009a; Chen et al. 2017). Thus, the cytoplasmic delivery of small-molecule model drugs and bioactive macromolecules (e.g. therapeutic proteins and siRNA) could be achieved *in vitro* and in *vivo* (Khormaee et al. 2013; Song et al. 2013; Ho et al. 2011).

In this Chapter, a hyperbranched topology was introduced to increase the membrane penetrating activity of poly(L-lysine isophthalamide). The synthetic route was developed, and their specific hyperbranched structures were carefully characterised. Furthermore, their pH-responsive hydrodynamic behaviour was investigated. Polymer-membrane interaction study was performed on model lipid systems including giant unilamellar vesicles and sheep red blood cells. Finally, the cytotoxicity was evaluated, and the efficient cytoplasmic delivery in mammalian cells was demonstrated.

3.2 Results and discussion

3.2.1 Model reactions

In order to have a good understanding of the crosslinker, 1,3,5-benzenetricarboxylic acid chloride, model reactions between the crosslinker and several model molecules were performed, including butylamine, L-phenylalanine methyl ester dihydrochloride and Boc-L-lysine. All of these model molecules have only one available primary amine group for reacting with 1,3,5-benzenetricarboxylic acid chloride. Instead of yielding crosslinked polymers, small-molecular products with similar structures to the crosslinking unit would be formed, and their structures provide useful information for NMR spectra

interpretation. For example, the chemical environment of the NH_2 group of butylamine was similar to the Nε amine of L-lysine. So the products of the model reaction between 1,3,5-benzenetricarboxylic acid chloride and butylamine would be a good reference for identification of amide, benzyl and other adjacent groups in ^{1}H-NMR.

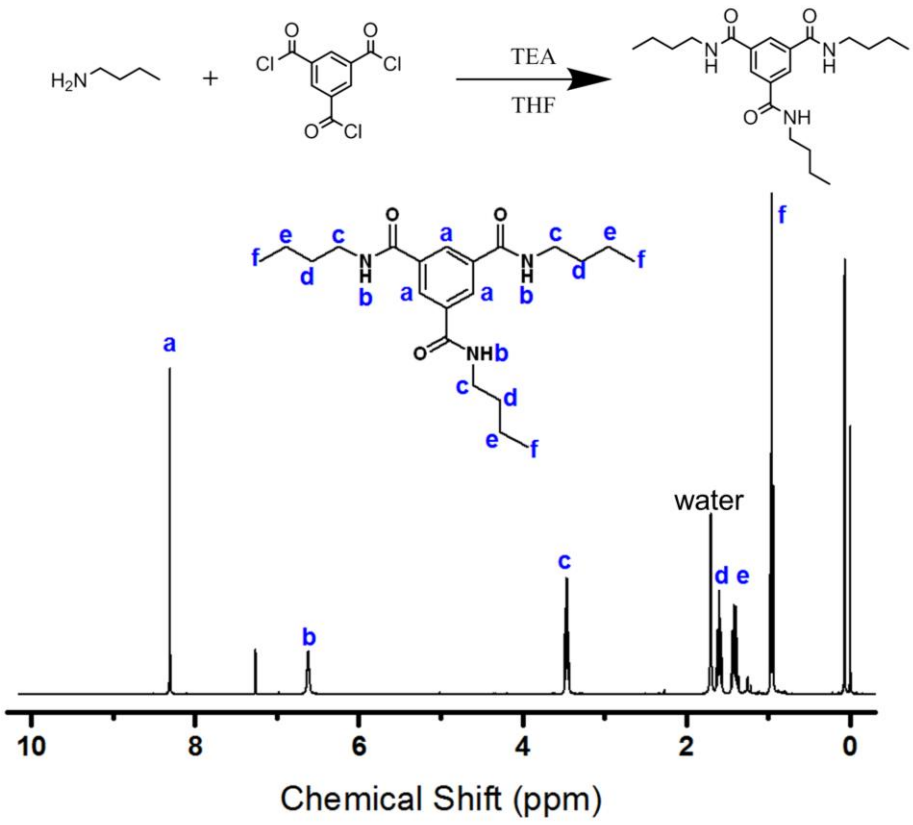

Figure 3.1: ^{1}H-NMR spectrum of the product of model reaction1. ^{1}H-NMR (400 MHz, $CDCl_3$): δ (ppm) 0.96 (9H, t, H_f, CH_3), 1.42 (6H, m, H_e, CH_2), 1.60 (6H, m, H_d, CH_2), 3.46 (6H, m, H_c, CH_2), 6.62 (3H, t, H_b, N*H*), 8.31 (3H, s, H_a, C*H*).

Figure 3.1 showed the ^{1}H-NMR spectrum of the purified product from this model reaction. When 1,3,5-benzenetricarboxylic acid chloride and butylamine reacted at a stoichiometric ratio of 1:3 in THF, which means all acyl chloride reacts with amine, a highly symmetric tri-substitute amide was formed. The formation of tri-substitutes means the reactivity of 1,3,5-benzenetricarboxylic acid chloride was sufficiently high for crosslinking

reaction. The NMR results also showed the chemical shift of the proton on the aromatic ring (H_b) was 8.31 ppm, much lower than the one on the reactant 1,3,5-benzenetricarboxylic acid chloride (9.09 ppm, NMR spectra in the appendix, Figure S1). Since amide had less electron negativity than acyl chloride, the electron density of aromatic rings in the tri-substituted product increased, which led to an increased shielding effect. The chemical shift, which reflected this effect, shifted to higher fields.

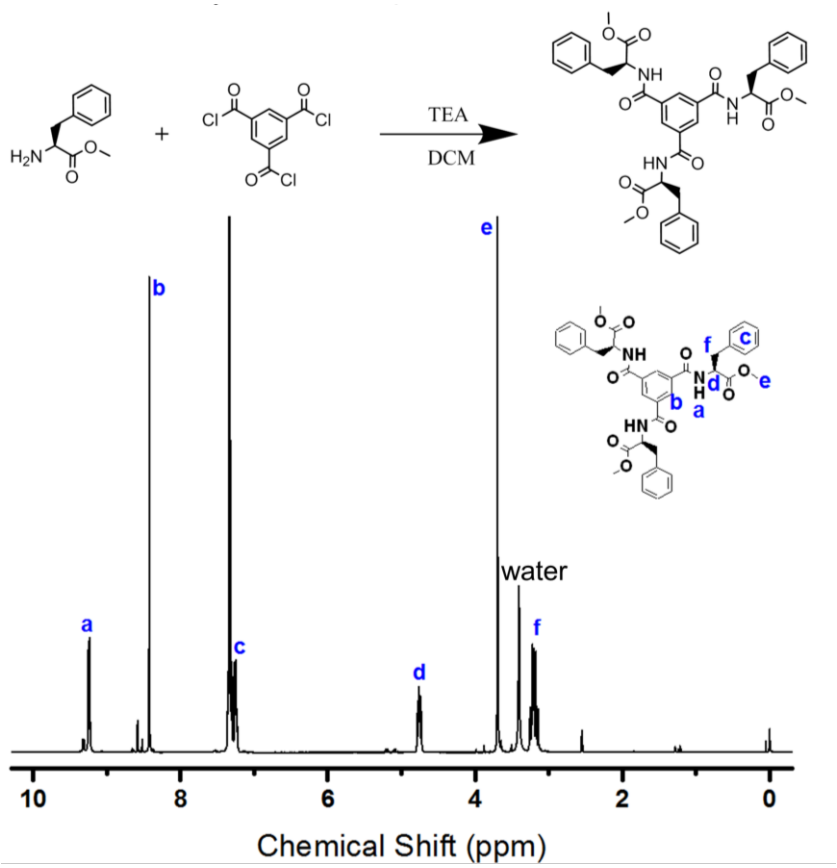

Figure 3.2: ^{1}H-NMR spectrum of the product of model reaction 2. ^{1}H-NMR (400 MHz, DMSO-d_6): δ (ppm) 3.20 (6H, m, H_f, CH_2), 3.69 (9H, s, H_e, CH_3), 4.76 (6H, m, H_d, C*H*), 7.38-7.21 (15H, m, H_c, C*H* on the phenylalanine aromatic ring), 8.43 (3H, s, H_b, C*H*), 9.23 (3H, d, H_a, N*H*).

To mimic the Nα amine of L-lysine, L-phenylalanine methyl ester was used. Though the side chain of these amino acids varied, the Nα amine and adjacent tertiary carbon environment remained the same. As shown in Figure 3.2, the product was also a tri-substituted amide, although the steric effects

hindered the reactivity of amine slightly. The chemical shift of the protons on the aromatic ring (H_b) was 8.43 ppm, similar to the one in the previous case (Figure 3.1 H_b). It was thus deduced that the tri-substituted crosslinking unit's peak would appear at around 8.3-8.5 ppm.

In the third model reaction, Boc-L-lysine was used as a better analogue to L-lysine. Instead of reacting in organic solvents, this time the reaction was performed in acetone and water mixture system, which was the same as the final reaction condition for polymer synthesis, in order to better mimic the polymerisation reaction. In this case, even though an excessive amount of Boc-L-lysine was presented, mono-, di- and tri- substitutes formed in the bi-solvent system, as shown in Figure 3.3.

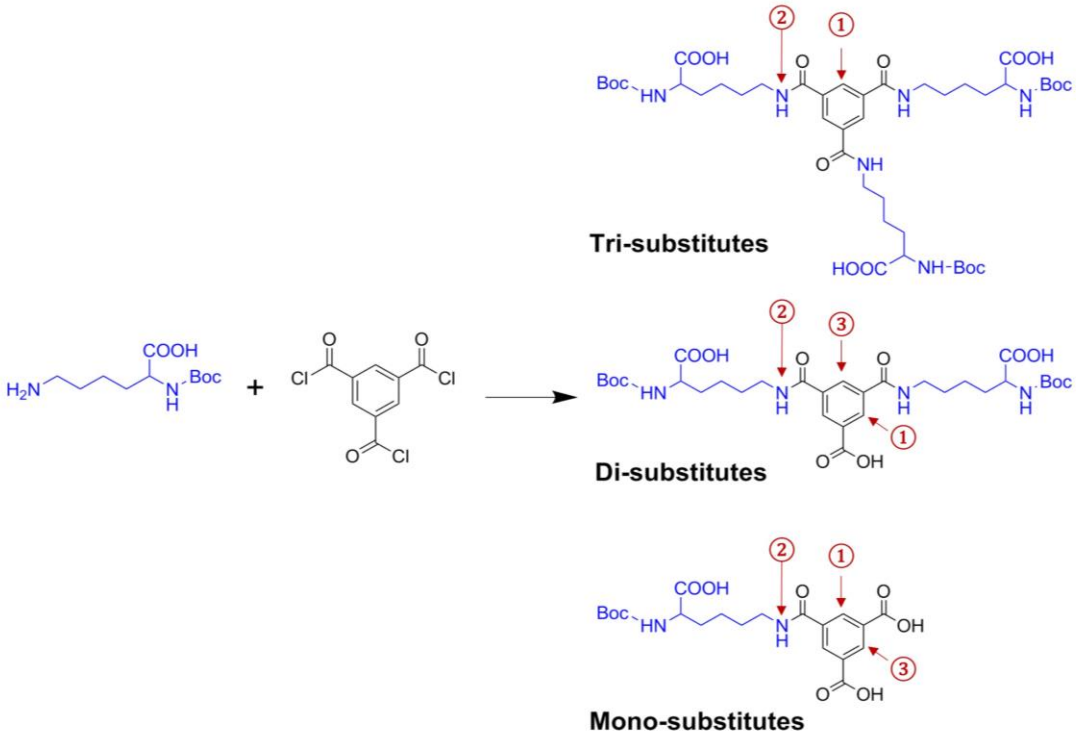

Figure 3.3 Scheme for the model reaction between the monomer analogue, Boc-L-lysine and the crosslinker, 1,3,5-benzenetricarboxylic acid chloride.

The characteristic peaks of each substitute were identified in Figure 3.4, and the chemical shifts and integrations were listed in Table 3.1. The peaks

were assigned by peak split, chemical shift and integrations altogether. The molar ratio of the three substitutes was calculated as below:

$$Trisubstitutes: disubstitutes: monosubstitutes = \frac{I_{T1}}{3}:\frac{I_{D1}}{2}:\frac{I_{M1}}{2} = 1: 0.46: 0.1$$

(Equation 3.1)

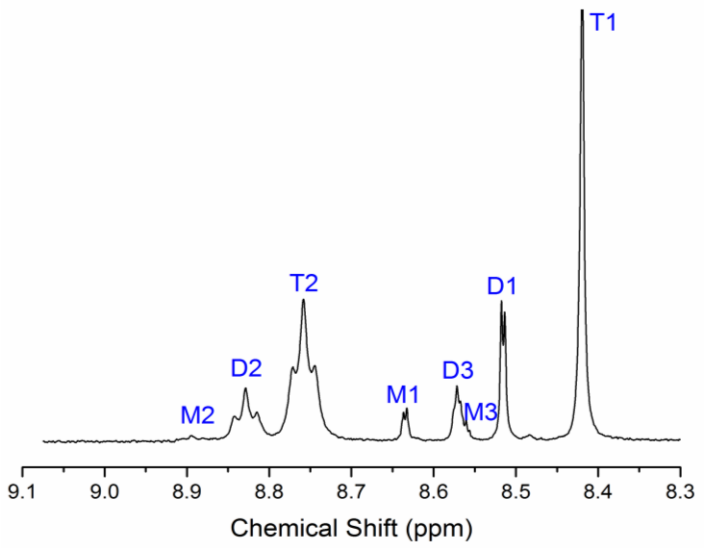

Figure 3.4 Zoomed-in ^{1}H-NMR spectrum of the product between 8.3 and 9.1 ppm where peaks corresponding to the protons on aromatic rings and amine groups locate.

Approximately two-thirds of the crosslinkers were substituted by Boc-L-lysine, indicating that the reactivity of the crosslinker was relatively high. In other words, in the polymerisation, approximately two-thirds of crosslinkers may form crosslinking units. At the same time, approximately one-third of the crosslinkers became di-substituted, which may contribute to the linear part in the polymerisation. Only 6% ended up being mono-substituted, which may become terminations of polymers.

The NMR spectra of unpurified products were also acquired (See appendix, Figure S2), and the ratio of three species was calculated (tri-substitutes: di-substitutes: mono- substitutes = 1: 0.43: 0.4). Before purification, the resolution of the spectrum was not good enough, which may lead to

integration errors. Nevertheless, the majority of the products were still tri-substitutes, which was in agreement with the results in Figure 3.4.

Table 3-1 Details of the peaks in Figure 3.3b.

Peak	Chemical shift (ppm)	Integration[a]
T1 (3H, s, C*H*)	8.42	3.00
T2 (3H, s, N*H*)	8.76	2.86
D1 (2H, d, C*H*)	8.52	0.93
D2 (2H, t, N*H*)	8.83	0.94
D3 (1H, d, C*H*)	8.57	0.43
M1 (2H, d, C*H*)	8.63	0.21
M2 (1H, t[b], N*H*)	8.89	0.06
M3 (2H, d[b], C*H*)	8.56	0.09

a Normalised by T1.

b Not very clear on the spectra due to overlapping with peak D2 or D3.

The last model reaction was performed between the crosslinker and the monomer used in the following polymer synthesis, which was L-lysine methyl ester dihydrochloride. It was carried out in the same water/acetone binary solvent system. Once the crosslinker was added to the monomer solution, immediate precipitation was observed. The resulting white precipitate could not be dissolved in all common solvents used, including water, methanol, ethanol, acetone, acetonitrile, chloroform, dichloromethane, tetrahydrofuran, dimethylformamide and DMSO. The poor solubility of the product indicates that a highly crosslinked polymer network was formed, making it impossible to carry out NMR characterisation. The results suggest that the reactivity of the crosslinker is sufficiently high for preparation of the hyperbranched polymers.

To sum up, in this Section, four model reactions were performed, and the products were characterised. NMR spectra showed that the reactivity of the

crosslinkers was high and the chemical shifts of related peaks were at around 8.4 ppm.

3.2.2 Polymer synthesis and structural characterisation

The novel HPLPs bearing different ratios of the crosslinker (1 mol%, 3 mol%, 5 mol%, 8 mol% and 10 mol% relative to L-lysine methyl ester dihydrochloride) were synthesised by the one-pot polycondensation of L-lysine methyl ester dihydrochloride, isophthaloyl chloride and 1,3,5-benzenetricarboxylic acid chloride, as detailed in Section 2.2.2.

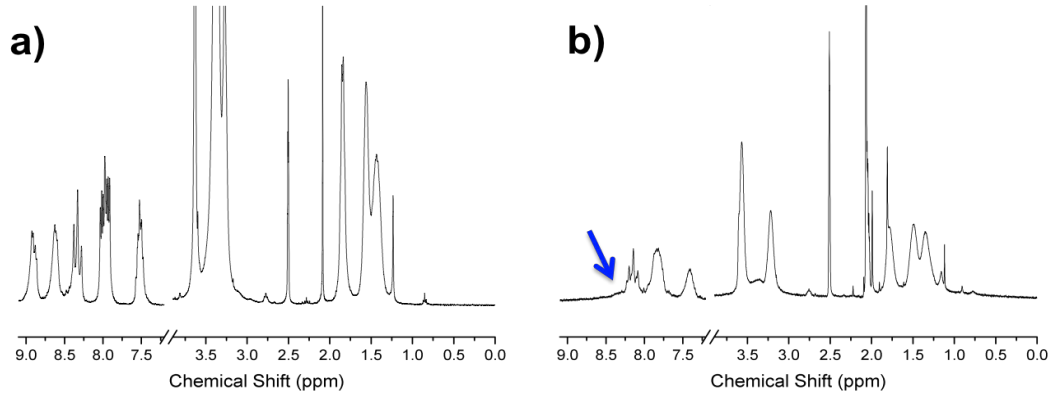

Figure 3.5 The NMR spectra of HPLP3 in different solvents. (a) in DMSO-d_6; (b) in DMSO-d_6 and D_2O (1:2 v/v). The arrow points to the peaks of crosslinkers.

NMR measurements were conducted to confirm the structures of the HPLPs and calculate the amount of crosslinkers incorporated. DMSO-d_6 was first used as an NMR solvent (Figure 3.5a). The overlap between the peaks of the crosslinker and those of the N-H groups in polymer backbones, however, made it difficult to calculate the integral areas. D_2O was then introduced to suppress the proton peaks of the N-H groups (Figure 3.5b). The peaks of the crosslinker were successfully revealed, though the resolution of the whole spectra was sacrificed a bit due to the slightly reduced solubility of the HPLPs (acid form) in the mixture of DMSO and D_2O.

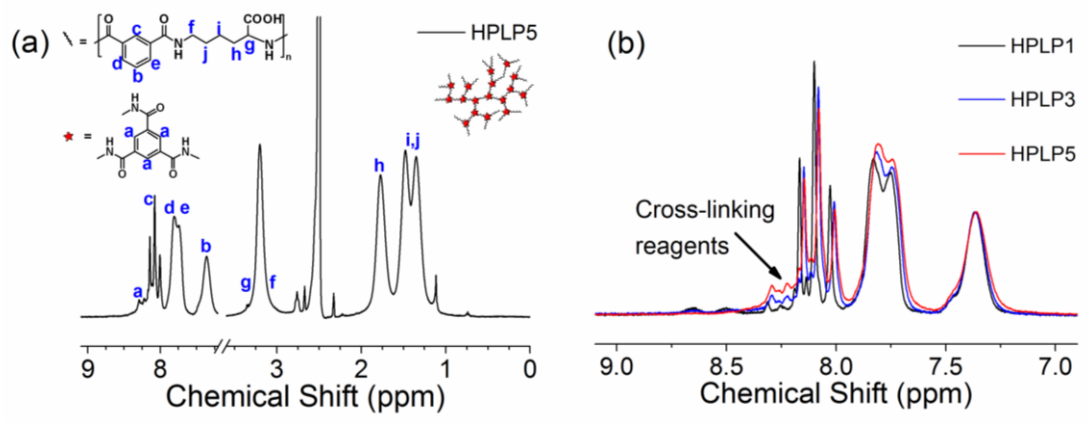

Figure 3.6 (a) ^{1}H NMR spectrum of HPLP5 with proton designations. (b) Zoomed-in ^{1}H NMR spectra of HPLP1, HPLP3 and HPLP5 between 6.9 and 9.1 ppm. Reprinted from (Wang & Chen 2017)**, copyright 2017, with permission from ACS publications.**

Via the optimisation of the NMR solvent, the presence of the crosslinker in the HPLPs at different branching degrees could be visualised with a relatively high resolution (Figure 3.6). All peaks were assigned as shown in Figure 3.5a. Because all these HPLPs had the same backbones, the majority of peaks in the H-NMR spectra were similar (See appendix, Figure S3) except those corresponding to the crosslinker (Figure 3.6b). It was obvious that the peaks between 7.95 and 8.45 ppm of the HPLP5, which had the highest amount of crosslinkers, were significantly larger than the HPLP1 with the lowest amount of crosslinkers. Though there was still a small overlapping area between the crosslinker-related peaks and another peak from polymer backbones, it is possible to calculate the amount of crosslinkers incorporated according to Equation 3.2. In this equation, the corresponding integral area in the H-NMR spectrum of the linear PLP was used as a negative control and was deducted from the calculation in order to minimise the effect of the overlapping peak from the polymer backbones. The calculated results are listed in Table 3-2.

$$Amount\ of\ incorporated\ crosslinkers = \frac{\int peaks\ (7.95{-}8.45\ ppm)\ of\ HPLPs - \int peaks\ (7.95{-}8.45\ ppm)\ of\ linear PLP}{3} \times 100\% \qquad \text{(Equation 3.2)}$$

Table 3-2 The amount of crosslinkers in the HPLPs characterised by H-NMR. Original data were presented in (Wang & Chen 2017)**, copyright 2017, with permission from ACS publications.**

Polymer	Theoretical crosslinker percentage [a]	Experimental crosslinker percentage [b]
HPLP1	1%	3%
HPLP2	3%	4%
HPLP3	5%	7%
HPLP4	8%	9%
HPLP5	10%	12%

a Determined by the stoichiometric ratio of crosslinkers in the polymerisation

b Calculated based on the NMR spectra of the HPLPs according to Equation 3.2.

According to Table 3-2, the calculated results of incorporated crosslinkers are similar to the theoretical data determined by stoichiometric ratio presented in the polymerisation, which proves that hyperbranched polymers with different crosslinking degrees were successfully prepared. Also, the crosslinking degrees could be adjusted by the feeding ratio of crosslinkers.

The branched structure of the HPLPs was further confirmed by GPC (Table 3-3). The PDI of HPLP1, HPLP2, HPLP3 and HPLP4 increased from 1.70 for HPLP1 to 2.65 for HPLP4, which probably resulted from the increase in the branching degrees of these polymers. Hyperbranched polymers with higher branching degrees tend to have more complicated structures with more diversified molecular weights, leading to higher polydispersities. However, with further increasing the branching degree up to 12% for HPLP5, the PDI was slightly decreased to 2.34. The PDI decrease was probably due to the poor solubility of some high-branching-degree fraction of the HPLP5 in the GPC solvent NMP. The insoluble species with higher molecular weights and

branching degrees might be filtrated before GPC measurement. As for the average molecular weight, both the number average molar mass (M_n) and the mass average molar mass (M_w) continuously increased from HPLP1 to HPLP5. Specifically, the M_w of HPLP5 was almost 2.5 times higher than that of HPLP1, which indicates an increase in the polymer molecular weight as result of the increase in the branching.

Table 3-3 The molecular weights and polydispersities of the HPLPs. Original data were presented in (Wang & Chen 2017)**, copyright 2017, with permission from ACS publications.**

Polymer	Mn (x 10^6)	Mw (x 10^6)	PDI
HPLP1	1.10	1.87	1.70
HPLP2	0.99	1.99	2.01
HPLP3	1.06	2.71	2.56
HPLP4	1.64	4.34	2.65
HPLP5*	1.99	4.67	2.34

* Not well-dissolved in NMP

FTIR results consolidated the successful polymerisation for all HPLPs (Figure 3.7). Typical amide I and II bands at 1623 and 1527 cm^{-1} respectively, were presented in the figure. However, it did not provide many structural details about the hyperbranched polymers. The spectra of all the HPLPs were similar, due to the high similarity of their backbones. Therefore, it is considerably difficult to characterise the branching degree by FTIR considering the relatively small amount of crosslinkers incorporated.

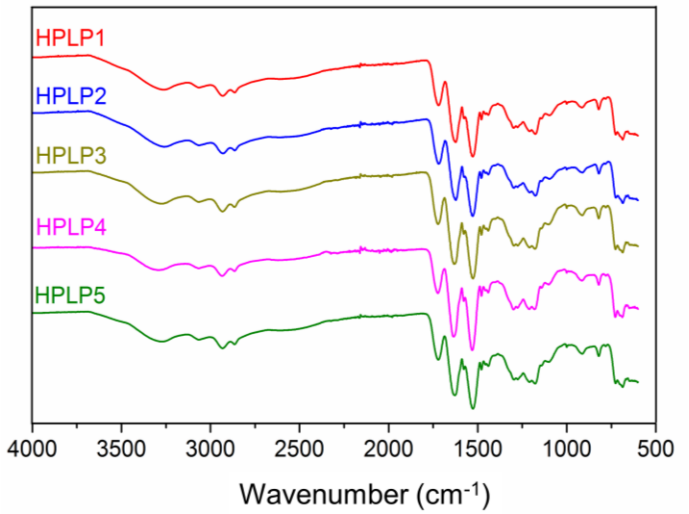

Figure 3.7 FTIR spectra of HPLPs. Reprinted from (Wang & Chen 2017)**, copyright 2017, with permission from ACS publications.**

DSC results in Figure 3.8 revealed an increased glass transition temperature T_g for the HPLP polymer with a higher branching degree, from 150.6 °C for HPLP1 to 172.3 °C for HPLP5, which is in agreement with the previous results of thermal analysis of amorphous polymers (Zhu et al. 2009). As the branching degree increased, the polymer architecture became more compact due to the introduction of more junction points. The compact structure hindered the free movement of polymer chains, resulting in an increased T_g.

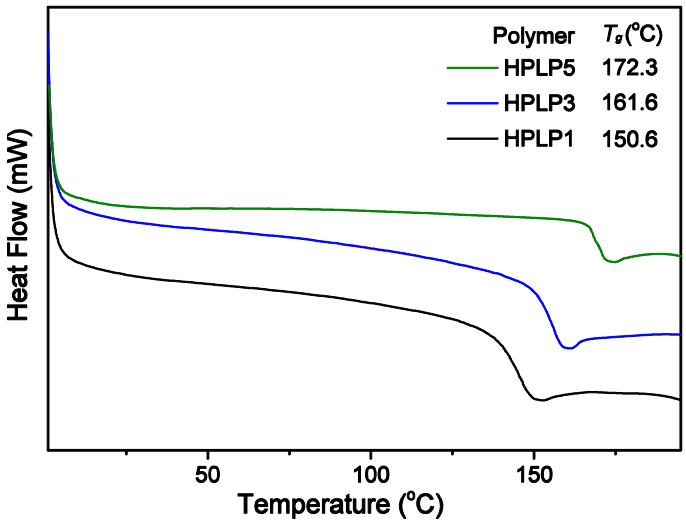

Figure 3.8 DSC curves of HPLP1, HPLP3 and HPLP5. Reprinted from (Wang & Chen 2017)**, copyright 2017, with permission from ACS publications.**

TGA data shown in Figure 3.9 compared the weight loss of HPLP5 and linear PLP during heating. The two identical curves both showed three weight loss stages. There was less than 10% of weight loss in the first stage until 250 °C, followed by a significant loss of 60% until 500 °C in the second stage. The final stage was from 500 to 600 °C, during which the polymers completely turned into ash. According to literature, the weight loss in the first stage may be due to the polymer terminal group degradation, while in the second stage the chain started to break, which required relatively high temperature (Khanna et al. 1981). At the final stage above 500 °C, any residue left would be degraded, hence the weight remained plunged to zero. Since the chemical composition of HPLP and PLP was similar, it was understandable that both polymers had similar TGA curves.

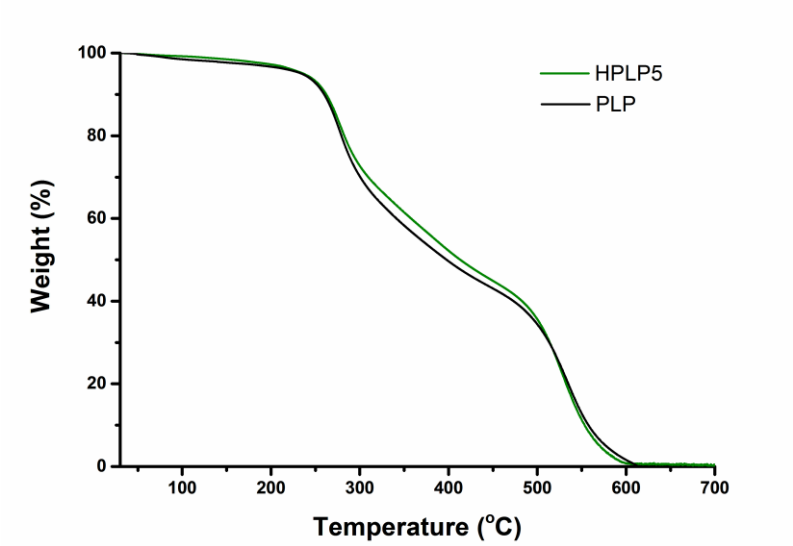

Figure 3.9 TGA curves of HPLP and linear PLP.

To sum up this section, HPLPs with different branching degrees were successfully prepared and characterised by various techniques. Results demonstrate that the branching degrees could be tuned by the amount of crosslinkers involved in the reaction.

3.2.3 Physiochemical properties

3.2.3.1 pH-Responsive phase transition behaviour of HPLPs

PLP and its modified polymers precipitated from aqueous solution under acidic conditions. Linear PLP precipitated at pH 4.7, which was previously reported by Eccleston et al. When hyperbranched structures were introduced, the pH-induced phase separation behaviour remained (Figure 3.10). HPLP1, which had the lowest branching degree, started precipitation at around 4.7 and the transition ended at around 4.3. However, HPLP5, with the highest branching degree, displayed a slightly broader transition range and its critical pH of precipitation shifted to a slightly higher value. This might be attributed to the enhanced chance of intermolecular confinement between polymer molecules with branched structures and the consequent gradual conformational change with increasing the branching degree.

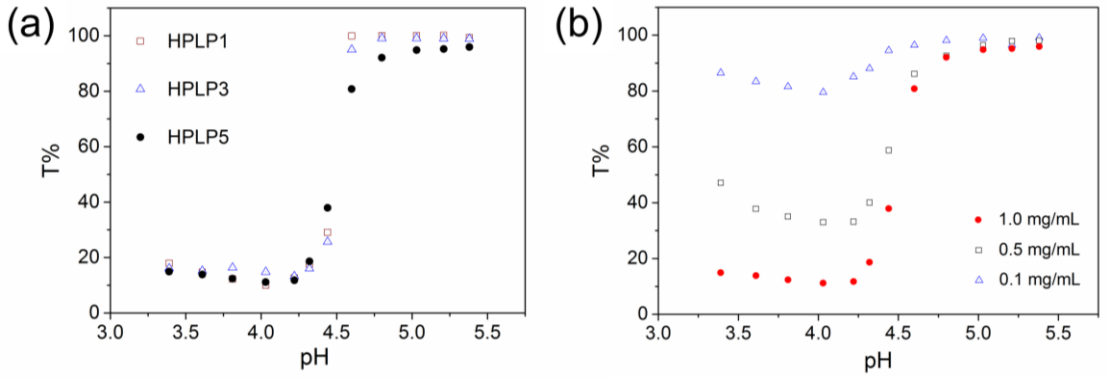

Figure 3.10 (a) pH-dependent transmittance of different HPLPs at 1.0 mg mL^{-1}; (b) pH-dependent transmittance of HPLP5 at different concentrations. (a) was reprinted from (Wang & Chen 2017)**, copyright 2017, with permission from ACS publications.**

All the HPLPs had almost the same trends in pH-dependent phase separation at different concentrations. The pH-dependent transmittance of HPLP3, as an example, at the concentration ranging from 0.05 to 1 mg mL^{-1}, was shown in Figure 3.10b. At a lower concentration ≤0.1 mg mL^{-1}, there was only a marginal phase transition. By increasing the polymer concentration ≥ 0.5

mg mL^{-1}, significant phase separation was observed with the critical precipitation pH at 4.7.

3.2.3.2 pH-Responsive conformational change of HPLPs

Pyrene, a hydrophobic fluorescent dye, has been commonly employed as a microenvironmental-polarity-sensitive probe to reveal the hydrophobicity of polymer structures in aqueous solution (Turro & Arora 1986; Chandar et al. 1988). Specifically, significant changes in both emission and excitation spectra of pyrene occur when it migrates from polar to non-polar environments, including a redshift from 333 to 338 nm in the excitation spectrum. Therefore, in this study, the ratio of the intensities at 338 nm to 333 nm (I_{338}/I_{333}) in the excitation spectra was used to indicate the polarity of pyrene environments; the higher the ratio, the more hydrophobic the pyrene environment.

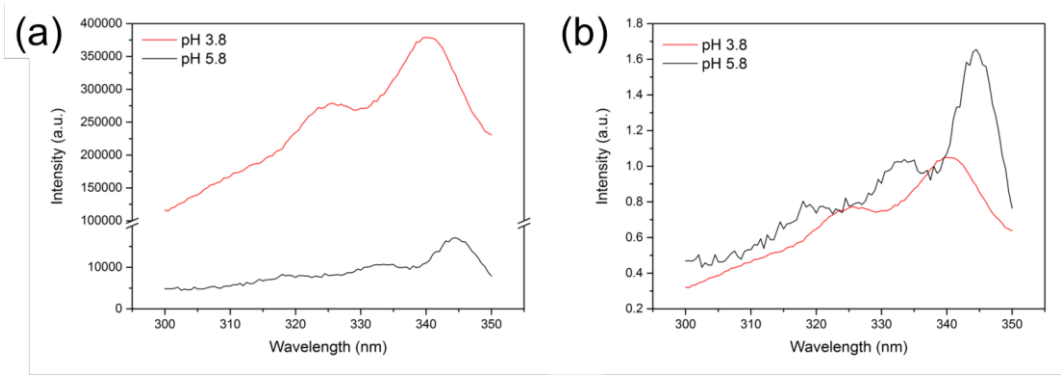

Figure 3.11 (a) The excitation spectra of pyrene containing 1.0 mg mL^{-1} PLP solution at pH 3.8 and 5.8. (λ_{em}=390 nm) (b) The intensities in figure (a) were normalised by I_{338}.

The excitation spectra of pyrene containing 1.0 mg mL^{-1} linear PLP solution at pH 3.8 and 5.8 are shown in Figure 3.11. When pyrene was in a polar solvent (in this case pH 5.8 buffer), the excitation intensity was extremely low compared with that in a non-polar microenvironment (in this case pH 3.8 buffer). When the intensity was normalised, a clear redshift of the maximum wavelength was observed, which indicated the presence of hydrophobic

microdomains in which pyrene was accommodated. The results shown here, about the pH-induced changes of the pyrene fluorescence in the PLP solution, were consistent with previously published work (Yue et al. 2005a).

Figure 3.12a illustrates the changes of I_{338}/I_{333} ratios as a function of pH for pyrene dissolved in the different HPLP solutions at a concentration of 0.1 mg mL^{-1}. All HPLPs depicted here had an increased I_{338}/I_{333} as pH decreased in the studied range. At pH 5.4, the I_{338}/I_{333} value was similar to that in deionised water, which suggested all HPLPs were hydrophilic. When pH dropped below 4.0, the I_{338}/I_{333} increased to 1.0 for HPLP1, 0.9 for HPLP3 and 0.8 for HPLP5. This indicated that all HPLPs formed hydrophobic microenvironments due to conformational changes. It is interesting to notice that the hyperbranched polymer with a higher branching degree showed a less steep transition. This could be attributed to the stronger steric hindrance within a more branched polymer, which impeded the pH-induced conformational change and hydrophobic domain formation.

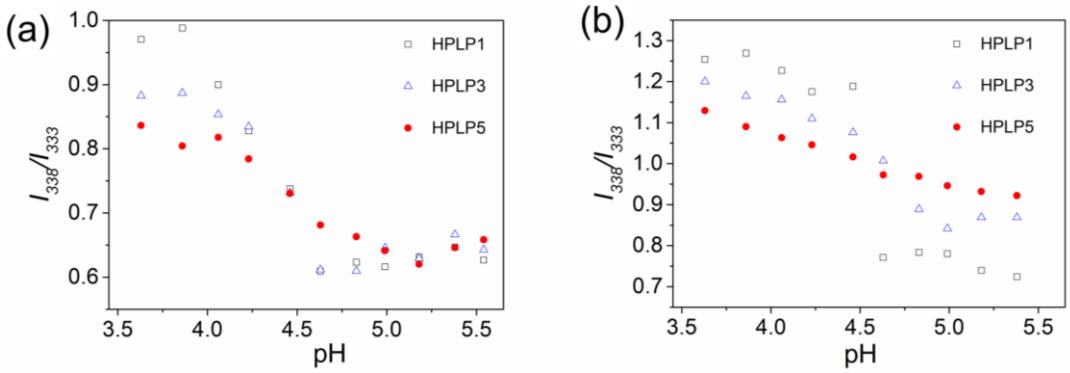

Figure 3.12 (a) Variations in I_{338}/I_{333} of HPLP1, HPLP3 and HPLP5 at 0.1 mg mL^{-1}. (b) Variations in I_{338}/I_{333} of HPLP1, HPLP3 and HPLP5 at 2 mg mL^{-1}. Reprinted from (Wang & Chen 2017)**, copyright 2017, with permission from ACS publications.**

Figure 3.12b depicts the pH-dependent variations of the I_{338}/I_{333} of pyrene in different HPLP solutions at a concentration of 2.0 mg mL^{-1}. The general trend was the same compared with Figure 3.11a. However, the value

of I_{338}/I_{333} of HPLP3 (0.85) and HPLP5 (0.9) at pH 5.4 were significantly higher than their I_{338}/I_{333} at 0.1 mg mL^{-1}, which suggested some hydrophobic domains already formed at this pH. It is then deduced that other than pH and hyperbranched structure, the hydrophobicity of polymers also depended on their concentration. Considering their amphiphilic nature, even at neutral pH, the polymers could form multimolecular aggregates thus bearing hydrophobic domains which accommodated pyrene.

To confirm this hypothesis, the critical aggregation concentration (CAC) was determined via the same method. This time, the I_{338}/I_{333} of pyrene was measured in pH 7.4 buffer with different concentrations of HPLP1 or HPLP5. As shown in Figure 3.13, the I_{338}/I_{333} remained around 0.6 when the concentration was below CAC (1 mg mL^{-1} for HPLP1 and 0.3 mg mL^{-1} for HPLP5 respectively). Above CAC, the I_{338}/I_{333} increased markedly, which means HPLPs tended to form multi-molecular aggregates with hydrophobic cores. The CAC of HPLP5 with higher branching degrees was found lower than that of HPLP1, due to the multivalency effect.

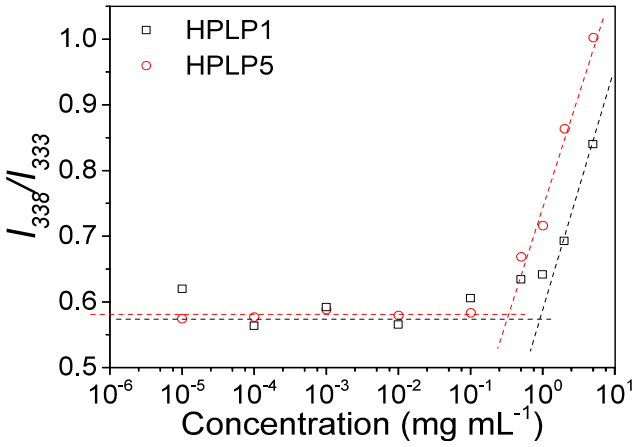

Figure 3.13 CAC determination for HPLP1 and HPLP5 at pH 7.4. Reprinted from (Wang & Chen 2017)**, copyright 2017, with permission from ACS publications.**

The CAC data provided a further explanation of the pH-dependent conformational alterations of the hyperbranched polymers at different concentrations. As shown in Figure 3.14, when the concentration of HPLP5 (0.1 mg mL^{-1}) was below the CAC (0.3 mg mL^{-1}), the pH-sensitive conformational changes predominantly resulted from intramolecular conformation alterations. However, when the concentration of HPLP5 (2 mg mL^{-1}) was sufficiently higher than its CAC, the HPLPs tended to form multimolecular aggregates due to intermolecular interactions. The hydrophobic cores of these aggregates were independent of pH, while their hydrophilic shells remained pH-responsive. As pH decreased, the carboxyl groups present in the hydrophilic shells were protonated, enabling the shells to become hydrophobic gradually and the consequent formation of the aggregates with more compact structures. It was interesting to notice that at a medium concentration of 1 mg mL^{-1}, $\Delta I_{338}/I_{333}$ was the greatest, which represented an intermediate stage of this conformational alteration.

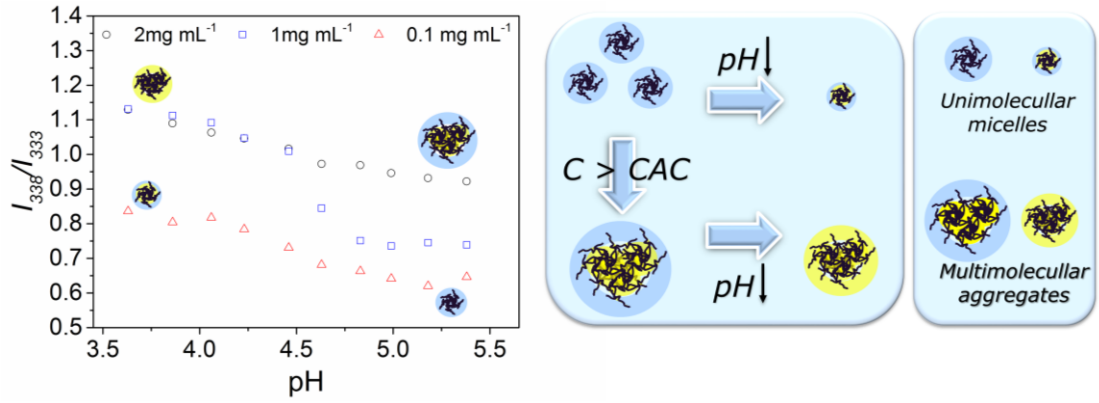

Figure 3.14 Variations in I_{338}/I_{333} of HPLP5 at 0.1, 1 and 2 mg mL^{-1} and the pH-responsive hydrophophobicity variation scheme.

DLS results shown in Figure 3.15 also confirmed pH- and concentration-dependent conformational alterations. At a concentration of 1 mg mL^{-1}, the average hydrodynamic size in diameter of HPLP1 was only 5.7 ± 1.6 nm at pH 7.4, which was comparable with a single polymer's size. This suggests that the

hyperbranched polymer might form unimolecular micelles. At lower pH (4.6), HPLP1 aggregated into hydrophobic assemblies, with an increased average size of 25.3 ± 2.2 nm. In comparison, the mean size of HPLP5 at pH 7.4 was much larger (256.7 ± 31.4 nm). It confirmed the formation of large multimolecular aggregates at the concentration sufficiently higher than its CAC as suggested in Figure 3.12. As pH dropped to 4.6, the shells of multimolecular aggregates became hydrophobic due to protonation of carboxyl groups and the whole aggregates shrank into compact assemblies (15.0 ± 2.0 nm). A similar size change in response to pH has been previously reported for the linear PLP (Chen et al. 2008).

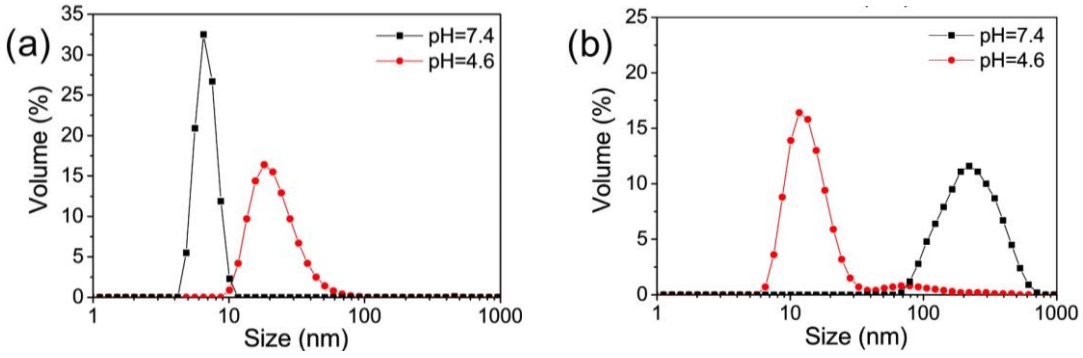

Figure 3.15 Hydrodynamic particle size distributions of (a) HPLP1 and (b) HPLP5 at 1 mg mL^{-1} in buffers at pH 4.6 (red) and pH 7.4 (black). Reprinted from (Wang & Chen 2017)**, copyright 2017, with permission from ACS publications.**

TEM was used to complement the DLS data, in order to characterise the polymer aggregates. The images of HPLP5 at pH 4.6 and pH 7.4 were presented in Figure 3.16, without staining. At pH 4.6, the contrast was better, showing dark compact aggregates, not necessarily spherical. The size was around 15 nm, similar to DLS measurement. At pH 7.4, more diffused irregular aggregates were found with the size of hundreds of nanometers. The contrast was not as good as the one at pH 4.6, so it was difficult to identify any detailed structure within the aggregates.

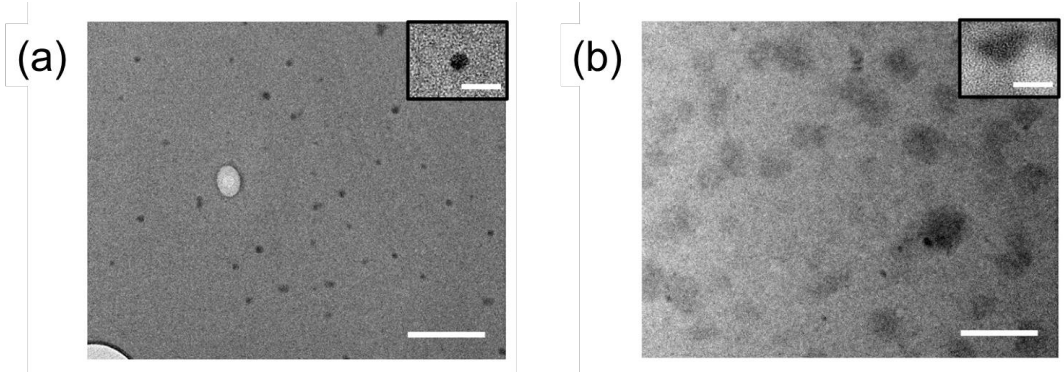

Figure 3.16 TEM images of HPLP5 at (a) pH 4.6 and (b) pH 7.4 (scale bar 200 nm) with one representative particle shown in their respective insets (scale bar 50 nm). Reprinted from (Wang & Chen 2017)**, copyright 2017, with permission from ACS publications.**

To sum up section 3.2.3, turbidimetry, spectrofluorimetry, DLS and TEM results revealed the relationship between the structure of the hyperbranched polymers and their physicochemical properties. Firstly, the pH-responsiveness of the HPLPs was dependent on their structures; secondly, the polymers with higher branching degrees showed a broader range of pH-responsive transitions and a lower ability to form hydrophobic microdomains due to the steric hindrance within the structure. Last but not least, the size and morphology of polymers varied a lot depending on their concentrations as well. At a concentration above CAC, polymers may form aggregates with larger size and hydrophobic inner cores.

3.2.4 pH-Mediated membrane permeability

3.2.4.1 HPLP interactions with GUVs

GUVs are artificial spherical lipid vesicles with a diameter of several tens of micrometres, made of one or several different kinds of lipids. They are considered as a simplified model system for membrane interaction study due to following reasons. Firstly, similar to mammalian cell membranes, GUV membranes are composed of lipid bilayers with a curvature. Secondly, these vesicles are large enough for visualisation under optical microscope; thus,

characterisation is much easier compared with liposomes and other small lipid vesicles. Finally, the membrane components are much simpler compared with cell membranes, which makes it easier to control the membrane properties, such as surface charge and rigidity.

In this study, GUVs were prepared by a well-established gel-assisted method (Weinberger et al. 2013). In this method, lipids containing solutions were spread on a dried PVA film, and the film was hydrated with sucrose buffer. During hydration, the PVA would absorb buffer and swell, which led to GUVs budding and formation. Before imaging, GUV dispersions were diluted in a glucose-containing buffer with similar salt composition and osmolality for two purposes. Since the vesicles were filled with sucrose buffer which was slightly denser than the glucose buffer in the outer side environment, vesicles were sedimented in the bottom of the observation chamber for imaging. Because the vesicle was sedimented, the focus of the image could be fixed on equator plane even during long-term observation or video recording. Besides that, the sucrose and glucose created a phase contrast between the inner and outer vesicle environment, which made them more accessible under the microscope.

The GUVs prepared were first examined under a phase contrast microscope to observe their morphology. A representative image was shown in Figure 3.17. GUVs shown in the image were polydispersed. The diameters varied from several micrometres up to around 40 micrometres. However, since the focus was just fixed on one vesicle, all the other vesicles were out of focus more or less, so their outlines shown here may not be the equator plane. As a result, their diameters measured from this image did not represent the actual size. Most of the GUVs were spherical, though a few had buddings.

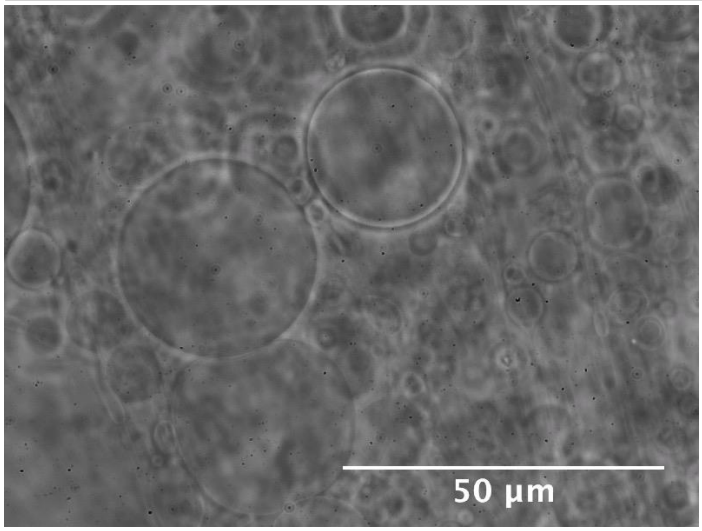

Figure 3.17 Phase contrast microscope image of GUVs made of DOPC and DOPS (9:1).

Afterwards, the effects of HPLP5 on GUV at acidic pH were imaged by confocal microscopy (Figure 3.18). The lipid membrane was composed of DOPC, a zwitterionic lipid without net charge, illuminated by Rhodamine B-labelled PE (red). In the buffer outside GUV, a membrane-impermeable dye HPTS (green) was used to indicate membrane integrity. When the membrane permeation was induced by HPLP5, HPTS was fluxed in, which led to the green signals both inside and outside GUVs.

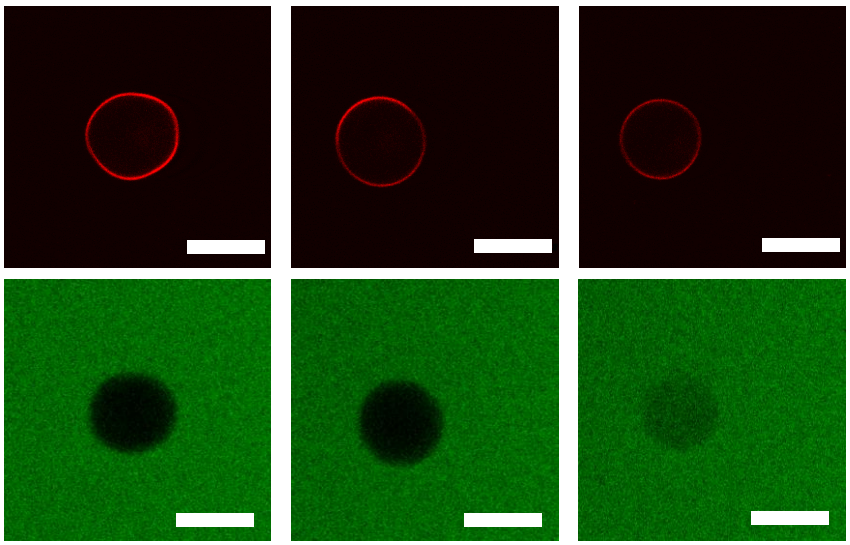

Figure 3.18 Selected frames from a time-lapse video of a typical GUV composed of DOPC and Rhodamine-labelled PE treated with HPTS at pH 5.0 in the presence of 1 mg mL^{-1} HPLP5 by confocal microscopy. Scale bar 20 µm.

It was shown in Figure 3.18 that HPLP5 could alter the GUV membrane permeability when at pH 5.0, characteristic of late endosomes. In the top left image of Figure 3.18, the membrane bending and possibly stretching were observed, which means the GUV's shape deviated from the energetically favourable spherical state. In spite of the fluctuations, the corresponding green channel showed that HTPS was not able to permeate into the GUV. In the top middle image, the GUV was a bit elongated and fluorescence intensity over the equator plane was not as homogenous as before, possibly due to the lipid reorganisation induced by HPLP5. In the last frame, though GUV appeared normal, HPTS gradually filled in the vesicle, indicating that the membrane was permeabilised by HPLP5.

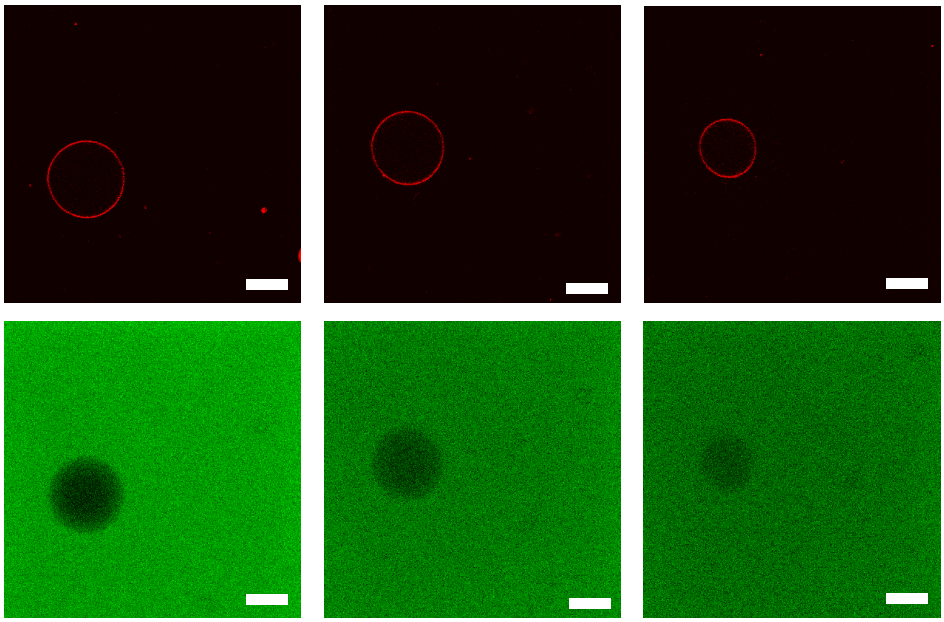

Figure 3.19 Selected frames from a time-lapse video of a typical GUV composed of DOPC, DOPS (9:1) and Rhodamine-labelled PE treated with HPTS at pH 5.0 in the presence of 1 mg mL^{-1} HPLP5 by confocal microscopy. Scale bar 20 µm.

To better mimic the negatively charged mammalian cell membrane, GUVs composed of a mixture of DOPC and DOPS (9:1) were prepared and incubated with HPLP5 at pH 5.0. DOPS is a negatively charged lipid, with a serine residue on the hydrophilic head. Images shown in Figure 3.19 confirmed

that HPLP5 also enhanced the permeability of the negatively charged GUV at this acidic pH. Although the membrane fluctuations were not as obvious as the one in Figure 3.18, it was found the vesicle shrank when HPTS fluxed in. After shrinking, it finally collapsed, leaving planar lipid bilayer patches on the glass substrate.

To better understand the HTPS fluxing and GUV collapsing process, a 3D-scan of GUV filled with HTPS was performed. As shown in Figure 3.20, the diameter reduction observed in Figure 3.19 was not because of shrinking of the vesicle. Instead, the GUV spread on the glass slide, which lowered the equator plane. As a result, the apparent size of the diameter became smaller. The spread of lipids on the glass led to the formation of a planar lipid bilayer, which was also in agreement with the patches observed after the collapse.

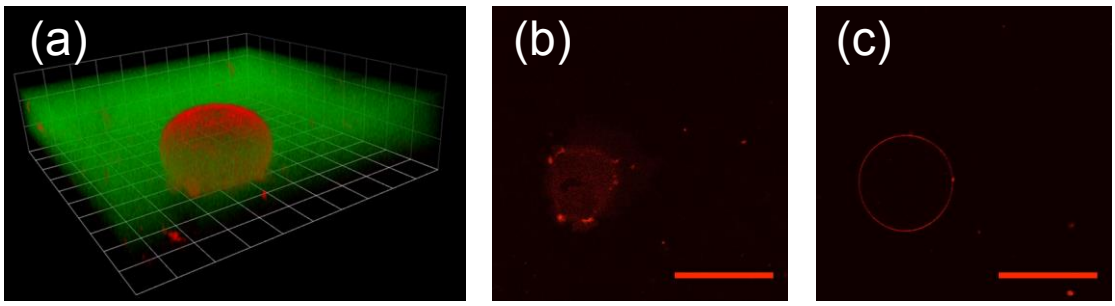

Figure 3.20 (a) 3D Confocal image of GUVs composed of DOPC, DOPS (9:1) and Rhodamine-labelled PE treated with HPTS at pH 5.0 in the presence of 1 mg mL^{-1} HPLP5. Red channel slices with the focal plane (b) at the supporting coverslip and (c) at the equator. Scale bar 50 μm.

The mechanism of glass-support bilayer formation from freestanding GUVs was not very clear. Similar events were observed by other researchers not only on glass-support but also on mica (Bhatia et al. 2014). Several mechanisms have been proposed, including a pore-expanding theory (Bhatia et al. 2014). Briefly, it was supposed that HPLP5 interacted with GUV membrane and possibly created pores or defects on the membrane, which

were energetically unstable due to the presence of a bilayer edge. When the opened lipid membrane came into contact with glass, it was absorbed and spread on the solid support, which was energetically favoured. Then as the glass-supported lipid layer expanded, the membrane tension on GUVs made them ruptured.

In summary, the results in this section indicated that HPLP5 could interact with GUVs and enhance the permeability of the membrane with a zero and negative net charge at pH 5.0. A hypothesised pore-expanding theory was proposed to explain the interaction between GUVs and HPLP5, which needs to be consolidated with further evidence.

3.2.4.2 HPLP interactions with sheep red blood cells

Sheep red blood cells (RBCs) were chosen as another model system to examine the membrane interaction of HPLPs because they are considered as the simplest mammalian cells. RBCs bear a membrane similar to other types of mammalian cells, with membrane proteins and polysaccharides, while they do not have cell nuclei or other organelles. The haemoglobin within RBCs serve as an indicator of RBC membrane integrity. In other words, by measuring the amount of haemoglobin leaked from RBCs (haemolysis), the membrane-lytic activity of specific molecules could be quantified.

Figure 3.21 shows the UV-vis absorbance spectra of HPLP5 and haemoglobin. It was clear that HPLP had no absorbance above 350 nm, while haemoglobin had characteristic peaks at 540 and 580 nm. This indicates that HPLPs did not interfere with haemoglobin in the UV-vis measurement.

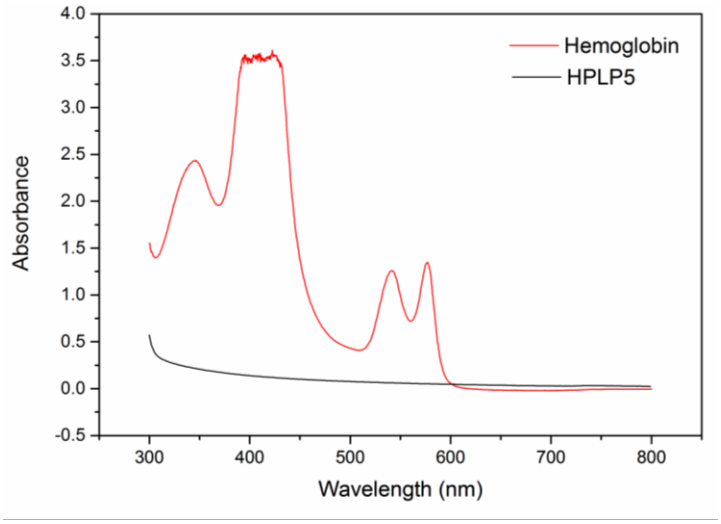

Figure 3.21 UV-vis absorbance spectra of HPLP5 solution (1 mg mL^{-1} in pH 7.4 phosphate buffer), and haemoglobin solution (prepared by lysing red blood cells in deionised water).

Then the haemolysis of HPLPs was studied at different pH values and concentrations. Figure 3.22a shows the concentration-dependent haemolysis of HPLPs at pH 5.0. At a concentration of 10 μg mL^{-1}, the haemolysis of all HPLPs studies were relatively low (< 20%). As concentration increased to 0.5 mg mL^{-1}, the haemolysis of all HPLPs slightly increased to 30%, without significant differences between each other. However, when the concentration was higher than 0.5 mg mL^{-1}, the HPLP with higher branching degrees exhibited a higher level of haemolysis. At 2 mg mL^{-1}, the haemolysis of HPLP5 even reached almost 100%, while that of HPLP1 was less than 40%. The dramatic increase in haemolysis was probably attributed to the multivalency effect of hyperbranched polymers. This effect was widely reported in literature about hyperbranched or dendritic polymers interacting with bio-targets. For example, a comparative study about linear/hyperbranched polyglycerol-based mannose conjugates showed that the hyperbranched structure significantly enhanced the interaction with target lectin compared with its linear counterpart (Kizhakkedathu et al. 2010). Moreover, nanoparticles coated mannose with dendritic displays even showed 1-2 orders of magnitude higher binding affinity

with target proteins than those coated with non-dendritic counterparts (Martin et al. 2009). Herein, although the binding with target molecules was not as complicated as binding with lipid membranes, multivalency could still contribute to the molecular recognitions, and thus facilitate the membrane interactions. In other words, the globular structure and higher density of surface groups of HPLP5 facilitated the interaction with lipid membranes, which led to considerably higher membrane binding affinity and membrane-lytic activity.

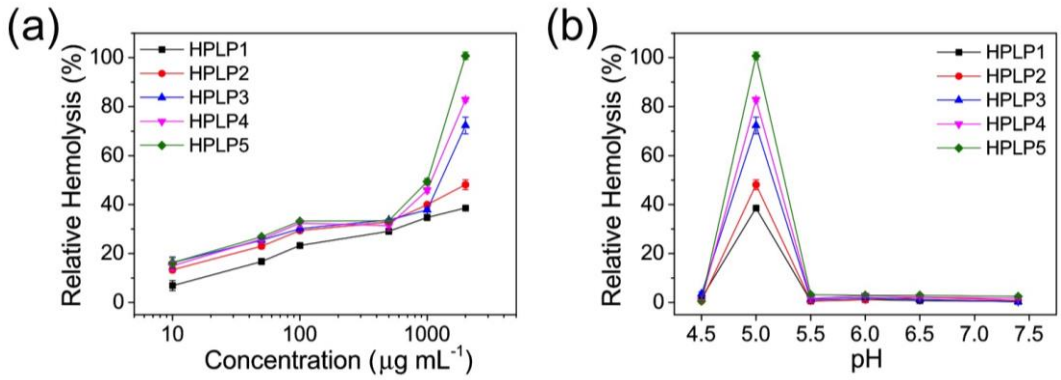

Figure 3.22 (a) Concentration-dependent relative haemolysis of sheep RBCs in the presence of different HPLPs at pH 5.0. (n=3). (b) pH-dependent relative haemolysis of sheep RBCs in the presence of different HPLPs at 2 mg mL^{-1}. (n=3). Reprinted from (Wang & Chen 2017)**, copyright 2017, with permission from ACS publications.**

Figure 3.22b showed the pH-dependent haemolysis of HPLPs. It was found that HPLPs had negligible haemolytic effects at physiological pH (7.4), which means they would not cause cell membrane damage in physiological conditions. In contrast, the haemolytic effects at late endosomal pH (5.0) were very efficient. The pH-responsive haemolysis resulted from the conformational changes. At pH 7.4, HPLPs were deprotonated and hydrophilic. The negative charge and hydrophilicity hindered their interaction with cell membranes due to electronic repulsion. At pH 5.0, however, HPLPs were partially protonated and hydrophobic domains formed as a consequence. This led to more efficient membrane interaction and subsequent haemolysis. When pH further

decreased to 4.5, most polymers precipitated out as turbidity study showed before. The available polymers for membrane interaction thus decreased, showing almost no membrane disruption.

The haemolysis of HPLPs were compared with several positive controls, including melittin, poly(L-lysine) and poly(L-arginine). Melittin is a commercially available, well-studied CPP, first discovered in bee venom (Habermann 1972). It was chosen as a positive control for its well-known high membrane-lytic activity (Tosteson et al. 1985; Murthy et al. 1999; Chen et al. 2006).

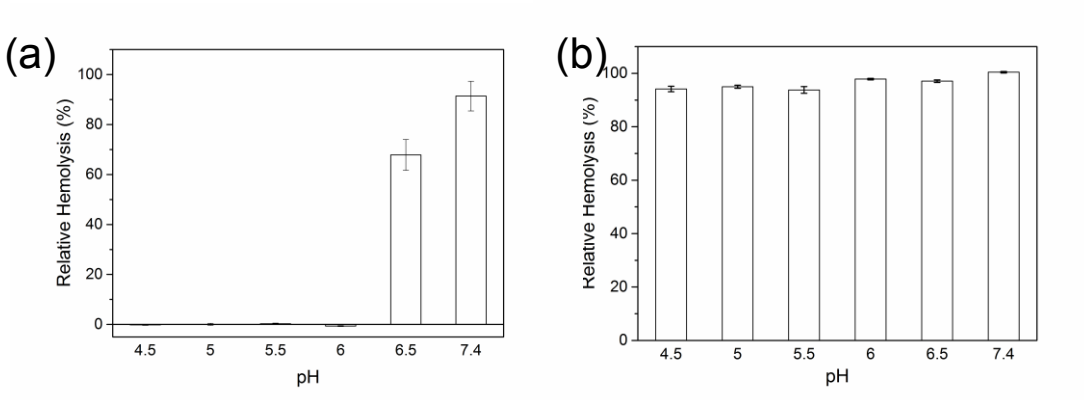

Figure 3.23 pH-dependent relative haemolysis of sheep RBCs in the presence of 5 μg mL^{-1} melittin in (a) 100 mM phosphate or citrate buffer and (b) in 150 mM NaCl. (n=3). (b) was reprinted from (Wang & Chen 2017)**, copyright 2017, with permission from ACS publications.**

Figure 3.23 showed the haemolysis of melittin at 5 μg mL^{-1}. It was interesting to find that the haemolytic effect of melittin was pH-dependent in Figure 3.23a. At pH 7.4, the haemolysis was more than 90%, which decreased to 70% at pH 6.5. When pH dropped to 6.0 or lower, no haemolysis was detected. This result was in contradictory to almost all published results which claimed that the haemolytic activity of melittin was independent of pH (Murthy et al. 1999; Chen et al. 2006). By re-examine the protocols, it was found that phosphate buffers were used for pH 7.4 and 6.5, while citric buffers were used for pH lower than 6.5. In other words, results with undetectable haemolysis

were all performed in citric buffers. This hint led to a hypothesis that it was citric in the buffers that affected melittin's haemolytic activity, which was confirmed with results in the literature (Tosteson et al. 1985). Tosteson *et al*. found both phosphate and citric ions had an inhibitory effect on haemolysis. A stronger inhibition of citric was observed than that of phosphate though.

So the pH-dependent haemolysis experiment was repeated in 150 mM NaCl solution with different pHs (Figure 3.23b). In NaCl solutions, the results were in accordance with previous reports. For the whole range of pH studied, the haemolysis was over 90%, without pH-responsiveness. The significant membrane-lytic activity of melittin was a potential concern for drug delivery application due to their potential cytotoxic effects. In comparison, HPLPs showed efficient haemolysis only within the narrow late endosomal pH range. This precisely controlled the membrane-lytic activity would minimise cytotoxic effects and the controlled release of payloads could be achieved in a specific step of the whole endocytosis pathway.

Besides melittin, another two commercially available poly(amino acid)s were also used as positive controls. Poly(L-lysine) and poly(L-arginine) have been investigated in literature for their endosomal escape ability and regarded as potential drug delivery vehicles (Rothbard et al. 2002; Murriel & Dowdy 2006). In Figure 3.24, it was shown both poly(L-lysine) and poly(L-arginine) had relatively low haemolytic activity within all the pH range studied even at a concentration of 2 mg mL^{-1}. As both polymers were positively charged at endosomal pH, it was expected they would interact with negatively charged cell membranes. However, at my experimental condition, the haemolysis was just 10%. The results suggest that both polymers did not induce significant membranes disruption, despite of their endosomal escape capability. This might

be due to the absence of their proton sponge effect in the haemolysis model, but present in endosomes.

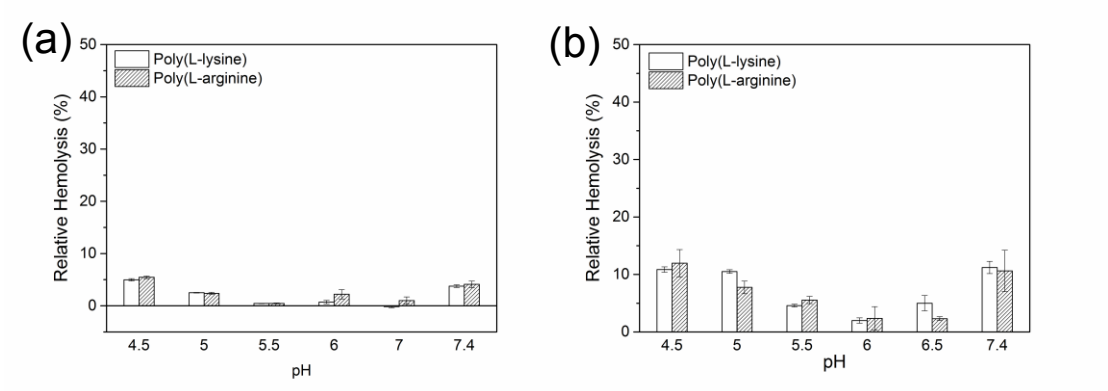

Figure 3.24 pH-dependent relative haemolysis of sheep RBCs in the presence of (a) 10 μg mL^{-1} poly(L-lysine) and poly(L-arginine); (b) 2 mg mL^{-1} poly(L-lysine) and poly(L-arginine). (n=3).

After haemolysis study, the mechanism of haemolysis was further investigated by confocal microscopy. Figure 3.25a showed the confocal images of RBCs haemolysed by HPLP5 at pH 5.0. After haemolysis, RBCs became ghost cells, which were transparent vesicles shown in the bright field and outlined in the red channel by Texas Red® hydrazide. Instead of complete disruption as GUVs, these ghost cells remained their spherical morphology without membrane collapse or fusion, though permeable to haemoglobin. In contrast, no ghost cells formed in the negative control (Figure 3.25d, pH 5.0 buffer without HPLPs), suggesting that the ghost cells formation was closely related to HPLP instead of other components or laser in the system.

To further examine the permeability of the ghost cell membrane, FITC-labelled dextran with different molecular weights was used as model molecules with different sizes. It was found that FITC-dextran 10K could efficiently diffuse into ghost cells. (Figure 3.25a) The green fluorescence intensity inside those ghost cells finally ended up the same as the background. However, FITC-

dextran 70K (Figure 3.25b) with a Stokes' radii of approximately 6 nm (Armstrong et al. 2004) and FITC-dextran 150K (Figure 3.25c) were found to be partially inside ghost cells. The green fluorescence intensity was lower than background, but higher than intact cells. This indicated that the ghost cell membrane was not permeable for every molecule. Those with a size larger than 6 nm were not able to diffuse across the membrane. It was deduced that HPLP5 interacted with RBC membrane and created defects with a size threshold of 6 nm. The defects were large enough for haemoglobin to diffuse out and FITC-dextran 10K to transfer in.

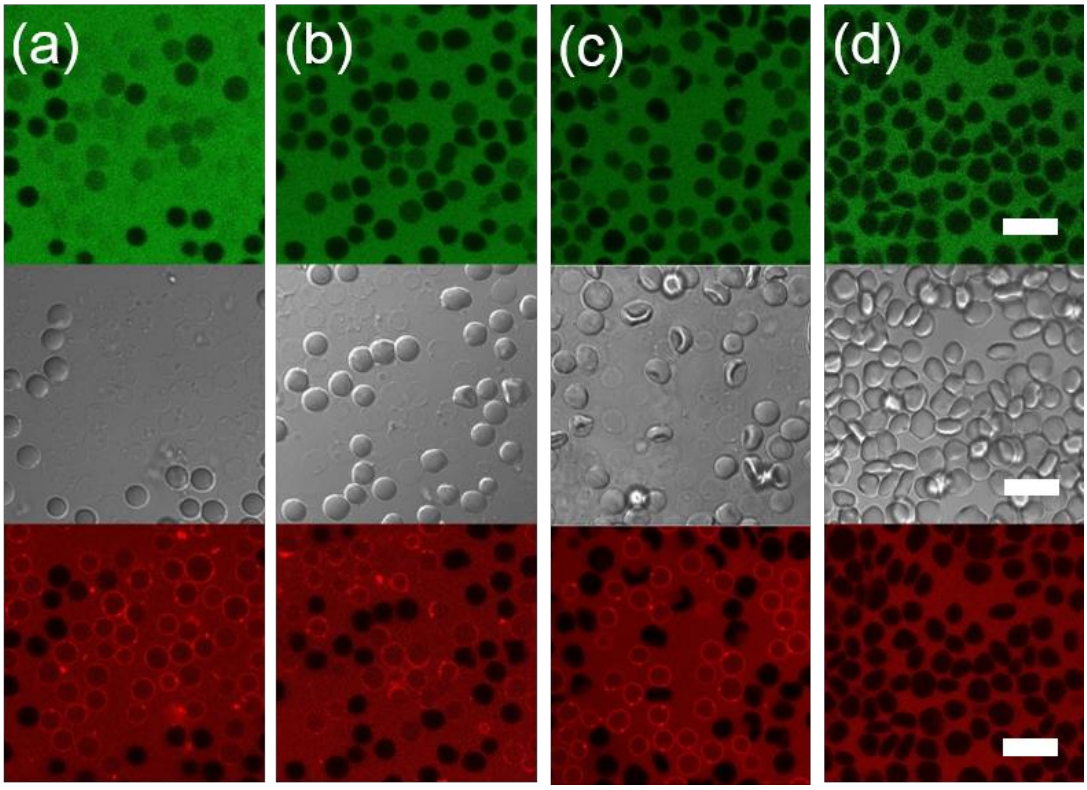

Figure 3.25 Confocal microscopy images of sheep RBCs treated with different sized FITC-dextran and Texas Red® hydrazide at pH 5.0 in the presence or absence of 1 mg mL^{-1} HPLP5: (a) FITC-dextran 10K and HPLP5; (b) FITC-dextran 70K and HPLP5; (c) FITC-dextran 150K and HPLP5; (d) FITC-dextran 10K in the absence of HPLP5. Scale bar 10 µm. Green channel, FITC-dextran; black and white channel, bright field; red channel Texas Red® hydrazide. Reprinted from (Wang & Chen 2017)**, copyright 2017, with permission from ACS publications.**

Figure 3.25 revealed some important information about the mechanism of HPLP and RBC membrane interaction. Firstly, HPLP5 could interact with RBCs at late endosomal pH and led to ghost cell formation. This means HPLP5 may interact with the membrane of late endosomes in a similar way. Instead of completely lysing late endosomes, HPLP5 just changed the membrane permeability and translocated potential payloads to the cytoplasm. The endosomal translocation, compared with other methods of cytosolic drug delivery pathways such as membrane disruption, caused less damage to cells, thus considered as less toxic. Secondly, there was a size threshold (around 6 nm) for the cargos to be translocated. This size threshold was roughly equal to the diameter of a 70 KDa globular protein. Peptides and proteins smaller than 70 KDa are potentially suitable for this delivery system, plus small molecular drugs. Thirdly, the pore-formation deduction was in agreement with previous observations on GUVs. Unlike GUVs which were nothing more than a vesicle made of lipids, RBCs had more complicated membrane anchored on their cytoskeleton. This may be the reason why ghost cells induced by HPLP5 were more stable than the GUVs in the similar condition.

Other negative controls for ghost cell formation included incubating HPLPs with RBCs at different pHs. As shown in Figure 3.26, at pH 7.4, no ghost cells were observed which was consistent with the haemolysis results shown in Figure 3.22. At pH 4.5, however, the quality of images was poor because HPLP5 precipitated and blocked the RBCs from visualisation.

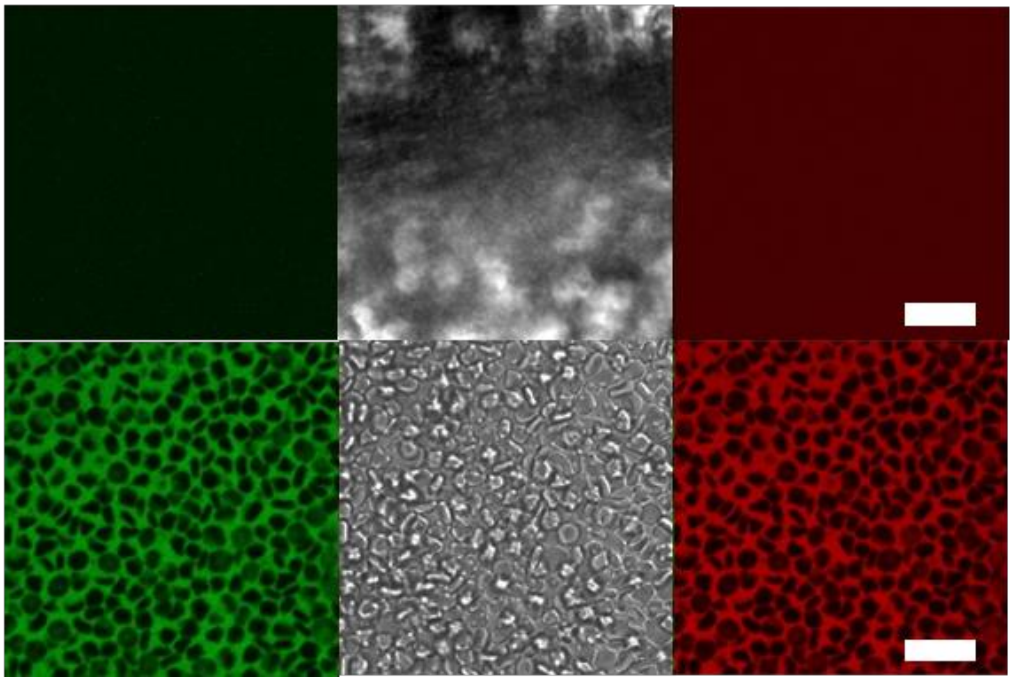

Figure 3.26 Confocal microscopy images of sheep RBCs treated with 10 μM FITC-dextran 10K, 1.5 μM Texas Red® hydrazide and 1 mg mL^{-1} HPLP5 at pH 4.5 (top) and pH 7.4 (bottom). Formation of HPLP5 precipitates at pH 4.5 prevented the RBCs being appropriately visualised. Scale bar 10 μm. Reprinted from (Wang & Chen 2017)**, copyright 2017, with permission from ACS publications.**

Furthermore, time-lapse confocal microscopy was performed to visualise the RBCs before ghost cell formation. It was found that the membrane of RBCs fluctuated vigorously when treated with HPLP5 at pH 5.0. Initially, all RBCs were discocytes, which were considered as the normal morphology. Then a significant number of stomatocytes were observed before evolving into spherocytes. Eventually those swollen spherical RBCs became ghosts. Before ghost formation, the cell membrane remained intact without internalization of either FITC-dextran or Texas Red®. However, the dramatic membrane rearrangement indicated the local tension changed continuously which led to membrane bending and stretching. It was thus possible that before ghost cell formation, the membrane defect under microscopic scale already formed and finally evolved into pores of several nanometers.

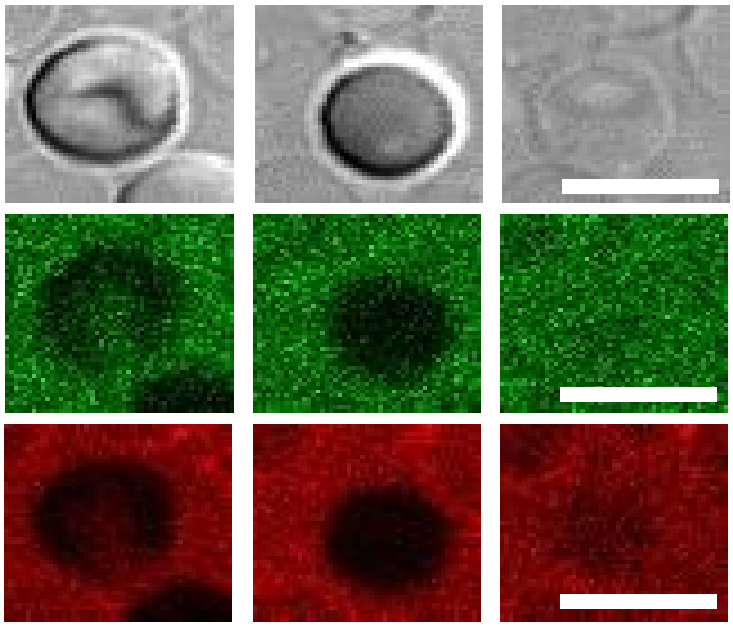

Figure 3.27 Time-lapse confocal microscopy images of sheep RBCs treated with 10 μM FITC-dextran 10K, 1.5 μM Texas Red® hydrazide and 1 mg mL^{-1} HPLP5 at pH 5.0. From top to bottom: bright field; green channel: FITC-dextran; red channel: Texas Red® hydrazide. From left to right, stomatocytes, spherocytes and ghost cells. Scale bar 5 μm. Reprinted from (Wang & Chen 2017)**, copyright 2017, with permission from ACS publications.**

It was interesting to find out similar morphology variations were also observed by other researchers on the erythrocytes treated with CPPs, e.g., snake venoms and the HA2-TAT peptide combining the HA2 peptide from influenza virus and the TAT peptide from HIV (Yau et al. 2012; Lee, Johnson, et al. 2010). Prior to ghost cell formation, erythrocytes always became spherocytes. According to the previous study, it was found that before spherocytes formation, the cytoskeleton underwent reversible arrangement, which means they were able to change back to discocytes. However, once spherocytes formed, not only membrane but also cytoskeleton proteins were irreversibly altered, which led to haemolysis subsequently.

To summarise this Section, the pH-dependent membrane-lytic activity of HPLPs was evaluated on GUVs and sheep RBCs, respectively. Quantitative haemolysis showed that all HPLPs were non-membrane-lytic at physiological

pH, but relatively active at late endosomal pH (5.0). Higher branching HPLPs had higher membrane-lytic activity due to multivalency effects. Further study on confocal imaging revealed more details about the interaction between HPLP5 and model lipid systems. For GUVs, the lipid membrane rupture led to plenary lipid bilayer formation, while for RBCs, the haemolysis led to ghost cell formation. Molecules smaller than 6 nm could diffuse into the resulting ghost cells, which indicated that the mechanism of haemolysis could be pore formation instead of membrane solubilization.

3.2.5 Cytotoxicity

The non-specific toxicity of HPLPs towards mammalian cells (e.g. HeLa cells) was characterised by alamarBlue® assay. As shown in Figure 3.28, all HPLPs showed negligible cytotoxicity even at a concentration of 5 mg mL^{-1}. The results indicated that the lysine-based hyperbranched polymers were quite biocompatible.

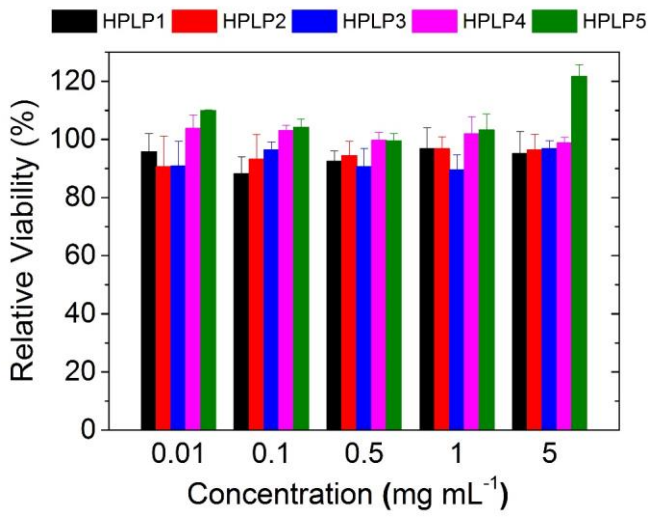

Figure 3.28 Concentration-dependent relative viabilities of HeLa cells treated with different HPLPs for 24 h as determined by alamarBlue® assay. (n=5). Reprinted from (Wang & Chen 2017)**, copyright 2017, with permission from ACS publications.**

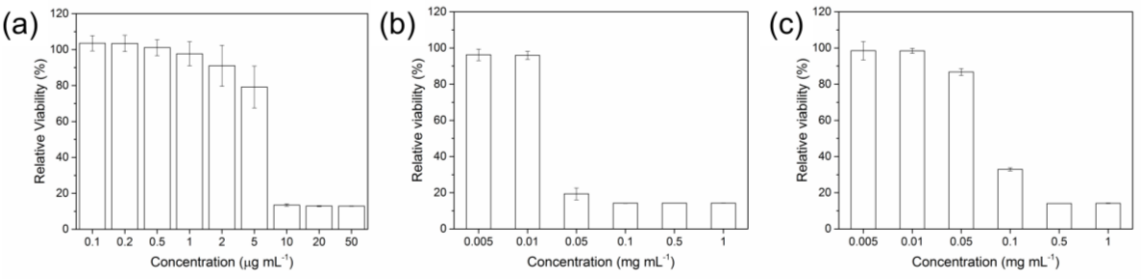

Figure 3.29 Concentration-dependent relative viabilities of HeLa cells treated with melittin (a), poly(L-lysine) (b) and poly(L-arginine) (c) for 24 h as determined by alamarBlue® assay. (n=5). (a) was reprinted from (Wang & Chen 2017)**, copyright 2017, with permission from ACS publications.**

In comparison, those positive controls showed significant cytotoxicity towards HeLa cells on the same condition. When the concentration was greater than 0.01 mg mL^{-1}, the relative viability for melittin was lower than 13%. It was inconsistent with the significant haemolysis results shown in Figure 3.23. For poly(L-lysine) and poly(L-arginine), the cytotoxicity was also considerably greater than HPLPs. The viability dropped to 18% and 37% at a concentration of 0.1 mg mL^{-1} respectively. Though both polymers did not show high haemolytic effects compared with melittin, their cytotoxic effects were comparable. This was possibly attributed to the fact that their toxic effects were more metabolic than membrane-lytic.

3.2.6 Intracellular delivery of model drugs

After membrane-lytic study of model lipid systems, intracellular delivery was evaluated to investigate whether HPLP5 could facilitate the endocomal escape of endocytosed cargos in mammalian cells. Here, calcein, a membrane-impermeable model drug, was used to visualise the endosomal escape. Specifically, Hela cells were co-incubated with both 1 mg mL^{-1} HPLP5 and 2 mg mL^{-1} calcein. After 1 hour of internalization at 37 ^{o}C, the cells were further incubated in fresh complete DMEM for 5 hours before imaging, to allow

maturation of endosomes and transformation of the polymer to a membrane-lytic state upon acidification.

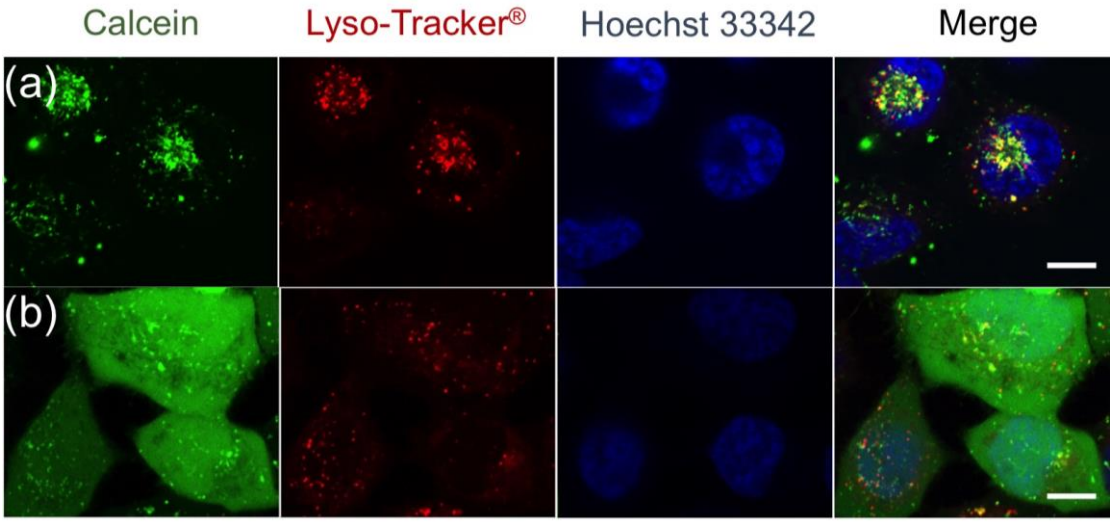

Figure 3.30 Confocal microscopy images of HeLa cells showing the intracellular distribution of the endocytosed calcein. The cells were treated with (a) 2 mg mL^{-1} calcein only, and (b) both 2 mg mL^{-1} calcein and 1 mg mL^{-1} HPLP5. Images were collected at 5 hours after 1 hour of uptake. Scale bar 10 μm. Reprinted from (Wang & Chen 2017)**, copyright 2017, with permission from ACS publications.**

As shown in Figure 3.30a, in the negative control without HPLP, calcein was trapped in endosomes/lysosomes, appearing as green spots, which were co-localised with LysoTracker®. In contrast, with HPLP5, calcein successfully escaped from endosomes into the cytoplasm, appearing as diffuse green fluorescence in the whole cell (Figure 3.30b). This suggests that upon protonation of HPLP5 in late endosome/lysosome, the hyperbranched polymer destabilised the membrane of intracellular vesicles and released calcein into the cell cytoplasm efficiently.

The intracellular delivery for positive controls is shown in Figure 3.31. Due to their significant cytotoxicity, lower concentration (1 μg mL^{-1} for melittin, 10 μg mL^{-1} for poly(L-arginine) and poly(L-lysine)) was used compared with HPLP5 (1 mg mL^{-1}). It was found that melittin had induced calcein cytoplasmic

delivery in a few cells. Poly(L-arginine) showed negligible delivery, while poly(L-lysine), among all positive controls, showed the best results.

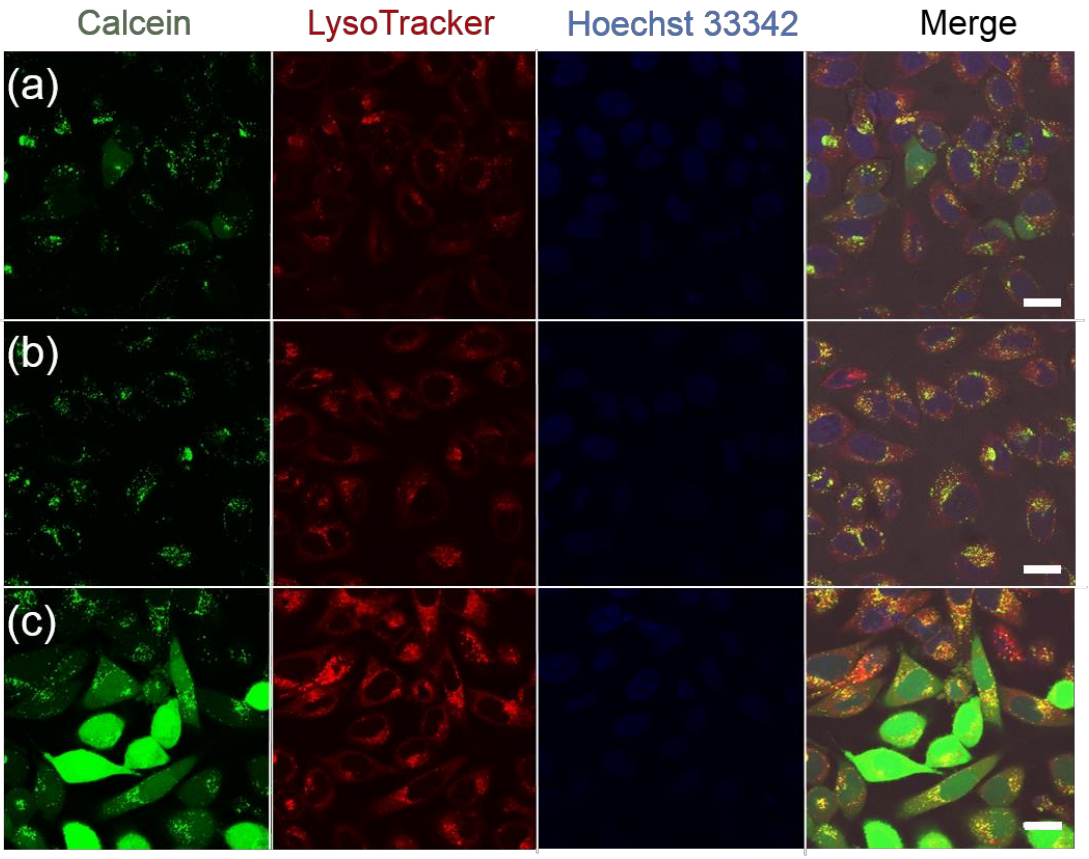

Figure 3.31 Confocal microscopy images of HeLa cells showing the intracellular distribution of the endocytosed calcein. The cells were treated with 2 mg mL^{-1} calcein and (a) 1 μg mL^{-1} melittin, (b) 10 μg mL^{-1} poly(L-arginine), (c) 10 μg mL^{-1} poly(L-lysine). Scale bar 20 μm.

The results suggested that positively charged poly(L-lysine) also facilitated the endosomal escape of calcein, possibly via a proton sponge mechanism as reported for most polycations. Upon acidification in endosomes, poly(L-lysine) became protonated thus positively charged. The dramatic increase in endosomal ionic strength led to osmotic imbalance and subsequent swelling of endosomes. The swelling eventually made endosomes burst and release cargos into cytoplasm. Compared with HPLP5, which changed the membrane permeability by creating defects, the complete membrane lysis of

poly(L-lysine) caused more severe damage to cells, thus leading to higher cytotoxicity.

3.3 Conclusions

A series of novel lysine-based, CPP-mimicking, hyperbranched polymers were successfully developed for intracellular drug delivery, as shown in Figure 3.32. To our knowledge, it is the first report of anionic, hyperbranched, CPP-mimicking polymers. The driving force behind the research in this Chapter was to study the structural effects on polymer-membrane interaction. It was expected that the novel hyperbranched structure could enhance the intracellular delivery efficiency by multivalency effects.

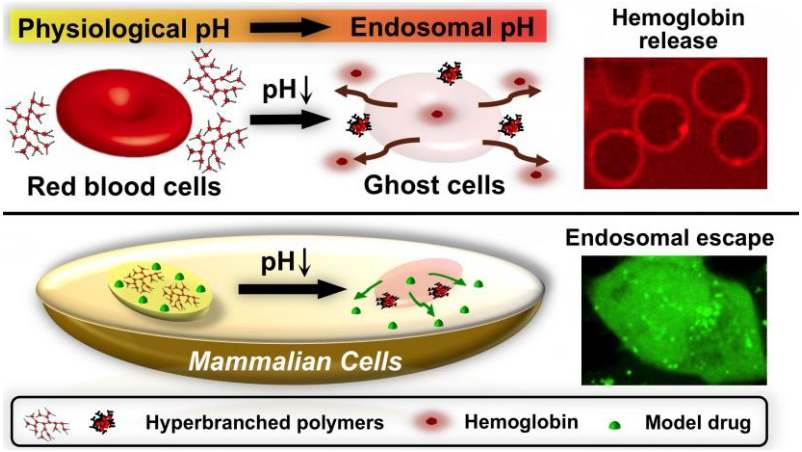

Figure 3.32 Summary scheme of hyperbranched polymers facilitating pH-responsive membrane penetration and endosomal escape. Reprinted from (Wang & Chen 2017)**, copyright 2017, with permission from ACS publications.**

HPLPs were synthesised via a one-pot polycondensation and their structures were characterised by a variety of techniques such as NMR, FTIR, GPC, DSC and TGA. The pH-responsive conformational changes were also evaluated by turbidimetry, fluorescence spectroscopy, DLS and TEM. Results showed that all HPLPs had pH-induced conformational changes. Unimolecular micelles or multimolecular aggregates with hydrophobic cores were formed at

neutral pH depending on if the polymer concentration was below or above the CAC, and both could become hydrophobic particles at acidic pH. Since the CAC was dependent on the branching degree, the pH-responsive conformational change could be manipulated by simply controlling the hyperbranched structure.

The pH-responsive polymer-membrane interactions were studied on GUVs and sheep RBCs as model lipid systems. The results of both studies confirmed that HPLP was only membrane-active at late endosomal pH but not physiological pH. A detailed study on the mechanism revealed that HPLP5 might create 6 nm pores on the membrane instead of solubilizing it completely. A quantitative study showed hyperbranching degrees affected the haemolytic effects. The higher branching species had higher haemolysis percentage.

All the HPLPs showed negligible cytotoxicity toward HeLa cells at a concentration as high as 5 mg mL^{-1}, but could facilitate the endocytosed payload to efficiently escape from intracellular vesicles into the cell cytoplasm. Compared with positive controls, HPLPs showed less cytotoxicity but efficient cytoplasmic delivery, thus suggesting their promising applications in intracellular drug delivery.

Chapter 4 Hydrogels for oral delivery

This Chapter describes the design and synthesis of PLP-based hydrogels for oral delivery applications. PLP was crosslinked with different crosslinkers via an EDC-coupling reaction. The swelling behaviour, SEM morphology and dynamic rheology of hydrogels were examined to reveal the network details and to evaluate the stimuli-responsive properties. The loading and release profiles were investigated on several model drugs, including probiotics.

This Chapter is partially based on the publication (Wang et al. 2016a) and another manuscript just submitted to *ACS Biomaterials Science & Engineering*. Some figures, tables and texts were reproduced and reprinted with permission from Wiley.

Note: MSc students Reva Attah and Xiaoxue Liu, undergraduate students Jiali Li and Yitong Chen in Dr. Rongjun Chen's group contributed to some results in this chapter. Reva Attah prepared samples used in the work presented from Figure 4.2 to Figure 4.17. Jiali Li and Yitong Chen prepared the samples used in Figure 4.18 and Figure 4.19. Xiaoxue Liu prepared samples used in the work presented from Figure 4.20 to Figure 4.28. The contribution of MSc students, undergraduate students and collaborators were specified in the captions of relevant figures.

4.1 Introduction

Oral drug administration is a preferable delivery route for patients due to its ease and convenience (Schoener & Peppas 2012; Tibbitt et al. 2016). It is also often less expensive than injective drugs which need to be produced in sterile clean rooms (Koetting & Peppas 2014; Sharpe et al. 2014). However,

the biological barriers in the gastrointestinal (GI) tract such as extreme pH in the stomach and high enzymatic activity in small intestine limit the application of oral delivery to many susceptible drugs, especially protein-based macromolecular drugs (Pinto 2010). Thus, drug delivery vehicles that protect payloads from exposure to these hostile environments are highly desirable.

Hydrogels, which are crosslinked three-dimensional polymer networks with high water content, have been extensively used in biomedical fields including tissue engineering and drug delivery (Hoffman 2012). Particularly, those hydrogels with stimuli-responsiveness are of great interests because of their ability to sense the environment and change physiochemical properties subsequently (Qiu & Park 2012; Koetting et al. 2015). Among all stimuli-responsive hydrogels, pH-responsive ones have been explored for oral delivery of various small hydrophilic drugs and macromolecular protein-based drugs (Gupta et al. 2002; Sharpe et al. 2014). These hydrogels usually collapse and protect the payloads in acidic stomach environment, while they swell and release in small intestine or colon (Serra et al. 2006). Due to pH-responsive controlled-release profile, these hydrogels are considered as promising carriers for oral administration.

However, the delivery of hydrophobic therapeutics remains a challenge for hydrogel carriers, because their intrinsic hydrophilic nature hinders the interaction with hydrophobic molecules. To overcome this limitation, there are two strategies commonly adapted (Gu et al. 2017). One method is to incorporate nanocarriers with hydrophobic moieties such as liposomes or polymer nanoparticles into hydrogels as composite materials (Grijalvo et al. 2016; Schoener et al. 2013). Though the encapsulation of hydrophobic moieties was reported as successful and efficient, the accumulative release percentage was relatively insufficient, possibly due to the entrapment of nanocarriers in

hydrogels (Lee et al. 2012; Liu et al. 2012). Another method is to introduce hydrophobic domains on hydrogel polymer networks to accommodate hydrophobic payloads (McKenzie et al. 2015). By adjusting the general hydrophobicity of various stimuli, the payloads could be released eventually. Compared with the previous method, the limitation of this strategy is a relatively low loading efficiency.

As previous reported, PLP is a lysine-based, metabolically derived pseudo-peptide with a pKa of 4.4 (Eccleston et al. 1999; Eccleston et al. 2000). It displays pH-dependent conformational changes and hydrophobicity variation, as well as good biocompatibility. Thus, it would be a promising hydrogel candidate in the field of hydrophobic therapeutics delivery. A previous report found that the hydrogels prepared by PLP crosslinked with an L-lysine derivative could accommodate a wide range of molecules and offer controlled release in different pH buffers (Watkins & Chen 2015). However, the effects of crosslinkers and the physiochemical properties were not well understood.

In this thesis, a systemic study of PLP-derived hydrogels was performed. A significant proportion of the work focuses on the effects of crosslinkers on hydrogel structure, as well as the controlled release in GI simulated buffers. As shown in Figure 4.1, PLP was first crosslinked by PEG (a biocompatible polymer) to make a pH-triggered hydrogel system. The crosslinking density and the length of PEG were studied to optimise the parameters for controlled delivery. Then, to precisely control the release, a redox-trigger was incorporated into the system via a disulfide-bond containing crosslinker, L-cystine dimethyl ester dihydrochloride (CDE). Since the redox-potential in human colon (-415 ± 72 mV) is much lower than the standard reduction potential for disulphide bands (around -250 mV), the cleavage of CDE would be possible to occur, leading to

degradation of hydrogels and complete release of payloads (Wilding et al. 1994).

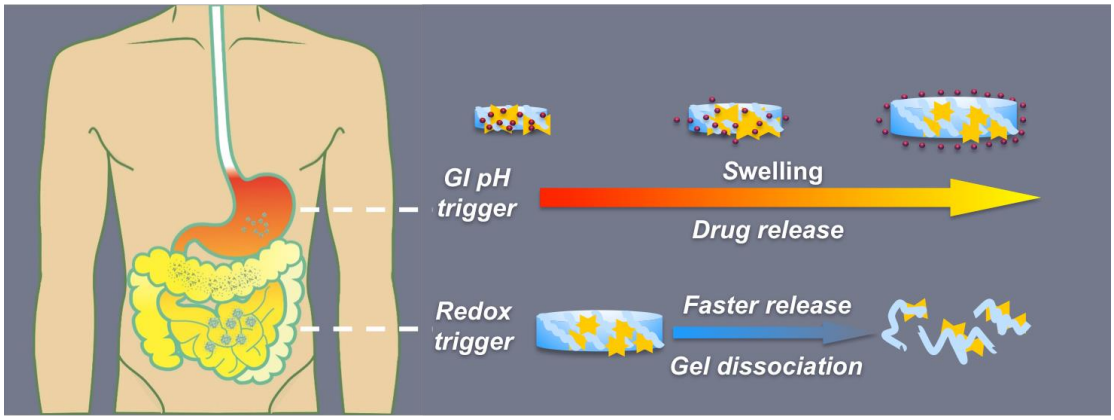

Figure 4.1 Schematic showing oral drug delivery hydrogels and their controlled-release behaviour. Adapted from literature (Wang et al. 2016b)**, copyright 2016, with permission from Wiley.**

Both hydrogel systems were developed with detailed structural characterisations. Swelling behaviour, SEM morphology and dynamic rheology were examined to reveal the hydrogel network and to evaluate the responsiveness. Crosslinkers' size, ratio, as well as the solid contents of the hydrogels were adjusted, to investigate the effects on hydrogel network and responsiveness. Finally, loading and release were investigated on several model drugs, including probiotics. The pH-trigger and redox-trigger were studied *in vitro*, with a GI-environment mimicking setting.

4.2 pH-Responsive amphiphilic hydrogels

4.2.1 Synthesis and structural characterisations

Hydrogels were prepared by a simple one-pot EDC-coupling reaction of PLP and PEG bisamine. The formulations and ingredients used are summarised in Table 4-1. During the reaction, the polymer mixture was originally viscous. Hydrogels formed after overnight treatment, which was

validated by vial tilting method. The unreacted molecules and impurities were removed by dialysis against water for 3 days. All hydrogels looked transparent after dialysis.

Table 4-1 PEG-crosslinked hydrogel formulations. *The hydrogel samples were prepared by Reva Attah in Dr. Chen's group.*

Name	PEG molecular weight (kDa)	PEG weight (mg)	Crosslinking ratio (mol%)[a]
Gel 1K	1.0	72	20
Gel 1.5K	1.5	108	20
Gel 3.4K	3.4	245	20
Gel 0.1	1.5	54	10
Gel 0.2 (Gel 1.5K)	1.5	108	20
Gel 0.5	1.5	270	50

a Feeding ratio of PEG compared with PLP residuals in the crosslinking reaction.

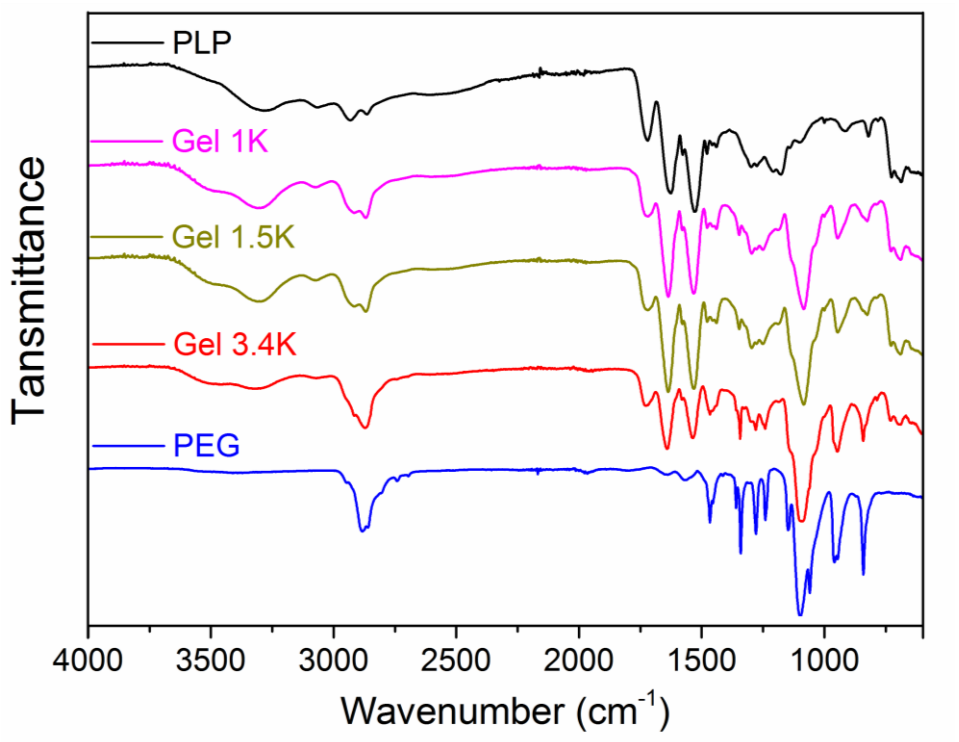

Figure 4.2 FTIR spectra of PLP, PEG and hydrogels of different crosslinkers.

The FTIR spectra of the lyophilised hydrogels are shown in Figure 4.2. All three hydrogels incorporated characteristic absorption bands of both PLP and PEG. The bands located at 1720 cm^{-1}(s, vs C=O of carboxylic acid groups), 1624 cm^{-1}(s, amide I) and 1527 cm^{-1}(s, amide II) were assigned to be on the backbone of PLP, while those located at 2882 cm^{-1} (s, vs C–H) and 1100 cm^{-1} (s, v C–O-C) were on PEG. The successful incorporation of all these bands mentioned above confirmed that the hydrogels were fabricated as designed. Interestingly, it was noticed that as the molecular weight of PEG crosslinkers increased the absorption of PEG bands (1100 cm^{-1}) increased. This was attributed to the increasing number of PEG repeating units of PEG with higher molecular weights, though the crosslinking density remained similar for Gel 1K Gel 1.5K and Gel 3.4K.

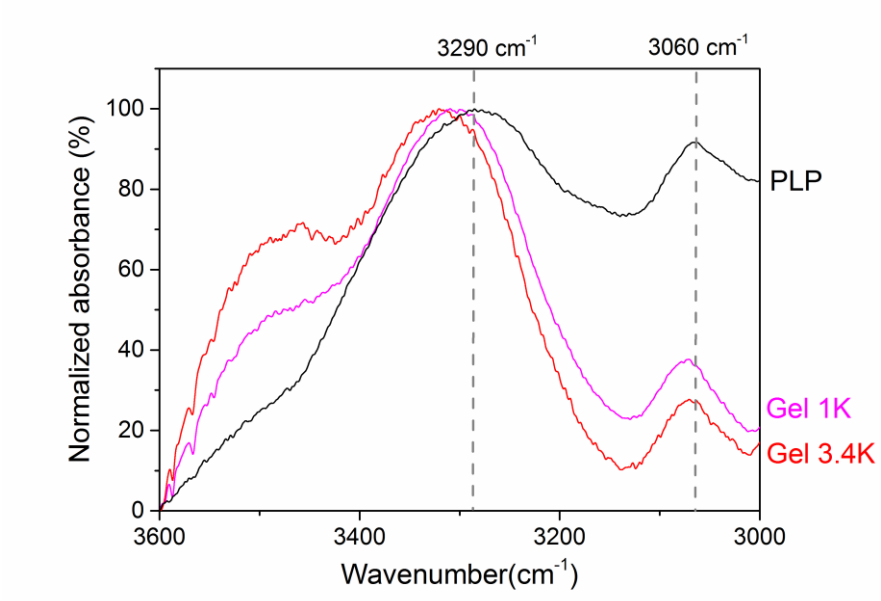

Figure 4.3 Zoomed-in FTIR spectra for Gel 1K, Gel 3.4K and PLP from 3000 to 3600 cm^{-1}.

In the FTIR spectra, it is also worth noticing that the hydrogel band shape from 3000 to 3500 cm^{-1} changed compared with PLP. The zoomed-in area is shown in Figure 4.3, in which the absorbance instead of transmittance was plotted. PLP had a broad band peaking at around 3290 and 3060 cm^{-1}

respectively. This broad band included the stretching of O-H and N-H, mostly in hydrogen-bonded forms. When the absorbance of all peaks were normalised to the absorbance of the peak at 3290 cm^{-1}, it was found that Gel 1K and Gel 3.4K showed significantly smaller peaks at 3060 cm^{-1}. Also, the peaks of hydrogels shifted to a higher frequency. The relative peak intensity variation and the blue shift were probably due to the hydrogen bonding exchanges between PLP and PEG. The structure of PLP suggested that the amide and carboxylic acid groups could form hydrogen bonds through inter- or intra-polymer chains. After crosslinking with PEG, the proton donor groups of PLP could also form hydrogen bonds with the ether oxygen of PEG. According to literature, the hydrogen-bond exchange changed the shape and ratio of different peaks in this broad band from 3000 cm^{-1} to 3600 cm^{-1} (Guo et al. 2010; Sharma & Pathak 2016; Van Duong et al. 2017). It was then concluded that the hydrogel network was not only constructed by chemically crosslinking but also hydrogen bonding.

As for hydrogels with different crosslinking ratios, the FTIR spectra are shown in Figure 4.4. Similar to Figure 4.2, for all Gels, both PLP and PEG characteristic bands were incorporated, even for GEL 0.1, which had the lowest crosslinking ratio. This suggests that PEG have been successfully incorporated into hydrogel networks for all the gels studied. The increased PEG band (1100 cm^{-1}) was also observed in hydrogels with a higher crosslinking ratio, which confirmed the increased amount of PEG in hydrogels with an increased crosslinking ratio.

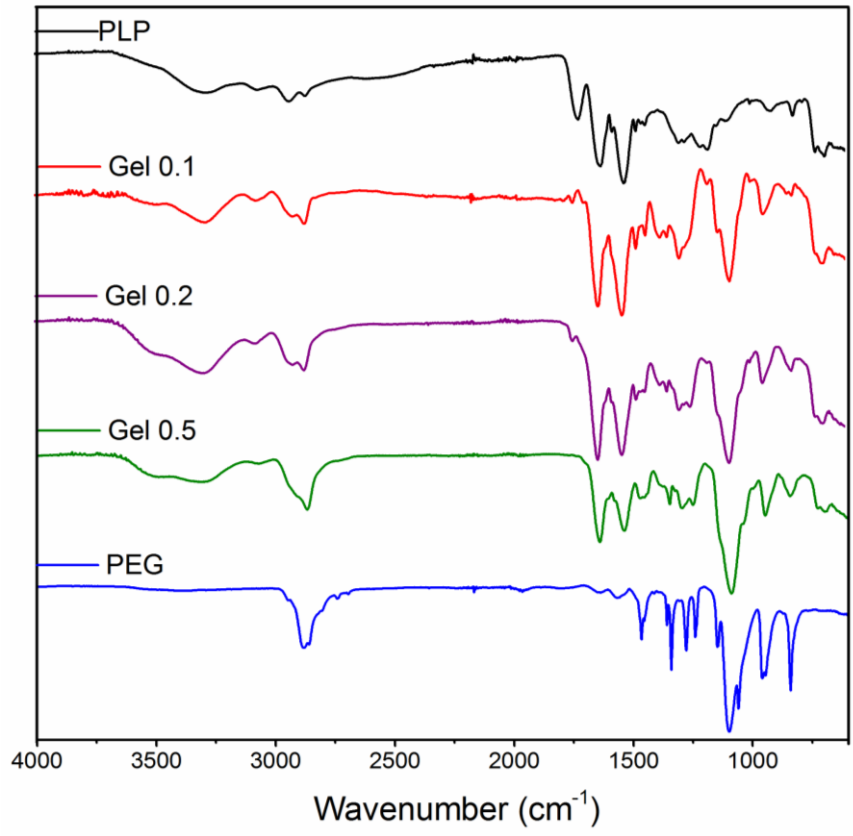

Figure 4.4 FTIR spectra of PLP, PEG and hydrogels of different crosslinking ratios.

The FTIR spectra also provided evidence about pH-responsiveness of the hydrogels. As shown in Figure 4.5, the band intensity at 1720 cm^{-1} (pointed with an arrow in Figure 4.5b) varied significantly when hydrogels were treated with different buffers before lyophilisation. This band was assigned to C=O stretching of carboxylic acid on PLP. At neutral pH, the carboxylic acid became deprotonated and thus formed COO^-. The C=O stretching band of COO^-, however, shifted to a lower frequency, which overlapped with amide I and amide II. Besides the variation of the band at 1720 cm^{-1}, the shape of the broad band at 3280 cm^{-1}, corresponding the NH stretching on the amide of PLP, also changed. Although not very obvious, this could possibly be related to hydrogen bond rearrangement at different pH environment (Kozlovskaya et al. 2012; Galande et al. 2011).

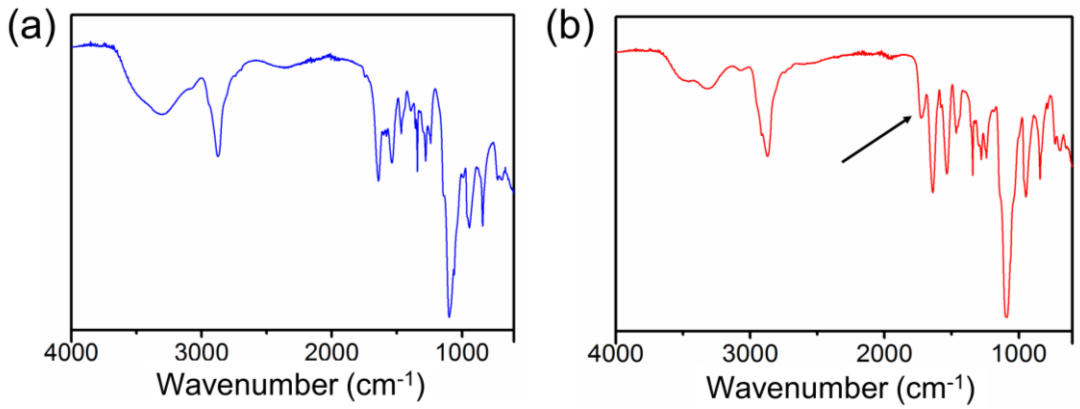

Figure 4.5 FTIR spectra of Gel 3.4K (a) at pH 7.4 and (b) at pH 3.0.

The hydrogels were also characterised by DSC (Figure 4.6). In a typical thermal cycle, the endothermic peaks of PEG (Mw=3.4 kDa) are shown at 29.1 °C and 34.6 °C. These peaks represent the melting transitions of PEG, which is a semi-crystalline polymer. PLP, on the other hand, is an amorphous polymer (DSC in Appendix, Figure S4). When PLP was crosslinked by PEG to prepare the hydrogels, the two polymers formed compact networks. In other words, the mobility of both polymer chains was reduced.

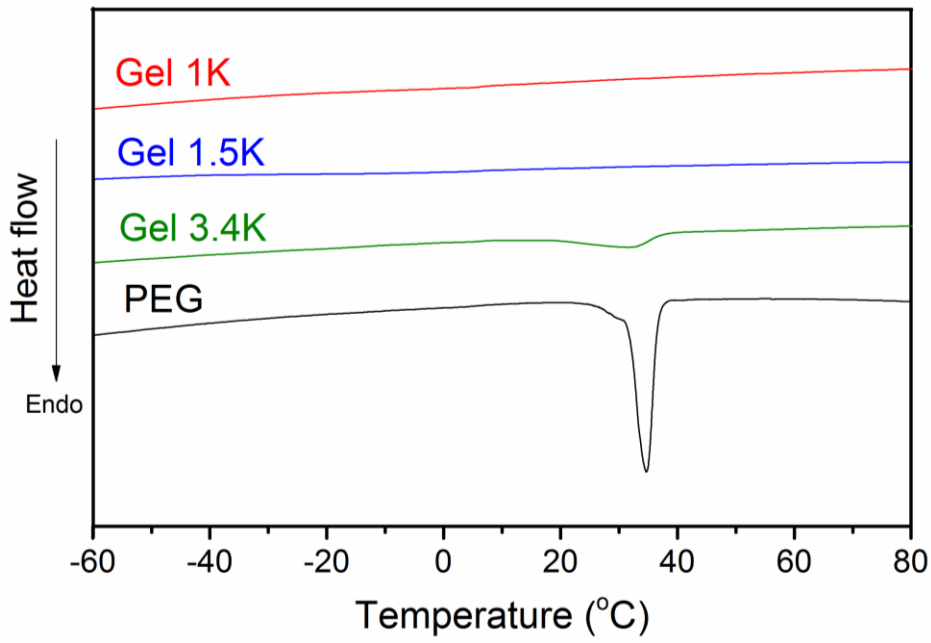

Figure 4.6 DSC of lyophilised Gel 1K, Gel 1.5K, Gel 3.4K and PEG. Before lyophilisation, all hydrogel gels were equilibrated in water.

In Figure 4.6, it was clear that the characteristic endothermic peaks of PEG disappeared in Gel 1K and Gel 1.5K. This suggests that after crosslinking, PEG was confined by PLP via chemical crosslinking and hydrogen bonding, thus not able to fold and form crystalised structures anymore. Gel 3.4K, however, had a broad peak from 16.9 °C to 40.3 °C. It suggests that the PEG within the network still had limited mobility to fold and form less regular semi-crystalline compared with pure PEG crystals. As a result, there appeared a much lower and broader peak. This suggested that the hydrogen bonding between PLP and PEG could inhibit the crystallization behaviour of PEG, which was also reported in other PEG-incorporated systems(Qiao et al. 2004; Li et al. 2013). In Gel 3.4K, however, the PEG and PLP in the network were not fully miscible, since the phase transitions of PEG were still detectable.

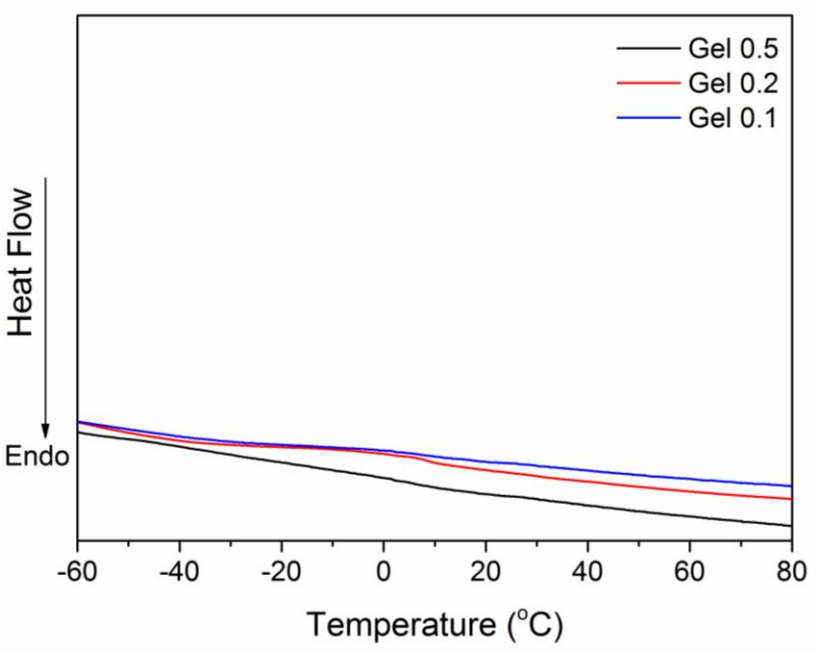

Figure 4.7 DSC of lyophilised Gel 0.1, Gel 0.2, Gel 0.5. Before lyophilisation, all hydrogel gels were equilibrated in water.

The DSC of lyophilised hydrogels of different crosslinking ratios were also performed. In Figure 4.7, despite the significant differences in crosslinking ratios, all three gels crosslinked by PEG 1.5 kDa showed no endothermic peak

within the studied range. It was then deduced that the crystallization peak was only detectable when the length of crosslinkers' chain was longer than a critical point.

To further prove the hypothesis above, a hydrogel crosslinked by PEG 8 kDa was prepared as a control. The DSC curve showed the endothermic peak, which was even more obvious than that of Gel 3.4K (See appendix, Figure S5). So the question is why longer PEG crosslinkers led to phase separation in the hydrogel? Considering the PEG crosslinkers were covalently tethered to the PLP backbone and non-covalently restrained by hydrogen bonds, then the crystallization was strictly confined in a polymer network. In this case, the longer the chain, the easier it was to fold and form crystals in nanoscale. The hypothesis was also supported by similar studies about confining crystallization of PEG. For instance, Qiao *et. al.* studied the crystallization of PEG network crosslinked by PEG dimethacrylate monomers (Qiao et al. 2004). The results suggested that the crystallinity of PEG 1K crosslinked network could not be detected by DSC, while crosslinked PEG 1.5K still had the endothermic peak with a lower T_m. Another study about the crystallization behaviour of PEG in a semi-interpenetrating polymer network also proved that the crystallinity was dependent on PEG's chain length (Li et al. 2013). When PEG's molecular weight was less than 2 kDa, the characteristic melting peak was not observed.

To sum up, this Section describes the synthesis and structural characterisation of PEG-crosslinked PLP hydrogels. FTIR and DSC results suggested that hydrogels were fabricated as designed. The two components were not only chemically crosslinked, but also physically crosslinked via hydrogen bonding.

4.2.2 Hydrogel morphology by SEM

SEM was used to characterise the morphology of hydrogels after lyophilisation. All the images shown here were cross-sections of hydrogels, to reveal the inner structures instead of surface morphology.

Figure 4.8 showed the morphology of hydrogels crosslinked by different molecular weight PEG, as well as PEG only. It was found that all three hydrogels had uniformed continuous network structure, while PEG itself formed irregular granules. Although the phase separation of Gel 3.4K was detected by DSC, it was relatively homogenous under SEM, without signs of PEG crystals. It was interesting to notice that Gel 1K had regular pores with a diameter of 5-10 μm. For Gel 1.5K, similar porous structures were observed but the pore size varied from 5 to more than 50 μm. In contrast, no pores were found in Gel 3.4K. Instead, there were just wrinkles of micrometre scales with a smooth surface.

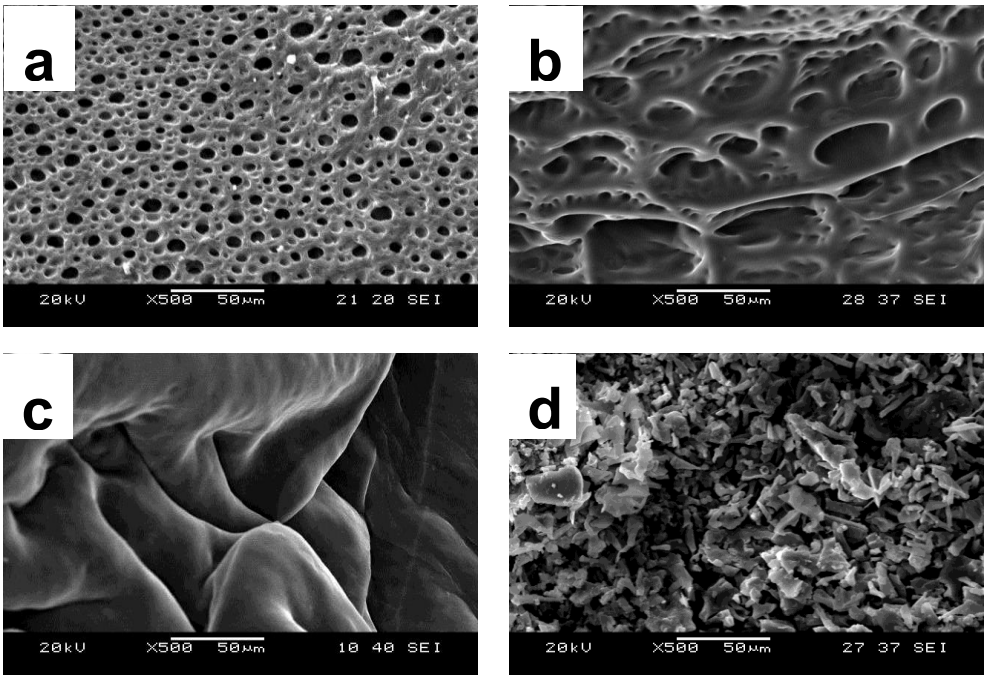

Figure 4.8 SEM images of (a) Gel 1K, (b) Gel 1.5K, (c) Gel 3.4K and (d) PEG only. All the hydrogels were equilibrated in pH 3 buffers before lyophilisation.

Similar porous structures were also observed in Gel 0.1 (Figure 4.9), however, this was not presented in Gel 0.5. The network appeared to be much denser with a few concave pits. This is attributed to the highest crosslinking density. The same trend was also observed in PLP-based hydrogels in the previous report (Watkins & Chen 2015). When the crosslinking density was higher than 20%, the porous structure became hardly identifiable.

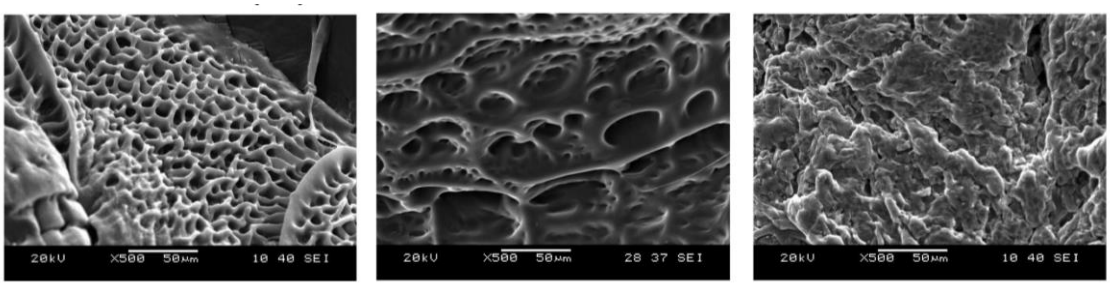

Figure 4.9 SEM images of Gel 0.1 (left), Gel 0.2 (middle), Gel 0.5 (right). All the hydrogels were equilibrated in pH 3 buffers before lyophilisation. *The images were collected by Reva Attah in Dr. Chen's group. Reproduced from Attah's Master Dissertation (2016).*

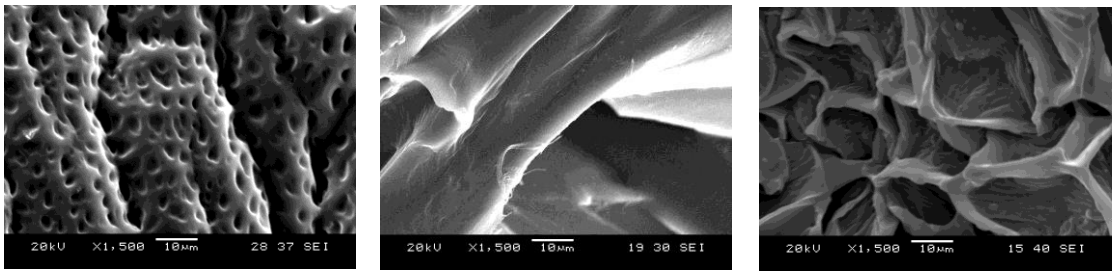

Figure 4.10 Images of Gel 1.5K equilibrated in different solutions before SEM. Left, at pH 3.0; middle, in water; right, at pH 7.4. *The images were collected by Reva Attah in Dr. Chen's group.*

It was interesting to notice there was a great difference between samples equilibrated in different solutions before lyophilisation (Figure 4.10). At pH 3.0, there were fine porous structures as discussed above. At pH 7.4 or in water, such pores disappeared. Instead, there were polymer networks with large wrinkles and relatively smooth details.

To explain the difference in SEM images shown in Figure 4.10, the author reviewed many papers about hydrogel morphology under SEM. Generally speaking, there were a great number of papers that reported similar porous structures (Chen & Park 2000; Serizawa et al. 2002; Annabi et al. 2010; Varghese et al. 2014). However, it was difficult to find the discussions about the cause of these porous structures. Most papers just reported it without further discussion, while some simply interpreted them as polymer meshes within the hydrogels (Varghese et al. 2014; Watkins & Chen 2015). Personally, I think this interpretation was not appropriate. The pores in SEM images were in micrometre scale, while polymer meshes were obviously in nanometer scale. Instead, the pores were more likely to be related to the water state within the hydrogels.

At pH 3.0, due to the protonation of COOH groups of PLP, the polymer became hydrophobic and changed its conformation in aqueous solution. In the hydrogel, although PLP was confined in a network crosslinked by PEG, it was still possible to become relatively hydrophobic, which means it has less affinity with water. Because of its hydrophobicity, it was supposed that the water within the hydrogels was able to form large ice crystals upon freezing. After ice sublimation during lyophilisation, the void left was the pore visualised by SEM. At neutral pH, the PLP was relatively hydrophilic, thus more approachable to water. It was supposed that the high affinity between the polymers and the surrounding water inhibit the formation of large crystals. As a result, the pores disappeared.

To support this hypothesis, the DSC of hydrated hydrogels was performed to study the freezing and thawing process of water within the hydrogels. Figure 4.11 showed the heating step in the second cycle. Though the endothermic peaks were heavily overlapping, it was still possible to identify

the trend of melting point. For hydrogels in pH 3 buffer, two melting peaks were identified, at -0.5°C and 2.3°C respectively. The majority of the peaks were above 0 °C. In contrast, for the hydrogels in water, the ratio of two peaks varied, with a significant decrease in the portion of the peak above 0 °C. For the hydrogels in pH 7.4 buffer, another peak at -3.4 °C was observed. The majority of the peak was shifted to minus 0 °C.

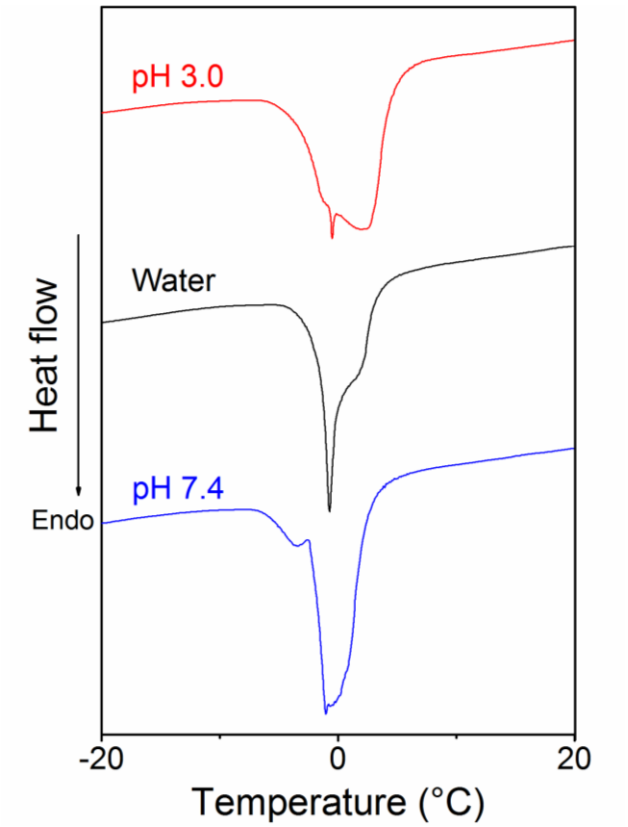

Figure 4.11 DSC curves of Gel 1.5K in pH 3.0 buffer, pH 7.4 buffer and water (second heating cycle).

According to literature, there were three types of water in the hydrogels: bonded, semi-bonded and free water (Yudianti et al. 2009). Bonded water, which was closely attached to the hydrogel via possibly hydrogen bonds, did not freeze or melt during the cycle and were thus not visible in the DSC diagram. Semi-bonded water, which was part of the hydration layer of hydrogel backbone, cannot freeze into perfect ice-crystals due to the interference from polymers. As a result, less energy was required for melting, which means the

melting point was usually lower than 0 °C. The free water was able to form large ice crystals, which required more energy to melt. Thus, the melting temperature can be even higher than 0 °C.

From Figure 4.11, it was inferred that pH 3 hydrogel had the largest ratio of free water that formed large ice crystals. This was due to the increased hydrophobicity of PLP, which preferred to interact with hydrophobic moieties instead of bonding to water. At a higher pH, PLP was deprotonated and more hydrophilic. The subsequent conformational changes made the polymer more approachable to water. Thus, more water became bonded or semi-bonded, which explains why the melting peak shifted to a lower temperature. These results were in agreement with the SEM observations. The large pores were probably due to sublimation of ice crystals at pH 3. While at pH 7.4 and in water, the ice was much smaller and irregular, which led to wrinkles but not pores.

4.2.3 pH-Responsive swelling properties

Following the water state analysis by DSC, the pH-dependent swelling behaviour of all hydrogels was studied (Figure 4.12). It was noticed that for all hydrogels, the swelling ratio (q) at pH 7.4 was higher than that at pH 3.0, due to hydrophobicity variation of PLP. Since the hydrophilic nature of PEG was not affected by pH, at pH 7.4, Gel 1K, Gel 1.5K and Gel 3.4 K had similar swelling ratios. However, at pH 3.0, it was found that Gel 3.4K had a significantly higher swelling ratio than Gel 1K and Gel 1.5K. The reason was that longer PEG chain hindered the shrinking of the hydrogel caused by hydrophobic PLP.

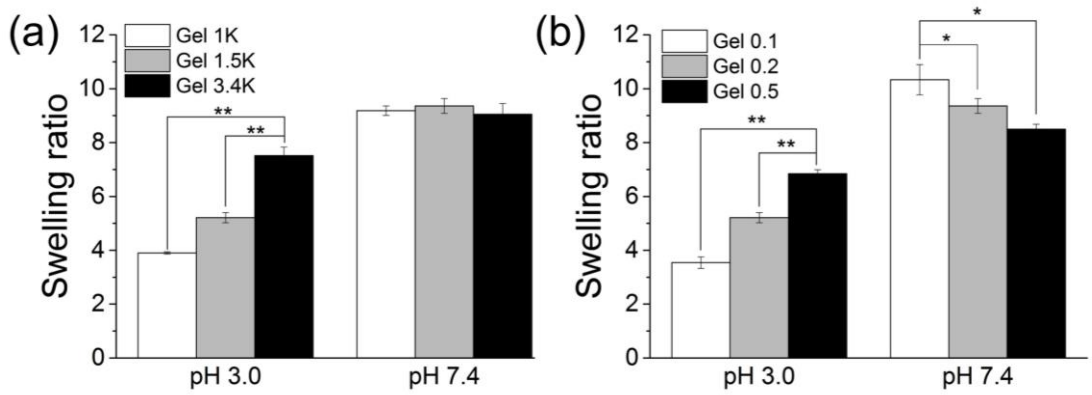

Figure 4.12 The swelling ratios (q) of hydrogels.* p<0.05, **p<0.01. (n=3). *The data were collected by Reva Attah in Dr. Chen's group. Reproduced from Attah's Master Dissertation (2016).*

In Figure 4.12b, it was found the higher crosslinker ratio led to smaller Δq. As the polymer network became denser, the chain mobility would decrease. Thus both shrinking and swelling caused by pH-responsive PLP conformational changes would be diminished. Similar results were also observed in the report of Kira *et. al.*, who also used pH-responsive PLP as backbones (Watkins & Chen 2015).

4.2.4 pH-Responsive rheology behaviour

Rheology is a critical factor for viscoelastic materials. For hydrogels, rheological measurements can reveal many architectural details, such as crosslinking density and chain entanglement (Peppas et al. 2000; Ghosh et al. 2005; Yan & Pochan 2010). The main rheological technique used for hydrogel samples is small-amplitude oscillatory shear. In this method, hydrogel disks are placed between two parallel plates and a small-amplitude sinusoidal shear stress is applied. The deformation response caused by shear (strain) is also sinusoidal with the same frequency but a phase lag. The storage modulus G' is defined as the coefficient with in-phase response and the loss modulus G'' is defined as the coefficient with out-of-phase response (Wyss 2016).

In a typical protocol for the rheological characterisation of hydrogels, strain sweep was first performed to determine the linear-viscoelastic regime (LVR). Within LVR, the stress amplitude changed with strain amplitude at the same scale. Thus, their viscoelastic properties, such as G' and G'', were independent of imposed strain and stress levels, which means the G' and G'' of different gels became comparable. That is the reason why LVR is so important in rheological measurement.

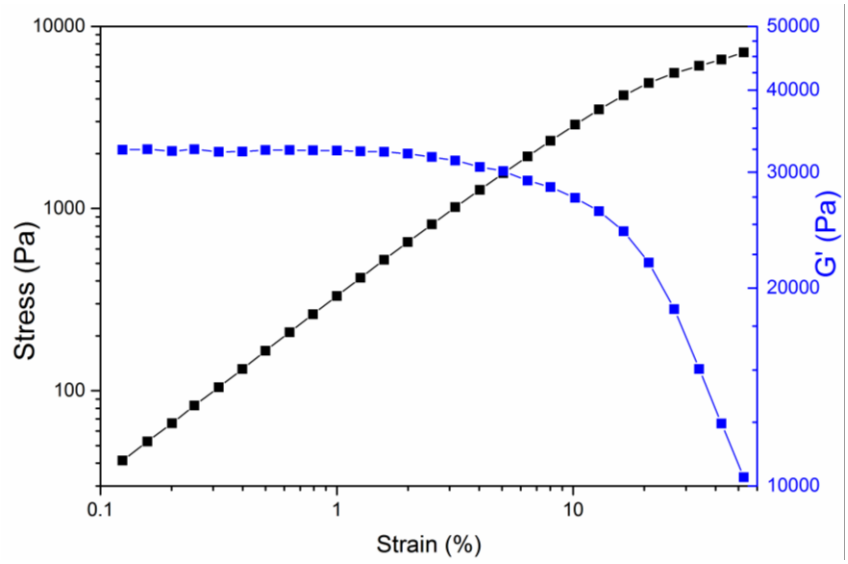

Figure 4.13 The correlation between G', oscillation stress and strain applied in the strain sweep of Gel 0.1. *The data were collected by Reva Attah in Dr. Chen's group.*

Figure 4.13 showed how LVR was identified in a typical strain sweep. G' and oscillation stress was measured against an increasing strain, while the frequency of oscillation was kept at a constant rate. When the strain was lower than 10%, the oscillation stress increased linearly with strain, with an R-squared of 0.9999. However, when it was higher than 10%, the increase deviated from the original linear curve. Storage modulus was more sensitive to the strain increase than oscillation stress. In Figure 4.13, G' remained almost the same until strain reached 2%. When strain was higher than 10%, G' dropped dramatically, which indicated strain was much higher than LVR limit and the gel interconnected structure was not able to generate a linear respond. So the LVR

of this gel was defined as 8% strain, when G' changed by more than 10% from the plateau.

After identification of LVR of all hydrogels by strain sweeps, frequency sweeps were performed to identify the G' and G'' of hydrogels. In a typical frequency sweep, a fixed strain with different frequencies was applied to a hydrogel. When the frequency was low, G' and G'' remained constant. However, as the frequency increased to a certain limit, the gel was not able to relax within the time frame, thus leading to deformations of networks. Herein, the frequency-independent G' is defined as the equilibrium shear modulus for the specific sample.

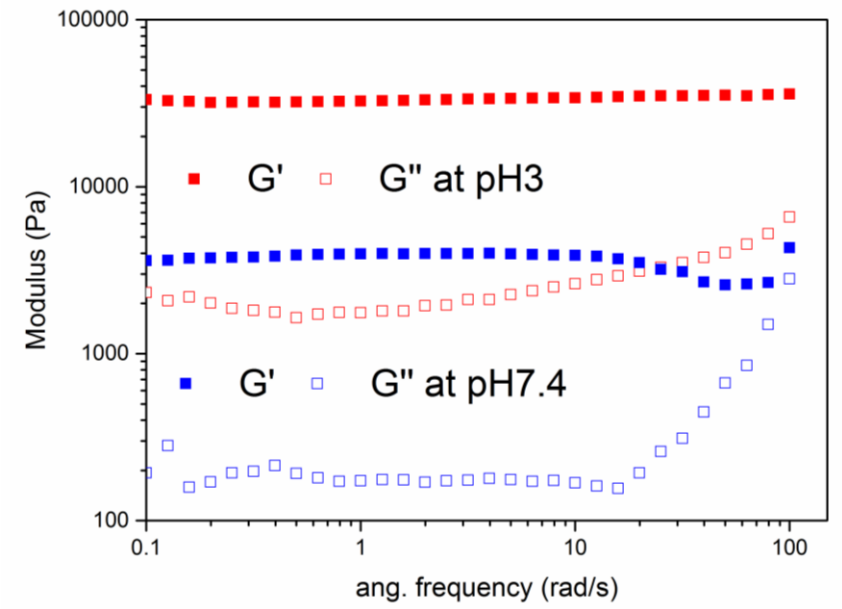

Figure 4.14 The variations of G' and G'' against angular frequency in the frequency sweep of Gel 0.1 at pH 3.0 and pH 7.4 respectively. *The data were collected by Reva Attah in Dr. Chen's group. Reproduced from Attah's Master Dissertation (2016).*

Figure 4.14 showed typical frequency sweep results for hydrogels at pH 3.0 and pH 7.4. It was found that both G' and G'' at pH 3.0 were much higher than those at pH 7.4. The higher modulus indicates that the gels were stiffer at acidic pH. Furthermore, G'' at pH 7.4 increased dramatically when the

frequency increased to 20 rad s^{-1}, and even almost surpassed G' at 100 rad s^{-1}. This means the gel network was unable to relax properly at a higher frequency and thus became more fluidic. In contrast, both G' and G'' kept almost constant within the studied frequency range at pH 3.0.

The differences of equilibrium shear modulus and gel relaxation at higher frequencies probably resulted from the pH-responsive protonation of PLP. At pH 3.0, the PLP was protonated and thus more hydrophobic. The hydrophobicity interaction between PLP chains enhanced the hydrogel network, leading to a more compact gel with a higher modulus. Moreover, when the network was rigid, the relaxation of applied stress was easy to dissipate and the hydrogel was able to recover in a relatively small timescale. At pH 7.4, however, the network was more expanded with more free water due to the electrostatic repulsion of COO^- groups. The critical time for relaxation was thus longer than the corresponding time at pH 3.0.

Based on all physiochemical characterisation results shown in Sections 4.2.2, 4.2.3 and 4.2.4, it was confirmed that the hydrogels had a pH-responsive amphiphilic structure. In an acidic environment, protonation of PLP led to formation of hydrophobic domains in the hydrogel, which repelled water but enhanced the polymer network by hydrophobic interaction. In a neutral environment, deprotonation of PLP made the hydrogel more hydrophilic, which incorporated more water in a more expanded network. This pH-responsive amphiphilicity made it a candidate for controlled hydrophobic drug loading and release.

4.2.5 Loading and release of model drugs

To study the capability of hydrogels in encapsulation of hydrophobic drugs, Nile red, which is a hydrophobic fluorescent probe with a logP of 5.0

(Bader et al. 2016), was used. The size and hydrophobicity of Nile red are similar to hydrophobic chemotherapeutics, e.g. paclitaxel (logP=3.96) (Surapaneni et al. 2012). Also, the strong fluorescence makes it easy to detect via spectrophotometre or fluorescence microscope (Sackett & Wolff 1987; Daban et al. 1991).

The loading was first performed in Nile red-saturated pH 3.0 buffer, since the hydrogels were expected to have hydrophobic domain due to protonation of PLP. Figure 4.15 shows the confocal images of Nile red loaded hydrogels as well as negative controls. From the fluorescent images, it was clear that Nile red had been successfully loaded into the hydrogels, which was confirmed by bright fluorescence in Figure 4.15a. In the bright field images, it was observed that negative control was very smooth without shades or contrast (Figure 4.15d). However, in the hydrogel, some dark tiny spots were shown, which were possibly Nile red aggregates. It was then deduced that hydrogels at pH 3.0 encapsulated Nile red sucessfully.

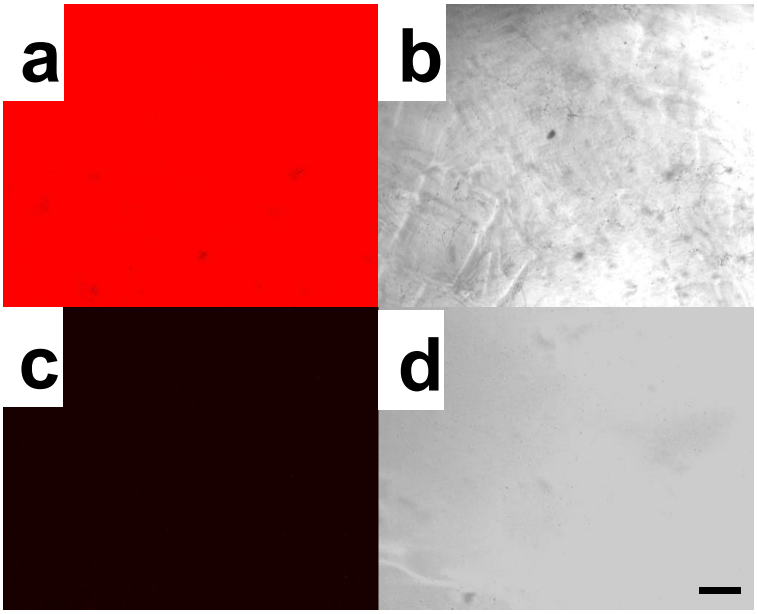

Figure 4.15 Confocal images of Nile red loaded hydrogel, fluorescent channel (a,c) and bright fields (b,d). (a), (b) PEG 1K Gel loaded with Nile red in pH 3.0 buffer. (c), (d) Negative control, gel without Nile red. Scale bar, 50 μm.

To study the relationship between hydrophobicity and Nile red encapsulation, the same loading experiment was performed in Nile red saturated pH 7.4 buffer. The 3D confocal images showed that the loading at pH 3.0 was much more efficient than that at pH 7.4 (Figure 4.16). The results confirmed that it was the hydrophobic domains formed at pH 3.0 that accommodated Nile red.

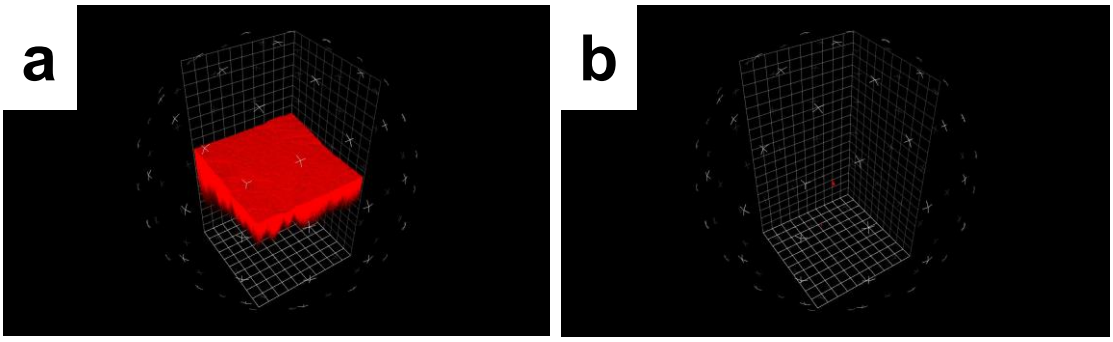

Figure 4.16 3D-Confocal images of Nile red loaded hydrogel in (a) pH 3.0 and (b) pH 7.4.

Though Nile red had a relatively high fluorescence efficiency, the measurement of fluorescence quantitatively in the release buffers was not applicable due to low loading capacity and thus insufficient fluorescence intensity. Instead of Nile red, another fluorescent model drug—fluorescein was used for quantitative study. Since fluorescein has a pKa of 6.35, it became hydrophobic at acidic pH and hydrophilic at neutral pH. This trend matched the hydrophobicity variation of hydrogels, which means the hydrophobic domains of hydrogels at acidic pH would accommodate fluorescein, while the hydrophilic network at neutral pH allowed for the release.

The drug loading was performed by a swelling-collapsing method previously reported by Peppas et al (Koetting & Peppas 2014). The hydrogel disks were first acidified to repel water from the network and then swelled in payloads buffers. The loaded gels were further acidified to ‘lock’ the payloads inside the compact network. Compared with the loading via soaking dried

hydrogels in payload buffers, this method maintained the hydrogel structure and avoided the dehydration which usually causes irreversible changes to the network.

The 24-hour cumulative fluorescein release was first studied in pH 3.0 and pH 7.4 buffers respectively (Figure 4.17). It was obvious that for every hydrogel sample studied, the release at pH 7.4 was significantly higher than that at pH 3.0. However, the differences between different hydrogel formulations were not that obvious. Gel 1K had slightly higher release percentage than Gel 3.4K at pH 3.0, but still lower than 10%. All gels had more than 80% release at pH 7.4, which proves to be very efficient. These preliminary results indicated that the hydrogels could be used for pH-stimulate controlled release of payloads.

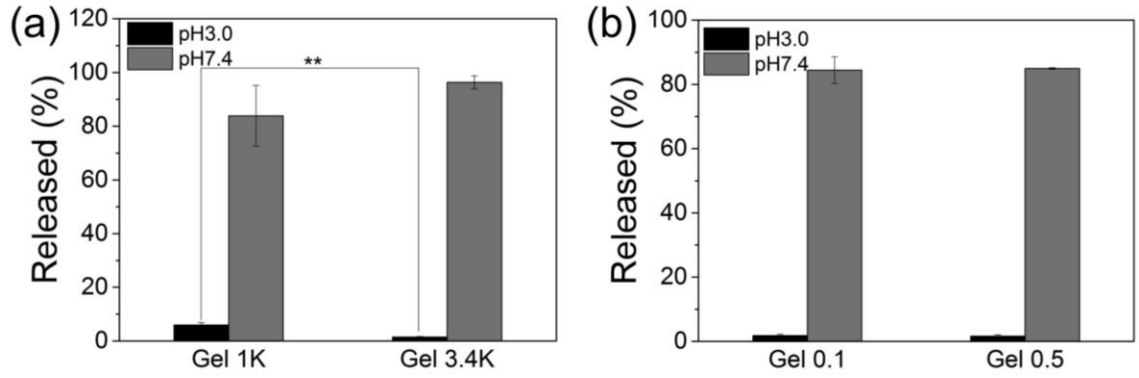

Figure 4.17 24-Hour cumulative release of fluorescein in pH 3.0 and pH 7.4 buffers. (a) Gel 1K and Gel 3.4K; (b) Gel 0.1 and Gel 0.5. ** p<0.01. (n=3). *The data were collected by Reva Attah in Dr. Chen's group.*

Then a kinetic study of release behaviour in bio-relevant buffers was performed. The hydrogels were first placed into simulated gastric fluid (SGF) for 2 hours, mimicking the digestion process in human stomach (1-3 hours), and then transferred into simulated intestinal fluid (SIF) for another 24 hours, which mimicked human intestinal environment. The results, shown in Figure 4.18, demonstrated that the fluorescein release in SGF was negligible in the

first 2 hours. Once transferred to SIF buffer, both gels quickly released more than 70% of the payload in the next 3 hours. Gel 3.4K reached the plateau at 81% after 3 hours in SIF while Gel 1K reached 71%, followed by a sustained release of another 10% of the payload. After 24 hours in SIF, both Gel 1K and Gel 3.4K released around 83% of fluorescein in total. During the time range studied, the fluorescein release from Gel 3.4 was slightly higher than that from Gel 1K at each time point. The reason might be that Gel 3.4K had a more expanded network due to long crosslinkers. Thus, the diffusion of payloads would be faster than that in Gel 1K which bore a slightly denser network.

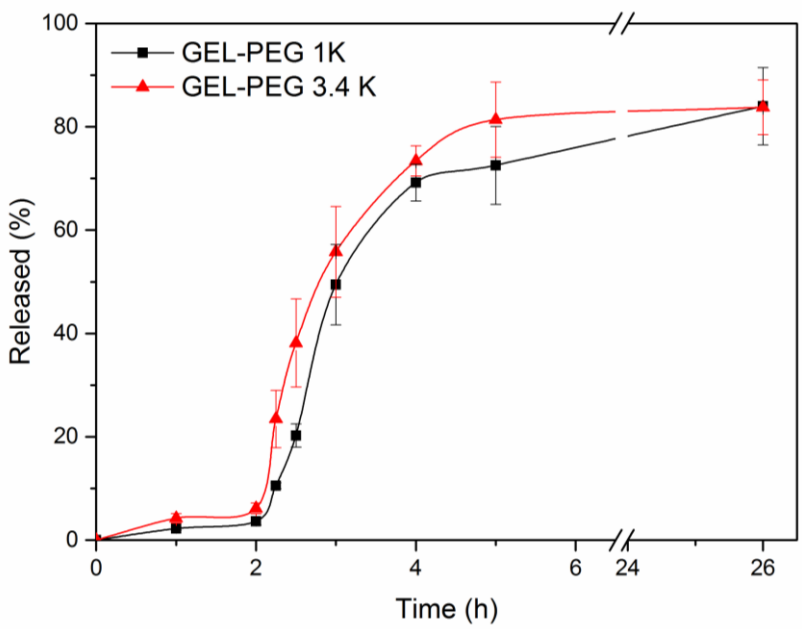

Figure 4.18 Release kinetics of fluorescein in biorelevent buffers (first 2 hours in SGF and then transferred to SIF for another 24 hours). (n=3). *The data were collected by undergraduate students Jiali Li and Yitong Chen in Dr. Chen's group. Reproduced from their undergraduate research report (2015).*

Based on the successful controlled release of fluorescein, FITC-dextran 10K, a fluorescent model drug with higher molecular weight, was used to mimic larger payloads such as peptides or proteins. The results in Figure 4.18 were surprisingly different from that in Figure 4.19. In the first 2 hours in SGF, almost half of the payloads were burst released (41% for Gel 1K and 51% for Gel 3.4

K). In SIF, the release slowed down. Gel 1K ended up with 70% total release and Gel 3.4 K ended up with 77% after 24 hours. But similar to the release of fluorescein, the Gel 3.4K release curve was slightly higher than the Gel 1K curve over the whole studied range.

The non-identical release behaviour of fluorescein and FITC-dextran 10K was attributed to their hydrophobicity. Since fluorescein is hydrophobic at a pH below its pKa, it could be successfully retained in the hydrogel in acidic environment like Nile red. At higher pH, as the hydrogel became more hydrophilic, the release was fast and efficient. Unlike fluorescein, FITC-dextran 10K was hydrophilic independent of environmental pH. So it could still be able to diffuse through the hydrogel even in SGF. The results indicated that these amphiphilic hydrogels were preferable for hydrophobic payloads oral delivery instead of hydrophilic ones.

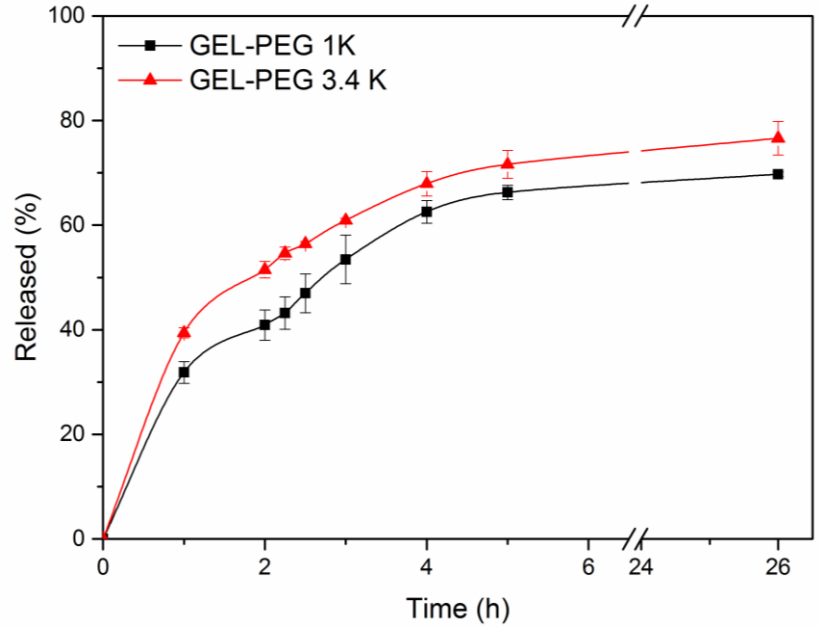

Figure 4.19 Release kinetics of FITC-dextran 10K in biorelevent buffers (first 2 hours in SGF and then transferred to SIF for another 24 hours). (n=3).

4.3 pH- and Redox-responsive hydrogels

4.3.1 Synthesis and structural characterisations

The synthesis of dual-responsive hydrogels was similar to the PEG-crosslinked hydrogels reported in section 4.2. By a one-pot EDC-coupling reaction, the hydrogels were prepared, followed by three-day dialysis for purification. The formulations and ingredients are summarised in Table 4-2.

Table 4-2 CDE-crosslinked hydrogel formulations. Readapted from published work (Wang et al. 2016a)**, copyright 2016, with permission from Wiley.** *The solid content data were collected by Xiaoxue Liu in Dr. Chen's group.*

Name	PLP (mg)	CDE (mg)	Polymer concentration (wt%)	Solid content (wt%)[a]
$Gel_{CDE}1$	100	25	10.0	7.5
$Gel_{CDE}2$	75	19	7.5	6.0
$Gel_{CDE}3$	50	13	5.0	5.3
$Gel_{CDE}4$	25	6	2.5	4.3

a The weight of a hydrogel disk after lyophilisation divided by its weight before lyophilisation (see Equation 2.1 in Chapter 2).

According to the previous study with PEG-crosslinked hydrogels, a medium crosslinking density (20%) was used for all CDE-crosslinked hydrogel formulations. By changing the polymer concentration in the hydrogel preparation, hydrogels with different solid contents were obtained, ranging from 7.5% for $Gel_{CDE}1$ to 4.3% to $Gel_{CDE}4$. When polymer concentrations were lower than 2.5%, the hydrogel could not form after overnight crosslinking.

FTIR was first used to characterise hydrogel structures. The spectra of all hydrogels and PLP were shown in Figure 4.20. All hydrogels spectra were nearly identical. Compared with PLP which had similar band intensity at 1300 cm^{-1} and 1190 cm^{-1}, the ratio of these two bands changed in the hydrogel

spectra. In PLP these two bands were correlated to amide III and COOH vibrations. In hydrogels, the increased intensity of band 1190 cm^{-1} was probably related to the ester group of CDE. Though the overlaps of ester and COOH bands made it a bit difficult to identify, the changes in band ratios confirmed the successful incorporation of CDE in the hydrogel structure. The vibration peak of CH_2-S was around 1315 cm^{-1} according to literature (A. Zhang et al. 2016). Unfortunately, it was not visible in Figure 4.20 because of the strong amide III band of PLP at around 1300 cm^{-1}, which overlapped with the CH_2-S peak.

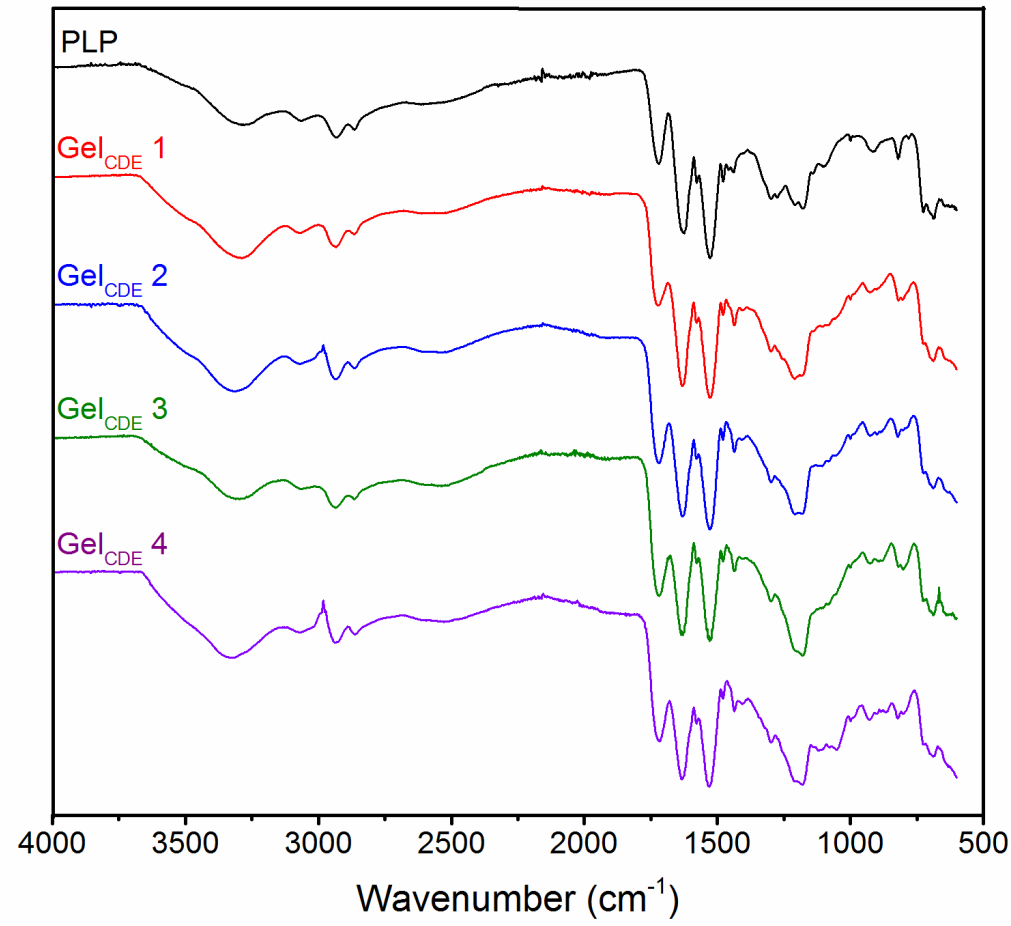

Figure 4.20 FTIR spectra of different hydrogels and PLP.

Since the CH_2-S peak was difficult to detect in FTIR spectra, X-ray photoelectron spectroscopy (XPS) was used to detect the sulfur in the hydrogels. According to Figure 4.21a, a clear sulfur peak (S 2p) at 164 eV was

identified along with carbon (C 1s) at 285 eV, nitrogen (N 1s) at 400 eV and oxygen (O 1s) at 532 eV. In the zoomed-in figure (Figure 4.21b), the sulfur peak was fitted with the S $2p_{3/2}$ and S $2p_{1/2}$ spin-orbit coupling contributions. The binding energy for S $2p_{3/2}$ was observed at 163.7 eV, which was characteristic for disulphide compounds (Qiu & Park 2012; Alvarez-Lorenzo et al. 2013). The XPS results, along with FTIR results, confirmed the incorporation of CDE crosslinkers in hydrogel samples.

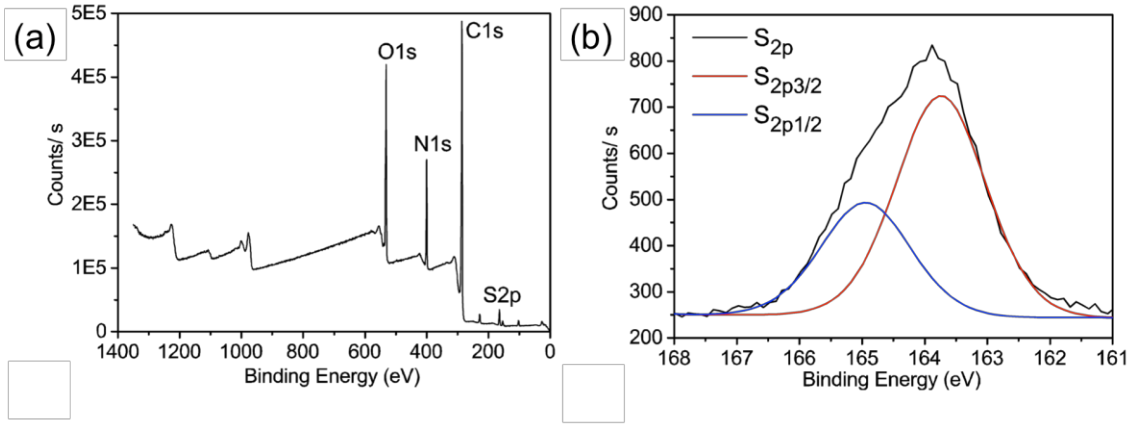

Figure 4.21 (a) the XPS spectrum of Gel_{CDE} 2; (b) the zoomed-in figure of the sulfur peak. Reprinted from published work (Wang et al. 2016a)**, copyright 2016, with permission from Wiley.**

Furthermore, the actual crosslinking ratio could be deduced from the atomic composition of polymer backbones and disulfide-bond containing crosslinkers (Table 4-3). In each PLP residue, there are two nitrogen atoms but no sulfur, while in each CDE crosslinker there are two nitrogen atoms and two sulfurs. The crosslinking ratio was calculated as shown in Equation 4.1. It was found that Gel_{CDE} 1 had the highest ratio of crosslinking, possibly due to higher crosslinking efficiency at the higher polymer concentration, while the other three gels had similar crosslinking degrees of around 13%.

Table 4-3 Atomistic compositions of each hydrogel by XPS and the crosslinking ratio. Readapted from published work (Wang et al. 2016a)**, copyright 2016, with permission from Wiley.**

Name	C (%)	O (%)	N (%)	S (%)	Crosslinking ratio (mol %)[a]
Gel_{CDE} 1	68.2	16.8	12.1	1.65	15.8
Gel_{CDE} 2	67.5	17.2	12.2	1.4	13.0
Gel_{CDE} 3	68.1	16.6	12.7	1.5	13.4
Gel_{CDE} 4	68.7	16.3	12.5	1.5	13.6

a Defined as the molar ratio of crosslinkers to PLP residues (see Equation 4.1).

$$Crosslinking\ ratio\ (\%) = \frac{2S(\%)}{2N(\%) - 2S(\%)} \times 100 \qquad \text{(Equation 4.1)}$$

To sum up, the FTIR and XPS results shown in this section confirmed the incorporation of the CDE crosslinkers and successful crosslinking of hydrogels.

4.3.2 Hydrogel morphology by SEM

The morphology of CDE-crosslinked hydrogels was also characterised by SEM via the same method as PEG-crosslinked hydrogels. As shown in Figure 4.22, all of the CDE-crosslinked hydrogels had porous structures. Compared with PEG-crosslinked hydrogels (Figure 4.8, 4.9 and 4.10), CDE-crosslinked hydrogels appeared more fragile and delicate. There were even small pieces observed in Gel_{CDE} 3 and Gel_{CDE} 4 with lower solid contents, which suggested that the hydrogel structures may have collapsed or even broken during the SEM sample preparation. This suggested that the presence of PEG strengthened the hydrogel network better than CDE.

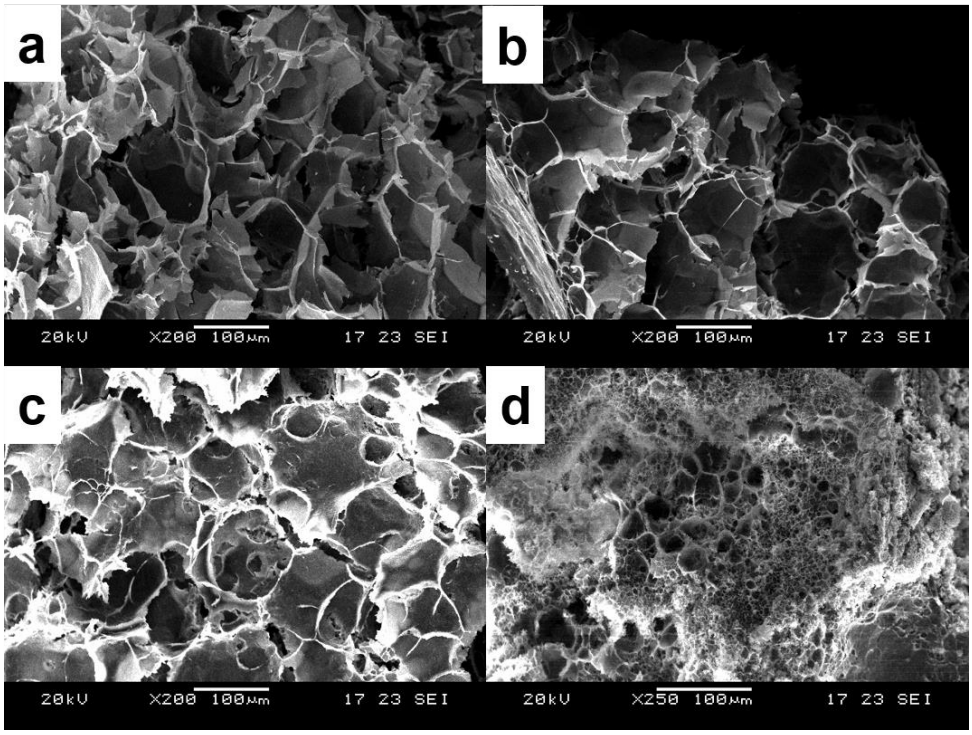

Figure 4.22 SEM images of different hydrogels. (a) Gel_{CDE} 4, (b) Gel_{CDE} 3, (c) Gel_{CDE} 2, (d) Gel_{CDE} 1. Reprinted from published work (Wang et al. 2016a)**, copyright 2016, with permission from Wiley.**

In Figure 4.22, the size of the pores was not perfectly uniform, but showed a general decreased trend with the increase of solid contents. The trend was similar to the trend with different crosslinking density (Figure 4.9). As the solid contents increased, the polymer network appeared to be denser which limited the water crystal formation, thus leading to smaller pores.

4.3.3 pH-Responsive swelling properties

As shown in Figure 4.23, the swelling ratio of all hydrogels at pH 7.4 was higher than that at pH 3.0 as expected. At both pHs, Gel_{CDE} 4 had a significantly higher swelling ratio than Gel_{CDE} 1. This indicated that a lower polymer network density would accompany more water in the hydrogel. Gel_{CDE} 2 had the highest Δq from pH 3.0 to pH 7.4, while Gel_{CDE} 1, Gel_{CDE} 3 and Gel_{CDE} 4 had similar $\Delta q<3$. This suggested that the pH-responsive swelling capacity probably

preferred the combination of a lower crosslinking degree and higher solid contents.

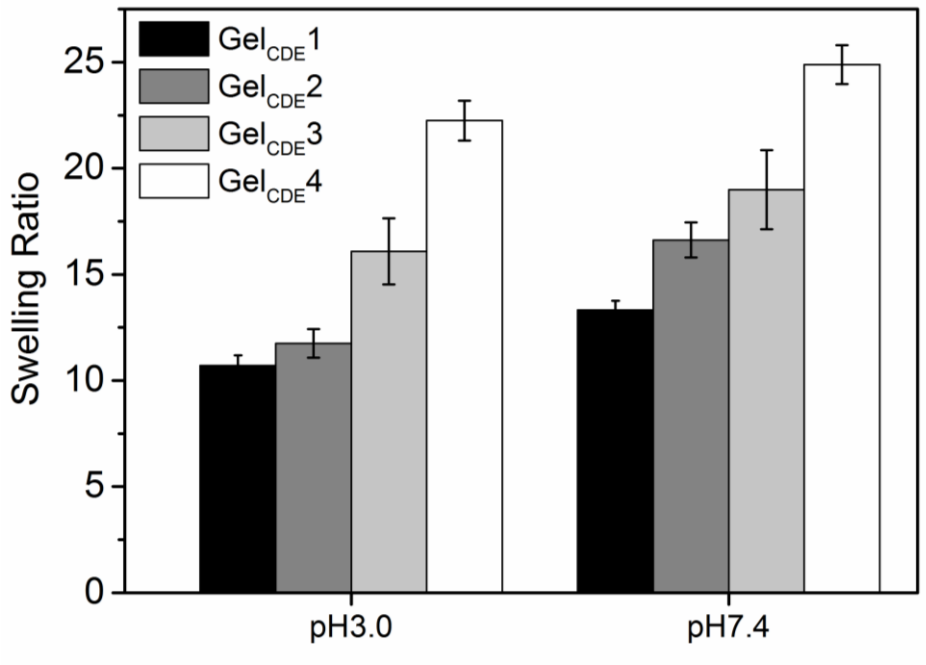

Figure 4.23 pH-responsive swelling behaviour of hydrogels. * p<0.05. (n=3). Reprinted from published work (Wang et al. 2016a)**, copyright 2016, with permission from Wiley.** *The data were collected by Xiaoxue Liu in Dr. Chen's group.i*

It was interesting to find out that the absolute swelling ratios of the CDE-crosslinked hydrogels were much higher than those of PEG-crosslinked hydrogels (Figure 4.12, q<10 for all hydrogel studied). This was not expected because PEG was considered much more hydrophilic than CDE. However, since PEG had both chemically and physically crosslinking effects, it was possible that the network was much more compact and thus unable to swell.

Another important fact was that PEG had a much higher molecular weight than CDE. So it was possible that PEG could crosslink most carboxylic acid groups that are distant from each other on different PLP chains, while CDE which may crosslink most carboxylic acid groups that are adjacent to each other on the same PLP backbone (Figure 4.24). In other words, the intramolecular

crosslinking instead of intermolecular crosslinking might be more likely to happen in CDE-crosslinked gels than PEG-crosslinked gels due to the differences in their molecular size. The intramolecular crosslinking had less limitation on polymer chain mobility compared with intermolecular crosslinking. So the swelling ratios of CDE-hydrogels appeared to be higher.

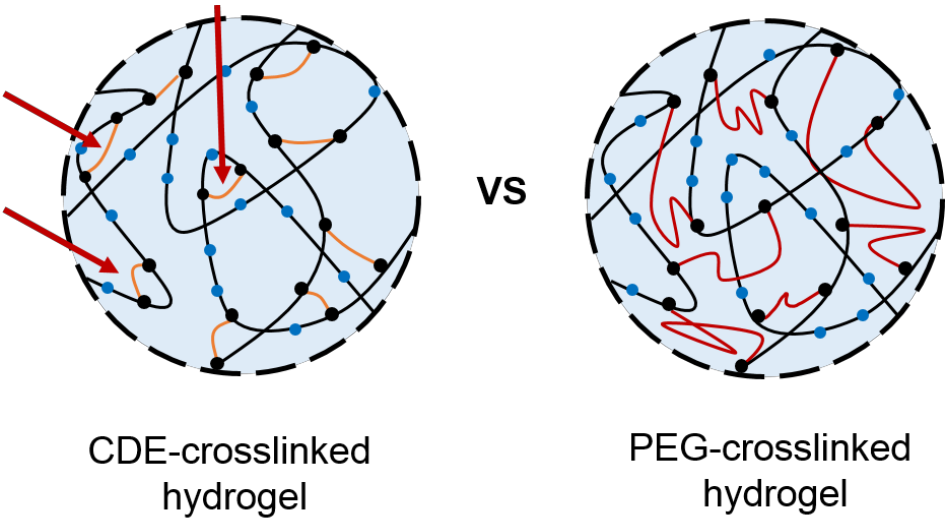

Figure 4.24 Schematic showing the differences of polymer network of CDE-crosslinked hydrogels and PEG-crosslinked hydrogels. Red arrows pointed to the intramolecular crosslinking of CDE-crosslinked hydrogels.

These intramolecular crosslinking also explained why the hydrogel could not form when the polymer concentration dropped to below 2.5% (wt). When the polymer concentration was low during gelation, intramolecular crosslinking became more prominent. Even though the ratio of polymer and crosslinkers was kept the same, the crosslinker was consumed by short-ranged intramolecular crosslinking, or even became daggling end without crosslinking. The gelation in this condition was thus inefficient.

4.3.4 Dual-responsive rheology behaviour

The pH- and redox-responsive rheology behaviour of CDE-crosslinked hydrogels was characterised similarly to PEG-crosslinked hydrogels via the

small-amplitude oscillatory shear method. The frequency sweep results are shown in Figure 4.25.

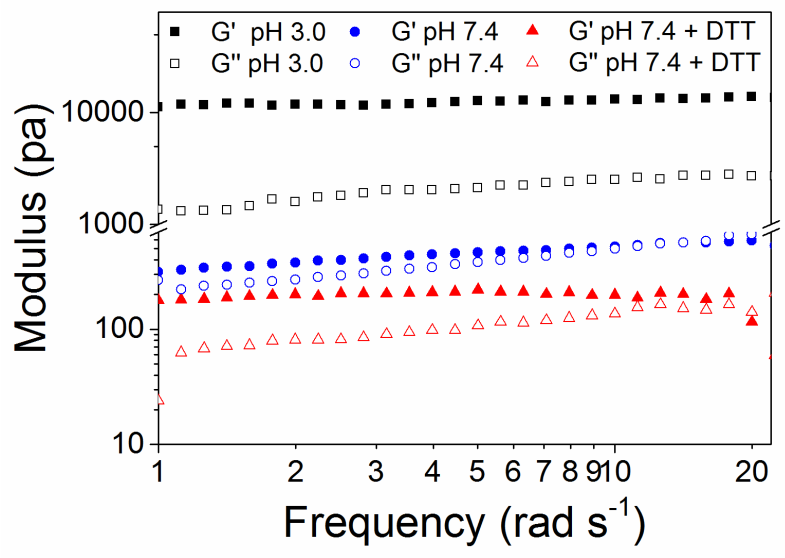

Figure 4.25 Frequency sweep of Gel_{CDE} 2 at pH 3.0, pH 7.4 and pH 7.4 with the addition of DTT. Reprinted from published work (Wang et al. 2016a)**, copyright 2016, with permission from Wiley.**

It was obvious that the G' at pH 3.0 was much higher than that at pH 7.4. Furthermore, at pH 3.0 the G' and G'' were almost independent of the frequency within the studied range, while at pH 7.4 the G'' surpassed G' when the frequency was higher than 14 rad s^{-1}. These two trends were similar to PEG-crosslinked hydrogels due to the pH-dependent protonation of PLP backbones. However, the G' of PEG-crosslinked hydrogels at pH 7.4 was almost 10 times higher than the corresponding G' of CDE-crosslinked hydrogels. This was attributed to the high water content and the loose network of CDE-crosslinked hydrogels, as discussed in Figure 4.24. The physical and chemical crosslinking of PEG led to compact networks and thus the hydrogels were stiffer.

When DTT was added to reduce the disulfide bonds of CDE, an even lower G' was observed (200 pa), only 1% of the corresponding G' at pH 3.0.

This suggested the addition of DTT further loosened the hydrogel network by the cleavage of disulfide bonds.

4.3.5 Loading and release of model drugs

After characterisation of dual-responsiveness by rheology, the loading and release profiles of the CDE-crosslinked hydrogels were investigated. From the previous study of PEG-crosslinked hydrogels shown in Section 4.2.5, hydrophobic payloads were favourable for encapsulation in the amphiphilic hyrogels. So fluorescein was chosen as the model drug for examining the loading and release profiles of the CDE-crosslinked hydrogels.

Figure 4.26 shows the cumulative release of fluorescein in different pH buffers. As Gel_{CDE} 4 was too fragile to handle, it was excluded from the release study. All the three hydrogels studied had distinctive pH-dependent cumulative release. Less than 5% of fluorescein was released at pH 3.0 and less than 10% at pH 5.0. In comparison, more than 90% was released at pH 7.4 after 24-hour incubation at 37 ^{o}C. The results indicate that these hydrogels could successfully retain drugs at gastric acid but release them at intestinal pH within 24 h.

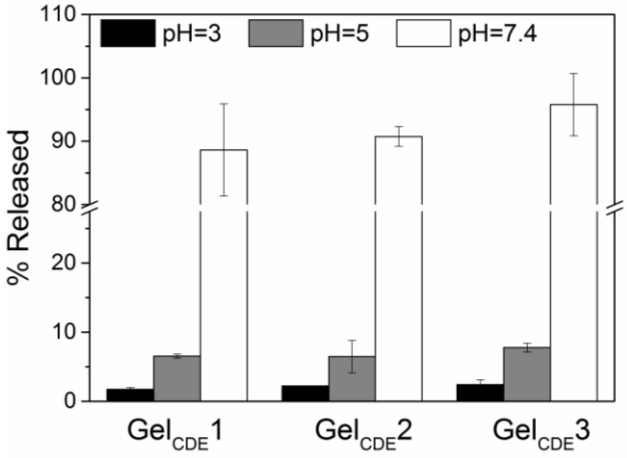

Figure 4.26 Cumulative release of fluorescein at pH 3.0 and 7.4 after 24 h of incubation. (n=3). Reprinted from published work (Wang et al. 2016a)**, copyright 2016, with permission from Wiley.** *The data were collected by Xiaoxue Liu in Dr. Chen's group.*

The kinetics of fluorescein release is shown in Figure 4.27. At pH 3.0 and 5.0, the release was all below 10% within the studied time-frame, thus considered as negligible. At pH 7.4, the release in the first 5 hours increased almost linearly with time. After 5 h, a 71% of release was reached and the kinetics was in a near zero-order release pattern. This might be due to the swelling of hydrogels, which was widely reported in pH-responsive ionic hydrogels, such as poly(N, N -dimethylacrylamide) hydrogels, and poly(acrylic acid) hydrogels (Siegel et al. 1988; Peppas & Khare 1993; Serra et al. 2006; Aimetti et al. 2009). Once DTT was introduced as a redox-trigger, a steeper release profile was observed, with almost complete release in 5 h. The results suggested that DTT could boost the release rate by dissociating the hydrogel.

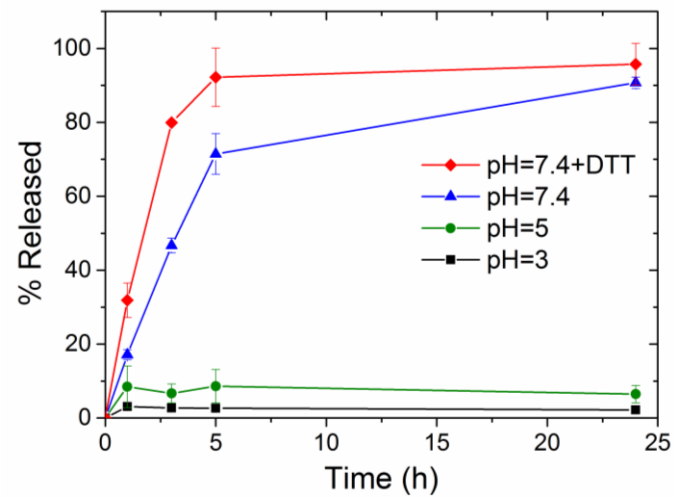

Figure 4.27 Released kinetics of Gel_{CDE} 2 at pH 3.0, pH 5.0, pH 7.4, and pH 7.4 with 0.1 M DTT. (n=3). Reprinted from published work (Wang et al. 2016a)**, copyright 2016, with permission from Wiley.**

The images shown in Figure 4.28 further confirmed the reducing effects of DTT on hydrogels. After 24 hours of release, Gel_{CDE} 3, which had a lower solid content and crosslinking density, was completely dissociated. For Gel_{CDE} 1 and Gel_{CDE} 2, instead of being dissolving completely, they swelled and disintegrated into small pieces. As Gel_{CDE} 1 and Gel_{CDE} 2 had higher solid contents, the denser polymer network made it less accessible to the reducing

reagent DTT. This explains why they were not completely disassociated like Gel_{CDE} 3.

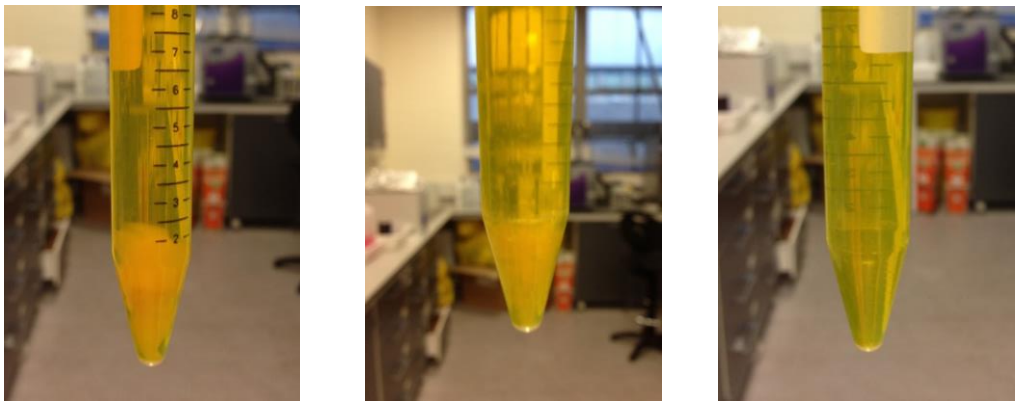

Figure 4.28 Images of hydrogels after drug release with 0.1 M DTT for 24h. From left to right: Gel_{CDE} 1, Gel_{CDE} 2 and Gel_{CDE} 3.

In summary, the hydrogels could retain the model drugs at gastric pH but release at intestinal pH. Furthermore, they could be dissociated under the colonic reducing environment. The dual-responsive controlled release behaviour made the hydrogels a potential candidate for colon-targeted delivery.

4.3.6 Cytotoxicity

Though all components of these hydrogels were previously reported to be biocompatible, the cytotoxicity of the hydrogels was evaluated *in vitro* by alamarBlue® assay on HeLa cells (Figure 4.29). It was found that all hydrogels had negligible cytotoxicity with cell viabilities higher than 90% even at a hydrogel concentration of 5 mg mL^{-1}. The biocompatibility of the hydrogels made it possible for further investigation into bio-related payloads loading and release.

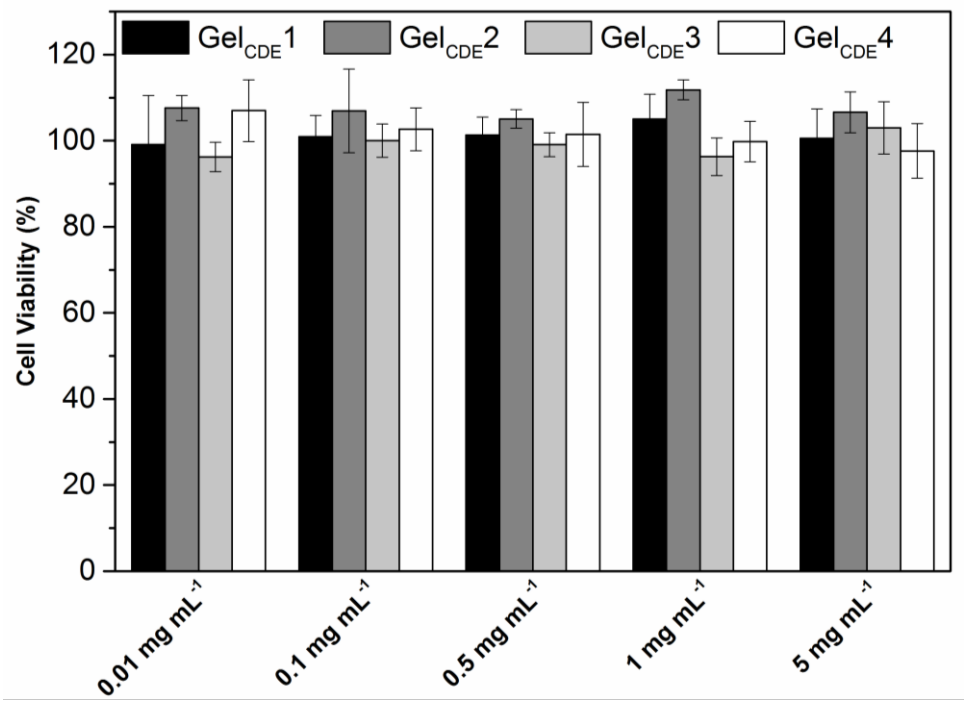

Figure 4.29 Cytotoxicity of gels evaluated by alamarBlue® assay on HeLa cells. (n=5). Reprinted from published work (Wang et al. 2016a)**, copyright 2016, with permission from Wiley.**

4.3.7 Loading and release of probiotics

Probiotics are considered as one of the favourable bio-related payloads. As microorganisms which benefit their hosts, gastrointestinal probiotics are capable of reducing the possibilities of inflammatory bowel disease (Jonkers et al. 2012; Sheil et al. 2007). Emerging evidence even shows that the imbalance of probiotics in gut is associated with metabolic disorders, which may lead to severe systemic diseases such as cancer (Yu & Li 2016; Warusavitarne & Stebbing 2017). However, oral delivery of probiotics remains to be a challenge due to the harsh GI environment, in which probiotics hardly survive (Livney 2010). Therefore, encapsulation of payloads in hydrogel carriers is important due to their protection effect towards acids in the stomach and enzymes in the small intestine. The disassociation of dual-responsive hydrogels in colon would also allow for an efficient release.

As one of the most commonly studied probiotic bacteria, *Lactobacillus rhamnosus GG* (LGG) is used here as a model probiotics for delivery study. This strain was a widely used food additive in yogurt (Yang et al. 2017). It was found to be beneficial in preventing viral infection by activating an immune response (Kawashima et al. 2011).

The loading of LGG was similar to that of fluorescein. Hydrogel slices were allowed for swelling in the LGG-containing MRS medium or PBS at pH 7.4. Figure 4.30 shows the amount of live bacteria in the hydrogels after loading. $Gel_{CDE}1$ and Gel_{CDE} 3 were used here to represent hydrogels with different networking densities. It was obvious that the loading efficiency in PBS solution was higher than that in MRS medium for both Gel_{CDE} 1 and Gel_{CDE} 3. Since MRS medium had a slightly acidic pH at 5, the hydrogels shrank. The consequent compact structure hindered the diffusion of LGG as well as the transportation of nutrition, thus leading to a lower bacterial loading efficiency. Gel_{CDE} 3 in PBS had the highest loading efficiency among all conditions used. It was used for the later release study.

Though LGG loading was performed in PBS, the release only worked in MRS medium. Significant differences were identified when using different release buffers. There were almost no living bacteria in either water or PBS release solution, while around 6 x 10^6 LGG mL^{-1} in MRS. The possible reason for the huge differences in survival rates might be bacteria's tendency towards nutrition. MRS broth provided an ideal environment for bacteria growth, so the bacteria encapsulated in the hydrogels tended to escape from the gels to MRS for better nutritional supplements. Moreover, the released free bacteria in MRS had the ability to grow in a biphasic pattern. So the number increased swiftly with time. By contrast, water and PBS buffer are nutrient-poor environments, which bacteria could not readily survive. Though hydrogels are more swollen

and have decent release profiles for small-molecule model drugs in water and PBS according to the previous study, MRS is proved to be a better release solution for bacteria.

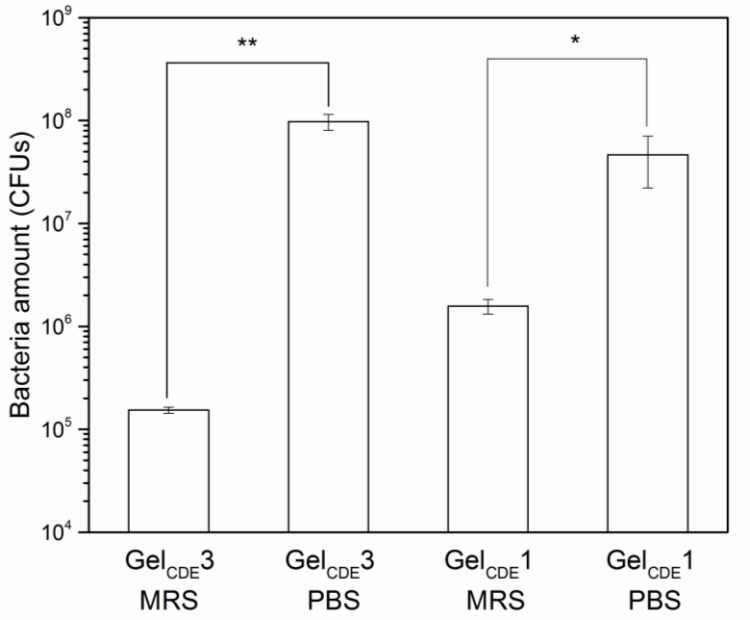

Figure 4.30 LGG loading capacity of Gel_{CDE} 1 and Gel_{CDE} 3 in MRS (pH 5.0) and PBS (pH 7.4) respectively. * p<0.05, **p<0.01. (n=3).

The release profile of LGG is shown in Figure 4.31. It is interesting to notice that the bacterial density in the hydrogel remained quite stable during the first 5-hour release process, while increased by an order of magnitude after 8 hours (Figure 4.31a). Although bacteria were continuously released from the hydrogel, those still within could reproduce, thus keeping the total number unchanged. Further elongation of release time to 8 hours even led to an increase in the number of bacteria in the hydrogel, which is another evidence of bacterial reproduction. Taking the advantage of this effect, the number of bacteria loaded could be increased if hydrogels were incubated with MRS after loading.

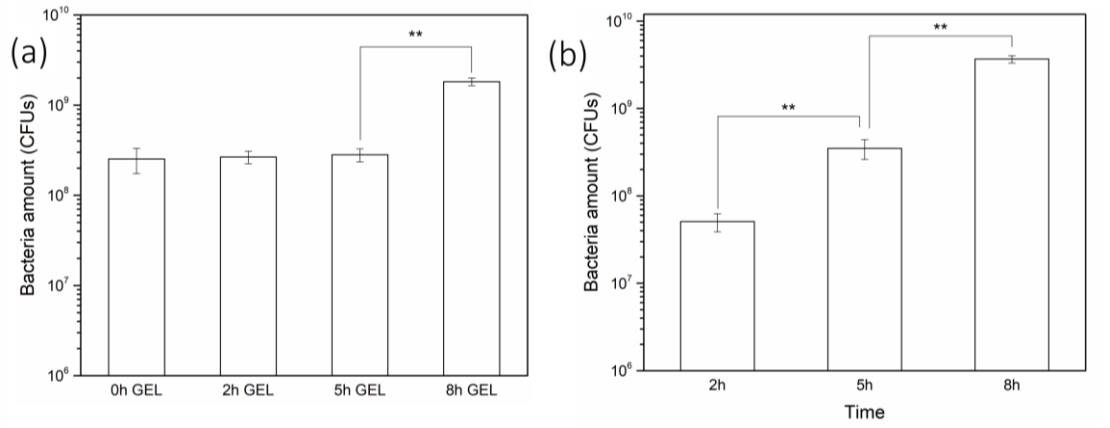

Figure 4.31 (a) LGG amount remained in the hydrogel during release. (b) LGG amount released in the MRS medium. **p<0.01. (n=3).

Figure 4.31b shows that the amount of released bacteria in MRS solution increased exponentially over time. The increased amount may come from both continuous release from hydrogels and bacteria reproduction. In an ideal environmental condition (sufficient nutrient and optimal temperature), bacteria grow in an exponential pattern after a short adaption to the growth conditions (Schlegel & Zaborosch 1993). Since the release was in LGG culture medium, the growth was likely to happen, which is consistent with the results in Figure 4.31a. However, it is difficult to quantify the amount of released LGG, with such a contribution from reproduction. Further experiments need to be performed to have a better understanding of the release pattern.

4.4 Conclusions

To conclude this Chapter, two series of stimuli-responsive hydrogels were developed by crosslinking PLP with different crosslinkers. The effects of crosslinking ratios, polymer concentration and crosslinker on hydrogel structures were systematically studied. The stimuli-responsive model drug release behaviour was demonstrated. The aim of this study was to investigate how crosslinkers affected the hydrogel structures and the consequent effects

on their behaviour of controlled release of model drugs, especially hydrophobic drugs.

The hydrogels were prepared by a facile EDC-coupling reaction in the aqueous system. The crosslinkers included CDE which is a small-molecular dimer of amino acid with disulfide bonds, and PEG which is a biocompatible polymer. The chemical components of the hydrogels were confirmed by FTIR and XPS. Further study of swelling, rheology, DSC and morphology under SEM proved that the PEG-crosslinked hydrogels had a more compact network than the CDE-crosslinked hydrogels, even at the same crosslinking density. This was attributed to the hydrogen bonding between PLP and PEG, as well as the higher intermolecular crosslinking.

Both PEG- and CDE-crosslinked hydrogels showed favourable profiles of controlled release of model hydrophobic drugs in the gastrointestinal mimicking environments. Although the networks of CDE- and PEG-crosslinked hydrogels had distinctive differences, all the hydrogels could retain the payloads in gastric acids while release in the intestinal-mimicking buffers. PEG-crosslinked hydrogels had a faster release than CDE-crosslinked hydrogels at neutral pH. When redox-trigger was induced, the release rate could be boosted and became comparable to PEG-crosslinked hydrogels.

Though comparable studies of the controlled-release behaviour of both hydrogels, it was found that the controlled-release was not only dependent on the carriers, the payload itself also played an important role. This hydrogel system, in particular, favoured hydrophobic payloads, such as Nile red and fluorescein.

Based on pH- and redox-triggered payload release behaviour of the hydrogels, an attempt was made on the delivery of super large payloads –

probiotics using the CDE-crosslinked hydrogels. The loading and release of LGG were evaluated *in vitro*. Preliminary results showed that LGG could be successfully incorporated into the hydrogels in PBS buffer at pH 7.4 and efficiently released in MRS medium. Further protective effects of hydrogels against gastrointestinal fluids and bile acids need to be investigated in the future to acquire a better understanding of the hydrogel system.

Chapter 5 Nanogels for oral drug delivery

Chapter 5 describes the design and synthesis of PLP-based nanogels, which combine the advantages of hydrogels and CPP-mimicking polymers. The nano-sized drug carriers were formulated by either physical or chemical crosslinking, with adjustable sizes. Cargos could be loaded in situ during nanogel formation and the release with pH- or redox-triggers was investigated.

Note: MSc students Xiaozhen Huang and Youlim Ha, undergraduate students Sim Wen, Benjamin Chin and Wanyue Ouyang in Dr Rongjun Chen's group contributed to some results in this chapter. Nanogel samples used in Figure 5.4 and 5.5 were prepared by Xiaozhen Huang and those used in Figure 5.7 were prepared by Sim Wen and Benjamin Chin. Nnanogels used in Figure 5.15 and 5.16 were prepared by Wanyue Ouyang. The contribution of MSc and undergraduate students were acknowledged in the captions of the relevant figures and tables.

5.1 Introduction

Though hydrogels could achieve oral delivery at macroscopic level, they were not able to facilitate the subsequent delivery to diseased cells due to the size limitation. However, nanogels, which are defined as nano-sized hydrogels, combine the advantages of hydrogels with nanotechnology. On the one hand, nanogels inherit the 3D-polymer network structures of hydrogels, thus presenting the controlled release of payloads depending on the local environment. On the other hand, the nano size enables intracellular or transcellular transport via endocytosis or macropinocytosis. This helps to overcome the microscopic barrier-GI epithelium and the cellular barriers. Therefore, nanogels are considered as a multi-scale delivery system.

Similar to hydrogels, nanogels could be prepared by physical crosslinking (such as hydrogen bonding, hydrophobic interactions and supermolecular host-guest interactions) or chemical crosslinking. Akiyoshi et al. first reported physically crosslinked nanogels, composed of cholesterol-modified polysaccharides (Akiyoshi et al. 1993; Akiyoshi et al. 1998). The amphiphilic polymers self-assembled in an aqueous environment and formed stable nano-sized aggregates. After that, a series of physically crosslinked nanogels based on cholesterol-modified poly(L-lysine) (Akiyoshi et al. 2000), poly(N-isopropylacrylamide)-grafted pullulan (Morimoto et al. 2008) and alkyl chain-grafted PEI (Chattopadhyay et al. 2016) have been reported. The nanogels could be used for macromolecule delivery, such as cancer antigens, cytokines and siRNA (Tahara & Akiyoshi 2015).

Chemically crosslinked nanogels have also been developed for decades. Kabanov *et al.* first proposed a drug delivery system called NanoGel™ by chemically crosslinking PEI with carbonyldiimidazole-activated PEG via an emulsification/solvent evaporation method (Vinogradov et al. 1999). However, the nanogels obtained were not uniform, with sizes ranging from 20-220 nm. Others who used nano- or micro-emulsion polymerization had better control over the size and distribution (Yusa et al. 2009; Shi et al. 2008). Some new methods use top-down particle lithographic fabrication templates to obtain precisely defined nanogels (J. Xu et al. 2013). However, the complexity and relatively low yield remain a problem for its application at large scale.

As discussed in the previous chapters, PLP and its derivatives had pH-dependent conformational changes and hydrophobicity variation, which could be used for nanogel formulation. In this Chapter, the author first developed physically crosslinked nanogels, prepared by a recently developed alkyl chain-grafted PLP (PLP-NDA18). PLP-NDA18 is a pH-responsive, fusogenic, comb-

like polymer, with 18 mol% of decylamine (10 carbons) on the side chain (Chen et al. 2017). These hydrophobic chains aggregated by physical interactions, resulting in nanogel formation. Apart from crosslinking the nanogels, the hydrophobic segments could accommodate hydrophobic payloads, e.g. Nile red, for oral delivery. As shown in Figure 5.1a, in the acidic gastric fluid, the nanogel could retain the payloads. In neural intestinal fluid, however, the carboxylic acid of PLP-NDA18 gradually becomes ionised, and the subsequent electrostatic repulsion overcomes the hydrophobic interaction. This causes the nanogels dissociation and payload release. The free PLP-NDA18, as an amphiphilic fusogenic polymer, could further enhance the drug permeation in intestinal epithelium cells (Chen et al. 2017). In this context, the nanogels combine the advantages of hydrogels and CPP-mimetic polymer, overcoming both macroscopic and microscopic barriers in oral administration.

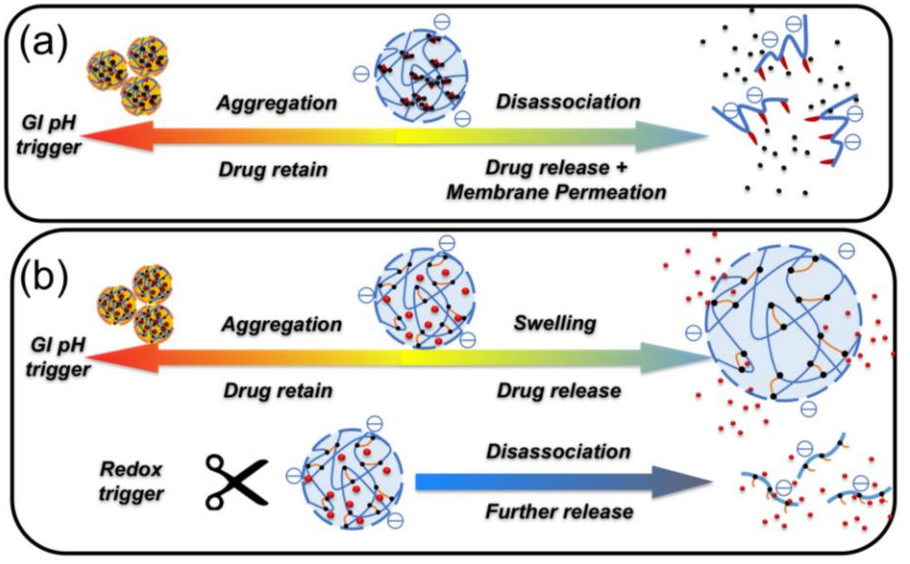

Figure 5.1 Schematic showing the responsive behaviour of physically crosslinked (a) and chemically crosslinked (b) nanogels.

Though physically crosslinked nanogels could control the release of hydrophobic payloads by pH-dependent dissociation, the burst release profile was not always favoured (Holowka & Bhatia 2014). The dramatically increased

local concentration after non-specific release may lead to toxic side effects. To enhance the stability of nanogels and to better control the drug release, chemically crosslinked nanogels, via another PLP derivative—PLP-Py20, are reported in this Chapter. PLP-Py20 has 20% pyridyldisulfide (Py) pendant groups for crosslinking. Compared with other disulfide containing crosslinkers, pyridyldisulfides react with free thiol groups with high efficiency over a broad pH range (Hermanson 2013), and thus considered as one the most popular crosslinkers. In this study, the Py crosslinkers were synthesised as previously reported, and were then conjugated to PLP via an EDC–coupling reaction to generate PLP-Py20. Then DTT was introduced to cleave half of the Py groups on PLP-Py20, to reveal free thiols. These free thiols were supposed to react with the remaining Py groups, forming nanogels via self-crosslinking. Since the nanogels prepared have both carboxylic acid groups and disulfide bonds, they are pH- and redox-responsive. When the local pH increased, the nanogels become swollen, but still not damaged. When a redox-trigger is presented, they become dissociated completely as shown in Figure 5.1b.

Both nanogel systems were developed with detailed characterisation. DLS and SEM were used to reveal the size and morphology. The stability of nanogels was studied, in different buffers with a range of pH and ion components. Finally, the loading and release of model drugs were investigated. The effects of pH-trigger and redox-trigger were studied *in vitro*, with a GI-environment mimetic setting.

5.2 Physically crosslinked nanogels

5.2.1 Synthesis and morphology

The physically crosslinked nanogels were prepared by nano-precipitation of PLP-NDA polymers as shown in Figure 2.4. PLP-NDA18 was

first dissolved in DMF and then dropped into water under vigorous stirring. The mixture became cloudy immediately after polymer addition. Then, the nanogel dispersion was dialysed against deionised water for DMF removal. The purified nanogels appeared uniformly dispersed in water without any visible agglomeration.

The effects of nanoprecipitation parameters on nanogel size and polydispersity were investigated systematically. The Z-average sizes of 18 different formulations are mapped in Figure 5.2. The hydrodynamic sizes measured by DLS are plotted against the initial polymer concentration in DMF and the final polymer concentration in water (details about all these formulations could be found in the Appendix, Table S1). The sloping lines refer to different water/DMF ratios.

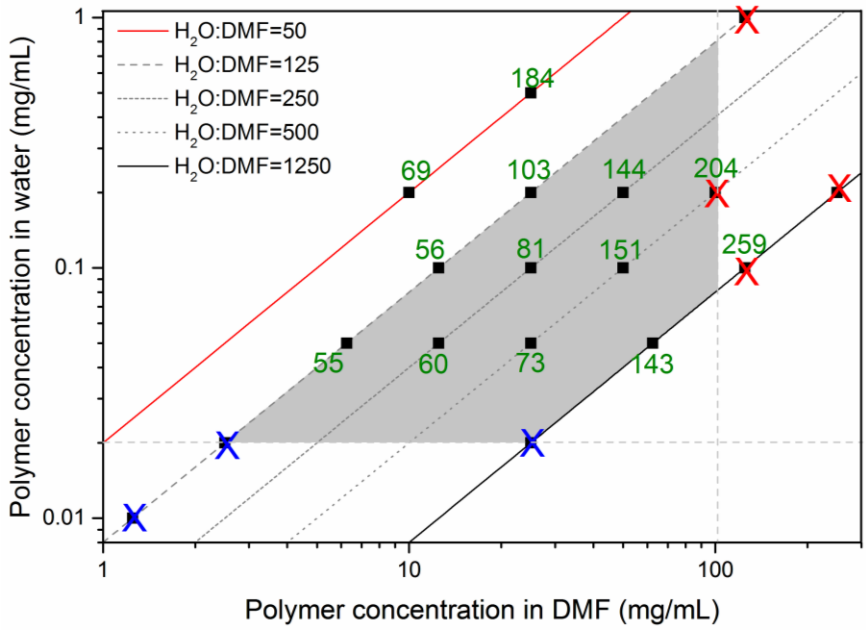

Figure 5.2 A 2D-map of nanogel hydrodynamic sizes as a function of polymer concentration in DMF and in water. Green numbers represent the Z-average size (nm) of the corresponding formulation measured by DLS; the blue cross means there were not enough particles in the sample for DLS measurement; the red cross means there were large particles in the sample and the data failed to pass the Malvern Zetasizer internal quality test. Each data point was the average of three measurements.

Figure 5.2 is quite informative, showing that the polymer concentration played a very important role in the particle formation process. The higher the concentration (either in DMF or water), the larger the size. When the initial concentration in DMF was too high (≥100 mg mL^{-1}, marked by red crosses), it was difficult for PLP-NDA18 to diffuse in water due to high local concentration. This contributed to large particle formation, which was shown in the DLS quality report. When the polymer was too dilute in water (≤0.02 mg mL^{-1}, marked by blue crosses), it was not favourable for particle formation as well. DLS measurements failed due to insufficient particles detected. The water/DMF volume ratio didn't seem to make a distinguished difference, compared with polymer concentration discussed above. However, it is worth noticing that lower water/DMF volume ratios should be favourable since less DMF would be used. Taking all these factors into consideration, the author defined a grey area shown in Figure 5.2 for nanogel preparation. Within this area, the nanogels with variable sizes could be synthesised, with a decent dispersity (PDI<0.2).

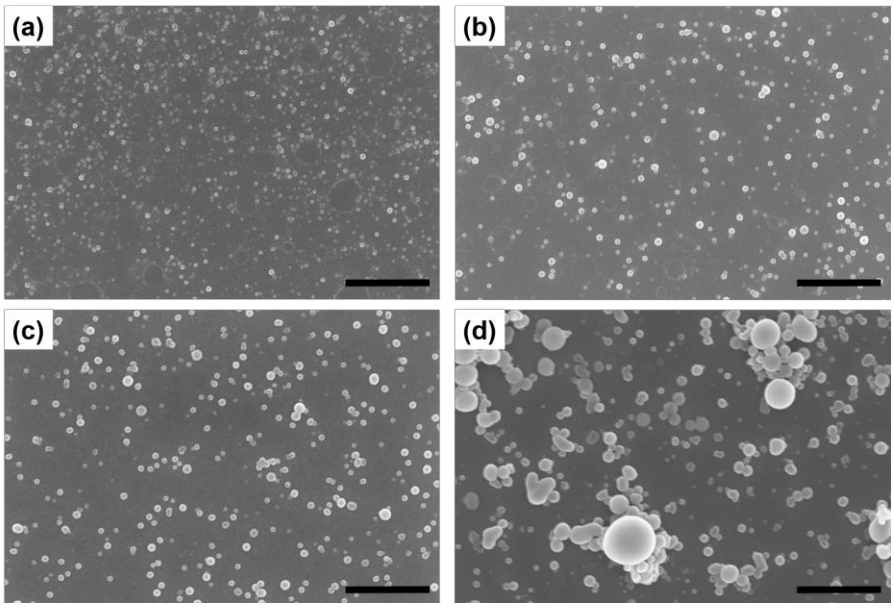

Figure 5.3 SEM of nanogels of different formulations. a, b, c and d represent formulations with an average hydrodynamic size of 55.7 ± 0.7 nm, 103.0 ± 2.8 nm, 151.4 ± 3.7 nm and 259.2 ± 3.3 nm respectively (according to DLS measurement). The scale bar represents 1 μm.

After purification, nanogels were visualised by SEM, to identify their morphology. Representative formulations were chosen to present here with an increased size from Figure 5.3a to 5.3d. Figure 5.3a shows the smallest nanogels obtained in the previous formulation trials. After purification, most of the particles maintained a spherical shape and individually distributed on the substrate. This suggests the nanogels prepared had good colloidal stability. The diameter of the particles varied from 30 to 100 nm, which correlates with DLS data. Figure 5.3b and 5.3c represent median-sized nanogels, which appeared similar in the SEM. Particles in these two images were also well-distributed with spherical shapes, though slightly larger than those in Figure 5.3a. Figure 5.3d shows an example formulation red-crossed in Figure 5.2. The morphology of these nanogels was significantly different from the other three. Large particle aggregates with irregular shapes were prevalent in the image. This is also consistent with DLS results, in which large particles were reported.

To summarise section 5.2.1, PLP-NDA18 based nanogels were successfully formulated by the nanoprecipitation method. The size of nanogels could be adjusted by changing the polymer concentration in the nanoprecipitation protocol. Furthermore, SEM images confirmed the nanosize and spherical morphology of the representative nanogels in this study.

5.2.2 pH-Sensitivity and ion tolerance

Since PLP-NDA18 was reported to have pH-responsive conformational changes (Chen et al. 2017), it is critical to identify how these changes affect nanogels. In this study, the nanogels were titrated by concentrated HCl or NaOH solutions, followed by DLS measurements. The nanogels with an average size of 103 nm were used in this study. As shown in Figure 5.4, the nanogels had little size variations between pH 3 to 9.5. When pH dropped below 3, the size started to increase, with an increase in PDI as well. This indicates

nanogels started to aggregate due to the protonation of carboxylic acid groups of the polymers. When pH increased beyond 9.5, the size dropped slightly. However, no particles were detected when pH reached 12. It was speculated that the strong alkaline made the nanogels disassociated because the ionisation of carboxylic acid groups overcame the hydrophobic interaction. Therefore, it was concluded that nanogels maintained good colloidal stability in slightly acidic or basic solution. However, strong acid or alkaline led to size variations.

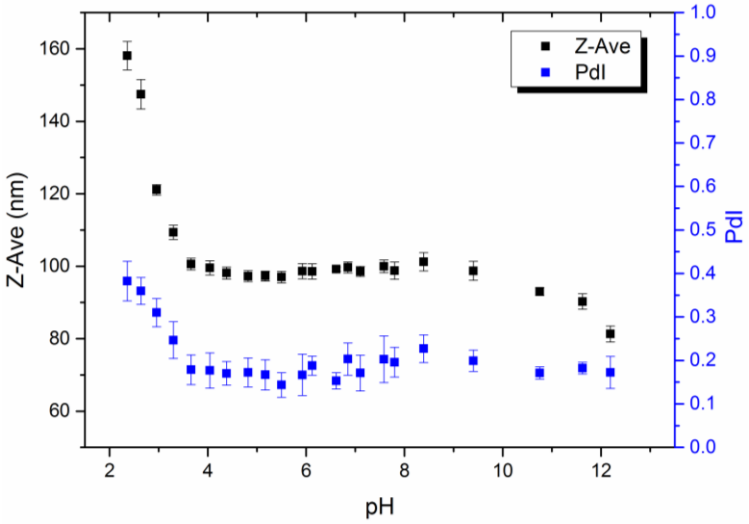

Figure 5.4 pH-responsive size and PDI variations of nanogels. (n=3).

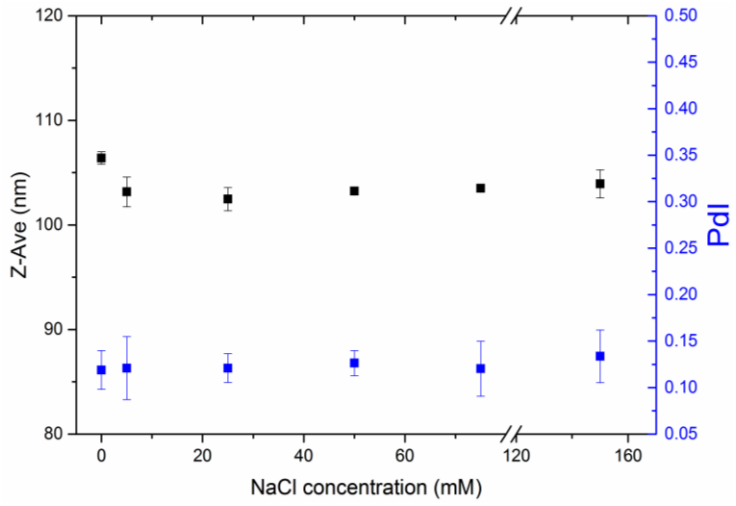

Figure 5.5 The effects of ionic strength on the size and PDI of nanogels. (n=3).

The effects of ionic strength of the NaCl solution on nanogels are shown in Figure 5.5. Within the concentration range tested (including the isotonic condition at 150 mM NaCl), no significant variation (both size and PDI) was observed. This means that the nanogels were not sensitive to ionic strength and the presence of counter ions Na^+ did not disturb the nanogel network.

The effects of different buffers are shown in Table 5-1. Commonly used biological buffers including HEPES, Tris and sodium phosphate were chosen, all adjusted to pH 7.0, at different molar concentrations (10 and 50 mM). It was found that the nanogels were sensitive to buffer ions. Among all three buffers, the tolerance for HEPES was the best. Even in 50 mM HEPES buffer, the size and PDI of nanogels were only a bit higher, suggesting the favourable stability of nanogels. Phosphate buffer was the least tolerated. In 10 mM phosphate buffer, the PDI was significantly higher than the sample in deionised water, and two peaks were identified in the distribution graph. With an increased buffering capacity, the nanogels could not be detected anymore, possibly due to dissolution.

Table 5-1 Nanogel size and distribution in common buffers

Sample medium	Size (nm)	PDI
Deionised water	99.8 ± 1.0	0.13 ± 0.05
HEPES 7.0 (10 mM)	98.7 ± 1.2	0.18 ± 0.03
HEPES 7.0 (50 mM)	103.6 ± 2.0	0.23 ± 0.06
Tris 7.0 (10 mM)	97.4 ± 1.7	0.21 ± 0.04
Tris 7.0 (50 mM)	NA[b]	NA[b]
Sodium phosphate 7.0 (10 mM)	103.7 ± 2.2	0.28 ± 0.02[a]
Sodium phosphate 7.0 (50 mM)	NA[b]	NA[b]

a Double peaks shown in DLS distribution results.

b NA means the DLS results failed to pass the internal quality test of Malvern Zetasizer.

The stability of nanogels is critical for their bioapplications. For physically crosslinked nanogels, it is often a serious concern, since physical interactions are less stable than chemical bonds. The possible dissolution or aggregation were often reported in buffers with different pH or ionic strength (Ogawa et al. 2003; Huang & Lapitsky 2012; Dyakonova et al. 2015).

The nanogels reported in this study were proved to be stable within a sufficiently wide ionic strength (up to 150 mM saline) and pH range (~3-9.5). However, it was sensitive to phosphate and Tris containing buffers at pH 7.0, especially those with higher buffering capacity. It has been reported that both pH and the ions affected the stability of nanogels (Huang & Lapitsky 2012; Huang et al. 2015). PLP-NDA18 is a polyanion with carboxylic acid groups (Chen 2017). In saline solution (pH~5.5), PLP-NDA18 was just slightly charged. In this case, the counter ions Na^+ were not a significant disturbance. However, in pH 7.0 buffers, the ionisation of the polymer was higher. The absorption of positively charged counter ions in the buffers due to ionised COO^- disturbed hydrophobic crosslinking. As a result, the dissolution of nanogels was observed.

To summarise 5.2.2, the pH-sensitivity and ion tolerance of physically crosslinked nanogels were characterised. The nanogels studied showed a good stability in mildly acidic and basic solutions (pH 3.0-9.5), and in saline solution with a sufficiently wide range of ionic strength. At neutral pH, the nanogels were more sensitive to phosphate and Tris containing buffers, which might be related to higher ionisation status.

5.2.3 Loading and release of model drugs

Since the dissolution of nanogels was observed only at neutral pH buffers, it was proposed that the nanogels could be a suitable oral delivery

candidate for intestinal delivery. In the acidic gastric environment, the nanogels were supposed to aggregate, withholding the payloads. In the intestinal environment, the disassociation caused by neutral phosphate containing fluids could facilitate the release. Considering the fact that nanogels had hydrophobic microdomains, a hydrophobic model drug—Nile red was selected for loading and release.

Nile red was loaded *in situ* during the nanogel preparation. The UV absorbance spectra were measured immediately after loading. According to Figure 5.6a, the UV absorbance at 570 nm was significantly enhanced when Nile red was loaded into nanogels. The enhancement was caused by the increased solubility of Nile red in the system, which means the hydrophobic microdomains in nanogels accommodated Nile red. After loading, the Nile-red encapsulated nanogel dispersion was uniform with an average size of 126.5 ± 2.3 nm, and a zeta potential of -38.4 ± 3.7 mV. The negative charge was attributed to the deprotonation of the carboxylic acid groups in PLP-NDA18. The absolute zeta potential value was between 30 to 40 mV, suggesting the nanogels were moderately stable in the dispersion. The particle size and zeta potential were monitored for one month and the results showed that neither varied during the one-month storage (Huang 2017).

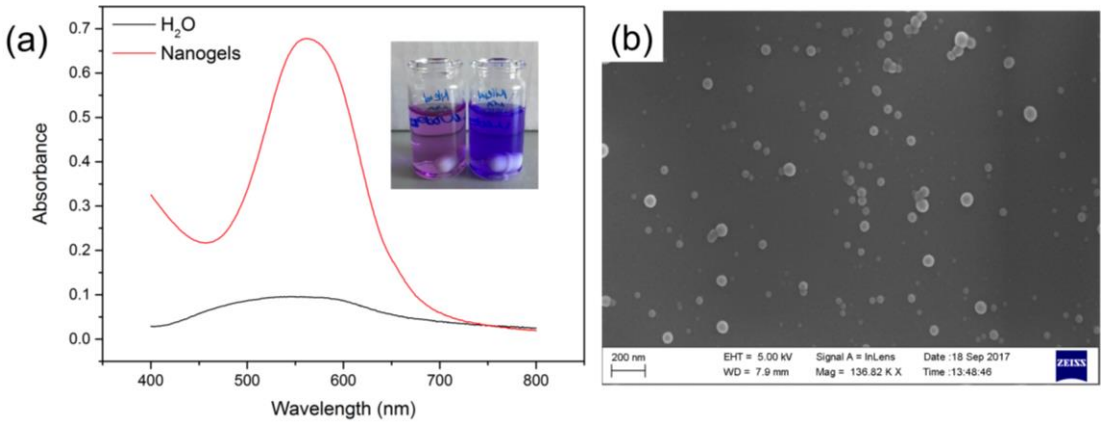

Figure 5.6 (a) UV absorbance spectra of Nile red loaded nanogels and Nile red in water. Inset figure is the photo of two samples: left, Nile red in water and right, Nile red loaded nanogels. (b) SEM of Nile-red loaded nanogels.

The morphology of the Nile red-loaded nanogels was shown in Figure 5.6b. Most of the particles were spherical, though some aggregations were observed. To remove any possible aggregations formed in the loading process, Nile red-loaded nanogels were all filtered via a 0.22 μm filter unit after loading. After filtration, the average size dropped to 87.8 ± 4.2 nm, but the zeta potential remained similar to unfiltered samples (-41.9 ± 3.1 mV).

Nile red release study was performed in bio-relevant buffers including simulated fasted gastric fluid (FaSSGF) and simulated fasted intestinal fluid (FaSSIF). Unlike SGF and SIF used in chapter 4, FaSSGF and FaSSIF contain biosurfactants, lecithin and sodium taurocholate. Lecithin is a mixture of phospholipids, which are one type of prevalent lipids in biosystems. Sodium taurocholate is a major component of bile, which aids to digest fat in daily meals (Wheeler & Ramos 1960). Both lecithin and sodium taurocholate are bio-derived emulsifying reagents for hydrophobic drug absorption (Holm et al. 2013). Compared with previous hydrophobic drug release studies, which used artificial surfactants for drug solubilisation, the release system in this study would better mimic the *in vivo* environment and provided a better understanding of the bioavailability of hydrophobic drugs *in vivo*.

Though the release buffer with biosurfactants has advantages listed above, the quantification of released Nile red in FaSSIF and FaSSGF became a problem. Since Nile red is a hydrophobic fluorophore, measuring its fluorescence intensity would be the most convenient way. However, as previously reported, Nile red was sensitive to its surrounding environment (Greenspan & Fowler 1985; Mukherjee et al. 2007). When its environment is changed, the fluorescence spectra and intensity may vary significantly. In this study, Nile red could be either encapsulated in nanogels composed of PLP-NDA18 or dispersed in emulsions formed by biosurfactants. Though nanogels contained hydrophobic domains, they also contained water and appeared more hydrophilic than the hydrophobic core of emulsions. So the environmental variations might introduce artefacts in fluorescence measurement.

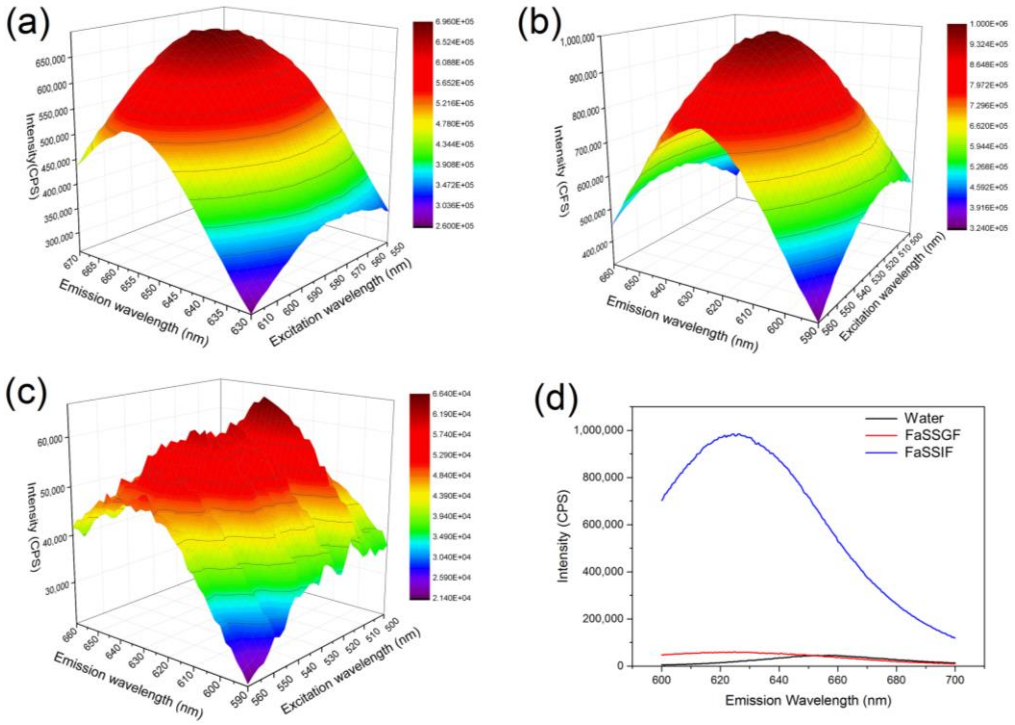

Figure 5.7 The 3D-fluorescence spectra of Nile red in loaded nanogels in (a) water, (b) FaSSIF and (c) FaSSGF. (d) The emission spectra of Nile red loaded nanogels in water, FaSSGF and FaSSIF.

To investigate the Nile red fluorescence in nanogels and biosurfactant solution, the 3D fluorescence spectra were recorded in three different cases: nanogels dispersed in water, in FaSSIF and in FaSSGF. Figure 5.7a showed the spectra of Nile red loaded nanogel dispersion in water. The excitation peak and the emission peak were at 570 nm and 660 nm respectively. When these Nile red loaded nanogels were added to FaSSIF, the excitation peak shifted to 520 nm and the emission peak shifted to 630 nm respectively (Figure 5.7b). The significant blue shift of both peaks indicated the increased hydrophobicity of the surrounding environment of Nile red. Considering the previous ion tolerance results, the nanogels would be dissociated in FaSSIF. As a result, Nile red was released, and emulsified by biosurfactants subsequently. When exposed to FaSSGF, similar blue shifts of both excitation and emission peaks were also observed, though less obvious than that in FaSSIF. The excitation peak appeared to be much broader, spanning from 510 to 550 nm, and the emission peak was also broader than that in FaSSIF. This suggests that Nile red was partially released and emulsified by biosurfactants, while some still remained encapsulated in nanogels.

Figure 5.7d compared the absolute peak intensity of Nile red in the emission spectra of the three solutions. Nile red in FaSSIF solution showed more than 10 times higher intensity than the other two, which also suggests the enhanced hydrophobicity of Nile red environment. However, it also suggests that the fluorescence intensities of Nile red containing nanogels in FaSSGF or FaSSIF were not comparable with those of free Nile red dissolved in FaSSGF or FaSSIF directly, due to the differences in the surrounding environment of Nile red. Therefore, the fluorescence measured in the release system had to be carefully normalised for quantification.

As previously reported, the extraction of Nile red via organic solvents could normalise the local environment of Nile red, no matter what surfactant was present or what environment Nile red was refined to (Frank et al. 2014; Lee & Kim 2015). Thus, in this study, the released Nile-red containing solutions were lyophilised and then redissolved in DMSO. The local environment of Nile red was thus normalised and the fluorescence intensity became comparable.

Figure 5.8a showed the release kinetics of Nile red in FaSSIF and FaSSGF, respectively. The release in FaSSIF was quick and efficient. More than 70% payloads were released within the first 5 hours and almost complete release was achieved after 24 hours. Considering the average time of human intestinal transition was around 3-4 hours, the release rate was sufficient for intestinal delivery. The release in FaSSGF was not significant. A burst release of 30% was observed in the first 3 hours, which is the average gastric transition time. More than half of the payloads were still retained in the nanogels even after 24-hour treatment in FaSSGF. The results suggested that the nanogels could control the release of Nile red in simulated GI fluids.

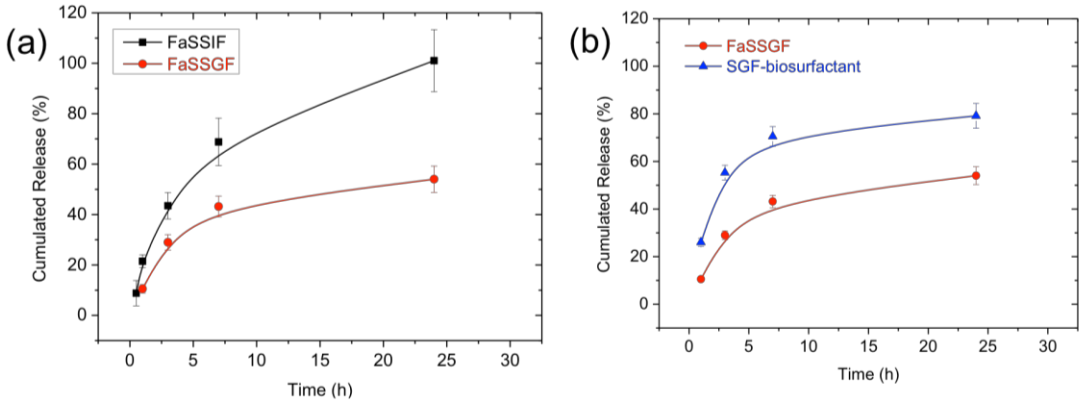

Figure 5.8 Nile red release kinetics in bio-relevant buffers, including FaSSIF, FaSSGF and SGF with higher biosurfactant contents. (n=3). *The data were provided by Xiaozhen Huang in Dr Chen's group. Reproduced from Huang's Master Dissertation (2017).*

The efficient release in FaSSIF was probably attributed to the dissociation of the nanogels. As shown in Figure 5.7b and 5.7d, the fluorescence intensity increased considerably with accompanying peak blue shifts after the addition of Nile red-loaded nanogels into FaSSIF. It was observed by DLS that nanogels disappeared in SIF, suggesting the dissolution-caused release.

High surfactant concentration in FaSSIF also facilitated the release. A control buffer was prepared (SGF-biosurfactant) with the same biosurfactant concentration compared to FaSSIF. However, the salt composition and pH was exactly the same as FaSSGF. As shown in Figure 5.8b, the release in SGF-biosurfactant was higher than that in FaSSGF (54% in the first 3 hours), but almost stopped after 5 hours and did not reach 100% after 24 hours, which also differed from the profile in FaSSIF. This suggests that the release was controlled by both biosurfactant concentration and pH.

5.2.4 pH-Mediated membrane activity

As previously reported in the literature (Chen et al. 2017), PLP-NDA18 polymer had pH-dependent membrane-lytic activity, which could facilitate the intracellular delivery of drugs. Therefore, the author wondered whether the nanogels formulated by physically crosslinking of PLP-NDA18 had similar behaviour. To validate this idea, haemolysis was performed in different pH buffers.

As shown in Figure 5.9, PLP-NDA18 and nanogels demonstrated similar pH-dependent membrane-lytic activities. The haemolytic activity of both materials increased when pH dropped from 7.4 to 5.5, and then decreased when pH further decreased to 4.5. PLP-NDA18 nanogels had almost the same hemolytic activity (65.6%±0.1%) at pH 5.5, compared with PLP-NDA18

polymer (65.5%±0.6%) at the same concentration (quantified by polymer mass). At other pHs studied in Figure 5.9, the haemolytic activities of nanogels were also comparable to polymers. This means the membrane-lytic activity of PLP-NDA18 polymers were well retained in nanogel samples.

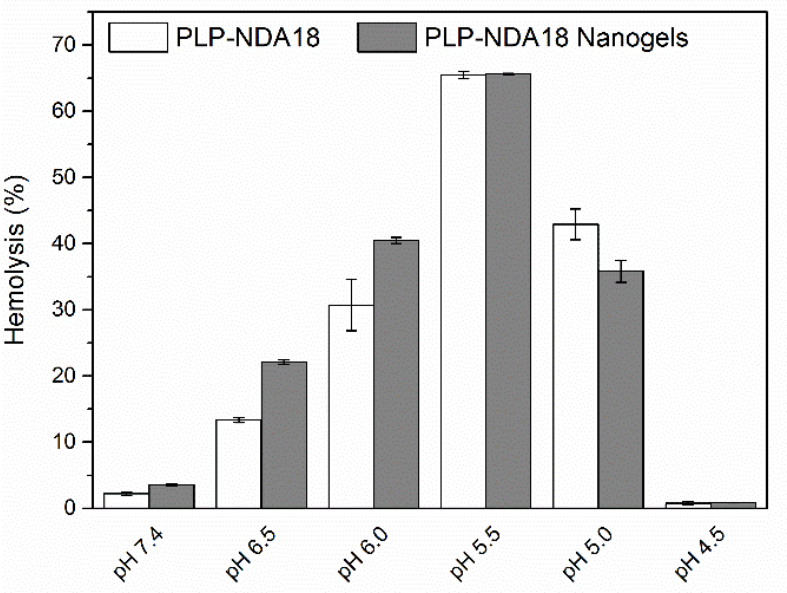

Figure 5.9 The membrane-lytic activity of PLP-NDA18 and the physically crosslinked PLP-NDA18 nanogels from pH 4.5 to 7.4. The final concentration of both polymers and nanogels in different buffers is 0.02 mg mL^{-1}. (n=3).

The similar pH-dependent membrane-lytic activity of PLP-NDA18 and nanogels were probably due to nanogel disassociation in buffers. As shown in Section 5.2.2, nanogels disassociated in neutral phosphate containing solutions. Results in Section 5.2.3 also proved that the drug release in FaSSIF was accompanied by nanogel disassociation. Since recovered polymers after nanogel disassociation demonstrated similar membrane-lytic activities compared with free PLP-NDA18, it is expected that the bioavailability of drugs released in FaSSIF could be further boosted by changing the permeability of intestinal cells.

To sum up Section 5.2, pH-responsive nanogels were developed via physical crosslinking of PLP-NDA18 polymer. The sizes of nanogels could be

adjusted easily by varying parameters in the synthetic step. pH and ion tolerance studied suggested that the nanogels could be dissociated in neutral phosphate-containing buffers. A hydrophobic model drug Nile red could be loaded *in situ* and the kinetic profile suggested the release favoured intestinal simulated fluids with high biosurfactant conents. Furthermore, the membrane-lytic activity of nanogels was comparable to free PLP-NDA18 polymers, which may further improve the bioavailability by changing the permeability of intestinal cells.

5.3 Chemically crosslinked nanogels via EDC coupling

Though physically crosslinked nanogels were able to control the release of Nile red by pH-dependent dissolution, the burst release profile was not always favoured. The dramatically increased local concentration after non-specific release may lead to toxic side effects. Thus, more stable nanogels in physiological buffers were developed via chemically crosslinking.

Inspired by the synthetic method of hydrogels in Chapter 4, the EDC-coupling reaction was first applied for preparation of nanogels through chemical crosslinking. The idea was to prepare the physically crosslinked PLP-NDA18 nanogels first, followed by addition of EDC, NHS and crosslinkers for chemical crosslinking. High EDC and NHS amounts (10 times higher than the crosslinkers) were used to activate the carboxylic acid on the surface of the resulting nanogels. Relatively low amounts of crosslinkers (CDE, cystamine or PEG 220 diamine) were used to avoid the crosslinking between nanogels and the subsequent agglomeration.

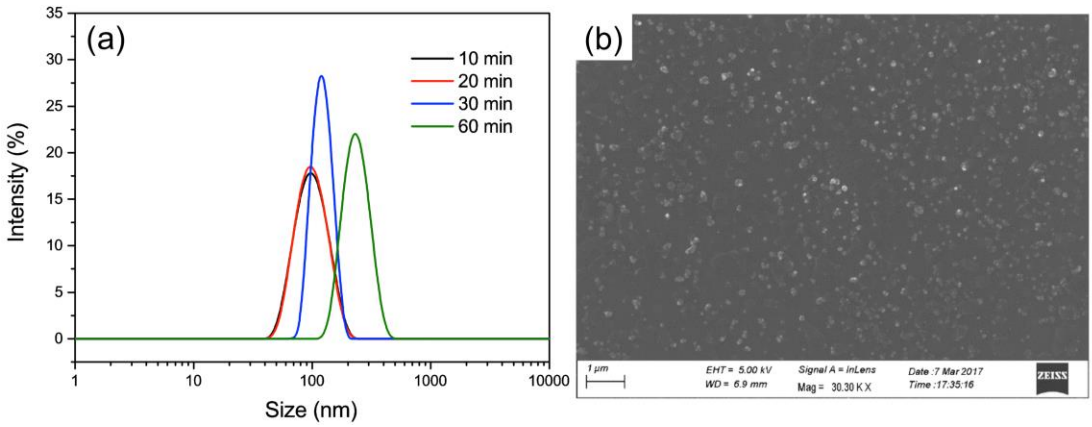

Figure 5.10 (a) Size variations of the chemically crosslinked nanogels during synthesis. (b) SEM of purified EDC-coupling nanogels.

As shown in Figure 5.10a, the size variation during the EDC-coupling reaction was monitored. After addition of all components, the size kept almost constant in the first 20 min at 94.4 ± 0.7 nm, similar with the size of the physically crosslinked nanogels. Afterwards, the size increased to 126.3 ± 2.0 nm at 30 min and 235.8 ± 9.4 nm after 1 hour. The increased size was probably due to the crosslinking between nanogels, though no large aggregates were observed in the size distribution graph (figure 5.10). From the kinetic study, it was found 30 min should be enough for crosslinking, and the reaction was quenched by adding sodium carbonate to hydrolyse the intermediates. After purification by dialysis, the SEM image suggests that most of the nanogels were around 100 nm in diameter (Figure 5.10b).

After synthesis and purification, the pH-responsibility and the phosphate ion tolerance of these nanogels were investigated. As shown in Table 5-2, the chemically crosslinked nanogels showed better stability in phosphate buffers in the pH range from 5.0 to 7.4, compared with physically crosslinked ones shown in Table 5-1. The increased stability also validates that the chemical crosslinking was successful. However, when pH dropped below 5.5, the nanogel size increased dramatically. This means the crosslinked nanogels still aggregated in the acidic environment.

Table 5-2 pH Responsibility of chemically crosslinked nanogels, which were prepared via EDC-coupling, in 50 mM phosphate buffer at different pHs.

pH	Size (nm)	PDI
5.0	283.4 ± 28.1	0.19 ± 0.01
5.5	122.3 ± 0.6	0.25 ± 0.07
6.0	109.6 ± 1.9	0.19 ± 0.06
6.5	108.2 ± 2.0	0.14 ± 0.02
7.0	110.8 ± 0.6	0.12 ± 0.02
7.4	108.5 ± 1.0	0.19 ± 0.06

Though successful crosslinking was proved by the increased stability in phosphate buffers, the crosslinked nanogels did not disassociate by reducing reagents. Table 5-3 showed the size of nanogels crosslinked by CDE and cystamine (CA), before and after the treatment of 50 mM DTT. Even after three days of treatment, the size of nanogels did not change for both nanogels. As shown in Figure 2.5, both CDE and cystamine have disulfide bonds, which means the cleavage by DTT should lead to the dissociation of nanogels completely. The uncleavable crosslinking suggests that the crosslinkers might not get incorporated.

Table 5-3 CDE and cystamine crosslinked nanogels before and after treatment of DTT

Sample	Size (nm)	PDI
CDE nanogels	103.0 ± 2.0	0.12 ± 0.04
CDE nanogels + DTT 3 hours	104.6 ± 1.4	0.11 ± 0.01
CDE nanogels + DTT 3 days	118.7 ± 1.6	0.09 ± 0.03
CA nanogels	149.5 ± 8.3	0.12 ± 0.02
CA nanogels + DTT 3 hours	155.4 ± 5.5	0.11 ± 0.01
CA nanogels + DTT 3 days	148.0 ± 5.4	0.11 ± 0.03

To investigate the contradictory results about crosslinking, another crosslinker (PEG 220 diamine) was used, and the FTIR spectra of nanogels, the crosslinker and PLP-NDA18 polymer without crosslinking were presented in Figure 5.11. PEG 220 diamine is a small molecular diamine crosslinker without disulfide group. The critical structure is the repeating ether groups which show a strong band at 1100 cm^{-1} (s, v C-O-C). However, this band was not apparent in nanogels. The whole spectra of nanogels were very identical to that of PLP-NDA18. This is also against the incorporation of crosslinkers in nanogels.

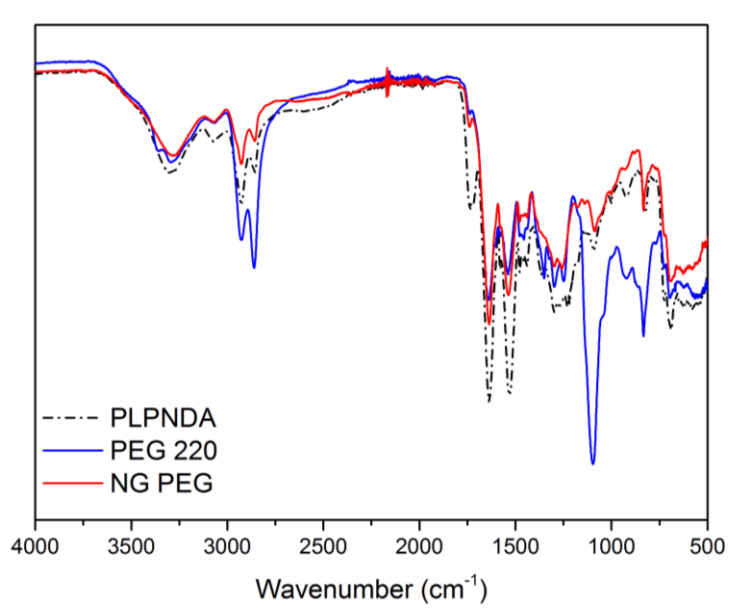

Figure 5.11 FTIR spectra of EDC-coupling nanogels crosslinked by PEG 220 diamine (solid red), crosslinker (solid blue) and PLP-NDA18 polymer (black dash).

Since both DLS and FTIR spectra denied the incorporation of crosslinkers, whether the chemical crosslinking was successful became questionable. Thus, a control experiment was designed. The nanogel preparation was repeated, in the same conditions with EDC and NHS, but without any crosslinkers. The DLS results show that nanogels formed after the addition of EDC and NHS, with a size of 125.8 ± 2.9 nm. Further ion tolerance test in phosphate buffers suggested these nanogels were more stable than

those physically crosslinked without EDC and NHS. Therefore, the addition of EDC and NHS enhanced the nanogel structure somehow, chemically or physically.

In literature, there were reports about side reactions in EDC-coupling. The mechanism of EDC-coupling with NHS on a silicon surface was shown in Figure 5.12 (Sam et al. 2010). At high concentration of EDC and NHS, urea side products were dominant, while a low concentration of EDC and NHS led to anhydride side products. The formation of these side products (anhydrides and urea) was irreversible. Therefore, one would speculate that the surface of the nanogels in this study were probably self-crosslinked forming anhydride. This explains why the stability of nanogels improved but no crosslinker was detected.

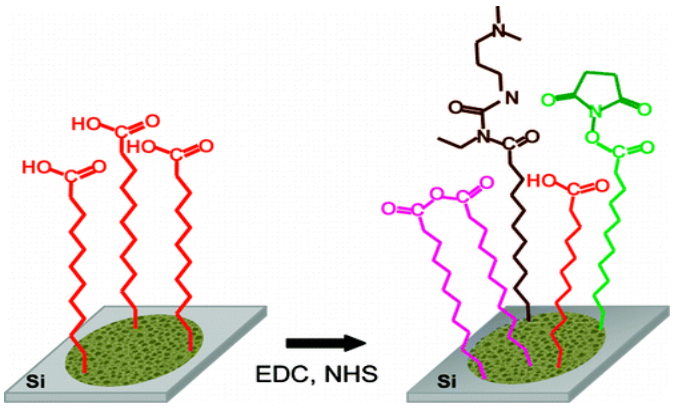

Figure 5.12 Surface EDC-coupling reaction scheme. Intermediates and side products include anhydride (pink), urea (brown) and NHS succinate (green). Reproduced from literature (Sam et al. 2010)**, copyright 2010, with permission from ACS Publications.**

Since the self-crosslinking speculation was difficult to prove and hard to control in practice, the EDC-coupling chemical crosslinking strategy was abandoned.

5.4 Chemically crosslinked nanogels via thiol-exchange

Instead of EDC-coupling between the carboxylic acid groups of polymers with the amines containing crosslinkers, a thiol-exchange strategy was proposed. As shown in Figure 5.13, a disulfide-containing crosslinker was first synthesised and conjugated to polymer backbone. When reducing reagent (such as DTT) was introduced, the crosslinkers could be partially cleaved to reveal thiol groups. The revealed thiol groups could react with the remaining crosslinkers on the polymers, resulting in self-crosslinked nanogels.

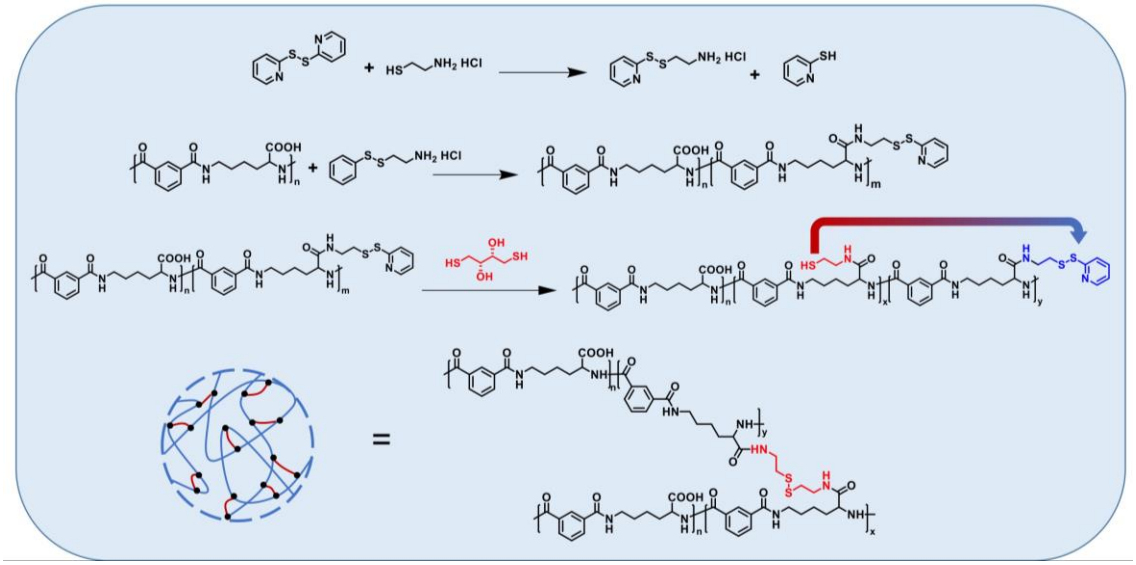

Figure 5.13 Synthetic scheme of chemically crosslinked dual-responsive nanogels.

Compared with the EDC-coupling strategy previously used, thiol-exchange strategy has three advantages. Firstly, it avoids the use of coupling reagents such as EDC and NHS, thus reducing possible side reactions. Secondly, the reaction condition is less sensitive to local concentrations of reactants, compared with EDC-coupling. This means the reaction efficiency is high even in a dilute system, which is exactly the case in nanogel synthesis. Finally, the disulfide crosslinker introduced here provides anchors for other functional moieties to conjugate. For instance, thiol containing pre-drugs or imaging reagents could be easily conjugated via thiol exchange reaction before

or after nanogel synthesis. However, the shortcoming of this strategy is that the disulfide crosslinkers (pyridine dithioethylamine, Py) are not commercially available. Therefore, they have to be synthesised and conjugated before nanogel preparation.

5.4.1 Synthesis of polymer precursors (PLP-Py20)

The synthesis of Py crosslinkers followed the protocol reported in literature (Lelle & Peneva 2014). ^{1}H-NMR and ^{13}C-NMR results showed in Figure 5.14 proved that the crosslinkers were successfully prepared. All the peaks were carefully designated, and the chemical shifts were consistent with literature. The products obtained were in salt forms, appeared as white crystals. The author chose to synthesise salt form crosslinker instead of amine form due to the ease of purification.

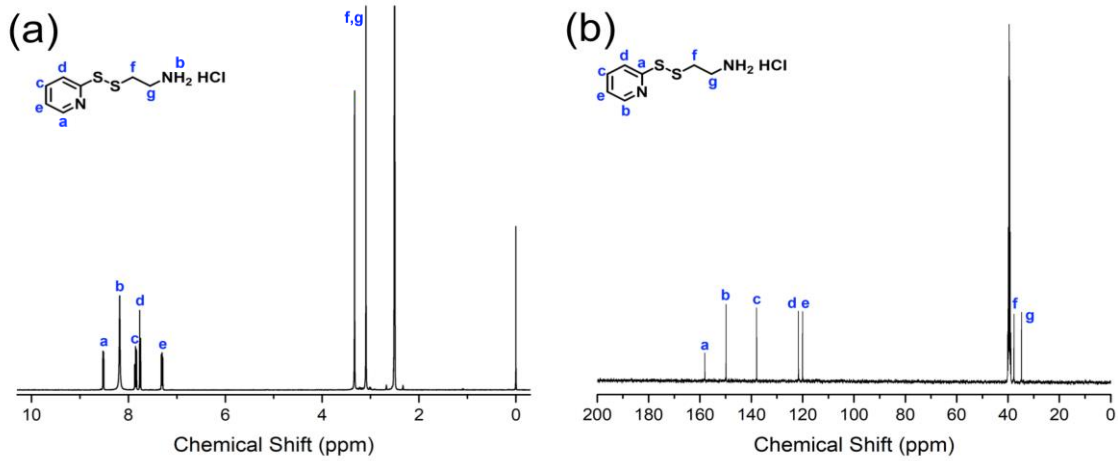

Figure 5.14 ^{1}H-NMR spectrum (a) and ^{13}C-NMR spectrum (b) of Py crosslinker. ^{1}H-NMR (400 MHz, DMSO-d$_6$): δ (ppm) 3.10 (4H, m, H$_f$, C*H*$_2$; H$_g$, C*H*$_2$), 7.31 (1H, m, H$_e$, C*H*), 7.77 (1H, m, H$_d$, C*H*), 8.18 (3H, s, H$_b$, N*H*$_3$), 8.52 (1H, m, H$_a$, C*H*). ^{13}C-NMR (400 MHz, DMSO-d$_6$): δ (ppm) 34.76 (C$_g$), 37.67 (C$_f$), 120.03 (C$_e$), 121.63 (C$_d$), 137.93 (C$_c$), 149.84 (C$_b$), 158.09 (C$_a$).

The conjugation of crosslinkers was first tried on PLP, via EDC-coupling reaction in pH 7.4 phosphate buffer. The ^{1}H-NMR spectrum of purified polymers was shown in Figure 5.15. The percentage of conjugated was calculated based

on ratio of peak a' on the crosslinker and the peak f on PLP backbone, as shown in the equation below.

$$\%Py\ conjugated = \frac{I_{a'}}{I_f} \times 100 \qquad \text{(Equation 5.1)}$$

where $I_{a'}$ represents the integral area of peak a' and I_f represents the integral area of peak f. For a stoichiometric ratio of 20% conjugation, the percentage of conjugation calculated was 22%. These results indicate that almost 100% reaction conversion was achieved.

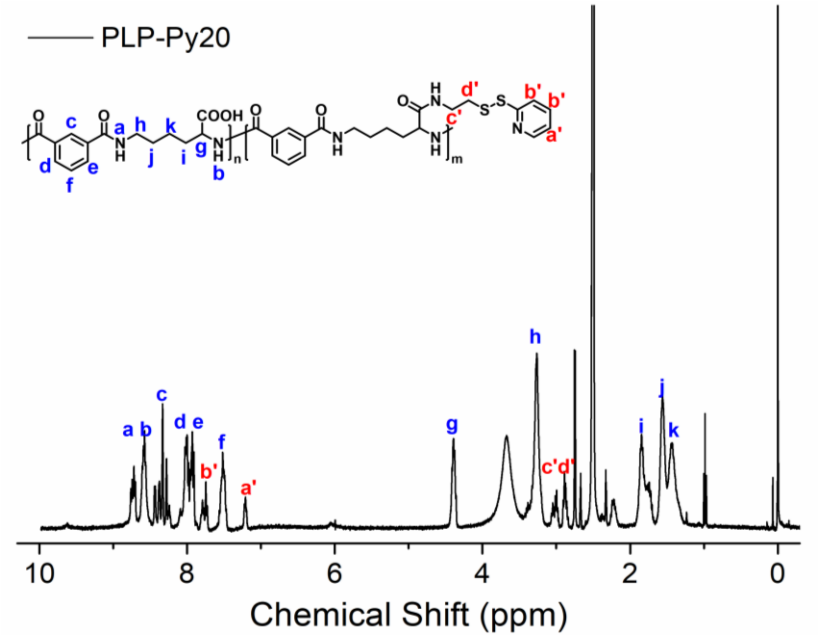

Figure 5.15 ^{1}H-NMR spectrum of PLP-Py conjugate, in DMSO-d_6.

5.4.2 Nanogel synthesis and morphology

The chemical crosslinking was also achieved by preparing physically crosslinked nanogels first, and then DTT was added to induce self-crosslinking. The cleavage of Py crosslinker could be monitored by the release of 2-mercaptopytidine, which is a side product after disulfide cleavage. This compound has a typical UV absorbance at 343 nm, which is widely used for quantification. During the nanogel formation, an increase in UV absorbance

was observed, which indicated the cleavage of disulfide bonds and thiol exchange happened. However, in this system, the nanogel formation introduced artefacts for UV measurement. The scattering effect of nanoparticles decreased the light transmittance. Therefore, the increase in UV absorbance was just interpreted as a qualitative evidence, rather than quantitative evidence.

The nanogel formation was also characterised by DLS measurement. Before adding DTT, the size of physically crosslinked nanogels was 330.5 ± 2.9 nm. After chemically crosslinking, the size increased to 464.4 ± 3.3 nm. After purification and dialysis against deionised water, the sizes of both nanogels decreased, to 228.8 ± 3.1 nm and 258.1 ± 3.3 nm respectively. The slightly increased size indicated that the chemical self-crosslinking did not introduce nanogel aggregation. One would speculate the crosslinking only happened within nanogels, but not between different nanogels.

SEM images of chemically-crosslinked nanogels are shown in Figure 5.16. The overview in Figure 5.16a indicated most nanogels were individually distributed without agglomeration, similar to the physically crosslinked ones in Figure 5.3b and 5.3c. In the zoomed-in image (Figure 5.16b), the nanogels were not perfectly spherical, and their size ranged from 50 to 100 nm, smaller than DLS average size. Some aggregates were observed, which might be contributed to the large particles in DLS distribution.

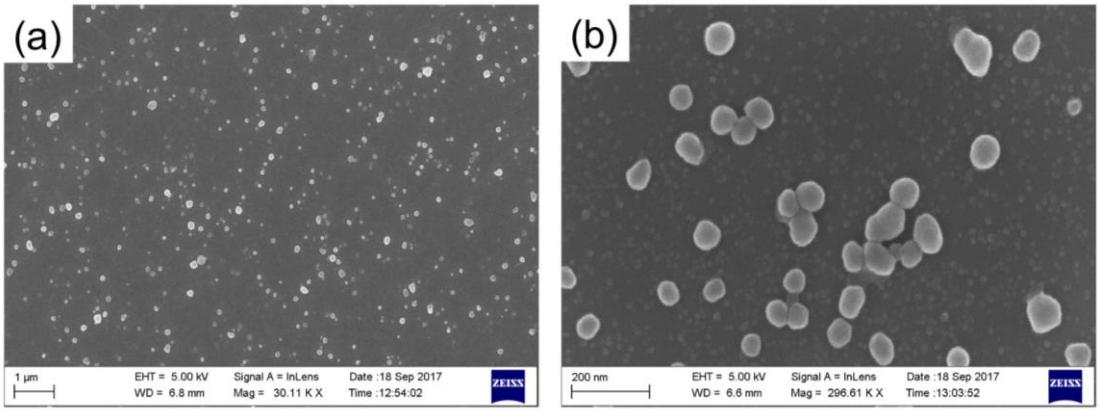

Figure 5.16 (a) SEM of chemically-crosslinked nanogels. (b) The zoomed-in image showing individual nanogels.

To summarise 5.4.1 and 5.4.2, chemically crosslinked nanogels could be synthesised via thiol-exchange strategy. The synthesis of Py crosslinkers and PLP-Py polymers was successful with high reaction efficiency. Self-crosslinked nanogels with an average size of 258.1 ± 3.3 nm were formed, with a medium polydispersity (PDI= 0.13 ± 0.02).

5.4.3 pH-sensitivity, ion tolerance and redox-sensitivity

The size and PDI of nanogels prepared by thiol-exchange in different pH phosphate buffers were shown in Table 5-4. The nanogels were found to be stable in 100 mM phosphate buffers (isotonic condition) from pH 5.0 to 7.4. Furthermore, the results showed a slight increase in size at higher pH. This was probably attributed to the swelling of nanogels, caused by ionisation of carboxylic acid groups of PLP-Py20. Interestingly, the swelling was not observed either in physically crosslinked or EDC-coupling nanogels. Instead of swelling, the physically crosslinked nanogels were dissociated in phosphate buffer at pH 7.0. The difference in nanogel behaviour indicated that chemically crosslinking via disulfide bond significantly enhanced the stability of nanogels. Even in an ionised state, the nanogel network expanded but still remained

associated, which is close to the behaviour of CDE or PEG-crosslinked hydrogels discussed in Chapter 4.

Table 5-4 pH sensitivity and ion tolerance of chemically crosslinked nanogels via thiol-exchange

Sample medium	Size (nm)	PDI
Deionised water	258.1 ± 3.3	0.13 ± 0.02
100 mM phosphate buffer pH 5.0	292.2 ± 5.5	0.23 ± 0.01
100 mM phosphate buffer pH 6.0	342.1 ± 0.2	0.08 ± 0.04
100 mM phosphate buffer pH 7.0	344.9 ± 8.6	0.15 ± 0.04
100 mM phosphate buffer pH 7.4	358.9 ± 2.5	0.15 ± 0.02
Phosphate saline pH 7.4 (PBS)	327.8 ± 6.3	0.14 ± 0.03
HEPES pH 7.0 (10 mM)	313.8 ± 5.0	0.14± 0.04
HEPES pH 8.0 (10 mM)	326.5 ± 5.3	0.09 ± 0.07

The effects of ions and different buffers are also shown in Table 5-4. The nanogels were stable in HEPES buffers and phosphate buffers (with or without saline). The similar swelling was observed in HEPES and PBS buffers. This indicated that the nanogels crosslinked by thiol-exchange had good ion tolerance.

Since nanogels were crosslinked via disulfide bond, they should be susceptible to reducing reagents such as DTT. To validate the redox-sensitivity, nanogels were treated with 50 mM DTT. As shown in Table 5-5, the addition of DTT in deionised water did not change the size of nanogels, even after 24-hour treatment. However, in PBS buffer, the same amount of DTT made nanogels disassociated. The results suggest that the nanogels could be cleaved by DTT. In deionised water, the cleaved nanogels were able to keep the nano-sized morphology via physical crosslinking, such as hydrophobic interaction. In PBS

buffer, the nanogels became completely disassociated, due to the cleavage of chemical crosslinking and the ionisation which diminished physical crosslinking.

Table 5-5 The size and distribution of nanogels after 50 mM DTT treatment for 24h.

Sample medium	Size (nm)	PDI
Deionised water	258.1 ± 3.3	0.13 ± 0.02
50 mM DTT in deionised water	256.0 ± 2.5	0.09 ± 0.02
PBS pH 7.4	327.8 ± 6.3	0.14 ± 0.03
50 mM DTT in PBS pH 7.4	NA[a]	NA[a]

a NA means the DLS results failed to pass the internal quality test of Malvern Zetasizer.

To sum up section 5.4.3, the nanogels crosslinked by thiol-exchange were more stable in buffers at neutral pH with good ion tolerance, due to disulfide bonding. The disulfide bond could be cleaved in the presence of the redox trigger such as DTT. The cleaved nanogels could partially maintain the structure via hydrophobic interaction but completely dissociated in PBS buffer with the DTT trigger.

5.4.4 Loading and release of anti-cancer drugs

After investigation of the stability of nanogels in different conditions, their drug loading capacity and controlled release behaviour were investigated. Successful *in situ* loading of hydrophobic payloads in the physically crosslinked PLP-NDA18 nanogels was demonstrated in Section 5.2.3. The author chose to load Nile red following the previous protocol. However, many precipitates formed immediately after the addition of Nile red, possibly due to less hydrophobicity of the PLP-Py polymer compared with PLP-NDA18. Therefore, a less hydrophobic payload—doxorubicin (DOX, logP=1.27 (Morton et al. 2013)), a widely used anti-cancer drug, was chosen here as an example.

DOX was loaded into the nanogels *in situ* during nanogel formation. After loading, the FTIR spectra of PLP-Py polymer, DOX and DOX-loaded nanogels were acquired, as shown in Figure 5.17. The DOX-loaded nanogels showed both typical bands of DOX, from 1000 to 1300 cm^{-1} (pointed with black arrows) and typical bands of PLP-Py at 1624 cm^{-1} (amide I) and 1527 cm^{-1} (amide II). This confirmed that DOX has been successfully incorporated into the nanogels.

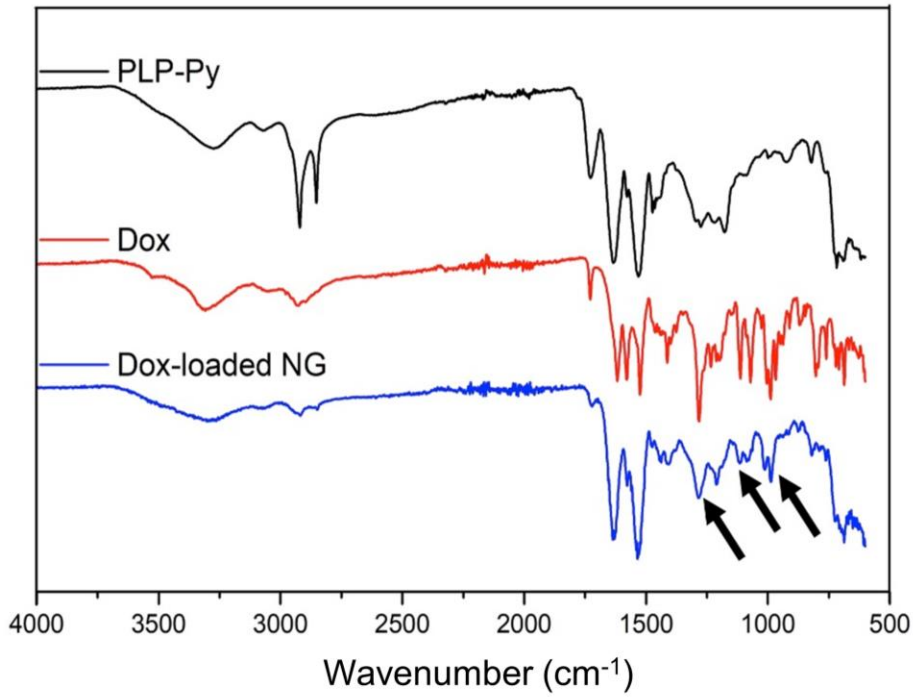

Figure 5.17 FTIR spectra of PLP-Py polymer, DOX and DOX-loaded nanogels. Black arrows pointed to typical DOX bands incorporated in nanogels.

Fluorescence spectra of free DOX and DOX-loaded nanogels also confirmed the successful loading. As shown in Figure 5.18, free DOX showed two emission peaks at 560 nm and 590 nm, respectively. DOX-loaded nanogels, however, showed only one peak at 590 nm. The disappearance of emission peak at 560 nm was attributed to the high local concentration of DOX, according to literature (Motlagh et al. 2016; Changenet-Barret et al. 2013). When the local concentration is higher than 5 μg mL^{-1}, the dimerised and aggregated DOX diminish the fluorescence and emission peaks shift to higher

wavelengths. This means the DOX loaded in the nanogels were in an aggregated state, with a relatively high local concentration.

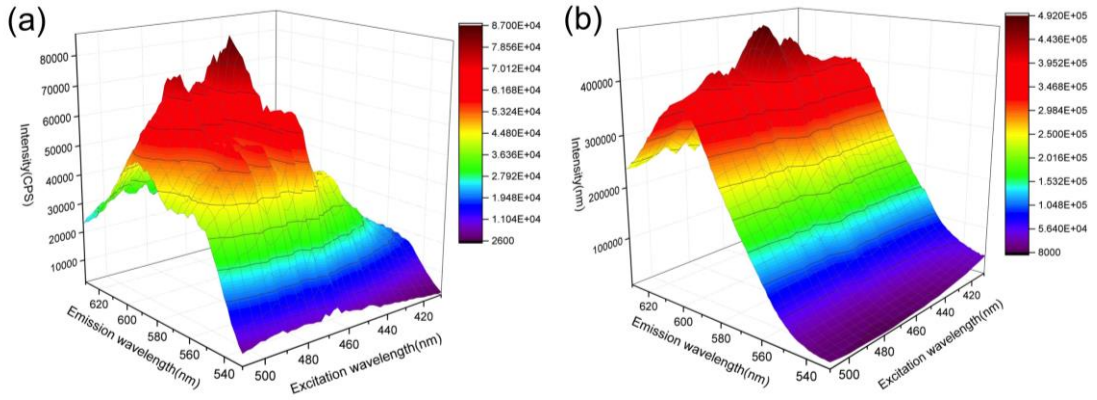

Figure 5.18 3D-fluorescence spectra of (a) free DOX in water and (b) DOX-loaded nanogels.

A preliminary study of DOX release was investigated by measuring the fluorescence spectra. Figure 5.19 shows the emission spectra of DOX-loaded nanogels after dispersion in different media for 2 hours. No matter what medium was used, there were two peaks in the spectra with similar shapes compared to free DOX shown in Figure 5.18a. This indicates that the DOX released from nanogels recovered from the aggregated state. Thus, the fluorescence intensity of the peak at 590 nm was correlated to the amount of DOX released. Interestingly, the intensity in SGF was higher than that in SIF but lower than that in SIF with the DTT trigger. This indicates that the release in SIF with the DTT trigger was the most efficient, due to the complete dissociation of nanogels. The release in SGF was also significant, despite the hydrophobicity of nanogels.

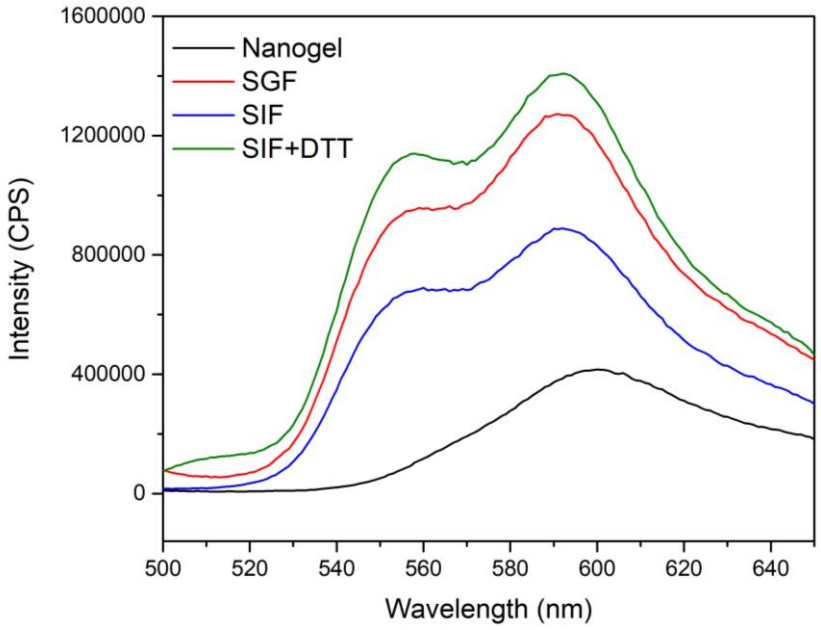

Figure 5.19 The emission spectra of DOX-loaded nanogels in water, and nanogels in different release media for 2 h. The excitation wavelength was 480 nm.

The higher release profile in SGF than that in SIF was not expected. From pH-responsive DLS data shown in Table 5-4, the nanogels were able to swell at higher pH, which is favourable for the release of payloads. However, this seemed not applicable to DOX. The reason for the preferable release in SGF might be related to the structure of DOX and the interaction between DOX and nanogels. As shown in Figure 5.20a, DOX is composed of a hydrophobic anthraquinone and a hydrophilic daunosamine sugar (Cagel et al. 2017). The pKa of the daunosamine (highlighted in red in Figure 5.20a) is 7.84 ± 0.05 (Sanli et al. 2014). Therefore, in SIF and SGF, the amine kept protonated, which made DOX soluble in both buffers. In SIF, PLP-Py was deprotonated and negatively charged, while DOX was positively charged. The electrostatic interaction limited the release, even though nanogels were swollen. The lower pH in SGF, however, facilitated the protonation of both DOX and PLP-Py of nanogels. The protonated PLP-Py lost its charge and became more hydrophobic, while protonated DOX was hydrophilic. The differences in hydrophobicity made them less compatible, resulting in fast release.

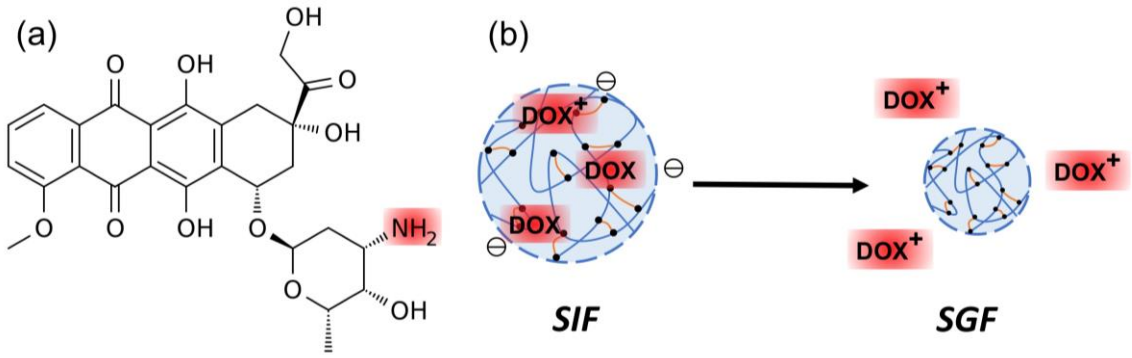

Figure 5.20 (a) Chemical Structure of DOX. (b) A schematic showing of DOX and nanogel in SGF and DIF.

5.5 Conclusions

To conclude this Chapter, two series of stimuli-responsive nanogels were developed by either physical crosslinking via hydrophobic interaction or chemical crosslinking via the thiol-exchange reaction and the subsequent disulfide-bond formation.

The nanogels prepared by physically crosslinking PLP-NDA18 were spherical nanoparticles with negative charges on the surface. The sizes of nanogels could be adjusted easily by varying parameters in the synthetic step. Hydrophobic model drugs Nile red could be loaded *in situ*, incorporated in the hydrophobic segments of the nanogels. The release of Nile red in simulated gastrointestinal buffers was controlled by pH-dependent dissolution of nanogels. In SGF, nanogels aggregated and the drugs were retained. In SIF, nanogels were quickly disassociated due to the ionisation of polymers, leading to complete release of payloads. After disassociation, the polymer retained membrane-lytic activities, which may further facilitate the drug delivery into intestinal cells. The controlled release behaviour and the membrane-activity of these physically crosslinked nanogels made them promising candidates for hydrophobic payloads delivery.

An attempt to chemically crosslink nanogels via EDC-coupling reaction was made. However, due to the unexpected side reactions, it was not successful. Another strategy for chemical crosslinking was to introduce Py crosslinkers onto the polymer backbone first and use thiol-exchange reaction for self-crosslinking. Nanogels were successfully prepared via this strategy, with better stability and ion tolerance, compared with physically crosslinked counterparts. Preliminary studies on drug loading and release proved that DOX could be loaded *in situ*. However, the release of DOX favoured gastric fluid than intestinal fluid, possibly due to the stronger electrostatic interaction of DOX and PLP-Py at neutral pH. This means the nanogels might be useful for treatment of stomach diseases, instead of intestinal diseases. Otherwise, the dual-responsive nanogels could be administrated via other routes to achieve intracellular delivery. Further research would be performed to reveal the full potential of this delivery system.

Chapter 6 Conclusions and future perspectives

6.1 Conclusions

A series of novel stimuli-responsive biomimetic polymer-based materials have been successfully developed for overcoming biological barriers at different levels. First, anionic hyperbranched CPP-mimetic polymers were synthesised and their pH-responsive membrane-lytic activity was systematically examined. These polymers had less cytotoxicity, but comparable intracellular delivery potency compared with commercially available CPPs. Second, PLP-based hydrogels with pH- or dual-responsiveness were developed for oral delivery. Payloads with different sizes and hydrophobicity could be encapsulated, and the pH-responsive hydrogels had an intestine-favoured release profile. Redox-responsive hydrogels could degrade upon redox-triggers, and thus favoured colonic release. Third, PLP-based nanogels were developed via either physically or chemically crosslinking. The resulted nanogels had good stability and stimuli-responsive disassociation, which was used for controlled release of hydrophobic cargos.

The main findings and impacts of the hyperbranched polymers, hydrogels and nanogels are summarised below.

6.1.1 HPLP for intracellular drug delivery

A series of hyperbranched CPP-mimetic polymers with pH-responsive membrane-lytic activity were developed in chapter 3. This is the first known report of anionic non-linear CPP-mimicking polymers. The impact of the hyperbranching structure on physiological behaviour (e.g. pH-dependent aggregation, hydrophobicity variation, conformational change and hydrodynamic size) of polymers has been systematically studied. It was found

that the polymers with higher branching degrees showed a broader range of pH-responsive transitions and a lower ability to form hydrophobic microdomains due to the steric hindrance within the structure. The results of the polymer-membrane interaction studies on artificial lipid particles and red blood cells confirmed that HPLPs were only membrane-active at late endosomal pH but not at physiological pH and the membrane permeability was independent of membrane charge. The mechanism of membrane permeability at acidic pH was found to be pore formation rather than membrane solubilisation. All HPLPs showed negligible cytotoxicity toward HeLa cells at a concentration as high as 5 mg mL^{-1} and could facilitate the endocytosed payload to efficiently escape from intracellular vesicles into the cell cytoplasm. Compared with cationic CPPs, HPLPs showed lower cytotoxicity but efficient cytoplasmic delivery, thus suggesting their promising applications in intracellular drug delivery.

6.1.2 PLP-based hydrogels for oral drug delivery

A series of PLP-based hydrogels were developed in Chapter 4. The pH-responsive swelling and rheological behaviour of the hydrogels could be adjusted by changing crosslinkers, crosslinking density and solid contents. The effects of crosslinkers on hydrogel network were investigated in detail. Hydrogels crosslinked by small molecular crosslinker CDE had less compact networks than those crosslinked by PEG, due to the hydrogen bonding between PLP and PEG, as well as the higher intermolecular crosslinking. Both PEG- and CDE-crosslinked hydrogels favoured hydrophobic payloads and showed good controlled-release profiles in the gastrointestinal mimic environments on the model drug fluorescein. The introduction of redox-triggers could lead to complete hydrogel disassociation. Further investigation of loading probiotics in CDE-crosslinked hydrogels showed that a probiotic (LGG) could be successfully loaded and released by hydrogels.

6.1.3 PLP-based nanogels as a multi-scale delivery system

PLP-based nanogels were prepared by a simple and reproducible nanoprecipitation method via either physically or chemically crosslinking. The sizes of nanogels prepared by physically crosslinked NDA18 were adjustable by varying synthetic parameters. The nanogels synthesised were negatively charged with a good stability in mild acidic and basic solutions (pH 3-9.5), and in saline solution within a sufficiently wide ionic strength. However, these nanogels dissolute in neutral phosphate-containing buffers, which led to cargo release. A hydrophobic model drug (Nile red) could be loaded via hydrophobic interaction with NDA18, and efficiently released in SIF due to nanogel dissolution. Chemically crosslinked nanogels could be crosslinked via a thiol-exchange strategy with both pH- and redox-responsiveness. Compared with physically crosslinked counterparts, chemically crosslinked nanogels had better stability and ion tolerance. pH-Responsive swelling and redox-responsive disassociation were observed in the DLS study. Preliminary studies on loading and release proved that an anticancer drug DOX could be loaded *in situl*, and the release favoured gastric environment instead of intestinal environment.

6.2 Future perspectives

Based on the findings listed above, some further research is recommended, in order to fully explore their potentials for drug delivery. Particularly, the following topics are worth investigating in the future.

6.2.1 Further modification of HPLPs

In Chapter 3, the haemolysis results suggested that a higher branching degree facilitated the membrane permeation at late endosomal pH. However, the highest branching degree studied was 10%. The author tried to prepare

more hyperbranched HPLPs, but the resulting polymers had relatively poor solubility, which limited further investigation on membrane permeability. The modification of hydrophilic moieties on HPLPs could be a solution to solve the solubility problem. For instance, conjugating PEG to the end COOH groups of HPLPs via an acid-liable bond (ester or hydrazone) is a feasible strategy to increase the solubility at physiological pH. In an acidic environment, the cleavage of an acid-liable linker reveals the membrane-lytic HPLP which leads to endosomal escape.

Except from solubility enhancement, further modifications of HPLPs also include the introduction of target ligands, to help improve the selectively of cell internalisation. As introduced in chapter 1, TPPs facilitated tumour penetration and cellular uptake of drugs and nanoparticles. Therefore, conjugating TPPs on the end COOH groups of HPLPs via an acid-liable bond may achieve both tumour targeting and intracellular release. Ideally, the acid-liable bond breaks in the acidic TME, to release TPPs for receptor binding. The activation of CendR pathway enables the uptake of drugs and HPLPs, which facilitates the following endosomal escape.

6.2.2 Co-delivery of double payloads and multiple stages of release

The preliminary results in Chapter 4 proved that both small molecular model drugs and probiotics could be loaded and released in the CDE-crosslinked hydrogels. Thus, it would be interesting to encapsulate double payloads with different properties to achieve a combined therapy (Zhang et al. 2011). For instance, for the treatment of chronic GI disorders, the co-delivery of drugs and probiotics may have synergetic effects, which may not only relieve the diseases but also help to restore normal bacterial microflora (Kim et al. 2015; Jonkers et al. 2012). The sequential release of both payloads from

hydrogels by swelling and redox-triggered disassociation may improve the efficacy of DDS.

Combining hydrogels with nanogels may lead to multiple stage drug delivery systems. As shown in Chapter 5, nanogels are relatively sensitive to environmental pH and the undesirable release of DOX was observed in SGF. If DOX-loaded nanogels could be encapsulated into bulky hydrogels to generate a double gel system, the protection of hydrogels may prevent the leakage of DOX in a gastric environment. In an intestinal environment, nanogels could be released either by swelling or hydrogel degradation and facilitate the following intracellular delivery. The nanogel-integrated system may improve the stability of nanogels by hydrogel protection and a more sustained and controllable release profile may be achieved.

6.2.3 *Ex vivo and in vivo* performance characterisation

The aim of this thesis was to develop new materials and prove the concept *in vitro*. Due to the limitation of time and facilities, there was no *ex vivo* models or *in vivo* characterisation involved. However, it would be interesting to investigate further the drug release behaviour in a more biorelevant setting. For instance, an *ex vivo* intestinal epithelium model was reported using a monolayer of Caco-2 cells (human epithelial colorectal adenocarcinoma cell line) seeded in Transwell plate (Sharpe et al. 2014). The Caco-2 cells form a confluent layer connected by tight junctions, which mimic the intestinal epithelium barrier. This model has been widely used for mucoadhesion and transport studies. An advanced *ex vivo* model is the co-culture of Caco-2 cells and another human adenocarcinoma cell line HT29. Compared with single cell culture model, the co-culture model is closer to the intestinal layers with similar mucus-secreting characteristics (Pan et al. 2015). Other *ex vivo* models include using primary intestinal cells to rebuild intestinal layers *in vitro* or induced

pluripotent stem cells to mimic normal intestinal cells, rather than diseased cells (Kauffman et al. 2013). These *ex vivo* models could be useful platforms to investigate how drug carriers interact with the biological barrier at microscopic level. The results may provide feedback for formulation optimisation.

Pharmacokinetics animal studies using these carriers could reveal more information about the drug release kinetics, biodistribution and toxicity *in vivo*. Since the *in vivo* physiological system is much more complex than *in vitro* and *ex vivo* models, the performance of the materials may deviate from previous results *in vitro*. In this case, the design of materials and the encapsulation strategy may need to be revisited to optimise the profile. Furthermore, the systemic toxicity and degradability are also important factors that need to be clarified for clinical applications.

Bibliography

Abd Karim, K.J. et al., 2014. Enhanced drug toxicity by conjugation of platinum drugs to polymers with guanidine containing zwitterionic functional groups that mimic cell-penetrating peptides. *Polymer Chemistry*, 5(22), pp.6600–6610.

Aburub, A., Risley, D.S. & Mishra, D., 2008. A critical evaluation of fasted state simulating gastric fluid (FaSSGF) that contains sodium lauryl sulfate and proposal of a modified recipe. *International Journal of Pharmaceutics*, 347(1–2), pp.16–22.

Aimetti, A.A., Machen, A.J. & Anseth, K.S., 2009. Poly(ethylene glycol) hydrogels formed by thiol-ene photopolymerization for enzyme-responsive protein delivery. *Biomaterials*, 30(30), pp.6048–6054.

Akashi, Y. et al., 2014. Anticancer effects of gemcitabine are enhanced by co-administered iRGD peptide in murine pancreatic cancer models that overexpressed neuropilin-1. *British Journal of Cancer*, 110, pp.1481–1487.

Akiyoshi, K. et al., 1993. Self-Aggregates of Hydrophobized Polysaccharides in Water. Formation and Characteristics of Nanoparticles. *Macromolecules*, 26(12), pp.3062–3068.

Akiyoshi, K. et al., 1998. Self-assembled hydrogel nanoparticle of cholesterol-bearing pullulan as a carrier of protein drugs: Complexation and stabilization of insulin. *Journal of Controlled Release*, 54(3), pp.313–320.

Akiyoshi, K. et al., 2000. Self-association of cholesteryl-bearing poly(L-lysine) in water and control of its secondary structure by host-guest interaction with cyclodextrin. *Macromolecules*, 33(18), pp.6752–6756.

Alvarez-Lorenzo, C. et al., 2013. Crosslinked ionic polysaccharides for stimuli-sensitive drug delivery. *Advanced Drug Delivery Reviews*, 65(9), pp.1148–1171.

Alvarez-Lorenzo, C. et al., 2016. Stimuli-responsive polymers for antimicrobial therapy: drug targeting, contact-killing surfaces and competitive release. *Expert Opinion on Drug Delivery*, 13(8), pp.1109–1119.

Angeles-Boza, A.M. et al., 2010. Generation of Endosomolytic Reagents by Branching of Cell-Penetrating Peptides: Tools for the Delivery of Bioactive Compounds to Live Cells in Cis or Trans. *Bioconjugate Chemistry*, 21(12), pp.2164–2167.

Annabi, N. et al., 2010. Controlling the porosity and microarchitecture of hydrogels for tissue engineering. *Tissue Engineering Part B: Reviews*, 16(4), pp.371–383.

Armstrong, J.K. et al., 2004. The Hydrodynamic Radii of Macromolecules and Their Effect on Red Blood Cell Aggregation. *Biophysical Journal*, 87(6), pp.4259–4270.

Attah, R., 2016. *Development of novel hydrogels for efficient drug delivery and controlled release Drug Release.* Master Dissertation. Imperial College London.

Bader, C.A. et al., 2016. A Molecular Probe for the Detection of Polar Lipids in Live Cells S. N. Witt, ed. *PLoS ONE*, 11(8), e0161557.

Bae, J. et al., 2015. Novel Redox-Responsive Amphiphilic Copolymer Micelles for Drug Delivery: Synthesis and Characterization. *The AAPS Journal*, 17(6), pp.1357–1368.

Bae, J. et al., 2014. Quinone propionic acid-based redox-triggered polymer nanoparticles for drug delivery: Computational analysis and in vitro evaluation. *Journal of Applied Polymer Science*, 131(13), pp.40461–40471.

Banerjee, R., 2012. Redox outside the Box: Linking Extracellular Redox Remodeling with Intracellular Redox Metabolism. *The Journal of Biological Chemistry*, 287(7), pp.4397–4402.

Bang, E.K. et al., 2013. Substrate-initiated synthesis of cell-penetrating poly(disulfide)s. *Journal of the American Chemical Society*, 135(6), pp.2088–2091.

Barany, G., Kneib Cordoiner, N. & Mullen, D.G., 1987. Solid phase peptide synthesis: a silver anniversary report. *Chemical Biology & Drug Design*, 30(6), pp.705–739.

Bertrand, O. et al., 2016. Redox-controlled upper critical solution temperature behaviour of a nitroxide containing polymer in alcohol-water mixtures. *Polymer Chemistry*, 7(5), pp.1088–1095.

Bhatia, T. et al., 2014. Fluid domain patterns in free-standing membranes captured on a solid support. *Biochimica et Biophysica Acta (BBA) - Biomembranes*, 1838(10), pp.2503–2510.

Binder, W.H., 2008. Polymer-induced transient pores in lipid membranes. *Angewandte Chemie - International Edition*, 47(17), pp.3092–3095.

Bobko, A.A. et al., 2012. In vivo monitoring of pH, redox status, and glutathione using L-band EPR for assessment of therapeutic effectiveness in solid tumors. *Magnetic Resonance in Medicine*, 67(6), pp.1827–1836.

Bolhassani, A., 2011. Potential efficacy of cell-penetrating peptides for nucleic acid and drug delivery in cancer. *Biochimica et Biophysica Acta (BBA) - Reviews on Cancer*, 1816(2), pp.232–246.

Bouwstra, J.A. et al., 2003. Structure of the skin barrier and its modulation by vesicular formulations. *Progress in Lipid Research*, 42(1), pp.1–36.

Brewster, M.E. & Loftsson, T., 2007. Cyclodextrins as pharmaceutical solubilizers. *Advanced Drug Delivery Reviews*, 59(7), pp.645–666.

Brock, R., 2014. The Uptake of Arginine-Rich Cell-Penetrating Peptides: Putting the Puzzle Together. *Bioconjugate Chemistry*, 25(5), pp.863–868.

Buerkli, C. et al., 2014. Amphipathic Homopolymers for siRNA Delivery: Probing Impact of Bifunctional Polymer Composition on Transfection. *Biomacromolecules*, 15(5), pp.1707–1715.

Cagel, M. et al., 2017. Doxorubicin: nanotechnological overviews from bench to bedside. *Drug Discovery Today*, 22(2), pp.270–281.

Carberry, T.P. et al., 2012. Dendrimer functionalization with a membrane-interacting domain of herpes simplex virus type 1: Towards intracellular delivery. *Chemistry - A European Journal*, 18(43), pp.13678–13685.

Chandar, P., Somasundaran, P. & Turro, N.J., 1988. Fluorescence probe investigation of anionic polymer-cationic surfactant interactions. *Macromolecules*, 21(4), pp.950–953.

Changenet-Barret, P. et al., 2013. Unravelling molecular mechanisms in the fluorescence spectra of doxorubicin in aqueous solution by femtosecond fluorescence spectroscopy. *Physical Chemistry Chemical Physics*, 15(8), p.2937.

Chattopadhyay, S. et al., 2016. Waterborne physically crosslinked antimicrobial nanogels. *Polymer Chemistry*, 7(2), pp.364–369.

Chen, C.-P. et al., 2006. Gene Transfer with Poly-Melittin Peptides. *Bioconjugate Chemistry*, 17(4), pp.1057–1062.

Chen, J. et al., 2011. pH and Reduction Dual-Sensitive Copolymeric Micelles for Intracellular Doxorubicin Delivery. *Biomacromolecules*, 12(10), pp.3601–3611.

Chen, J. & Park, K., 2000. Synthesis and characterization of superporous hydrogel composites. *Journal of Controlled Release*, 65(1), pp.73–82.

Chen, L. & Harrison, S.D., 2007. Cell-penetrating peptides in drug development: enabling intracellular targets. *Biochemical Society Transactions*, 35(4), pp.821–825.

Chen, R. et al., 2008. Aqueous solution behaviour and membrane disruptive activity of pH-responsive PEGylated pseudo-peptides and their intracellular distribution. *Biomaterials*, 29(32), pp.4333–4340.

Chen, R., Khormaee, S., et al., 2009a. Effect of l-Leucine Graft Content on Aqueous Solution Behavior and Membrane-Lytic Activity of a pH-Responsive Pseudopeptide. *Biomacromolecules*, 10(9), pp.2601–2608.

Chen, R. et al., 2005. Modulation of cell membrane disruption by pH-responsive pseudo-peptides through grafting with hydrophilic side chains. *Journal of Controlled Release*, 108(1), pp.63–72.

Chen, R., Eccleston, M.E., et al., 2009. Synthesis and pH-responsive properties of pseudo-peptides containing hydrophobic amino acid grafts. *Journal of Materials Chemistry*, 19(24), pp.4217–4224.

Chen, R., Khormaee, S., et al., 2009b. The role of hydrophobic amino acid grafts in the enhancement of membrane-disruptive activity of pH-responsive pseudo-peptides. *Biomaterials*, 30(10), pp.1954–61.

Chen, S., 2017. *Biomimetic Nanoscale Systems for pH-Triggered Intracellular Drug Delivery*. PhD Thesis. Imperial College London.

Chen, S. et al., 2017. Membrane-Anchoring, Comb-Like Pseudopeptides for Efficient, pH-Mediated Membrane Destabilization and Intracellular Delivery. *ACS Applied Materials & Interfaces*, 9(9), pp.8021–8029.

Cheng, R. et al., 2013. Dual and multi-stimuli responsive polymeric nanoparticles for programmed site-specific drug delivery. *Biomaterials*, 34(14), pp.3647–3657.

Cheng, R. et al., 2011. Glutathione-responsive nano-vehicles as a promising platform for targeted intracellular drug and gene delivery. *Journal of Controlled Release*, 152(1), pp.2–12.

Cho, H. et al., 2012. Redox-sensitive polymeric nanoparticles for drug delivery. *Chemical Communications*, 48(48), pp.6043–6045.

Choonara, B.F. et al., 2014. A review of advanced oral drug delivery technologies facilitating the protection and absorption of protein and peptide molecules. *Biotechnology Advances*, 32(7), pp.1269–1282.

Cooley, C.B. et al., 2009. Oligocarbonate Molecular Transporters: Oligomerization-Based Syntheses and Cell-Penetrating Studies. *Journal of the American Chemical Society*, 131(45), pp.16401–16403.

Daban, J.R., Samsó, M. & Bartolomé, S., 1991. Use of Nile red as a fluorescent probe for the study of the hydrophobic properties of protein-sodium

dodecyl sulfate complexes in solution. *Analytical Biochemistry*, 199(2), pp.162–168.

Daffre, S. et al., 2008. Bioactive natural peptides. *Studies in Natural Products Chemistry*, 35(C), pp.597–691.

Dai, J. et al., 2011. Interlayer-Crosslinked Micelle with Partially Hydrated Core Showing Reduction and pH Dual Sensitivity for Pinpointed Intracellular Drug Release. *Angewandte Chemie International Edition*, 50(40), pp.9404–9408.

David, A.E. et al., 2012. Immobilized thermolysin for highly efficient production of low-molecular-weight protamine—An attractive cell-penetrating peptide for macromolecular drug delivery applications. *Journal of Biomedical Materials Research Part A*, 100A(1), pp.211–219.

Deas, T.S. et al., 2007. In Vitro Resistance Selection and In Vivo Efficacy of Morpholino Oligomers against West Nile Virus. *Antimicrobial Agents and Chemotherapy* , 51(7), pp.2470–2482.

Deming, T.J., 1997. Facile synthesis of block copolypeptides of defined architecture. *Nature*, 390(6658), pp.386–399.

Deming, T.J., 2000. Living polymerization of α-amino acid- N -carboxyanhydrides. *Journal of Polymer Science Part A: Polymer Chemistry*, 38(17), pp.3011–3018.

Deng, B., Ma, P. & Xie, Y., 2015. Reduction-sensitive polymeric nanocarriers in cancer therapy: a comprehensive review. *Nanoscale*, 7(30), pp.12773–12795.

Ding, H., Portilla-Arias, J., et al., 2013. Distinct mechanisms of membrane

permeation induced by two polymalic acid copolymers. *Biomaterials*, 34(1), pp.217–225.

Ding, H. et al., 2010. Inhibition of brain tumor growth by intravenous poly(-L-malic acid) nanobioconjugate with pH-dependent drug release. *Proceedings of the National Academy of Sciences*, 107(42), pp.18143–18148.

Ding, H., Helguera, G., et al., 2013. Polymalic acid nanobioconjugate for simultaneous immunostimulation and inhibition of tumor growth in HER2/neu-positive breast cancer. *Journal of Controlled Release*, 171(3), pp.322–329.

Ding, H. et al., 2017. Polymalic Acid Tritryptophan Copolymer Interacts with Lipid Membrane Resulting in Membrane Solubilization. *Journal of Nanomaterials*, 2017, Article ID: 4238697.

Ding, H. et al., 2011. The optimization of polymalic acid peptide copolymers for endosomolytic drug delivery. *Biomaterials*, 32(22), pp.5269–5278.

Dowdy, S.F., 2017. Overcoming cellular barriers for RNA therapeutics. *Nature Biotechnology*, 35, pp.222–229.

Van Duong, T. et al., 2017. Spectroscopic Investigation of the Formation and Disruption of Hydrogen Bonds in Pharmaceutical Semicrystalline Dispersions. *Molecular Pharmaceutics*, 14(5), pp.1726–1741.

Dyakonova, M.A. et al., 2015. Salt-Induced Changes in Triblock Polyampholyte Hydrogels: Computer Simulations and Rheological, Structural, and Dynamic Characterization. *Macromolecules*, 48(22), pp.8177–8189.

Eccleston, M.E. et al., 2000. pH-responsive pseudo-peptides for cell membrane

disruption. *Journal of Controlled Release*, 69(2), pp.297–307.

Eccleston, M.E., Slater, N.K.H. & Tighe, B.J., 1999. Synthetic routes to responsive polymers; co-polycondensation of tri-functional amino acids with diacylchlorides. *Reactive and Functional Polymers*, 42(2), pp.147–161.

Eggimann, G.A. et al., 2014. Designed cell penetrating peptide dendrimers efficiently internalize cargo into cells. *Chemical Communications*, 50(55), pp.7254–7257.

El-Sayed, M.E.H., Hoffman, A.S. & Stayton, P.S., 2005. Smart polymeric carriers for enhanced intracellular delivery of therapeutic macromolecules. *Expert Opinion on Biological Therapy*, 5(1), pp.23–32.

Ensign, L.M., Cone, R. & Hanes, J., 2012. Oral drug delivery with polymeric nanoparticles: The gastrointestinal mucus barriers. *Advanced Drug Delivery Reviews*, 64(6), pp.557–570.

Espelin, C.W. et al., 2016. Dual HER2 targeting with trastuzumab and liposomal-encapsulated doxorubicin (MM-302) demonstrates synergistic antitumor activity in breast and gastric cancer. *Cancer Research*, 76(6), pp.1517–1527.

FDA/Center for Drug Evaluation and Research, 2017. Inactive Ingredient Search for Approved Drug Products. Available at: https://www.accessdata.fda.gov/scripts/cder/iig/index.cfm.

Feron, O., 2010. Tumor-Penetrating Peptides: A Shift from Magic Bullets to Magic Guns. *Science Translational Medicine*, 2(34), p.34ps26.

Fischer, H., Erdmann, S. & Holler, E., 1989. An Unusual Polyanion from

Physarum polycephalum That Inhibits Homologous DNA Polymerase α in Vitro. *Biochemistry*, 28(12), pp.5219–5226.

Fox, M.E., Szoka, F.C. & Fréchet, J.M.J., 2009. Soluble Polymer Carriers for the Treatment of Cancer: The Importance of Molecular Architecture. *Accounts of Chemical Research*, 42(8), pp.1141–1151.

Frank, L.A. et al., 2014. Chitosan gel containing polymeric nanocapsules: A new formulation for vaginal drug delivery. *International Journal of Nanomedicine*, 9(1), pp.3151–3161.

Fu, H. et al., 2010. Redox-controlled “smart” polyacrylamide solubility. *Polymer Chemistry*, 1(5), pp.631–633.

Fu, J. et al., 2015. Intracellular Delivery of Functional Proteins and Native Drugs by Cell-Penetrating Poly(disulfide)s. *Journal of the American Chemical Society*, 137(37), pp.12153–12160.

Futaki, S. et al., 2001. Arginine-rich peptides An abundant source of membrane-permeable peptides having potential as carriers for intracellular protein delivery. *Journal of Biological Chemistry*, 276(8), pp.5836–5840.

Futaki, S. et al., 2002. Translocation of branched-chain arginine peptides through cell membranes: flexibility in the spatial disposition of positive charges in membrane-permeable peptides. *Biochemistry*, 41(25), pp.7925–7930.

Galande, C. et al., 2011. Quasi-molecular fluorescence from graphene oxide. *Scientific Reports*, 1, Article number: 85.

Gao, W., Chan, J.M. & Farokhzad, O.C., 2010. pH-Responsive Nanoparticles for Drug Delivery. *Molecular Pharmaceutics*, 7(6), pp.1913–1920.

Gasparini, G. et al., 2014. Cellular Uptake of Substrate-Initiated Cell-Penetrating Poly(disulfide)s. *Journal of the American Chemical Society*, 136(16), pp.6069–6074.

Ghosh, K. et al., 2005. Rheological Characterization of in Situ Cross-Linkable Hyaluronan Hydrogels. *Biomacromolecules*, 6(5), pp.2857–2865.

Gillies, E.R. & Fréchet, J.M.J., 2005. Dendrimers and dendritic polymers in drug delivery. *Drug Discovery Today*, 10(1), pp.35–43.

Greenspan, P. & Fowler, S.D., 1985. Spectrofluorometric studies of the lipid probe, nile red. *Journal of Lipid Research* , 26(7), pp.781–789.

Grijalvo, S. et al., 2016. Biodegradable liposome-encapsulated hydrogels for biomedical applications: a marriage of convenience. *Biomaterials Science*, 4(4), pp.555–574.

Gu, D. et al., 2017. Hydrogels with smart systems for delivery of hydrophobic drugs. *Expert Opinion on Drug Delivery*, 14(7), pp.879–895.

Guidotti, G., Brambilla, L. & Rossi, D., 2017. Cell-Penetrating Peptides: From Basic Research to Clinics. *Trends in Pharmacological Sciences*, 38(4), pp.406–424.

Guo, L. et al., 2010. FTIR study on hydrogen-bonding interactions in biodegradable polymer blends of poly(3-hydroxybutyrate) and poly(4-vinylphenol). *Macromolecules*, 43(8), pp.3897–3902.

Gupta, P., Vermani, K. & Garg, S., 2002. Hydrogels: from controlled release to pH-responsive drug delivery. *Drug Discovery Today*, 7(10), pp.569–579.

Habermann, E., 1972. Bee and Wasp Venoms. *Science*, 177(4046), pp.314–322.

Hadjichristidis, N. et al., 2009. Synthesis of Well-Defined Polypeptide-Based Materials via the Ring-Opening Polymerization of α-Amino Acid N-Carboxyanhydrides. *Chemical Reviews*, 109(11), pp.5528–5578.

Hamid Akash, M.S., Rehman, K. & Chen, S., 2015. Natural and synthetic polymers as drug carriers for delivery of therapeutic proteins. *Polymer Reviews*, 55(3), pp.371–406.

He, B., Wan, E. & Chan-Park, M.B., 2006. Synthesis and Degradation of Biodegradable Photo-Cross-Linked Poly(α,β-malic acid)-Based Hydrogel. *Chemistry of Materials*, 18(17), pp.3946–3955.

Herce, H.D., Garcia, A.E. & Cardoso, M.C., 2014. Fundamental Molecular Mechanism for the Cellular Uptake of Guanidinium-Rich Molecules. *Journal of the American Chemical Society*, 136(50), pp.17459–17467.

Hermanson, G.T., 2013. Chapter 2 - Functional Targets for Bioconjugation BT - Bioconjugate Techniques (Third edition). In Boston: Academic Press, pp. 127–228.

Ho, V.H.B., Slater, N.K.H. & Chen, R., 2011. pH-responsive endosomolytic pseudo-peptides for drug delivery to multicellular spheroids tumour models. *Biomaterials*, 32(11), pp.2953–8.

Hoffman, A.S., 2012. Hydrogels for biomedical applications. *Advanced Drug Delivery Reviews*, 64, pp.18–23.

Holm, R., Müllertz, A. & Mu, H., 2013. Bile salts and their importance for drug absorption. *International Journal of Pharmaceutics*, 453(1), pp.44–55.

Holowka, E.P. & Bhatia, S.K., 2014. *Drug Delivery*, New York, NY: Springer New York.

Huang, X., 2017. *Model Drug Release Profile of a pH-Responsive Nanocarrier*. Master Dissertation. Imperial College London.

Huang, Y., Cai, Y. & Lapitsky, Y., 2015. Factors affecting the stability of chitosan/tripolyphosphate micro- and nanogels: resolving the opposing findings. *Journal of Materials Chemistry B*, 3(29), pp.5957–5970.

Huang, Y. & Lapitsky, Y., 2012. Salt-Assisted Mechanistic Analysis of Chitosan/Tripolyphosphate Micro- and Nanogel Formation. *Biomacromolecules*, 13(11), pp.3868–3876.

Huang, Z.W. et al., 2012. New functional degradable and bio-compatible nanoparticles based on poly(malic acid) derivatives for site-specific anti-cancer drug delivery. *International Journal of Pharmaceutics*, 423(1), pp.84–92.

Huo, M. et al., 2014. Redox-responsive polymers for drug delivery: from molecular design to applications. *Polymer Chemistry*, 5(5), pp.1519–1528.

Jain, K. et al., 2010. Dendrimer toxicity: Let's meet the challenge. *International Journal of Pharmaceutics*, 394(1–2), pp.122–142.

Jia, X. et al., 2000. Antimicrobial Peptides Protect Coho Salmon fromVibrio anguillarum Infections. *Applied and Environmental Microbiology* , 66(5), pp.1928–1932.

Jin, E. et al., 2013. Acid-Active Cell-Penetrating Peptides for in Vivo Tumor-Targeted Drug Delivery. *Journal of the American Chemical Society*, 135(2), pp.933–940.

Jones, M., 2010. An example of Dynamic Light Scattering. Available at: https://commons.wikimedia.org/w/index.php?curid=10502233.

Jonkers, D. et al., 2012. Probiotics in the Management of Inflammatory Bowel Disease. *Drugs*, 72(6), pp.803–823.

Juliano, R.L., 2006. Intracellular Delivery of Oligonucleotide Conjugates and Dendrimer Complexes. *Annals of the New York Academy of Sciences*, 1082(1), pp.18–26.

Kanamala, M. et al., 2016. Mechanisms and biomaterials in pH-responsive tumour targeted drug delivery: A review. *Biomaterials*, 85, pp.152–167.

Kang, H. et al., 2005. Tat-conjugated PAMAM dendrimers as delivery agents for antisense and siRNA oligonucleotides. *Pharmaceutical Research*, 22(12), pp.2099–2106.

Kauffman, A.L. et al., 2013. Alternative functional in vitro models of human intestinal epithelia. *Frontiers in Pharmacology*, 4, Article number: 79.

Kauffman, W.B. et al., 2015. Mechanism matters: a taxonomy of cell penetrating peptides. *Trends in Biochemical Sciences*, 40(12), pp.749–764.

Kaufman, E.A. et al., 2017. Generation effect of Newkome dendrimers on cellular uptake. *Polymer*, 113, pp.67–73.

Kawashima, T. et al., 2011. Lactobacillus plantarum strain YU from fermented foods activates Th1 and protective immune responses. *International Immunopharmacology*, 11(12), pp.2017–2024.

Kelley, K.E. et al., 2012. Identification of phthalates in medications and dietary supplement formulations in the United States and Canada. *Environmental Health Perspectives*, 120(3), pp.379–384.

Kesharwani, P., Tekade, R.K. & Jain, N.K., 2014. Generation dependent cancer targeting potential of poly(propyleneimine) dendrimer. *Biomaterials*,

35(21), pp.5539–5548.

Khanna, Y.P. et al., 1981. Aromatic polyamides. II. Thermal degradation of some aromatic polyamides and their model diamides. *Journal of Polymer Science: Polymer Chemistry Edition*, 19(11), pp.2817–2834.

Khine, Y.Y. et al., 2016. Direct Correlation Between Zeta Potential and Cellular Uptake of Poly(methacrylic acid) Post-Modified with Guanidinium Functionalities. *Macromolecular Chemistry and Physics*, 217(20), pp.2302–2309.

Khormaee, S. et al., 2013. Endosomolytic Anionic Polymer for the Cytoplasmic Delivery of siRNAs in Localized In Vivo Applications. *Advanced Functional Materials*, 23(5), pp.565–574.

Khormaee, S. et al., 2010. The Influence of Aromatic Side-Chains on the Aqueous Properties of pH-Sensitive Poly(L-lysine iso-phthalamide) Derivatives. *Journal of Biomaterials Science, Polymer Edition*, 21(12), pp.1573–1588.

Khramtsov, V. V & Gillies, R.J., 2014. Janus-Faced Tumor Microenvironment and Redox. *Antioxidants & Redox Signaling*, 21(5), pp.723–729.

Kim, Y., Binauld, S. & Stenzel, M.H., 2012. Zwitterionic Guanidine-Based Oligomers Mimicking Cell-Penetrating Peptides as a Nontoxic Alternative to Cationic Polymers to Enhance the Cellular Uptake of Micelles. *Biomacromolecules*, 13(10), pp.3418–3426.

Kim, Y. Il et al., 2015. Development of a novel bi-coated combination capsule containing mosapride and probiotics for irritable bowel syndrome. *Pharmaceutical Development and Technology*, 20(8), pp.949–956.

Kizhakkedathu, J.N. et al., 2010. High Molecular Weight Polyglycerol-Based Multivalent Mannose Conjugates. *Biomacromolecules*, 11(10), pp.2567–2575.

Kluzek, M. et al., 2017. Influence of a pH-sensitive polymer on the structure of monoolein cubosomes. *Soft Matter*, 13(41), pp.7571–7577.

Koetting, M.C. et al., 2015. Stimulus-responsive hydrogels: Theory, modern advances, and applications. *Materials Science and Engineering: R: Reports*, 93, pp.1–49.

Koetting, M.C. & Peppas, N.A., 2014. pH-Responsive poly(itaconic acid-co-N-vinylpyrrolidone) hydrogels with reduced ionic strength loading solutions offer improved oral delivery potential for high isoelectric point-exhibiting therapeutic proteins. *International Journal of Pharmaceutics*, 471(1–2), pp.83–91.

Koren, E. & Torchilin, V.P., 2012. Cell-penetrating peptides: breaking through to the other side. *Trends in Molecular Medicine*, 18(7), pp.385–393.

Kozlovskaya, V. et al., 2012. pH-triggered shape response of cubical ultrathin hydrogel capsules. *Soft Matter*, 8(38), pp.9828–9839.

Kumar, S., Roy, S.G. & De, P., 2012. Cationic methacrylate polymers containing chiral amino acid moieties: controlled synthesis via RAFT polymerization. *Polymer Chemistry*, 3(5), pp.1239–1248.

Kuppusamy, P. et al., 2002. Noninvasive Imaging of Tumor Redox Status and Its Modification by Tissue Glutathione Levels. *Cancer Research*, 62(1), pp.307–312.

Laakkonen, P. et al., 2002. A tumor-homing peptide with a targeting specificity

related to lymphatic vessels. *Nature Medicine*, 8, pp.751–755.

Lackey, C.A. et al., 1999. Hemolytic Activity of pH-Responsive Polymer-Streptavidin Bioconjugates. *Bioconjugate Chemistry*, 10(3), pp.401–405.

Lau, Y. & Lim, V., 2016. Colon targeted drug delivery of branch-chained disulphide cross-linked polymers: design, synthesis, and characterisation studies. *Chemistry Central Journal*, 10(1), Article number: 77.

Leader, B., Baca, Q.J. & Golan, D.E., 2008. Protein therapeutics: a summary and pharmacological classification. *Nature Reviews Drug Discovery*, 7(1), pp.21–39.

Lee, B.-S. & Holler, E., 2000. β-Poly(L-malate) production by non-growing microplasmodia of Physarum polycephalum. *FEMS Microbiology Letters*, 193(1), pp.69–74.

Lee, J.-H. et al., 2012. Biopolymer-Connected Liposome Networks as Injectable Biomaterials Capable of Sustained Local Drug Delivery. *Biomacromolecules*, 13(10), pp.3388–3394.

Lee, J. & Kim, J.C., 2015. Photothermally triggerable solid lipid nanoparticles containing gold nanospheres. *Colloids and Surfaces A: Physicochemical and Engineering Aspects*, 484, pp.441–448.

Lee, S.-M. et al., 2007. Polymer-Caged Lipsomes: A pH-Responsive Delivery System with High Stability. *Journal of the American Chemical Society*, 129(49), pp.15096–15097.

Lee, S.H. et al., 2014. Activatable Cell Penetrating Peptide–Peptide Nucleic Acid Conjugate via Reduction of Azobenzene PEG Chains. *Journal of the American Chemical Society*, 136(37), pp.12868–12871.

Lee, Y.-J., Erazo-Oliveras, A. & Pellois, J.-P., 2010. Delivery of Macromolecules into Live Cells by Simple Co-incubation with a Peptide. *ChemBioChem*, 11(3), pp.325–330.

Lee, Y.-J., Johnson, G. & Pellois, J.-P., 2010. Modeling of the Endosomolytic Activity of HA2-TAT Peptides with Red Blood Cells and Ghosts. *Biochemistry*, 49(36), pp.7854–7866.

Lelle, M. & Peneva, K., 2014. An amino acid-based heterofunctional cross-linking reagent. *Amino Acids*, 46(5), pp.1243–1251.

Li, D. et al., 2016. Facile Construction of pH- and Redox-Responsive Micelles from a Biodegradable Poly(β-hydroxyl amine) for Drug Delivery. *Biomacromolecules*, 17(1), pp.291–300.

Li, J. et al., 2017. Smart Asymmetric Vesicles with Triggered Availability of Inner Cell-Penetrating Shells for Specific Intracellular Drug Delivery. *ACS Applied Materials & Interfaces*, 9(21), pp.17727–17735.

Li, W., Nicol, F. & Szoka, F.C., 2004. GALA: a designed synthetic pH-responsive amphipathic peptide with applications in drug and gene delivery. *Advanced drug delivery reviews*, 56(7), pp.967–985.

Li, Y. et al., 2013. Crystallization of Poly (ethylene glycol) in Poly methyl methacrylate) Networks. *Materials Science (Medžiagotyra)*, 19(2), pp.147–151.

Liechty, W.B. et al., 2009. Synthetic pH-Responsive Polymers for Protein Transduction. *Advanced Materials*, 21, pp.3910–3914.

Lim, V., Peh, K.K. & Sahudin, S., 2013. Synthesis, characterisation, and evaluation of a cross-linked disulphide amide-anhydride-containing

polymer based on cysteine for colonic drug delivery. *International Journal of Molecular Sciences*, 14(12), pp.24670–24691.

Liu, J. et al., 2014. PH-Sensitive nano-systems for drug delivery in cancer therapy. *Biotechnology Advances*, 32(4), pp.693–710.

Liu, R. et al., 2011. Anti-tumor drug delivery of pH-sensitive poly(ethylene glycol)-poly(L-histidine)-poly(L-lactide) nanoparticles. *Journal of Controlled Release*, 152(1), pp.49–56.

Liu, Y., Li, Z. & Liang, D., 2012. Behaviors of liposomes in a thermo-responsive poly(N-isopropylacrylamide) hydrogel. *Soft Matter*, 8(16), pp.4517–4523.

Livney, Y.D., 2010. Milk proteins as vehicles for bioactives. *Current Opinion in Colloid and Interface Science*, 15(1–2), pp.73–83.

Lo, S.L. & Wang, S., 2008. An endosomolytic Tat peptide produced by incorporation of histidine and cysteine residues as a nonviral vector for DNA transfection. *Biomaterials*, 29(15), pp.2408–2414.

Lorents, A. et al., 2012. Cell-penetrating Peptides Split into Two Groups Based on Modulation of Intracellular Calcium Concentration. *Journal of Biological Chemistry* , 287(20), pp.16880–16889.

Lv, H. et al., 2006. Toxicity of cationic lipids and cationic polymers in gene delivery. *Journal of Controlled Release*, 114(1), pp.100–109.

Ma, N. et al., 2010. Dual Redox Responsive Assemblies Formed from Diselenide Block Copolymers. *Journal of the American Chemical Society*, 132(2), pp.442–443.

Mäde, V., Els-Heindl, S. & Beck-Sickinger, A.G., 2014. Automated solid-phase peptide synthesis to obtain therapeutic peptides. *Beilstein Journal of*

Organic Chemistry, 10, p.1197.

Marie, E. et al., 2014. Amphiphilic Macromolecules on Cell Membranes: From Protective Layers to Controlled Permeabilization. *Journal of Membrane Biology*, 247(9–10), pp.861–881.

Martens, T.F. et al., 2014. Intracellular delivery of nanomaterials: How to catch endosomal escape in the act. *Nano Today*, 9(3), pp.344–364.

Martin, A.L., Li, B. & Gillies, E.R., 2009. Surface Functionalization of Nanomaterials with Dendritic Groups: Toward Enhanced Binding to Biological Targets. *Journal of the American Chemical Society*, 131(2), pp.734–741.

Mat Yusuf, N.S. et al., 2017. Characterisation and Evaluation of Trimesic Acid Derivatives as Disulphide Cross-Linked Polymers for Potential Colon Targeted Drug Delivery. *Polymers*, 9(8), p.331.

McKenzie, M. et al., 2015. Hydrogel-based drug delivery systems for poorly water-soluble drugs. *Molecules*, 20(11), pp.20397–20408.

McKinlay, C.J., Waymouth, R.M. & Wender, P.A., 2016. Cell-Penetrating, Guanidinium-Rich Oligophosphoesters: Effective and Versatile Molecular Transporters for Drug and Probe Delivery. *Journal of the American Chemical Society*, 138(10), pp.3510–3517.

Melikov, K. et al., 2015. Efficient entry of cell-penetrating peptide nona-arginine into adherent cells involves a transient increase in intracellular calcium. *Biochemical Journal*, 471(2), pp.221–230.

Merrifield, R.B., 2006. Solid-phase peptide synthesis. *Advances in Enzymology and Related Areas of Molecular Biology, Volume 32*, pp.221–296.

Mi, F.-L. et al., 2008. Oral Delivery of Peptide Drugs Using Nanoparticles Self-Assembled by Poly(γ-glutamic acid) and a Chitosan Derivative Functionalized by Trimethylation. *Bioconjugate Chemistry*, 19(6), pp.1248–1255.

Miller, K. et al., 2016. HERMIONE: a randomized Phase 2 trial of MM-302 plus trastuzumab versus chemotherapy of physician's choice plus trastuzumab in patients with previously treated, anthracycline-naïve, HER2-positive, locally advanced/metastatic breast cancer. *BMC Cancer*, 16, p.352.

Milletti, F., 2012. Cell-penetrating peptides: classes, origin, and current landscape. *Drug Discovery Today*, 17(15), pp.850–860.

Min, K.H. et al., 2010. Tumoral acidic pH-responsive MPEG-poly(β-amino ester) polymeric micelles for cancer targeting therapy. *Journal of Controlled Release*, 144(2), pp.259–266.

Mishra, V., Gupta, U. & Jain, N.K., 2010. Influence of different generations of poly(propylene imine) dendrimers on human erythrocytes. *Pharmazie*, 65(12), pp.891–895.

Mitragotri, S., Burke, P.A. & Langer, R., 2014. Overcoming the challenges in administering biopharmaceuticals: formulation and delivery strategies. *Nature Reviews Drug Discovery*, 13(9), pp.655–672.

Monti, S.M., Supuran, C.T. & De Simone, G., 2013. Anticancer carbonic anhydrase inhibitors: a patent review (2008 – 2013). *Expert Opinion on Therapeutic Patents*, 23(6), pp.737–749.

Morimoto, N. et al., 2008. Dual Stimuli-Responsive Nanogels by Self-Assembly of Polysaccharides Lightly Grafted with Thiol-Terminated Poly(N-isopropylacrylamide) Chains. *Macromolecules*, 41(16), pp.5985–5987.

Morton, S.W., Poon, Z. & Hammond, P.T., 2013. The architecture and biological performance of drug-loaded LbL nanoparticles. *Biomaterials*, 34(21), pp.5328–5335.

Motlagh, N.S.H. et al., 2016. Fluorescence properties of several chemotherapy drugs: doxorubicin, paclitaxel and bleomycin. *Biomedical Optics Express*, 7(6), pp.2400–2406.

Mukherjee, S., Ghosh, R.N. & Maxfield, F.R., 1997. Endocytosis. *Physiological Reviews*, 77(3), pp.759–803.

Mukherjee, S., Raghuraman, H. & Chattopadhyay, A., 2007. Membrane localization and dynamics of Nile Red: Effect of cholesterol. *Biochimica et Biophysica Acta (BBA) - Biomembranes*, 1768(1), pp.59–66.

Mura, S., Nicolas, J. & Couvreur, P., 2013. Stimuli-responsive nanocarriers for drug delivery. *Nature Materials*, 12(11), pp.991–1003.

Murriel, C.L. & Dowdy, S.F., 2006. Influence of protein transduction domains on intracellular delivery of macromolecules. *Expert Opinion on Drug Delivery*, 3(6), pp.739–746.

Murthy, N. et al., 1999. The design and synthesis of polymers for eukaryotic membrane disruption. *Journal of Controlled Release*, 61(1), pp.137–143.

Neri, D. & Supuran, C.T., 2011. Interfering with pH regulation in tumours as a therapeutic strategy. *Nature Reviews Drug Discovery*, 10, p.767.

Niazi, S.K., 2009. Handbook of Pharmaceutical Manufacturing Formulations: Compressed Solid Products. *Informa Healthcare*, 1, 2nd , p.648.

O'Brien, M.E.R. et al., 2004. Reduced cardiotoxicity and comparable efficacy in a phase III trial of pegylated liposomal doxorubicin HCl (CAELYX™/Doxil®)

versus conventional doxorubicin for first-line treatment of metastatic breast cancer. *Annals of Oncology*, 15(3), pp.440–449.

Ogawa, K., Nakayama, A. & Kokufuta, E., 2003. Preparation and Characterization of Thermosensitive Polyampholyte Nanogels. *Langmuir*, 19(8), pp.3178–3184.

Opstad, K.S. et al., 2003. Detection of elevated glutathione in meningiomas by quantitative in vivo 1H MRS. *Magnetic Resonance in Medicine*, 49(4), pp.632–637.

Orive, G. et al., 2003. Drug delivery in biotechnology: Present and future. *Current Opinion in Biotechnology*, 14(6), pp.659–664.

Osanai, S. & Nakamura, K., 2000. Effects of complexation between liposome and poly(malic acid) on aggregation and leakage behaviour. *Biomaterials*, 21(9), pp.867–876.

Pack, D.W. et al., 2005. Design and development of polymers for gene delivery. *Nature Reviews Drug Discovery*, 4(7), pp.581–593.

Palm-Apergi, C. et al., 2009. The membrane repair response masks membrane disturbances caused by cell-penetrating peptide uptake. *The FASEB Journal* , 23(1), pp.214–223.

Pan, F. et al., 2015. Optimization of Caco-2 and HT29 co-culture in vitro cell models for permeability studies. *International Journal of Food Sciences and Nutrition*, 66(6), pp.680–685.

Patra, C.N. et al., 2017. Pharmaceutical significance of Eudragit: A review. *Future Journal of Pharmaceutical Sciences*, 3(1), pp.33–45.

Peppas, N.A. et al., 2000. Hydrogels in pharmaceutical formulations. *European*

Journal of Pharmaceutics and Biopharmaceutics, 50(1), pp.27–46.

Peppas, N.A. & Khare, A.R., 1993. Preparation, structure and diffusional behavior of hydrogels in controlled release. *Advanced Drug Delivery Reviews*, 11(1–2), pp.1–35.

Pinto, J.F., 2010. Site-specific drug delivery systems within the gastro-intestinal tract: from the mouth to the colon. *International Journal of Pharmaceutics*, 395(1–2), pp.44–52.

Proksch, E., Brandner, J.M. & Jensen, J., 2008. The skin: an indispensable barrier. *Experimental Dermatology*, 17(12), pp.1063–1072.

Qiao, C. et al., 2004. The Critical Lowest Molecular Weight for PEG to Crystallize in Cross-Linked Networks. *Macromolecular Rapid Communications*, 25(5), pp.659–663.

Qiu, Y. & Park, K., 2012. Environment-sensitive hydrogels for drug delivery. *Advanced Drug Delivery Reviews*, 64, pp.49–60.

Ramsey, J.D. & Flynn, N.H., 2015. Cell-penetrating peptides transport therapeutics into cells. *Pharmacology and Therapeutics*, 154, pp.78–86.

Rizzuti, M. et al., 2015. Therapeutic applications of the cell-penetrating HIV-1 Tat peptide. *Drug Discovery Today*, 20(1), pp.76–85.

Roldo, M. et al., 2007. Azo compounds in colon-specific drug delivery. *Expert Opinion on Drug Delivery*, 4(5), pp.547–560.

Rothbard, J.B. et al., 2002. Arginine-rich molecular transporters for drug delivery: Role of backbone spacing in cellular uptake. *Journal of Medicinal Chemistry*, 45(17), pp.3612–3618.

Rothbard, J.B. et al., 2000. Conjugation of arginine oligomers to cyclosporin A facilitates topical delivery and inhibition of inflammation. *Nature Medicine*, 6, pp.1253–1257.

Ruoslahti, E., 2017. Tumor penetrating peptides for improved drug delivery. *Advanced Drug Delivery Reviews*, 110–111, pp.3–12.

Sackett, D.L. & Wolff, J., 1987. Nile red as a polarity-sensitive fluorescent probe of hydrophobic protein surfaces. *Analytical Biochemistry*, 167(2), pp.228–234.

Saito, G., Swanson, J.A. & Lee, K.-D., 2003. Drug delivery strategy utilizing conjugation via reversible disulfide linkages: role and site of cellular reducing activities. *Advanced Drug Delivery Reviews*, 55(2), pp.199–215.

Saleh, A.F. et al., 2010. Synthesis and splice-redirecting activity of branched, arginine-rich peptide dendrimer conjugates of peptide nucleic acid oligonucleotides. *Bioconjugate Chemistry*, 21(10), pp.1902–1911.

Sam, S. et al., 2010. Semiquantitative Study of the EDC/NHS Activation of Acid Terminal Groups at Modified Porous Silicon Surfaces. *Langmuir*, 26(2), pp.809–814.

Sanli, S., Altun, Y. & Guven, G., 2014. Solvent effects on pKa values of some anticancer agents in acetonitrile–water binary mixtures. *Journal of Chemical & Engineering Data*, 59(12), pp.4015–4020.

Schlaad, H. & Antonietti, M., 2003. Block copolymers with amino acid sequences: Molecular chimeras of polypeptides and synthetic polymers. *The European Physical Journal E*, 10(1), pp.17–23.

Schlegel, H.G. & Zaborosch, C., 1993. *General Microbiology*, Cambridge

University Press.

Schmalz, A. et al., 2010. Double stimuli-responsive behavior of linear and star-shaped poly(N,N-diethylaminoethyl methacrylate) in aqueous solution. *Polymer*, 51(6), pp.1213–1217.

Schoener, C.A., Hutson, H.N. & Peppas, N.A., 2013. PH-responsive hydrogels with dispersed hydrophobic nanoparticles for the oral delivery of chemotherapeutics. *Journal of Biomedical Materials Research - Part A*, 101 A(8), pp.2229–2236.

Schoener, C.A. & Peppas, N.A., 2012. Oral delivery of chemotherapeutic agents: background and potential of drug delivery systems for colon delivery. *Journal of Drug Delivery Science and Technology*, 22(6), pp.459–468.

Serizawa, T., Wakita, K. & Akashi, M., 2002. Rapid deswelling of porous poly (N-isopropylacrylamide) hydrogels prepared by incorporation of silica particles. *Macromolecules*, 35(1), pp.10–12.

Serra, L., Doménech, J. & Peppas, N.A., 2006. Drug transport mechanisms and release kinetics from molecularly designed poly(acrylic acid-g-ethylene glycol) hydrogels. *Biomaterials*, 27(31), pp.5440–51.

Sharma, V. & Pathak, K., 2016. Effect of hydrogen bond formation/replacement on solubility characteristics, gastric permeation and pharmacokinetics of curcumin by application of powder solution technology. *Acta Pharmaceutica Sinica B*, 6(6), pp.600–613.

Sharpe, L.A. et al., 2014. Therapeutic applications of hydrogels in oral drug delivery. *Expert Opinion on Drug Delivery*, 11(6), pp.901–915.

Sheil, B., Shanahan, F. & O'Mahony, L., 2007. Probiotic Effects on Inflammatory Bowel Disease. *The Journal of Nutrition*, 137(3), p.819S–824.

Shete, H.K., Prabhu, R.H. & Patravale, V.B., 2014. Endosomal escape: a bottleneck in intracellular delivery. *Journal of Nanoscience and Nanotechnology*, 14(1), pp.460–474.

Shi, D. et al., 2008. Photo-Cross-Linking and Cleavage Induced Reversible Size Change of Bio-Based Nanoparticles. *Macromolecules*, 41(21), pp.8167–8172.

Shi, N.-Q. et al., 2012. Enhancing cellular uptake of activable cell-penetrating peptide–doxorubicin conjugate by enzymatic cleavage. *International Journal of Nanomedicine*, 7, pp.1613–1621.

Siegel, R.A. et al., 1988. pH-Controlled release from hydrophobic/polyelectrolyte copolymer hydrogels. *Journal of Controlled Release*, 8(2), pp.179–182.

Sigma-Aldrich, 2012. *SAFETY DATA SHEET (Sigma-L0645)*,

Söderlind, E. et al., 2010. Simulating Fasted Human Intestinal Fluids: Understanding the Roles of Lecithin and Bile Acids. *Molecular Pharmaceutics*, 7(5), pp.1498–1507.

Song, L. et al., 2013. Efficient, pH-Triggered Drug Delivery Using a pH-Responsive DNA-Conjugated Gold Nanoparticle. *Advanced Healthcare Materials*, 2(2), pp.275–280.

Song, Z. et al., 2017. Synthetic polypeptides: from polymer design to supramolecular assembly and biomedical application. *Chemical Society Reviews*, 46, pp.6570–6599.

Stayton, P.S., Foster, S. & Hoffman, A.S., 2010. *pH-Responsive Polymer Carrier Compositions for Cytosolic Protein Delivery.* US20100150952A1.

Sugahara, K.N. et al., 2010. Coadministration of a Tumor-Penetrating Peptide Enhances the Efficacy of Cancer Drugs. *Science*, 328(5981), pp.1031–1035.

Sugahara, K.N. et al., 2009. Tissue-Penetrating Delivery of Compounds and Nanoparticles into Tumors. *Cancer Cell*, 16(6), pp.510–520.

Surapaneni, M.S., Das, S.K. & Das, N.G., 2012. Designing Paclitaxel Drug Delivery Systems Aimed at Improved Patient Outcomes: Current Status and Challenges. *ISRN Pharmacology*, 2012, pp.1–15.

Tabujew, I. et al., 2014. The Guanidinium Group as a Key Part of Water-Soluble Polymer Carriers for siRNA Complexation and Protection against Degradation. *Macromolecular Rapid Communications*, 35(13), pp.1191–1197.

Tahara, Y. & Akiyoshi, K., 2015. Current advances in self-assembled nanogel delivery systems for immunotherapy. *Advanced Drug Delivery Reviews*, 95, pp.65–76.

Tan, Z., Dhande, Y.K. & Reineke, T.M., 2017. Cell Penetrating Polymers Containing Guanidinium Trigger Apoptosis in Human Hepatocellular Carcinoma Cells unless Conjugated to a Targeting N-Acetyl-Galactosamine Block. *Bioconjugate Chemistry*, 28(12), pp.2985–2997.

Tang, H. et al., 2013. Helical poly(arginine) mimics with superior cell-penetrating and molecular transporting properties. *Chemical Science*, 4(10), pp.3839–3844.

Tarallo, R. et al., 2013. Dendrimers functionalized with membrane-interacting peptides for viral inhibition. *International Journal of Nanomedicine*, 8, pp.521–534.

Teesalu, T. et al., 2009. C-end rule peptides mediate neuropilin-1-dependent cell, vascular, and tissue penetration. *Proceedings of the National Academy of Sciences*, 106(38), pp.16157–16162.

Teesalu, T., Sugahara, K. & Ruoslahti, E., 2013. Tumor-Penetrating Peptides. *Frontiers in Oncology*, 3, p.216.

Thakral, S., Thakral, N.K. & Majumdar, D.K., 2013. Eudragit®: a technology evaluation. *Expert Opinion on Drug Delivery*, 10(1), pp.131–149.

Tian, L. & Bae, Y.H., 2012. Cancer nanomedicines targeting tumor extracellular pH. *Colloids and Surfaces B: Biointerfaces*, 99, pp.116–126.

Tibbitt, M.W., Dahlman, J.E. & Langer, R., 2016. Emerging Frontiers in Drug Delivery. *Journal of the American Chemical Society*, 138(3), pp.704–717.

Tiwari, G. et al., 2012. Drug delivery systems: An updated review. *International Journal of Pharmaceutical Investigation*, 2(1), pp.2–11.

Torchilin, V.P., 2014. Multifunctional, stimuli-sensitive nanoparticulate systems for drug delivery. *Nature Reviews Drug Discovery*, 13(11), pp.813–827.

Tosteson, M.T. et al., 1985. Melittin lysis of red cells. *The Journal of Membrane Biology*, 87(1), pp.35–44.

Traverso, N. et al., 2013. Role of glutathione in cancer progression and chemoresistance. *Oxidative Medicine and Cellular Longevity*, 2013, Article ID: 972913.

Treat, N.J. et al., 2012. Guanidine-Containing Methacrylamide (Co)polymers via aRAFT: Toward a Cell-Penetrating Peptide Mimic. *ACS Macro Letters*, 1(1), pp.100–104.

Tünnemann, G. et al., 2006. Cargo-dependent mode of uptake and bioavailability of TAT-containing proteins and peptides in living cells. *The FASEB Journal* , 20(11), pp.1775–1784.

Turro, N.J. & Arora, K.S., 1986. Pyrene as a photophysical probe for intermolecular interactions of water-soluble polymers in dilute solutions. *Polymer*, 27(5), pp.783–796.

Varghese, J.S., Chellappa, N. & Fathima, N.N., 2014. Gelatin–carrageenan hydrogels: role of pore size distribution on drug delivery process. *Colloids and Surfaces B: Biointerfaces*, 113(1), pp.346–351.

Vial, F. et al., 2007. Long-living channels of well defined radius opened in lipid bilayers by polydisperse, hydrophobically-modified polyacrylic acids. *Soft Matter*, 3(1), pp.75–78.

Vinogradov, S., Batrakova, E. & Kabanov, A., 1999. Poly(ethylene glycol)–polyethyleneimine NanoGel™ particles: novel drug delivery systems for antisense oligonucleotides. *Colloids and Surfaces B: Biointerfaces*, 16(1), pp.291–304.

Vivès, E., Schmidt, J. & Pèlegrin, A., 2008. Cell-penetrating and cell-targeting peptides in drug delivery. *Biochimica et Biophysica Acta (BBA) - Reviews on Cancer*, 1786(2), pp.126–138.

Vlieghe, P. et al., 2010. Synthetic therapeutic peptides: science and market. *Drug Discovery Today*, 15(1), pp.40–56.

Wadia, J.S., Stan, R. V & Dowdy, S.F., 2004. Transducible TAT-HA fusogenic peptide enhances escape of TAT-fusion proteins after lipid raft macropinocytosis. *Nature Medicine*, 10, pp.310–315.

Wang, F. et al., 2014. Recent progress of cell-penetrating peptides as new carriers for intracellular cargo delivery. *Journal of Controlled Release*, 174(1), pp.126–136.

Wang, J. et al., 2014. Preparation and pH controlled release of polyelectrolyte complex of poly(l-malic acid-co-d,l-lactic acid) and chitosan. *Colloids and Surfaces B: Biointerfaces*, 115, pp.275–279.

Wang, L. et al., 2010. Biodegradable magnetic-fluorescent magnetite/poly(dl-lactic acid-co-α,β-malic acid) composite nanoparticles for stem cell labeling. *Biomaterials*, 31(13), pp.3502–3511.

Wang, S. et al., 2016a. Amino acid based hydrogels with dual responsiveness for oral drug delivery. *Macromolecular Bioscience*, 16(9), pp.1258–1264.

Wang, S. et al., 2016b. Macromol. Biosci. 9/2016. *Macromolecular Bioscience*, 16(9), p.1251.

Wang, S. & Bresme, F., 2017. Simulation Studies on the Lipid Interaction and Conformation of Novel Drug-Delivery Pseudopeptidic Polymers. *The Journal of Physical Chemistry B*, 121(39), pp.9113–9125.

Wang, S. & Chen, R., 2017. pH-Responsive, Lysine-Based, Hyperbranched Polymers Mimicking Endosomolytic Cell-Penetrating Peptides for Efficient Intracellular Delivery. *Chemistry of Materials*, 29(14), pp.5806–5815.

Warusavitarne, J. & Stebbing, J., 2017. Probiotics and cancer: ready for meal time? *The Lancet Oncology*, 16(4), pp.371–372.

Watkins, K.A. & Chen, R., 2015. pH-responsive, lysine-based hydrogels for the oral delivery of a wide size range of molecules. *International Journal of Pharmaceutics*, 478(2), pp.496–503.

Weinberger, A. et al., 2013. Gel-Assisted Formation of Giant Unilamellar Vesicles. *Biophysical Journal*, 105(1), pp.154–164.

Wender, P.A. et al., 2008. The design of guanidinium-rich transporters and their internalization mechanisms. *Advanced Drug Delivery Reviews*, 60(4), pp.452–472.

Wheeler, H.O. & Ramos, O.L., 1960. Determinants of the flow and composition of bile in the unanesthetized dog during constant infusions of sodium taurocholate. *Journal of Clinical Investigation*, 39(1), p.161.

Whitehead, K.A., Langer, R. & Anderson, D.G., 2009. Knocking down barriers: advances in siRNA delivery. *Nature Reviews Drug Discovery*, 8(2), pp.129–138.

Wilding, I.R., Davis, S.S. & O'Hagan, D.T., 1994. Targeting of drugs and vaccines to the gut. *Pharmacology & Therapeutics*, 62(1–2), pp.97–124.

Wyss, H.M., 2016. Rheology of Soft Materials. In *Fluids, Colloids and Soft Materials: An Introduction to Soft Matter Physics*. Hoboken, NJ, USA: John Wiley & Sons, Inc, pp. 149–164.

Xu, H., Cao, W. & Zhang, X., 2013. Selenium-Containing Polymers: Promising Biomaterials for Controlled Release and Enzyme Mimics. *Accounts of Chemical Research*, 46(7), pp.1647–1658.

Xu, J. et al., 2013. Future of the particle replication in nonwetting templates (PRINT) technology. *Angewandte Chemie - International Edition*, 52(26),

pp.6580–6589.

Yan, C. & Pochan, D.J., 2010. Rheological properties of peptide-based hydrogels for biomedical and other applications. *Chemical Society Reviews*, 39(9), pp.3528–3540.

Yang, G.-Y. et al., 2017. Oral Administration of Lactobacillus rhamnosus GG Ameliorates Salmonella Infantis-Induced Inflammation in a Pig Model via Activation of the IL-22BP/IL-22/STAT3 Pathway. *Frontiers in Cellular and Infection Microbiology*, 7, p.323.

Yang, H. et al., 2016. Smart pH/Redox Dual-Responsive Nanogels for On-Demand Intracellular Anticancer Drug Release. *ACS Applied Materials & Interfaces*, 8(12), pp.7729–7738.

Yau, T.W. et al., 2012. Cytoskeletal rearrangements in human red blood cells induced by snake venoms: light microscopy of shapes and NMR studies of membrane function. *Cell Biology International*, 36(1), pp.87–97.

Yu, A.-Q. & Li, L., 2016. The Potential Role of Probiotics in Cancer Prevention and Treatment. *Nutrition and Cancer*, 68(4), pp.535–544.

Yudianti, R. et al., 2009. DSC analysis on water state of salvia hydrogels. *Macromolecular Research*, 17(12), pp.1015–1020.

Yue, Z., Eccleston, M.E. & Slater, N.K.H., 2005a. Modulation of the pH-responsive properties of poly(L-lysine iso-phthalamide) grafted with a poly(ethylene glycol) analogue. *Biomaterials*, 26(32), pp.6357–6366.

Yue, Z., Eccleston, M.E. & Slater, N.K.H., 2005b. PEGylation and aqueous solution behaviour of pH responsive poly(l-lysine iso-phthalamide). *Polymer*, 46(8), pp.2497–2505.

Yusa, S. et al., 2009. Preparation and Characterization of a pH-Responsive Nanogel Based on a Photo-Cross-Linked Micelle Formed From Block Copolymers with Controlled Structure. *Langmuir*, 25(9), pp.5258–5265.

Zeng, J. et al., 2013. Organoselenium compounds: development of a universal “living” free radical polymerization mediator. *Polymer Chemistry*, 4(12), pp.3453–3457.

Zhang, A. et al., 2016. Suppressed blinking behavior of CdSe/CdS QDs by polymer coating. *Nanoscale*, 8(9), pp.5006–5014.

Zhang, D., Wang, J. & Xu, D., 2016. Cell-penetrating peptides as noninvasive transmembrane vectors for the development of novel multifunctional drug-delivery systems. *Journal of Controlled Release*, 229, pp.130–139.

Zhang, H., Wang, G. & Yang, H., 2011. Drug delivery systems for differential release in combination therapy. *Expert Opinion on Drug Delivery*, 8(2), pp.171–190.

Zhang, J. et al., 2012. pH and Reduction Dual-Bioresponsive Polymersomes for Efficient Intracellular Protein Delivery. *Langmuir*, 28(4), pp.2056–2065.

Zhang, R.X. et al., 2017. Design of nanocarriers for nanoscale drug delivery to enhance cancer treatment using hybrid polymer and lipid building blocks. *Nanoscale*, 9(4), pp.1334–1355.

Zhu, Q. et al., 2009. Role of Branching Architecture on the Glass Transition of Hyperbranched Polyethers. *The Journal of Physical Chemistry B*, 113(17), pp.5777–5780.

Zorko, M. & Langel, Ü., 2005. Cell-penetrating peptides: mechanism and kinetics of cargo delivery. *Advanced Drug Delivery Reviews*, 57(4),

pp.529–545.

Appendix A Supplement Figures and Tables

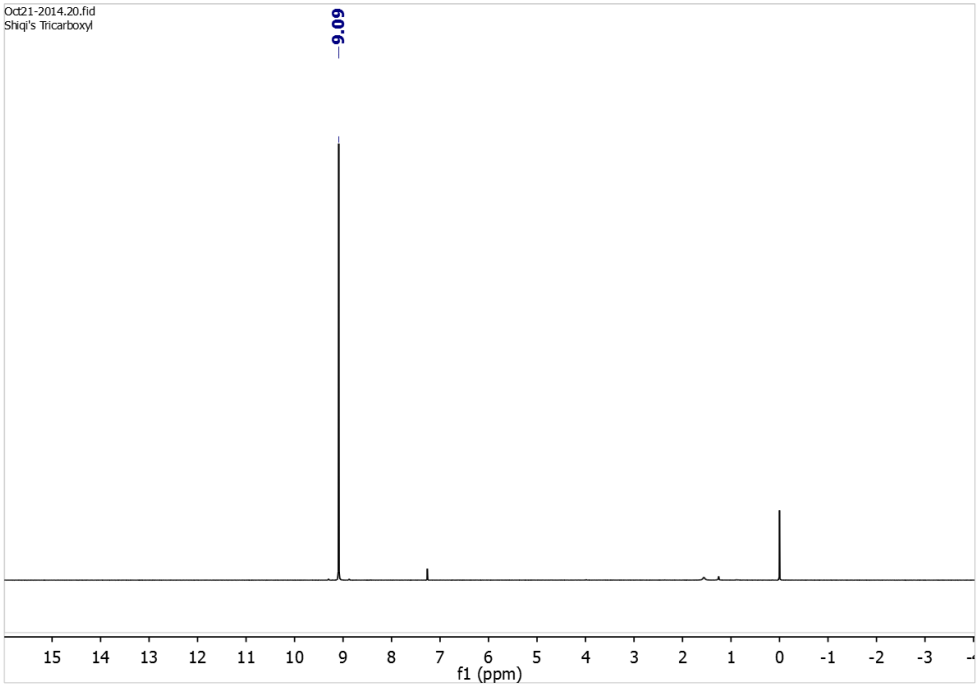

Figure S1 ^{1}H-NMR spectrum of 1,3,5-benzenetricarboxylic acid chloride (in $CDCl_3$).

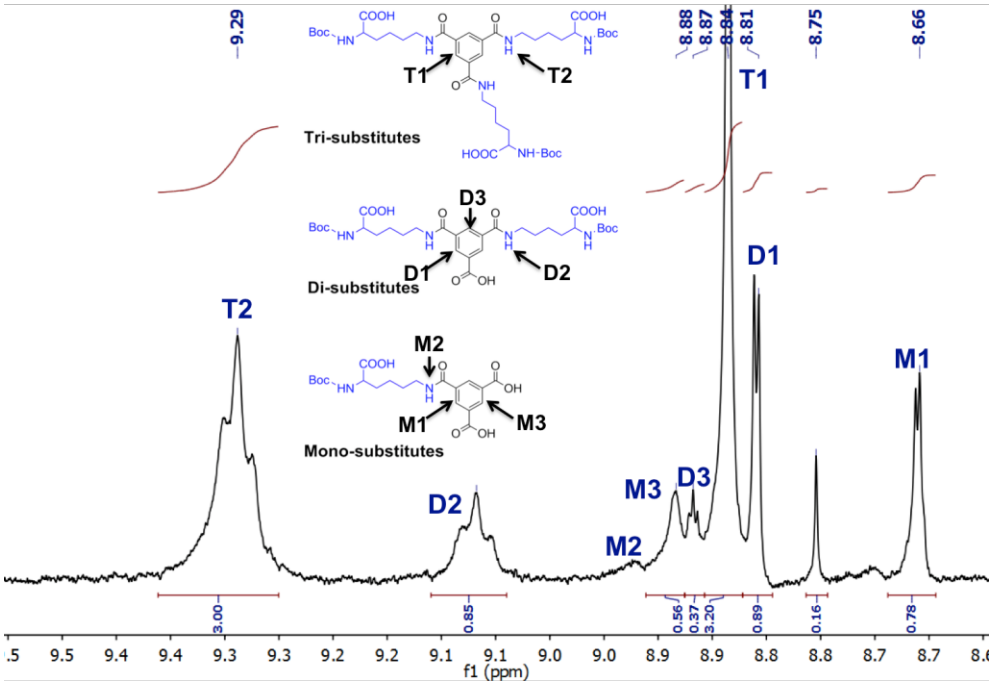

Figure S2 ^{1}H-NMR spectrum of unpurified products of model reaction 3 in DMSO-d_6.

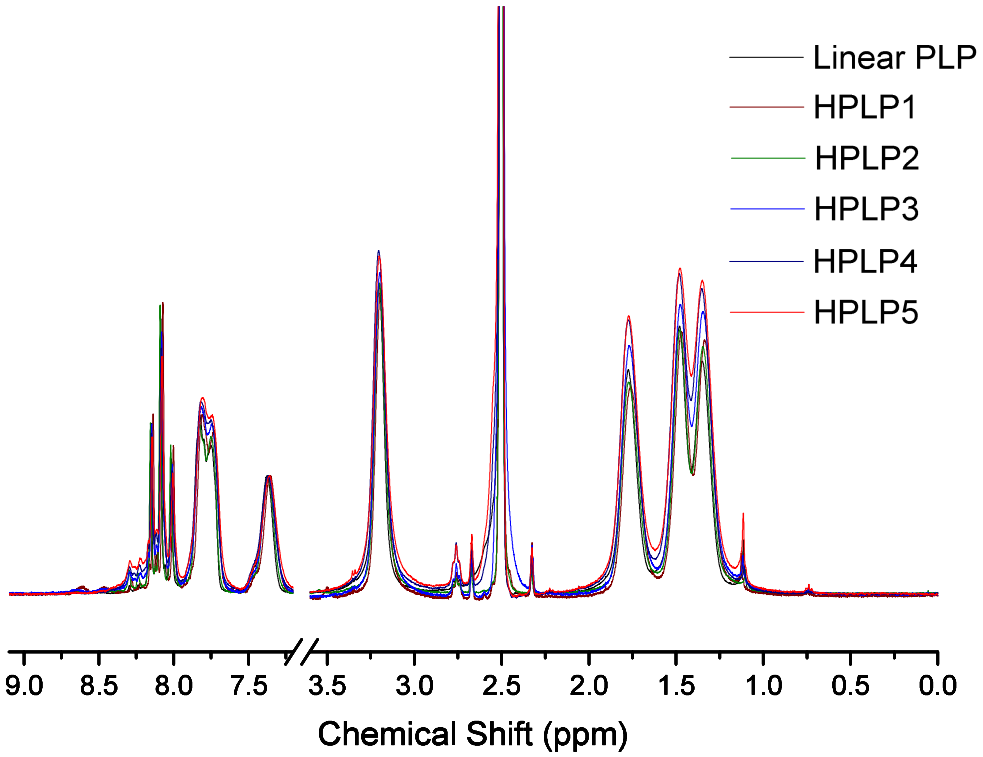

Figure S3 ^{1}H-NMR spectrum of HPLPs and linear PLP in DMSO-d_6.

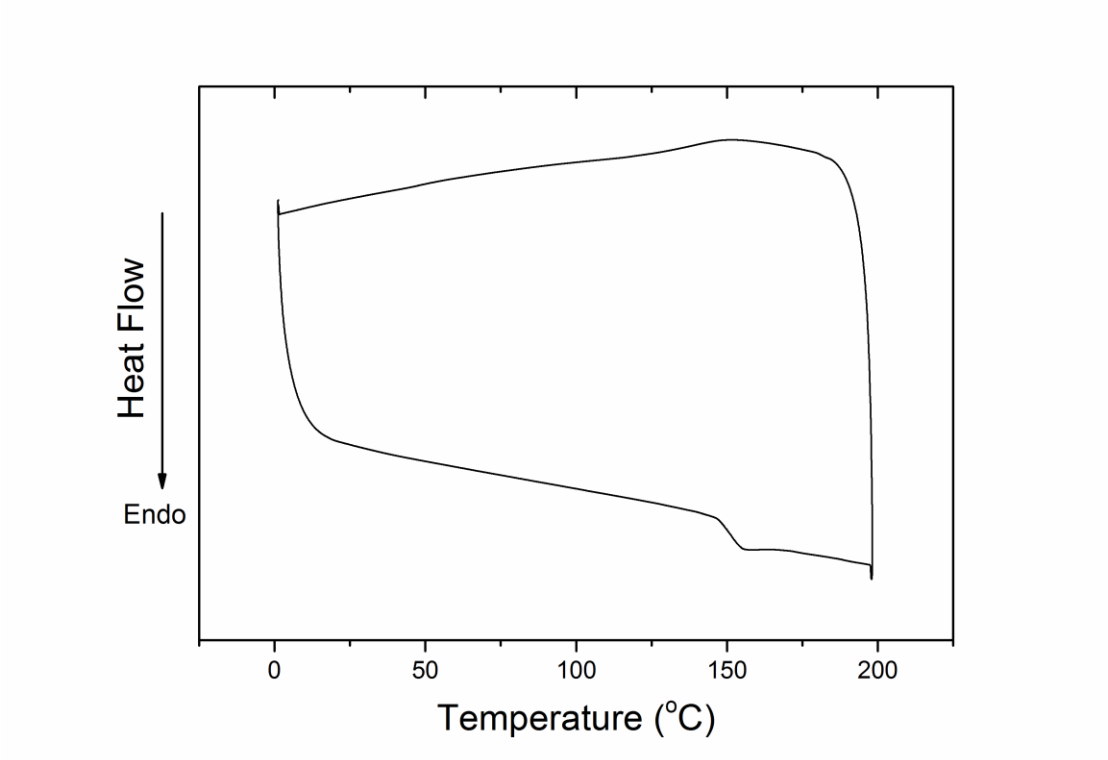

Figure S4 DSC curve of PLP in a heating-cooling cycle.

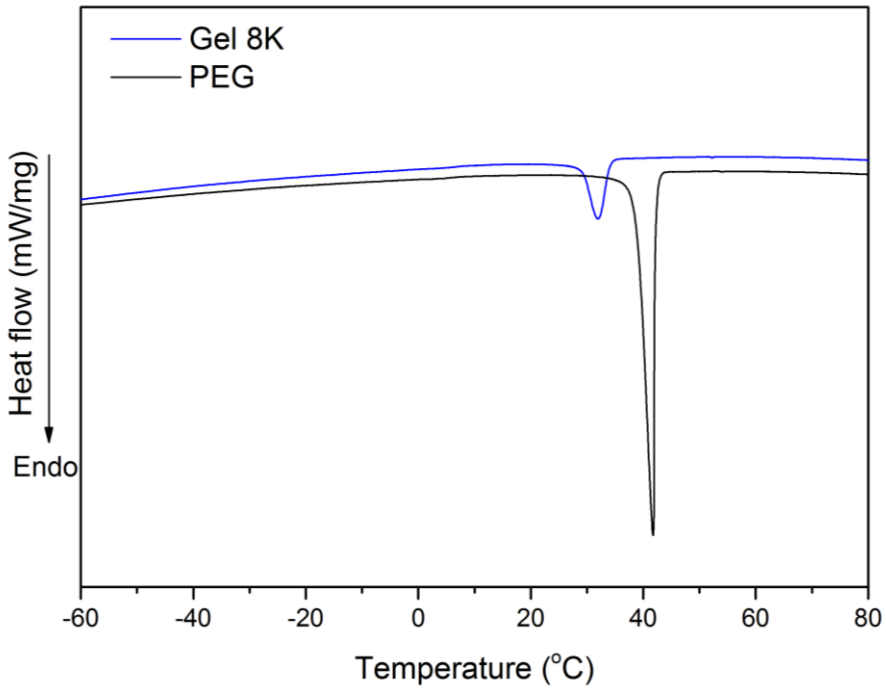

Figure S5 DSC of lyophilised Gel 8K and PEG 8K.

Table S1 Formulations of nanogels. In A, B, C series, the polymer concentration in water was kept the same (0.2, 0.1, 0.05 mg mL^{-1} respectively). In D series, the Water: DMF ratio was kept the same (125). In E series, the polymer concentration in DMF was kept the same (25 mg mL^{-1}).

No.	DMF volume (μL)	Water volume (mL)	Polymer (mg)	Ratio (Water:DMF, v/v)	Polymer concentration in DMF (mg mL^{-1})	Polymer concentration in water (mg mL^{-1})	Size (nm)	PDI
A1	4	5	1	1250	250	0.2	NA	NA
A2*	10	5	1	500	100	0.2	204.0 ± 3.4	0.14 ± 0.01
A3	20	5	1	250	50	0.2	143.7 ± 2.3	0.10 ± 0.04
A4 (D2,E4)	40	5	1	125	25	0.2	103.0 ± 2.9	0.10 ± 0.02
A5	100	5	1	50	10	0.2	68.8 ± 1.0	0.12 ± 0.02
B1*	4	5	0.5	1250	125	0.1	259.2 ± 3.3	0.24 ± 0.09
B2	10	5	0.5	500	50	0.1	151.4 ± 3.7	0.12 ± 0.04
B3 (E3)	40	10	1	250	25	0.1	81.2 ± 2.9	0.18 ± 0.04
B4 (D3)	40	5	0.5	125	12.5	0.1	55.7 ± 0.7	0.10 ± 0.03
C1	4	5	0.25	1250	62.5	0.05	143.0 ± 1.8	0.09 ± 0.03
C2 (E2)	40	20	1	500	25	0.05	72.8 ± 1.2	0.19 ± 0.00
C3	20	5	0.25	250	12.5	0.05	60.4 ± 1.5	0.10 ± 0.01
C4 (D4)	40	5	0.25	125	6.25	0.05	54.6 ± 1.2	0.18 ± 0.01
D1	40	5	5	125	125	1	NA	NA

D2 (A4,E4)	40	5	1	125	25	0.2	103.0 ± 2.9	0.10 ± 0.02
D3 (B4)	40	5	0.5	125	12.5	0.1	55.7 ± 0.7	0.10 ± 0.03
D4 (C4)	40	5	0.25	125	6.25	0.05	54.6 ± 1.2	0.18 ± 0.01
D5	40	5	0.1	125	2.5	0.02	NA	NA
D6	40	5	0.05	125	1.25	0.01	NA	NA
E1	40	50	1	1250	25	0.02	NA	NA
E2 (C2)	40	20	1	500	25	0.05	72.8 ± 1.2	0.19 ± 0.00
E3 (B3)	40	10	1	250	25	0.1	81.2 ± 2.9	0.18 ± 0.04
E4 (A4,D2)	40	5	1	125	25	0.2	103.0 ± 2.9	0.10 ± 0.02
E5	40	2	1	50	25	0.5	183.9 ± 7.2	0.15 ± 0.02

* The quality test suggested that there were large particles in the sample. NA means the measured data failed to pass the Malvern Zetasizer internal quality test.

Appendix B Permissions summary table for third party copyright works

Name of work	Source of work	Copyright holder and contact	Permission requested date	I have permission Yes / No	Permission note
Figure 1.1 Multiple biological barriers to intravenous delivery of tumour-targeting drugs.	Synthetic polypeptides: from polymer design to supramolecular assembly and biomedical application, Chem. Soc. Rev., 2017,46, 6570-6599	© 2017 The Royal Society of Chemistry	05/01/2018	Yes	Rightslink® by Copyright Clearance Centre License Number 4262770563932
Figure 1.2 Biological barriers at different scales in oral drug delivery. Figure 4.1 Schematic showing oral drug delivery hydrogels and their controlled-release behaviour.	Cover picture, Macromol. Biosci., 2016, 16, 1251	© 2016 Wiley	03/01/2018	Yes	Rightslink® by Copyright Clearance Centre License Number 4261700439067
Figure 1.3 Design of pH-responsive drug delivery systems.	pH-Responsive nanoparticles for drug delivery, Mol. Pharm. 2010, 7, 1913	© 2010 ACS Publications	05/01/2018	Yes	Rightslink® by Copyright Clearance Centre

Figure 1.10 Schematic representation of the CendR trans-tissue transport pathway.	Tumor penetrating peptides for improved drug delivery, Adv. Drug Deliv. Rev. 2017, 3,110	© 2017 Elsevier B.V.	04/01/2018	Yes	Rightslink® by Copyright Clearance Centre License Number 4261730006379
Figure 1.11 CPP internalization pathways.	Cell-penetrating peptides: breaking through to the other side, Trends Mol. Med. 2012, 18, 385.	© 2012 Elsevier B.V.	04/01/2018	Yes	Rightslink® by Copyright Clearance Centre License Number 4261730685976
Figure 1.12 (a) Schematic illustration of a redox-responsive colon targeting system utilizing PEGylated CPP.	Activatable cell penetrating peptide–peptide nucleic acid conjugate via reduction of azobenzene peg chains, J. Am. Chem. Soc. 2014, 136, 12868.	© 2014 ACS Publications	04/01/2018	Yes	Rightslink® by Copyright Clearance Centre
Figure 1.12 (b) TME enzyme-cleavable drug delivery system.	Cell-penetrating peptides as noninvasive transmembrane vectors for the development of novel multifunctional drug delivery systems, J. Control. Release 2016, 229, 130	Open access	NA	Yes	Open access under the Creative Common License (CC BY-NC-ND 4.0)

Figure 1.13 (a) Guanidine-containing polyacrylates and copolymers synthesised from RAFT polymerization.	Guanidine-containing methacrylamide (co)polymers via aRAFT: toward a cell-penetrating peptide mimic, ACS Macro Lett. 2012, 1, 100	© 2012 ACS Publications	04/01/2018	Yes	Rightslink® by Copyright Clearance Centre
Figure 1.13 (b) Polyarginine derivatives synthesised by NCA polymerization.	Synthetic polypeptides: from polymer design to supramolecular assembly and biomedical application, Chem. Soc. Rev. 2017, 46, 6570	© 2017 The Royal Society of Chemistry	04/01/2018	Yes	Rightslink® by Copyright Clearance Centre License Number 4262200173634
Figure 1.14 Schematic illustration of zwitterionic and cationic micelles and their cytotoxicity.	Zwitterionic guanidine-based oligomers mimicking cell-penetrating peptides as a nontoxic alternative to cationic polymers to enhance the cellular uptake of micelles, Biomacromolecules 2012, 13, 3418	© 2012 ACS Publications	04/01/2018	Yes	Rightslink® by Copyright Clearance Centre
Figure 1.15 Chemical structures of anionic amphiphilic membrane-lytic polymers.	Polymer-induced transient pores in lipid membranes, Angew. Chemie - Int. Ed. 2008, 47, 3092	© 2008 Wiley	04/01/2018	Yes	Rightslink® by Copyright Clearance Centre License Number 4262210531066

Figure 1.17 (a) Concentration-dependent relative haemolysis by PLP, PV-75, PL-75, PP-75 at pH 6.5. (b) pH-induced haemolysis by PLP, PV-75, PL-75,PP-75 at 0.025 mg/ml.	The role of hydrophobic amino acid grafts in the enhancement of membrane-disruptive activity of pH-responsive pseudo-peptides, Biomaterials 2009, 30, 1954	© 2012 Elsevier B.V.	04/01/2018	Yes	Rightslink® by Copyright Clearance Centre License Number 4262220165159
Figure 3.5 (a) ^{1}H NMR spectrum of HPLP5 with proton designations. (b) Zoomed-in ^{1}H NMR spectra of HPLP1, HPLP3 and HPLP5 between 6.9 and 9.1 ppm. Table 3-2 The amount of crosslinkers in the HPLPs characterised by H-NMR. Table 3-3 The molecular weights and polydispersities of the HPLPs. Figure 3.6 FTIR spectra of HPLPs. Figure 3.7 DSC curves of HPLP1, HPLP3 and HPLP5. Figure 3.9 (a) pH-dependent transmittance of different HPLPs at 1.0 mg mL^{-1} Figure 3.11 (a) Variations in I_{338}/I_{333} of HPLP1, HPLP3 and HPLP5 at 0.1 mg	pH-Responsive, lysine-based, hyperbranched polymers mimicking endosomolytic cell-penetrating peptides for efficient intracellular delivery, Chem. Mater. 2017, 29, 5806	© 2017 ACS Publications	03/01/2018	Yes	Rightslink® by Copyright Clearance Centre License is granted to use the full article as the author's original work

mL^{-1}. (b) Variations in I_{338}/I_{333} of HPLP1, HPLP3 and HPLP5 at 2 mg mL^{-1}. Figure 3.12 CAC determination for HPLP1 and HPLP5 at pH 7.4. Figure 3.14 Hydrodynamic particle size distributions of (a) HPLP1 and (b) HPLP5 at 1 mg mL^{-1} in buffers at pH 4.6 (red) and pH 7.4 (black). Figure 3.15 TEM images of HPLP5 at (a) pH 4.6 and (b) pH 7.4. Figure 3.22. (a) Concentration-dependent relative haemolysis of sheep RBCs in the presence of different HPLPs at pH 5.0. (b) pH-dependent relative haemolysis of sheep RBCs in the presence of different HPLPs at 2 mg mL^{-1}. Figure 3.23 (b) pH-dependent relative haemolysis of sheep RBCs in the presence of 5 □g mL^{-1} melittin in 150mM NaCl. Figure 3.25 Confocal microscopy images of sheep RBCs treated with different sized FITC-dextran and Texas Red® hydrazide at pH 5.0 in the	pH-Responsive, lysine-based, hyperbranched polymers mimicking endosomolytic cell-penetrating peptides for efficient intracellular delivery, Chem. Mater. 2017, 29, 5806	© 2017 ACS Publications	03/01/2018	Yes	Rightslink® by Copyright Clearance Centre License is granted to use the full article as the author's original work

presence or absence of 1 mg mL^{-1} HPLP5. Figure 3.26 Confocal microscopy images of sheep RBCs treated with 10 μM FITC-dextran 10K, 1.5 μM Texas Red® hydrazide and 1 mg mL^{-1} HPLP5 at pH 4.5 and pH 7.4. Figure 3.27 Time-lapse confocal microscopy images of sheep RBCs treated with 10 μM FITC-dextran 10K, 1.5 μM Texas Red® hydrazide and 1 mg mL^{-1} HPLP5 at pH 5.0. Figure 3.28 Concentration-dependent relative viabilities of HeLa cells treated with different HPLPs for 24 hours as determined by alamarBlue® assay. Figure 3.29 (a) Concentration-dependent relative viabilities of HeLa cells treated with melittin for 24 hours as determined by alamarBlue® assay. Figure 3.30 Confocal microscopy images of HeLa cells showing the intracellular distribution of the endocytosed calcein.	pH-Responsive, lysine-based, hyperbranched polymers mimicking endosomolytic cell-penetrating peptides for efficient intracellular delivery, Chem. Mater. 2017, 29, 5806	© 2017 ACS Publications	03/01/2018	Yes	Rightslink® by Copyright Clearance Centre License is granted to use the full article as the author's original work

Figure 3.32 Summary scheme of hyperbranched polymers facilitating pH-responsive membrane penetration and endosomal escape.	pH-Responsive, lysine-based, hyperbranched polymers mimicking endosomolytic cell-penetrating peptides for efficient intracellular delivery, Chem. Mater. 2017, 29, 5806	© 2017 ACS Publications	03/01/2018	Yes	Rightslink® by Copyright Clearance Centre License is granted to use the full article as the author's original work
Figure 4.9 SEM images of Gel 0.1 (left), Gel 0.2 (middle), Gel 0.5 (right). Figure 4.12 The swelling ratios of hydrogels. Figure 4.14 The variations of G' and G'' against angular frequency in the frequency sweep of Gel 0.1 at pH 3.0 and pH 7.4 respectively.	Development of novel hydrogels for efficient drug delivery and controlled release, Master Dissertation, 2016	Open access	NA	Yes	Open access under the Creative Common License (CC BY-NC-ND 4.0)
Table 4-2 CDE-crosslinked hydrogel formulations. Figure 4.21 (a) the XPS spectrum of Gel 2; (b) the zoomed-in figure of the sulfur peak. .	Amino acid based hydrogels with dual responsiveness for oral drug delivery, Macromol. Biosci. 2016, 16, 1258.	© 2016 Wiley	03/01/2018	Yes	Rightslink® by Copyright Clearance Centre License Number 4261680833498

Table 4-3 Atomistic compositions of each hydrogel by XPS and the crosslinking ratio Figure 4.22 SEM images of different hydrogels. (a) Gel 4, (b) Gel 3, (c) Gel 2, (d) Gel 1. Figure 4.23 pH-responsive swelling behaviour of hydrogels. Figure 4.25 Frequency sweep of Gel 2 at pH 3.0, pH 7.4 and pH 7.4 with the addition of DTT. Figure 4.26 Cumulative release of fluorescein at pH 3.0 and 7.4 after 24 h of incubation. Figure 4.27 Released kinetics of Gel 2 at pH 3.0, pH 5.0, pH 7.4, and pH 7.4 with 0.1 M DTT. Figure 4.29 Cytotoxicity of gels evaluated by alamarBlue® assay on Hela cells.	Amino acid based hydrogels with dual responsiveness for oral drug delivery, Macromol. Biosci. 2016, 16, 1258.	© 2016 Wiley	03/01/2018	Yes	Rightslink® by Copyright Clearance Centre License Number 4261680833498 License is granted to use the full article as the author's original work

Figure 5.8 Nile red release kinetics in bio-relevant buffers, including FaSSIF, FaSSGF and SGF with higher biosurfactant contents.	Model drug release profile of a pH-responsive nanocarrier, Master Dissertation, 2017	Open access	NA	Yes	Open access under the Creative Common License (CC BY-NC-ND 4.0)
Figure 5.12 Surface EDC-coupling reaction scheme. Intermediates and side products	Semiquantitative study of the EDC/NHS activation of acid terminal groups at modified porous silicon surfaces, Langmuir 2010, 26, 809	© 2010 ACS Publications	03/01/2018	Yes	Rightslink® by Copyright Clearance Centre

Imperial College London

Appendix C Bio1 Form of Haemolysis

FORM BIO1

PROJECT REGISTRATION AND RISK ASSESSMENT FOR WORK INVOLVING BIOLOGICAL MATERIAL

For Safety Dept use only	Project Assessment I.D.: **TIIC-2586**	If updated, date of first consent:	
	Consent date for this version: **23.04.2014**	CL with derogation ☐	GM Class

PLEASE READ THIS CAREFULLY

This form acts to register projects involving the use of Biological Agents and / or Genetically Modified Micro-Organisms, or of materials (such as cells and tissues) that may be contaminated with these agents. It also aids in assessing the hazards and risks associated with the project as well as in identifying those at risk and the measures necessary for preventing, or controlling these risks. Please ensure that sufficient detail is provided when completing this form and that the relevant written protocols are referenced where required. Note that the written protocols (e.g. Code of Practice (CoP) or Standard Operating Procedures (SOPs)) containing details of the working procedures must accompany these risk assessments at submission for work requiring Containment Level 2 or above. Once completed and approved, all risk assessments plus the protocols must be held together and supplied to all those working within this project, or who may otherwise be at risk from exposure.

Any queries during the preparation of these documents should be directed to your Safety Officer or directly to the BioSafety Team before submission. This form plus protocols should be reviewed in the first instance by your FSM/CSM and then must be submitted to biosafety@imperial.ac.uk

The work described within this Project Registration must not commence until the Principal Investigator has received a completed Biological Project Certificate.

Any changes to the work, or the persons involved, must be notified via the above email address. All changes requested must be incorporated within an amended version of this form as well as within the Code of Practice plus details of what has been changed recorded within the risk assessment change control form (Form C).

Principal Investigator	
Name: **Dr. Rongjun Chen**	CID: Other employee no:
Department / Section: **Chemical Engineering**	
Faculty: **Lecturer**	

Details of person conducting the risk assessment	
Name: **Shiqi Wang**	CID: **00839434** Other employee no:
Department / Section: **Chemical Engineering**	
Faculty:	

The activity
Title: **Haemolysis Assay**

Change history *(list all previous versions of this risk assessment)*	
Date	Risk Assessment ID and version no.
N/A	**N/A**

The following declaration must be completed by the PI responsible for this project

- ☒ All information contained in this form is accurate and comprehensive.
- ☒ All workers involved will be instructed that their work must remain within the boundaries of this Project Registration.
- ☒ It is understood that this Registration does not comprise operating protocols or all risk assessment required for specific tasks. Such written protocols and risk assessments of individual tasks is still required. Where these must be submitted with this form is indicated within the relevant sections.
- ☒ All changes to the work covered by this form will be reassessed and the changes submitted to biosafety@imperial.ac.uk before those changes are made to the work.

☒ All workers have been given, or will be given before they become involved, this risk assessment, adequate training and where necessary, their competency assessed and recorded.

☒ All workers have, or will be before their involvement begins, enrolled with Occupational Health for health clearance where necessary.

☒ It is understood that this risk assessment shall not be transferred to a third party without the PI named in this form either taking responsibility for the new activities, or ensuring that a new proposal is submitted to Safety Department.

GUIDANCE ON THE COLOUR SCHEME FOR THIS FORM:				
Blue fill = mandatory for all work	No fill = for all work above CL2 only	Pink fill = tissues, cells, etc specific	Green fill - non-GM biological agents specific	Orange fill – GMM specific

1. INTRODUCTION

This section must be completed in all cases

1.1 Background and aim of the project	**To assess the membrane-disruptive activity of polymers, liposomes, nanoparticles or hydrogels on red blood cells.**
1.2 Description of the experimental procedures	**Buffer solutions in the pH range 4-7.4 will be prepared.** **Red blood cells (RBCs) will be centrifuged and washed multiple times to prepare RBC stock suspension.** **Polymers and liposomes will be left in buffered solutions for 48 hours, then certain amounts of RBC suspension will be added to the solutions at certain concentrations.** **The solutions will be incubated in a water bath for 1 hour, then the UV/Vis absorabance will be measured.**
1.3 Where will this work be carried out? List all areas to be used e.g. the main lab, CBS, shared incubator rooms, shared storage facilities	Rooms or area(s): **ACEX 319, Bone 433** Building(s): **Bone Building, ACE Extension Building** Campus: **South Kensington**

A brief background to the project provides the reviewer a better understanding of the aims of the work. For Q1.2, the author is encouraged to cover as much of their activities with a particular agent or material as possible within this form. The intention of this Project Registration is primarily to agree the scope of the proposed works, and not to focus on the risk assessment of individual procedures. Note however that risk assessment of specific procedures remains essential and must be carried out.

2. NATURE OF WORK & ASIC HAZARD IDENTIFICATION

If this material is to be used then all relevant parts of this section must be completed

TISSUES, CELLS, BODY FLUIDS OR EXCRETA

2.1 If human or animal tissues, cells, body fluids or excreta will NOT be used then hatch here ☐ and proceed to Q2.9

2.2 List all the tissues, cells, body fluids or excreta to be used (species, type, where obtained)	**Sheep's red blood cells, defibrinated, TCS Biosciences** *Details on the source of the material must be included*
2.3 Describe what infectious agents this material has been screened for	**Viruses and pathogens**

2.4 Will any clinical history or veterinary screening (if relevant) be provided?	Yes ☐ No ☒		N/R ☐
If yes, detail what this will include:			
If yes, will a policy of rejection of samples from diseased donors be adopted? Explain:			
If yes and for human material, how will the information be disseminated in the course of the project?			N/R ☐
If yes and for human material, will this information be anonomised?	Yes ☐ No ☐		N/R ☐
2.5 What is the likelihood of infection of any of this material? Please consider the worse case in this answer if multiple tissues, cells, etc are being used.	Medium risk ☐ High risk ☐ If medium or high risk of infection go to next question		None ☐ Low risk ☒ If none or low risk proceed to Question 2.10
2.6 If medium or high risk of infection name and classify the biological agents this material could be infected with	Tissue, cell, fluids or excreta	Name of agent	ACDP/defra classification
2.7 Describe the type and severity of the disease that can be caused to humans or animals by each of the agents that could be present			
2.8 Do any of the materials listed require a licence or a permit before work commences?	For example, IAPPO1, SAPO, defra, or FERA licenses? If yes, please list these and attach them with this form.		

BIOLOGICAL AGENTS

2.9 If non-Genetically-Modified Biological Agents will NOT be used then hatch here ☒ and proceed to Q2.13

2.10 List the non-GM biological agents to be used	Name of agent	Strain(s)	ACDP/defra classification

2.11 Describe the type and severity of the disease that can be caused to humans, animals or plants by each of the agents, and if relevant, the particular strains in use	
2.12 Do any of the organisms listed require a licence or a permit before work commences?	For example, IAPPO1, SAPO, defra, or FERA licenses? If yes, please list these and attach them with this form.

GENETICALLY MODIFIED MICRO-ORGANISMS

2.13 If Genetically-Modified Micro-Organisms (GMMs) will NOT be used then hatch here ☒ and proceed to Question 3.1

2.14 Provide an overview of the different types of GMM that will be constructed. Please ensure that the scope and boundaries of the work are made clear	

2.15	List all recipient species and strains to be used, their ACDP or defra classification	
2.16	List of vector systems to be used and their particular functional properties	
2.17	List the names and functional properties of all altered genes	
2.18	Identify the most hazardous GMM(s) to be constructed giving consideration both to human health and the environment	

3. DECLARATION

This section must be completed in all cases

3.1 Are you confident that any non-GM organism, tissue, cell, blood, body fluid or any component of any GMM covered by this assessment cannot potentially pose a threat to humans or the environment?	Yes ☒ *Hatch here if you believe that this project comprises work requiring only **Containment Level 1** proceed to Q5.1 of this form*	No ☐ *Hatch here if you believe that **Containment Level 2 (or higher**) is required and then answer Q3.2 and proceed to Q4.1 of this form*
3.2 Do any of the materials contain pathogens or toxins covered by the Anti-Terrorism (Crime and Security Act)?	Yes ☐ No ☒ A list of the agents and toxins is available at the Safety Dept website. If yes, then Section 4 must still be completed even if only Containment Level 1.	

PLEASE READ THIS CAREFULLY

You must only answer 'YES' to Q3.1 if you believe that you have sufficient information to classify the project as requiring only Containment Level 1, as defined in the Genetically Modified Organisms (Contained Use) Regulations or by COSHH. In order to do this you must be confident that even in the event of a total breach of containment all the biological agents, genetically modified organisms or cultured material would be of no or of negligible risk to human health or to the environment.

For ALL projects requiring Containment Level 2, or higher, or those covered by the Anti-Terrorism (Crime and Security) Act, submissions of this form must be accompanied by a Code of Practice, or at the very least, all the SOPs relevant to the work.

4. FURTHER ASSESSMENT

All relevant parts of this section must be completed if you answered 'No' to Q3.1

TISSUES, CELLS, BODY FLUIDS OR EXCRETA

4.1	If human or animal tissues, cells, body fluids or excreta will NOT be used then hatch here ☐ and proceed to Q4.8		
4.2	Will any culturing of the material described in Q2.2 take place? If yes, describe which cell(s) will be cultured and under what conditions.	Yes ☐	No ☐
4.3	If culturing, could HIV permissive cells be present? If yes, describe the cells and for how long these cultures will be allowed to grow.	Yes ☐	No ☐ N/R ☐
4.4	If culturing, what is the maximum volume of culture grown?	Per flask:	Number of flasks: N/R ☐
4.5	Will the tissues, cells, body fluids or excreta be manipulated in any way that could result in the concentration of	Yes ☐	No ☐

	any adventitious biological agent present? If yes, explain.		
4.6	What will the most hazardous procedure involving the use of this material be?		
4.7	Will any of the fluids, tissues or cells be donated by you or your colleagues?	Yes ☐	No ☐
	If yes, detail who will provide these		N/R ☐
	If yes, explain the special risks associated		N/R ☐
	If yes, provide justification for not using material from another safer source e.g. National Blood Service		N/R ☐
	If yes, how will confidentiality be assured?		N/R ☐
	If yes, has written consent been obtained from the donor?		N/R ☐
	If yes, has Ethics Committee approval been obtained?	Yes ☐	No ☐

BIOLOGICAL AGENTS

4.8 If non-Genetically-Modified Biological Agents will NOT be used then hatch here ☐ and proceed to Q4.14

4.9	Describe ALL the route(s) of infection (relevant to the laboratory setting) and the minimum infectious dose(s), if known	Name of agent	Route(s) of infection	Minimum infectious dose

4.10	What is the highest concentration and volume of agent(s) to be worked with?	Per experiment: Total stored:
4.11	Are there any known drug resistances amongst the strains to be used? If yes, explain what these are and the consequences	
4.12	What forms of the agent will be used e.g. spores, vegetative forms and are there any issues over the robustness of these particular forms e.g. resistance to disinfectants or increased stability on dry surfaces	
4.13	What will the most hazardous procedure involving the use of this material be?	

GENETICALLY MODIFIED MICRO-ORGANISMS

4.14 If GMMs will NOT be used then hatch here ☐ and proceed to Q5

4.15	Identify the hazards to human health or to the environment of the recipient microorganism(s)	

4.16	Identify any of the hazards to human health or to the environment associated directly with the vector systems in use			
4.17	Identify all of the known or potential hazards associated with all the GMMs to be generated. It is important that the boundaries of this project are clearly explained here			
4.18	Describe the likelihood and consequences of the modifications being transferred to related microorganisms			
4.19	Identify the most hazardous GMM(s) to be constructed giving consideration both to human health and the environment			
4.20	Describe ALL the potential route(s) of infection (relevant to the laboratory setting) of the GMM(s)	Name of agent	Route(s) of infection	Minimum infectious dose
4.21	What is the highest concentration and volume of the GMM(s) to be worked with?	Per experiment:	Total stored:	

5. RISKS AND CONTROL MEASURES

All questions in this section must be answered and further details supplied when indicated

NOTE that a Code of Practice (CoP) or Standard Operating Procedure (SOP) reference must be provided for CL2 or higher work, or work covered by the Anti-Terrorism (Crime and Security) Act

Risk			If yes, how will this be controlled?	Reference for SOP, CoP other written protocol providing details on usage, training, decontamination, etc.
5.1	Might infectious droplets or aerosols be created, either deliberately or by accident?	Yes ☐ No ☒	For example, will a safety cabinet or any other form of Local Exhaust Ventilation be required? Are there any particular requirements for the room ventilation?	**N/A**
5.2	Will material be transported within the laboratory?	Yes ☒ No ☐	**Materials will be carried in contrained, water-proof trays.** For example, cultures being transported between the safety cabinet and the incubator must be double contained so as to prevent spillage if dropped	**N/A**
5.3	Will the material be transported locally on campus but outside of the laboratory?	Yes ☒ No ☐	**Materials will be carried in contained, water-proof, sealed containers.** For example, material transported from the primary laboratory to CBS must be double contained so as to prevent spillage if dropped, adequately labelled and no gloves must be worn outside of the laboratory	**N/A**
5.4	Will this material be shipped elsewhere in the UK or abroad?	Yes ☐	Provide details of material to be shipped and the packing instructions to be followed. For example, MTb cultures shipped as Category A infectious substance	**N/A**

		No ☒	in PI620 packaging. Further guidance is available on the Safety Dept website	
	5.5 Will this material be received from elsewhere?	Yes ☒ No ☐	**The material will be purchased and received from TC Biosciences in an appropriate package.** Provide details of material to be received, how this will be arranged and what steps will be taken to ensure that the material is correctly packaged. Further guidance is available on the Safety Dept website	**N/A**
	5.6 Will this material be stored?	Yes ☒ No ☐	**The material will be stored in the refrigerator in a sealed glass jar, separate from any other samples.** Provide details of how, where and in what this material will be stored. If stored in Liquid Nitrogen describe the additional precautions in place	**N/A**
	5.7 Will infectious material be centrifuged?	Yes ☒ No ☐	Will the primary containers be sealed? **Yes** Will sealed rotors or sealed buckets be used? **Yes, an eppendorf centrifuge will be used with the following ratings:** **LI-C, CI-C, SI-C** Include details on the protection factor afforded by the bio containment arrangements fitted to the centrifuge. This information is available from the manufacturer and in the operators instructions e.g. where release of micro-organisms is to be prevented, a centrifuge should be used which is classified LI-C, CI-B and SI-C or better. Where L is leaktightness, C is cleanability and S is sterilizability. Performance is graded A to C (C is best)	**Centrifuge - ARAF**
			Where will these rotors be opened? **In a secure position on the lab bench** For example, within a safety cabinet	**N/A**
			Describe the procedures in place to deal with leaks or spillages in the centrifuge or rotor **Add 70% ethanol or water to an spillage or leak, and then use towels to wipe down an spillage or leaks**	**N/A**
	5.8 Are biological samples to be cultured in an incubator?	Yes ☐ No ☒	What type of incubator (e.g. shaking or static shelf) is this and describe the measures to be used to prevent and contain any spillages	**N/A**
	5.9 Are sharps to be used at any stage during this activity?	Yes ☐ No ☒	Describe the sharps, justify their use and describe the precautions in place to protect the user and others from injury	**N/A**
	5.10 Are animals to be used as part of this project?	Yes ☐ No ☒	What procedures will be undertaken?	**N/A**
			Where will this aspect of the work be undertaken?	**N/A**

			Is shedding of biological agent or GMMs by the infected animals possible? If yes, detail routes of shedding, risk periods for such shedding and the additional precautions required to control exposure	**N/A**
			Who will perform the inoculations/exposure of the animals? What training will they have received and where will this be recorded	**N/A**
			Provide details on any additional training required for those handling these animals	**N/A**
			Provide details on any additional precautions necessary	**N/A**
	5.11 Will a fermenter be used to culture the pathogen	Yes ☐ No ☒	What size and type is this and are any supplementary containment measures required, for example, the use of a safety cabinet or spill tray?	**N/A**
			Where is this fermenter located and who is in charge of the area?	**N/A**
	5.12 Is there any stage within the experimental procedures when the infectious material is inactivated (other than for disposal)?	Yes ☐ No ☒	If yes, how will this be done and what will then happen to the material?	**N/A**
	5.13 Are any of the following to be used in conjunction with this project? If yes provide details and the SOP/CoP reference		Liquid Nitrogen ☐ Radioactive materials ☐ Carcinogens ☐ Toxins ☐ Lasers ☐ Fieldwork ☐ Lone working ☒	**N/A** **N/A** **N/A** **N/A** **N/A** **N/A** **N/A**

6. PPE & HYGIENCE

All questions in this section must be answered in all cases

NOTE that a Code of Practice (CoP) or Standard Operating Procedure (SOP) reference must be provided for CL2 or higher work, or work covered by the Anti-Terrorism (Crime and Security) Act

Control measure	Details	Reference for SOP, CoP other written protocol
6.1 When will gloves be worn?	**Always**	**N/A**
6.2 What type are these and where will they be stored?	**Purple nitrile gloves, stored on the lab bench**	**N/A**
6.3 When will laboratory coats be worn and what type are these?	**Always, long-sleeved, knee length laboratory designed coats**	**N/A**

	6.4 Where will the lab coats be stored and what are the arrangements for cleaning or disposal?	**On the back of the door, to be laundered by the Chemical Engineering departmental store every few weeks.**	**N/A**
	6.5 Is any other type of personal protective equipment to be used? If yes, provide details	**Laboratory goggles.**	**N/A**
	6.6 Describe the lab hygiene facilities	**Eye wash and sink**	**N/A**

7. WASTE

All questions in this section must be answered in all cases

NOTE that a Code of Practice (CoP) or Standard Operating Procedure (SOP) reference must be provided for CL2 or higher work, or work covered by the Anti-Terrorism (Crime and Security) Act

7.1 How will waste be treated prior to disposal?

(Note that all differently treated wastes must be included e.g. if some liquid is autoclaved, but others not, then describe both)	**Treatment prior to disposal**	**SOP/CoP/ protocol**
Liquid waste	**Dilute in deionized water and dispose of in the sink**	**N/A**
Solid waste	**Contaminated plastic will be placed in the biological waste bins, autoclaved, and disposed of with the Chemistry departmental biological waste.**	**N/A**
Other waste (specify): **N/A**	**N/A**	**N/A**

7.2 If waste is to be autoclaved confirm the following;

All cycles have been validated for the actual load types used	Yes ☒ No ☐	No SOP required but documentary evidence of this validation must be available
The successful completion of every load is checked prior to disposal?	Yes ☒ No ☐	**N/A**

7.3 How will liquid waste be disposed of?

To drain?	Yes ☒ No ☐	**N/A**
As solid waste?	Yes ☐ No ☒	
Other (specify)?	Yes ☐ No ☒	

7.4 How will solid waste be disposed of?

Categorisation	Colour code	Disposal method	SOP/CoP/ protocol
☐ Sharps	Yellow	Yellow sharps bin > autoclave sterilisation if known or potentially infected >clinical waste disposal (incineration)	
☐ Human body parts, organs including blood bags and blood preserves and excreta (unless identified as medium or high risk or known infected in Q2.5 of this assessment in which case they must be pre-treated before disposal)	Yellow	Yellow rigid one way sealed tissue bins > clinical waste disposal (incineration) * Human tissue waste must be placed in separate containers from non-human waste and labelled 'HTA waste'	
☐ Animal body carcasses or recognisable parts (unless identified as medium or high risk or known infected in Q2.5 of this assessment in which case they must be pre-treated before disposal)	Yellow	Yellow rigid one way sealed tissue bins > clinical waste disposal (incineration)	
☐ Potentially or known infected lab wastes (including sharps) of Hazard Group 2, GM Class 2, DEFRA Category 2 or higher, that have not been pre-treated before leaving site	Special case – contact Safety Department	This is not a route of preference and is subject to special requirements	
☒ Infected or potentially infected lab wastes that have been pre-treated before leaving site	Orange	Disinfection or sterilisation in the laboratory suite > orange clinical waste bags > clinical waste disposal (alternative treatment)	
☐ Infected or potentially infected animal or human body parts, organs or excreta that have been pre-treated before leaving site	Yellow	Disinfection or sterilisation in the laboratory suite >yellow one way sealed tissue bins > clinical waste disposal (incineration) * Human tissue waste must be placed in separate containers from non-human waste and labelled 'HTA waste'	
☐ Packaging material that has been used for the importation of animal products subject to Defra licenses	Yellow	yellow clinical waste bags > clinical waste disposal (incineration or alternative treatment as described in the licence	

8. MAINTENANCE

All questions in this section must be answered for all work at CL2 or higher, or work covered by the Anti-Terrorism (Crime and Security) Act. In all cases the SOP/CoP or protocol reference is required.

8.1 List the maintenance regimes for all the following lab equipment

	Maintenance frequency	Maintenance carried out by	SOP/CoP/ protocol	N/R
Centrifuge(s)	**Daily**	**Users**	**Centrifuge - ARAF** **Centrifuge - SOP**	☐
Safety cabinets				☒
Autoclaves	**As needed**	**Autoclave owners**		☐
Shaking incubators				☒
Other (specify)				☒

9. TRAINING

All questions in this section must be answered for all work at CL2 or higher, or work covered by the Anti-Terrorism (Crime and Security) Act. In all cases the SOP/CoP or protocol reference is required.

9.1 Confirm that training to all workers is providing in at least the following aspects of this work

	Training frequency	Training carried out by	Is competency assessed?	SOP/CoP/ protocol	N/R
Hazards associated with this work	**one-time**	**ChemEng Safety Departmen**	Yes ☒ No ☐	**N/A**	☐
Safe working practices as described in this risk assessment	**one-time**	**ChemEng Safety Departmen**	Yes ☒ No ☐	**N/A**	☐
Spillage response within the safety cabinet	**one-time**	**ChemEng Safety Departmen**	Yes ☒ No ☐	**N/A**	☐
Spillage response within the centrifuge	**one-time**	**Centrifuge manufacturer**	Yes ☒ No ☐	**N/A**	☐
Spillage response elsewhere	**one-time**	**ChemEng Safety Department**	Yes ☒ No ☐	**N/A**	☐
Post-exposure protocols	**one-time**	**ChemEng Safety Departmen**	Yes ☒ No ☐	**N/A**	☐

10. EEMERGEN CY PROCEDURES

All questions in this section must be answered for all work at CL2 or higher, or work covered by the Anti-Terrorism (Crime and Security) Act. In all cases the SOP/CoP or protocol reference is required.

10.1 Describe the procedures in place for dealing with spillage of infectious or potentially infectious material

	Procedure	SOP/CoP/ protocol	N/R
Within the safety cabinet			☒

	Within the centrifuge	**Wipe up with towels and deionized water**		☐
	Within the laboratory but outside of any primary control measure e.g. safety cabinet	**Wipe up with towels and deionized water**		☐
	Outside of the laboratory	**Wipe up with towels and deionized water**		☐
	10.2 Describe the procedures in place for an accidental exposure			
	Immediate action	**Wipe up with towels and deionized water**		☐
	When and to whom to report the incident	**N/A**		☐

11. ACCESS

All questions in this section must be answered for all work at CL2 or higher, or work covered by the Anti-Terrorism (Crime and Security) Act. In all cases the SOP/CoP or protocol reference is required.		
		SOP/CoP/ protocol
11.1 Is the lab(s) adequately separated from other areas (e.g. offices)	Yes ☒ No ☐ If no, explain:	
11.2 Is/are the lab(s) or other work areas shared with other users not involved in this project	Yes ☐ No ☒ If yes, explain who and what procedures are in place to control any risk to them:	
11.3 Describe the measures in place to ensure that the infectious material is secured	**Blood will be kept in sealed container away from other chemicals.**	
11.4 What access colour code do the rooms used have?	Red ☐ Amber ☐ Yellow ☐	

12. OCCUPATIONAL HEALTH

This section to be completed for work with biological agents or GMMs in Hazard Group 2 or higher and for work with unscreened human tissues ONLY This must be completed the Occupational Physician only but note that where pre-activity requirements are identified, it is the responsibility of the Principal Investigator to ensure that these are carried out for all individuals working on this project, before they actually start work THE PRINCIPAL INVESTIGATOR MUST ENSURE THAT THE INFORMATION DESCRIBED IN THIS SECTION IS UNDERSTOOD BY ALL THOSE THAT WORK ON THIS PROJECT	
12.1 Medical risk assessment	
12.2 Pre-activity requirements	
select one	*Details:*
select one	*Details:*
select one	*Details:*
12.3 Periodic health surveillance requirements	
12.4 Post exposure action	

	12.5 Antibiotic treatment or chemoprophylaxis	
	12.6 Additional notes or comments	

13. CONTAINMENT LEVEL

This section must be completed in all cases

13.1 Confirm what Containment Level can be assigned to each aspect or component of this project. If different aspects of this work merit different Containment Levels, then all must be listed

Project aspect	Where work will be carried out	Containment Level (as required under COSHH or GMO (Contained Use) Regs	With extra controls (list these, if relevant. If required seek advice from your DSO or the College BSO)	With derogation from certain controls (list these, if relevant. If required seek advice from your DSO or the College BSO)
Haemolysis Assay	Bone 433, ACEX 319	CL1	N/A	N/A

14. GM CLASS

This section must be completed for work with Genetically Modified Micro-organisms only

14.1 Confirm the class of all GMMs in use

Project aspect	GM Class

Imperial College London

Appendix D Bio1 Form of Cell Culture

FORM BIO1

PROJECT REGISTRATION AND RISK ASSESSMENT FOR WORK INVOLVING BIOLOGICAL MATERIAL

For Safety Dept use only	Project Assessment I.D.: **GMIC-5100**	If updated, date of first consent:	
	Consent date for this version:	CL with derogation ☐	GM Class

PLEASE READ THIS CAREFULLY

This form acts to register projects involving the use of Biological Agents and / or Genetically Modified Micro-Organisms, or of materials (such as cells and tissues) that may be contaminated with these agents. It also aids in assessing the hazards and risks associated with the project as well as in identifying those at risk and the measures necessary for preventing, or controlling these risks. Please ensure that sufficient detail is provided when completing this form and that the relevant written protocols are referenced where required. Note that the written protocols (e.g. Code of Practice (CoP) or Standard Operating Procedures (SOPs)) containing details of the working procedures must accompany these risk assessments at submission for work requiring Containment Level 2 or above. Once completed and approved, all risk assessments plus the protocols must be held together and supplied to all those working within this project, or who may otherwise be at risk from exposure.

Any queries during the preparation of these documents should be directed to your Safety Officer or directly to the BioSafety Team before submission. This form plus protocols should be reviewed in the first instance by your FSM/CSM and then must be submitted to biosafety@imperial.ac.uk

The work described within this Project Registration must not commence until the Principal Investigator has received a completed Biological Project Certificate.

Any changes to the work, or the persons involved, must be notified via the above email address. All changes requested must be incorporated within an amended version of this form as well as within the Code of Practice plus details of what has been changed recorded within the risk assessment change control form (Form C).

Principal Investigator	
Name: **Dr Rongjun Chen**	CID: **00621851** Other employee no:
Department / Section: **Chemical Engineering**	
Faculty: **Engineering**	

Details of person conducting the risk assessment	
Name: **Shiqi Wang**	CID: **00839434** Other employee no:
Department / Section: **Chemical Engineering**	
Faculty: **Engineering**	

The activity
Title: **Cell Culture**

Change history *(list all previous versions of this risk assessment)*	
Date	Risk Assessment ID and version no.
N/A	**N/A**

The following declaration must be completed by the PI responsible for this project

- ☒ All information contained in this form is accurate and comprehensive.
- ☒ All workers involved will be instructed that their work must remain within the boundaries of this Project Registration.
- ☒ It is understood that this Registration does not comprise operating protocols or all risk assessment required for specific tasks. Such written protocols and risk assessments of individual tasks is still required. Where these must be submitted with this form is indicated within the relevant sections.
- ☒ All changes to the work covered by this form will be reassessed and the changes submitted to biosafety@imperial.ac.uk before those changes are made to the work.
- ☒ All workers have been given, or will be given before they become involved, this risk assessment, adequate training and where necessary, their competency assessed and recorded.

☒ All workers have, or will be before their involvement begins, enrolled with Occupational Health for health clearance where necessary.

☒ It is understood that this risk assessment shall not be transferred to a third party without the PI named in this form either taking responsibility for the new activities, or ensuring that a new proposal is submitted to Safety Department.

GUIDANCE ON THE COLOUR SCHEME FOR THIS FORM:				
Blue fill = mandatory for all work	No fill = for all work above CL2 only	Pink fill = tissues, cells, etc specific	Green fill - non-GM biological agents specific	Orange fill – GMM specific

1. INTRODUCTION

This section must be completed in all cases	
1.1 Background and aim of the project	**Mammalian cell lines will be cultured to provide biological models used for in vitro cell studies.**
1.2 Description of the experimental procedures	**Mammalian cell lines will be cultured using standard culturing methodology - For more information see the SOP attached**
1.3 Where will this work be carried out? *List all areas to be used e.g. the main lab, CBS, shared incubator rooms, shared storage facilities*	Rooms or area(s): **319** Building(s): **ACEX** Campus: **South Kensington**
A brief background to the project provides the reviewer a better understanding of the aims of the work. For Q1.2, the author is encouraged to cover as much of their activities with a particular agent or material as possible within this form. The intention of this Project Registration is primarily to agree the scope of the proposed works, and not to focus on the risk assessment of individual procedures. Note however that risk assessment of specific procedures remains essential and must be carried out.	

2. NATURE OF WORK AND BASIC HAZARD IDENTIFICATION

If this material is to be used then all relevant parts of this section must be completed		
TISSUES, CELLS, BODY FLUIDS OR EXCRETA		
2.1 If human or animal tissues, cells, body fluids or excreta will NOT be used then hatch here ☐ and proceed to Q2.9		
2.2 List all the tissues, cells, body fluids or excreta to be used (species, type, where obtained)	**Cell lines:** **- HeLa** **- SK-BR3 wild type (ATCC)** **- SK-BR3 Fluc/Rluc reporter (Transfected in house at MedImmune)** **- MDA-MB-231 wild type (ATCC)** **- MDA-MB-231 Fluc/Rluc reporter (Transfected in house at MedImmune)** **Other:** **- Fetal Bovine Serum, Heat Inactivated (Sigma-Aldrich)** *Details on the source of the material must be included*	
2.3 Describe what infectious agents this material has been screened for	**Mycoplasma screening at MedImmune**	
2.4 Will any clinical history or veterinary screening (if relevant) be provided?	Yes ☐ No ☒	N/R ☐

If yes, detail what this will include:		
If yes, will a policy of rejection of samples from diseased donors be adopted? Explain:		
If yes and for human material, how will the information be disseminated in the course of the project?		N/R ☒
If yes and for human material, will this information be anonomised?	Yes ☐ No ☐	N/R ☒

2.5 What is the likelihood of infection of any of this material? Please consider the worse case in this answer if multiple tissues, cells, etc are being used.	Medium risk ☐ High risk ☐ If medium or high risk of infection go to next question		None ☐ Low risk ☒ *If none or low risk proceed to Question 2.10*
2.6 If medium or high risk of infection name and classify the biological agents this material could be infected with	Tissue, cell, fluids or excreta	Name of agent	ACDP/defra classification
2.7 Describe the type and severity of the disease that can be caused to humans or animals by each of the agents that could be present	**n/a**		
2.8 Do any of the materials listed require a licence or a permit before work commences?	**No** *For example, IAPPO1, SAPO, defra, or FERA licenses? If yes, please list these and attach them with this form.*		

BIOLOGICAL AGENTS

2.9 If non-Genetically-Modified Biological Agents will NOT be used then hatch here ☒ and proceed to Q2.13

2.10 List the non-GM biological agents to be used	Name of agent	Strain(s)	ACDP/defra classification
2.11 Describe the type and severity of the disease that can be caused to humans, animals or plants by each of the agents, and if relevant, the particular strains in use			
2.12 Do any of the organisms listed require a licence or a permit before work commences?	*For example, IAPPO1, SAPO, defra, or FERA licenses? If yes, please list these and attach them with this form.*		

GENETICALLY MODIFIED MICRO-ORGANISMS

2.13 If Genetically-Modified Micro-Organisms (GMMs) will NOT be used then hatch here ☒ and proceed to Question 3.1

2.14 Provide an overview of the different types of GMM that will be constructed. Please ensure that the scope and boundaries of the work are made clear	
2.15 List all recipient species and strains to be used, their ACDP or defra classification	
2.16 List of vector systems to be used and their particular functional properties	

2.17	List the names and functional properties of all altered genes	
2.18	Identify the most hazardous GMM(s) to be constructed giving consideration both to human health and the environment	

3. DECLARATION

This section must be completed in all cases

3.1	Are you confident that any non-GM organism, tissue, cell, blood, body fluid or any component of any GMM covered by this assessment cannot potentially pose a threat to humans or the environment?	Yes ☐ *Hatch here if you believe that this project comprises work requiring only **Containment Level 1** proceed to Q5.1 of this form*	No ☒ *Hatch here if you believe that **Containment Level 2 (or higher)** is required and then answer Q3.2 and proceed to Q4.1 of this form*
3.2	Do any of the materials contain pathogens or toxins covered by the Anti-Terrorism (Crime and Security Act)?	Yes ☐ No ☒ *A list of the agents and toxins is available at the Safety Dept website. If yes, then Section 4 must still be completed even if only Containment Level 1.*	

PLEASE READ THIS CAREFULLY

You must only answer 'YES' to Q3.1 if you believe that you have sufficient information to classify the project as requiring only Containment Level 1, as defined in the Genetically Modified Organisms (Contained Use) Regulations or by COSHH. In order to do this you must be confident that even in the event of a total breach of containment all the biological agents, genetically modified organisms or cultured material would be of no or of negligible risk to human health or to the environment.

For ALL projects requiring Containment Level 2, or higher, or those covered by the Anti-Terrorism (Crime and Security) Act, submissions of this form must be accompanied by a Code of Practice, or at the very least, all the SOPs relevant to the work.

4. FURTHER ASSESSMENT

All relevant parts of this section must be completed if you answered 'No' to Q3.1

TISSUES, CELLS, BODY FLUIDS OR EXCRETA

4.1	If human or animal tissues, cells, body fluids or excreta will NOT be used then hatch here ☐ and proceed to Q4.8		
4.2	Will any culturing of the material described in Q2.2 take place? If yes, describe which cell(s) will be cultured and under what conditions.	Yes ☒ No ☐ **All the cell lines listed above will be cultured in flasks in standard conditions (Incubator, 37 oC, 5% CO2)**	
4.3	If culturing, could HIV permissive cells be present? If yes, describe the cells and for how long these cultures will be allowed to grow.	Yes ☐ No ☒	N/R ☐
4.4	If culturing, what is the maximum volume of culture grown?	Per flask: **5-67.5 mL** Number of flasks: **5-30**	N/R ☒
4.5	Will the tissues, cells, body fluids or excreta be manipulated in any way that could result in the concentration of any adventitious biological agent present? If yes, explain.	Yes ☐ No ☒	
4.6	What will the most hazardous procedure involving the use of this material be?	**Seeding cells for model assays**	

4.7	Will any of the fluids, tissues or cells be donated by you or your colleagues?	Yes ☐	No ☒
	If yes, detail who will provide these		N/R ☒
	If yes, explain the special risks associated		N/R ☒
	If yes, provide justification for not using material from another safer source e.g. National Blood Service		N/R ☒
	If yes, how will confidentiality be assured?		N/R ☒
	If yes, has written consent been obtained from the donor?		N/R ☒
	If yes, has Ethics Committee approval been obtained?	Yes ☐	No ☐

BIOLOGICAL AGENTS

4.8 If non-Genetically-Modified Biological Agents will NOT be used then hatch here ☒ and proceed to Q4.14

4.9	Describe ALL the route(s) of infection (relevant to the laboratory setting) and the minimum infectious dose(s), if known	Name of agent	Route(s) of infection	Minimum infectious dose

4.10	What is the highest concentration and volume of agent(s) to be worked with?	Per experiment: Total stored:
4.11	Are there any known drug resistances amongst the strains to be used? If yes, explain what these are and the consequences	
4.12	What forms of the agent will be used e.g. spores, vegetative forms and are there any issues over the robustness of these particular forms e.g. resistance to disinfectants or increased stability on dry surfaces	
4.13	What will the most hazardous procedure involving the use of this material be?	

GENETICALLY MODIFIED MICRO-ORGANISMS

4.14 If GMMs will NOT be used then hatch here ☒ and proceed to Q5

4.15	Identify the hazards to human health or to the environment of the recipient microorganism(s)	
4.16	Identify any of the hazards to human health or to the environment associated directly with the vector systems in use	
4.17	Identify all of the known or potential hazards associated with all the GMMs to be generated. It is important that the boundaries of this project are clearly explained here	
4.18	Describe the likelihood and consequences of the modifications being transferred to related microorganisms	

4.19	Identify the most hazardous GMM(s) to be constructed giving consideration both to human health and the environment			
4.20	Describe ALL the potential route(s) of infection (relevant to the laboratory setting) of the GMM(s)	Name of agent	Route(s) of infection	Minimum infectious dose
4.21	What is the highest concentration and volume of the GMM(s) to be worked with?	Per experiment:	Total stored:	

5. RISKS AND CONTROL MEASURES

All questions in this section must be answered and further details supplied when indicated

NOTE that a Code of Practice (CoP) or Standard Operating Procedure (SOP) reference must be provided for CL2 or higher work, or work covered by the Anti-Terrorism (Crime and Security) Act

Risk			If yes, how will this be controlled?	Reference for SOP, CoP other written protocol providing details on usage, training, decontamination, etc.
5.1	Might infectious droplets or aerosols be created, either deliberately or by accident?	Yes ☒ No ☐	**Operations will be performed in a safety biocabinet or by using sealed containers and sealed rotors when using centrifugation.** *For example, will a safety cabinet or any other form of Local Exhaust Ventilation be required? Are there any particular requirements for the room ventilation?*	**See - Standard Operation Procedure for Cell Culture**
5.2	Will material be transported within the laboratory?	Yes ☒ No ☐	**Materials will be containted prior to transport in containted boxes or trays.** *For example, cultures being transported between the safety cabinet and the incubator must be double contained so as to prevent spillage if dropped*	**See - Standard Operation Procedure for Cell Culture**
5.3	Will the material be transported locally on campus but outside of the laboratory?	Yes ☒ No ☐	**Materials will be carried in contained, sealed containers to areas with relevant analytical equipment (e.g. fluorometer).** *For example, material transported from the primary laboratory to CBS must be double contained so as to prevent spillage if dropped, adequately labelled and no gloves must be worn outside of the laboratory*	**See - Standard Operation Procedure for Cell Culture**
5.4	Will this material be shipped elsewhere in the UK or abroad?	Yes ☐ No ☒	*Provide details of material to be shipped and the packing instructions to be followed. For example, MTb cultures shipped as Category A infectious substance in PI620 packaging. Further guidance is available on the Safety Dept website*	**N/A**
5.5	Will this material be received from elsewhere?	Yes ☒ No ☐	**The material will be shipped from the University of Leeds. It will be shipped in containted vials. The cells will be frozen (in dry ice).** *Provide details of material to be received, how this will be arranged and what steps will be taken*	**See - Standard Operation Procedure for Cell Culture**

			to ensure that the material is correctly packaged. Further guidance is available on the Safety Dept website	
	5.6 Will this material be stored?	Yes ☒ No ☐	***The material will be stored in liquid nitrogen (cells) or fridge (FBS)*** *Provide details of how, where and in what this material will be stored. If stored in Liquid Nitrogen describe the additional precautions in place*	**See - Standard Operation Procedure for Cell Culture**
	5.7 Will infectious material be centrifuged?	Yes ☒ No ☐	Will the primary containers be sealed? **Yes** Will sealed rotors or sealed buckets be used? **Yes** *Include details on the protection factor afforded by the bio containment arrangements fitted to the centrifuge. This information is available from the manufacturer and in the operators instructions e.g. where release of micro-organisms is to be prevented, a centrifuge should be used which is classified LI-C, CI-B and SI-C or better. Where L is leaktightness, C is cleanability and S is sterilizability. Performance is graded A to C (C is best)*	**See - Standard Operation Procedure for Cell Culture**
			Where will these rotors be opened? **On the bench** *For example, within a safety cabinet*	**See - Standard Operation Procedure for Cell Culture**
			Describe the procedures in place to deal with leaks or spillages in the centrifuge or rotor **See SOP attached**	**See - Standard Operation Procedure for Cell Culture**
	5.8 Are biological samples to be cultured in an incubator?	Yes ☒ No ☐	**Thermo incubator with CO2 supply and static shelf** *What type of incubator (e.g. shaking or static shelf) is this and describe the measures to be used to prevent and contain any spillages*	**See - Standard Operation Procedure for Cell Culture**
	5.9 Are sharps to be used at any stage during this activity?	Yes ☒ No ☐	**Pippete tips of various size will be used - required for various operations such as handling the cells and addition of reagents. The tips are plastic and do not pose a big risk to the users. Nevertheless, users are trained in proper handling and disposal of the tips and will wear appropriat PPE.** *Describe the sharps, justify their use and describe the precautions in place to protect the user and others from injury*	**See - Standard Operation Procedure for Cell Culture**
	5.10 Are animals to be used as part of this project?	Yes ☐ No ☒	What procedures will be undertaken?	**N/A**
			Where will this aspect of the work be undertaken?	**N/A**
			Is shedding of biological agent or GMMs by the infected animals possible?	**N/A**

			If yes, detail routes of shedding, risk periods for such shedding and the additional precautions required to control exposure	
			Who will perform the inoculations/exposure of the animals? *What training will they have received and where will this be recorded*	**N/A**
			Provide details on any additional training required for those handling these animals	**N/A**
			Provide details on any additional precautions necessary	**N/A**
	5.11 Will a fermenter be used to culture the pathogen	Yes ☐ No ☒	What size and type is this and are any supplementary containment measures required, for example, the use of a safety cabinet or spill tray?	**N/A**
			Where is this fermenter located and who is in charge of the area?	**N/A**
	5.12 Is there any stage within the experimental procedures when the infectious material is inactivated (other than for disposal)?	Yes ☐ No ☒	If yes, how will this be done and what will then happen to the material?	**N/A**
	5.13 Are any of the following to be used in conjunction with this project? If yes provide details and the SOP/CoP reference		Liquid Nitrogen ☒ Radioactive materials ☐ Carcinogens ☐ Toxins ☐ Lasers ☐ Fieldwork ☐ Lone working ☒	**See - Standard Operation Procedure for Cell Culture**

6. PPE & HYGIENCE

All questions in this section must be answered in all cases

NOTE that a Code of Practice (CoP) or Standard Operating Procedure (SOP) reference must be provided for CL2 or higher work, or work covered by the Anti-Terrorism (Crime and Security) Act

Control measure	Details	Reference for SOP, CoP other written protocol
6.1 When will gloves be worn?	**Always**	**See - Standard Operation Procedure for Cell Culture**
6.2 What type are these and where will they be stored?	**Purple nitrile gloves, stored on the lab bench**	**See - Standard Operation Procedure for Cell Culture**
6.3 When will laboratory coats be worn and what type are these?	**Always, long-sleeved, knee length laboratory designed coats, suitable for CL2 activities**	**See - Standard Operation Procedure for Cell Culture**

	6.4 Where will the lab coats be stored and what are the arrangements for cleaning or disposal?	**On the back of the door, to be laundered by the Chemical Engineering departmental store every few weeks.**	**See - Standard Operation Procedure for Cell Culture**
	6.5 Is any other type of personal protective equipment to be used? If yes, provide details	**Laboratory goggles.**	**See - Standard Operation Procedure for Cell Culture**
	6.6 Describe the lab hygiene facilities	**Eye wash, soap, sink**	**See - Standard Operation Procedure for Cell Culture**

7. WASTE

All questions in this section must be answered in all cases

NOTE that a Code of Practice (CoP) or Standard Operating Procedure (SOP) reference must be provided for CL2 or higher work, or work covered by the Anti-Terrorism (Crime and Security) Act

7.1 How will waste be treated prior to disposal?

(Note that all differently treated wastes must be included e.g. if some liquid is autoclaved, but others not, then describe both)	**Treatment prior to disposal**	**SOP/CoP/ protocol**
Liquid waste	**Biological - By autoclaving or disinfection before discarding** **Chemical - sink or waste drum, depending on the hazard type**	**See - Standard Operation Procedure for Cell Culture**
Solid waste	**Contaminated plastic will be placed in the biological waste bins, autoclaved, and disposed of with the Chemistry departmental biological waste.**	**See - Standard Operation Procedure for Cell Culture**
Other waste (specify): **N/A**	**N/A**	**N/A**

7.2 If waste is to be autoclaved confirm the following;

All cycles have been validated for the actual load types used	Yes ☒ No ☐	*No SOP required but documentary evidence of this validation must be available*
The successful completion of every load is checked prior to disposal?	Yes ☒ No ☐	**See - Standard Operation Procedure for Cell Culture**

7.3 How will liquid waste be disposed of?

To drain?	Yes ☒ No ☐		**Disinfection with Virkon overnight and then dispose to the drain** **See - Standard Operation Procedure for Cell Culture**
As solid waste?	Yes ☐ No ☒		
Other (specify)?	Yes ☐ No ☒		

7.4 How will solid waste be disposed of?

Categorisation	Colour code	Disposal method	SOP/CoP/ protocol
☒ Sharps	Yellow	Yellow sharps bin > autoclave sterilisation if known or potentially infected >clinical waste disposal (incineration)	**See - Standard Operation Procedure for Cell Culture**
☐ Human body parts, organs including blood bags and blood preserves and excreta (unless identified as medium or high risk or known infected in Q2.5 of this assessment in which case they must be pre-treated before disposal)	Yellow	Yellow rigid one way sealed tissue bins > clinical waste disposal (incineration) * Human tissue waste must be placed in separate containers from non-human waste and labelled 'HTA waste'	
☐ Animal body carcasses or recognisable parts (unless identified as medium or high risk or known infected in Q2.5 of this assessment in which case they must be pre-treated before disposal)	Yellow	Yellow rigid one way sealed tissue bins > clinical waste disposal (incineration)	
☐ Potentially or known infected lab wastes (including sharps) of Hazard Group 2, GM Class 2, DEFRA Category 2 or higher, that have not been pre-treated before leaving site	Special case – contact Safety Department	This is not a route of preference and is subject to special requirements	
☒ Infected or potentially infected lab wastes that have been pre-treated before leaving site	Orange	Disinfection or sterilisation in the laboratory suite > orange clinical waste bags > clinical waste disposal (alternative treatment)	**See - Standard Operation Procedure for Cell Culture**
☐ Infected or potentially infected animal or human body parts, organs or excreta that have been pre-treated before leaving site	Yellow	Disinfection or sterilisation in the laboratory suite >yellow one way sealed tissue bins > clinical waste disposal (incineration) * Human tissue waste must be placed in separate containers from non-human waste and labelled 'HTA waste'	

	☐ Packaging material that has been used for the importation of animal products subject to Defra licenses	Yellow	yellow clinical waste bags > clinical waste disposal (incineration or alternative treatment as described in the licence	

8. MAINTENANCE

All questions in this section must be answered for all work at CL2 or higher, or work covered by the Anti-Terrorism (Crime and Security) Act. In all cases the SOP/CoP or protocol reference is required.

8.1 List the maintenance regimes for all the following lab equipment

	Maintenance frequency	Maintenance carried out by	SOP/CoP/ protocol	N/R
Centrifuge(s)	**Daily**	**Users**	**Centrifuge - SOP**	☐
Safety cabinets	**Daily**	**Users**	**Biological Safety Cabinet - SOP**	☐
Autoclaves	**As needed**	**Autoclave owners**	**See - Standard Operation Procedure for Cell Culture**	☐
Shaking incubators				☐
Other (specify)				☐

9. TRAINING

All questions in this section must be answered for all work at CL2 or higher, or work covered by the Anti-Terrorism (Crime and Security) Act. In all cases the SOP/CoP or protocol reference is required.

9.1 Confirm that training to all workers is providing in at least the following aspects of this work

	Training frequency	Training carried out by	Is competency assessed?	SOP/CoP/ protocol	N/R
Hazards associated with this work	**Once**	**Experienced colleagues**	Yes ☐ No ☒	**See - Standard Operation Procedure for Cell Culture**	☐
Safe working practices as described in this risk assessment	**Once**	**Experienced colleagues**	Yes ☐ No ☒	**See - Standard Operation Procedure for Cell Culture**	☐
Spillage response within the safety cabinet	**Once**	**Experienced colleagues**	Yes ☐ No ☒	**See - Standard Operation Procedure for Cell Culture**	☐
Spillage response within the centrifuge	**Once**	**Experienced colleagues**	Yes ☐ No ☒	**Centrifuge - SOP**	☐
Spillage response elsewhere	**Once**	**Experienced colleagues**	Yes ☐ No ☒	**See - Standard Operation Procedure for Cell Culture**	☐
Post-exposure protocols	**Once**	**Experienced colleagues**	Yes ☐ No ☒		☐

10. EM

All questions in this section must be answered for all work at CL2 or higher, or work covered by the Anti-Terrorism (Crime and Security) Act. In all cases the SOP/CoP or protocol reference is required.

	10.1 Describe the procedures in place for dealing with spillage of infectious or potentially infectious material			
		Procedure	**SOP/CoP/ protocol**	**N/R**
	Within the safety cabinet	**Wipe down all interior cabinet surfaces, all supplies and equipment with 1% Virkon or 70% ethanol.**	**See - Standard Operation Procedure for Cell Culture**	☐
	Within the centrifuge	**Wipe up with towels and deionized water**	**Centrifuge - SOP**	☐
	Within the laboratory but outside of any primary control measure e.g. safety cabinet	**Put on gloves and cover spill area with paper towels** **Disinfection with 1% Virkon solution, decontaminate all objects in spill area, clean the spillage with paper towels, mop floor if spill on the floor.**	**See - Standard Operation Procedure for Cell Culture**	☐
	Outside of the laboratory	**Notify other workers in the area of the spill and control traffic through area.** **Put on gloves and cover spill area with paper towels** **Disinfection with 1% Virkon solution, decontaminate all objects in spill area, clean the spillage with paper towels, mop floor if spill on the floor.**	**See - Standard Operation Procedure for Cell Culture**	☐
	10.2 Describe the procedures in place for an accidental exposure			
	Immediate action	**treated with 70% ethanol, then rinse well with water.** **Remove any contaminated lab coat and put in autoclavable bag. Be aware that autoclaving may damage fabric.**	**See - Standard Operation Procedure for Cell Culture**	☐
	When and to whom to report the incident	**After taking emergency action** **Report to PI and safety officer**		☐

11. ACCESS

All questions in this section must be answered for all work at CL2 or higher, or work covered by the Anti-Terrorism (Crime and Security) Act. In all cases the SOP/CoP or protocol reference is required.

		SOP/CoP/ protocol
11.1 Is the lab(s) adequately separated from other areas (e.g. offices)	Yes ☒ No ☐ *If no, explain:*	
11.2 Is/are the lab(s) or other work areas shared with other users not involved in this project	Yes ☐ No ☒ *If yes, explain who and what procedures are in place to control any risk to them:*	
11.3 Describe the measures in place to ensure that the infectious material is secured	**Double door with access code**	
11.4 What access colour code do the rooms used have?	Red ☐ Amber ☐ Yellow ☒	

12. OCCUPATIONAL HEALTH

This section to be completed for work with biological agents or GMMs in Hazard Group 2 or higher and for work with unscreened human tissues ONLY

This must be completed the Occupational Physician only but note that where pre-activity requirements are identified, it is the responsibility of the Principal Investigator to ensure that these are carried out for all individuals working on this project, before they actually start work

THE PRINCIPAL INVESTIGATOR MUST ENSURE THAT THE INFORMATION DESCRIBED IN THIS SECTION IS UNDERSTOOD BY ALL THOSE THAT WORK ON THIS PROJECT

12.1 Medical risk assessment	
12.2 Pre-activity requirements	
select one	*Details:*
select one	*Details:*
select one	*Details:*
12.3 Periodic health surveillance requirements	
12.4 Post exposure action	
12.5 Antibiotic treatment or chemoprophylaxis	
12.6 Additional notes or comments	

13. CONTAINMENT LEVEL

This section must be completed in all cases

13.1 Confirm what Containment Level can be assigned to each aspect or component of this project. If different aspects of this work merit different Containment Levels, then all must be listed

Project aspect	Where work will be carried out	Containment Level (as required under COSHH or GMO (Contained Use) Regs	With extra controls (list these, if relevant. If required seek advice from your DSO or the College BSO)	With derogation from certain controls (list these, if relevant. If required seek advice from your DSO or the College BSO)
Cell culturing	ACEX 319	CL2	N/A	N/A

14. GM CLASS

This section must be completed for work with Genetically Modified Micro-organisms only

14.1 Confirm the class of all GMMs in use

Project aspect	GM Class